EXPERIMENTAL EVALUATION OF DUCTILE IRON PIPELINE RESPONSE TO EARTHQUAKE-INDUCED GROUND DEFORMATION

A Dissertation

Presented to the Faculty of the Graduate School

of Cornell University

In Partial Fulfillment of the Requirements for the Degree of

Doctor of Philosophy

by

Chalermpat Pariya-Ekkasut

May 2018

EXPERIMENTAL EVALUATION OF DUCTILE IRON PIPELINE RESPONSE TO EARTHQUAKE-INDUCED GROUND DEFORMATION

Chalermpat Pariya-Ekkasut, Ph.D.

Cornell University 2018

This thesis addresses the performance of ductile iron (DI) pipelines with restrained axial slip joints subject to earthquake-induced ground deformation. DI pipelines account for 23% of U.S. water distribution systems (US.EPA, 2013), and have been used extensively for replacing aging cast iron (CI) pipelines. Under earthquake-induced ground deformation a jointed DI pipeline is vulnerable primarily to joint pullout and excessive joint rotation. Improvements in pipeline technology have led to the development of DI pipelines with restrained axial slip joints that move axially and rotate to conform to differential soil movements, but are restrained from pullout without leakage and loss of structural integrity.

A series of large-scale experiments was performed on DI pipelines with restrained axial slip joints to characterize tensile strength properties, direct axial compression and tension, moment vs rotation characteristics, soil axial restraint, and performance in response to fault rupture. Large-scale tests were performed primarily on 6-in. (150-mm)-diameter DI pipelines, but also included direct tension and bending tests on 12-in. (300-mm)-diameter DI pipelines.

The direct compression tests show either leakage or irrecoverable deformation in the form of large rotation at loads equal to or slightly higher than load consistent with

the proportional limit stress of DI pipe. The direct tension tests show that tensile failure of the pipeline depends on the locking mechanism of the joint. Joints that use full circumferential locking rings generate the highest resisting force. Failure and leakage under tension with these features occurred as DI ring shear fracture and bell fracture. In contrast, joints that use locking segments mobilized lower pullout force. Failure and leakage of joints with locking segments occurred as local deformation at the spigot caused by load concentration at the locking segments, allowing the weld bead to slip past the locking segments and cause leakage.

Large-scale fault rupture tests provide a comprehensive and detailed understanding of the sequence of joint movements, combined axial pullout and rotation at each joint, and the actual axial forces influenced by longitudinal frictional resistance and axial resistance to movement at the joints. The longitudinal frictional forces are controlled by at-rest (K_o) conditions, which set the initial state of stress along the pipeline near the north and south ends of the split basin, and the conditions of maximum lateral soil reaction during fault rupture, which establish the maximum longitudinal frictional resistance for the pipeline in the vicinity of fault rupture.

The joint axial resistance model proposed in this work is obtained from the expression for face resistance of the leading edge of a jacked pipe proposed by Meskele and Stuedlein (2015) from the work of Weber and Hurtz (1981). The model is used to predict the axial resistance from a restrained axial slip joint for DI pipe and the pullout restraints of PVCO and PVC pipelines. The proposed model provides for relatively close prediction under K_o conditions within ±15% of the actual maximum load measured during full scale soil axial resistance tests.

BIOGRAPHICAL SKETCH

Chalermpat Pariya-Ekkasut was born in Bangkok, Thailand on December, 5, 1989 as the second child of the family. His father, Sutep Pariya-Ekkasut, served for 44 years as an engineering officer and retired as a lieutenant general of the Royal Thai Army. Inspired by his father's work and achievement, Chalermpat decided to follow in his father's footsteps and join the national service at the age of 15, and without hesitation, the Army was his first choice.

His military career started at the Armed Forces Academies Military Preparatory School, where he engaged in rigorous academics, military training, and intensive physical activities. At the end of the three-year program, Chalermpat was ranked academically second in his class and earned an opportunity to pursue his bachelor's degree in a military college in the United States.

Chalermpat spent a year at Wyoming Seminary School in Kingston, PA to practice his English skill and experience the new culture. He then applied to the United States Military Academy at West Point and became one of twenty international cadets in the class of 2013. During his senior year, Chalermpat was one of the five members of the West Point steel bridge team. He graduated with a Bachelor of Science in Civil Engineering with honors and was promoted to second lieutenant in the Thai Army. Fascinated by large-scale testing at the Bovay Civil Infrastructure Laboratory, Chalermpat decided to take a leave from the military service and pursue a Ph.D. at Cornell University.

To Pariya-Ekkasut family

“It is not necessary to do extraordinary things to get extraordinary results.”

- Warren E. Buffett

ACKNOWLEDGEMENTS

First and foremost, I would like to thank my advisors, Professors Thomas D. O'Rourke and Harry E. Stewart, for the opportunity to pursue my graduate studies in the geotechnical engineering research group at Cornell.

I am sincerely grateful for Professor O'Rourke's invaluable research skills, professional development, and tremendous guidance during my studies and thesis writing.

I thank sincerely Professor Stewart for his council and professionalism with respect to my laboratory work, research, and teaching. I have learned many precious life lessons from him.

I extend my appreciation to Professor Mircea Grigoriu for his guidance in my studies, and for the excellent course he taught that I was able to take at Cornell University.

I am happy to have shared this difficult journey with my past and present geotechnical graduate students Dimitra Bouziou, Brad Wham, Christina Argyrou, and Dakota Price. I am especially thankful for Brad who dedicated uncountable hours training me in laboratory and research skills.

I extend my thanks and best wishes to Tim Bond, our excellent and irreplaceable lab manager. He was always there to help me through challenging times at Cornell. I am also grateful to have worked with the staff and students of the Bovay (Civil Infrastructure) Laboratory, including Blake Berger, Joe Chipalowski, Addie Lederman,

Andrew Shakalis, Kimberly Buhl, Margaret Stack, Mia Stewart, Sarah Weinberg, Corbin Atkins, and many others.

I would like to acknowledge all parties that have enhanced my Cornell experience. My utmost gratitude goes to my parents, LTG Sutep and Mrs. Achara Pariya-Ekkasut, for their support of this endeavor and for tolerating my long absence from home. It must have been difficult for them. In this respect, I would like to thank my sister, Ms. Pimchanok Pariya-Ekkasut, for taking care of our parents during my absence and for being a wonderful sister.

I also thank my beloved girlfriend, Ms. Siraphat (Fay) Taesuwan. Fay and I have been through the PhD journey together. I appreciate her patience and understanding. She is always by my side to cheer me up every time I feel upset. I hope we will have "good news" soon!

I appreciate the financial support provided by Cornell University and the School of Civil and Environmental Engineering through teaching assistantships, as well as funding from research sponsors American Cast Iron Pipe Company, Kubota Corporation, McWane Corporate, and U.S. Pipe.

TABLE OF CONTENTS

LIST OF FIGURES

LIST OF TABLES

CHAPTER 1

INTRODUCTION

1.1 Overview

Under earthquake-induced ground deformation a jointed pipeline is vulnerable primarily to joint pullout, but also vulnerable to excessive joint rotation or pipe barrel bending, as well as compressive axial movement that causes local, irrecoverable deformation where the spigot makes contact with the bell of a connecting pipe. Improvements in pipeline technology have led to a new generation of pipelines that can accommodate permanent ground deformation by either ductile flexure or axial deformation of the pipe barrel, axial movement and rotation of the joints, or a combination of both. Representative of the technology for improved response to earthquake-induced ground deformation are various ductile iron (DI) pipelines with joints that can move axially and rotate to conform to differential soil movements, but are restrained from pullout without leakage and loss of structural integrity. These pipelines are often referred to as earthquake resistant or hazard resilient DI pipelines. Because of their ability to slip axially and their restraint against pullout, in this work they are referred to as restrained axial slip joints.

Ductile iron (DI) pipelines account for nearly 23% of U.S. water distribution systems (US.EPA, 2013), and have been used extensively for replacing aging cast iron (CI) pipelines. Because of their ductility, DI pipelines are better suited for locations of differential soil movement than pipelines composed of relatively brittle materials, such

as CI and asbestos cement. The improvements in DI pipeline joints to resist pullout, slip in response to axial extension/compression, and rotate, represent a paradigm shift in the earthquake resistant design and construction of critical water supplies.

1.2 Previous Research

In recognition of the susceptibility of DI water pipelines to earthquakes, Singhal and Benavides (1984) conducted experiments on various sizes of DI push-on joints to determine their structural behavior when subjected to static loading and reloading conditions. Unpressurized pull-out and four-point bending tests were performed on joints under buried, semi-buried, and unburied condition until joint slippage. Pull-out force vs. joint displacement and bending moment vs. joint rotation were plotted on the basis of the test data. Unpressurized three-point bending test results on nominal 6-in. (150-mm), 8-in. (200-mm), and 12-in. (300-mm) diameter DI push-on joints were presented by Yang et al. (2011). The tests provide moment vs. rotation relationships of these joints and evidence that rubber gaskets can prevent leakage at flexible connections of jointed DI pipelines.

Maragakis et al. (1999) and Meis et al. (2001, 2003) tested different DI pipe joints in both static compression and tension. The DI pipe joints in these investigations include push-on joints and restrained joints, which utilized a retaining ring, gripper gasket, or bolted collar. The DI pipes in this research, however, were relatively short, and the internal water pressure was low [3 to 4 psi (20 to 28 kPa)]. Stress vs. strain relationships from tensile coupon were not presented. Only yield stress and Young's

modulus were given. The proportional limit stress is taken as 0.65 of yield stress obtained from tensile coupon tests performed in this work. The maximum compressive load measured for the nominal 6-in. (150-mm)-diameter push-on DI joints was 237 kips (1,054 kN), which is equivalent to 155% and 101% of the proportional limit and yield loads, respectively. The proportional limit load, P_{prop}, is defined as $P_{prop} = \sigma_{prop}A$, where σ_{prop} is the proportional limit stress and A is the pipe cross-sectional area. The yield load, P_y, is defined similarly as $P_{prop} = \sigma_y A$ where σ_y is the yield stress. The maximum tensile capacity of a nominal 6-in. (150-mm) diameter DI joint equipped with a retaining ring was 121 kips (538 kN). The peak loads reported by Meis et al. (2003) help define an ultimate limit state, but do not allow for an assessment of a serviceability limit state related to water leakage because the internal water pressure during the tests was well below typical operating pressures for water distribution pipelines in the field.

Wham and O'Rourke (2015) report on a series of specially designed four-point bending experiments under 55 psi (380 kPa) of internal water pressures in comparison with 3D finite-element (FE) simulations to characterize 6-in. (150-mm) diameter DI push-on joints. The results were used to develop a relationship between rotation and metal binding as a function of axial pullout, as well as to determine the magnitudes of rotation and moment that initiate joint leakage. Uniaxial tension and one-dimensional compression tests were performed on the elastomeric gasket material and used to develop a hyper elastic strain energy model of the gasket for application in numerical modeling to characterize behavior under extreme loading. Numerical models

demonstrate joint leakage to be independent of load path, and that a unique pressure boundary predicts leakage for many combinations of deformation.

Kishi et al. (2013) report on the performance of earthquake resistant DI pipelines in response to the 2011 Tohoku earthquake. As previously explained, earthquake resistant DI joints move axially and rotate, but are restrained against pullout. The investigators claim that no damage was incurred by these pipelines, either in response to the earthquake shaking, permanent ground movement, or undermining due to tsunami-induced flooding and erosion. The results of surveys of existing pipelines in locations of liquefaction, settlement, and flooding are reported in terms of joint rotation and expansion/contraction of the joints.

Oda et al. (2016) performed a large-scale fault rupture test on a nominal 8-in. (200-mm) earthquake resistance ductile iron pipeline. The test showed that the pipeline exhibited the behavior of a chain structure to accommodate fault movement. Pipeline behavior in the fault rupture test was numerically modeled and the analytical and experimental results were compared. The finite element model (FEM) was then used to design a DI pipeline system that could accommodate a large ground displacement.

More recently, US manufacturers have developed DI pipeline systems with special restrained joints that can slip and rotate to accommodate earthquake-induced ground deformation. These products add substantially to the inventory of jointed DI pipelines that can be used to enhance performance in response to earthquakes and other hazard-related sources of differential soil movement. Large-scale test results for these

types of DI pipeline systems are reported by Pariya-Ekkasut et al. (2015, 2016, 2017, 2018) and Stewart et al. (2015).

1.3 Restrained Axial Slip Joints

This work includes a systematic and detailed assessment of DI pipelines with restrained axial slip joints. The large-scale test results for four commercially available jointed DI pipelines are summarized with respect to DI tensile strength properties, direct axial compression and tension, moment vs rotation characteristics, soil axial restraint, and performance in response to fault rupture. The large-scale test results are associated primarily with nominal 6-in. (150-mm) diameter pipe. The physical characteristics of each commercially available DI pipeline with restrained axial slip joints are described under the four subheadings that follow.

1.3.1 AMERICAN Earthquake Joint System (EJS)

Three-dimensional (3D) views of the AMERICAN Earthquake Joint System (EJS) are shown in Figure 1.1. A 3D external view is provided in Figure 1.1 a), which shows a red EJS deep socket bell that connects a standard flex-ring bell and a spigot with set-back weld ring. Figure 1.1 b) provides a cut-away view of the EJS joint. The deep socket (SE) and flex-ring (FR) bells have rubber gaskets to prevent leakage and are equipped with DI locking rings. In each joint the weld ring, which has an approximate thickness of 0.5 in. (13 mm), bears against the locking ring to resist pullout.

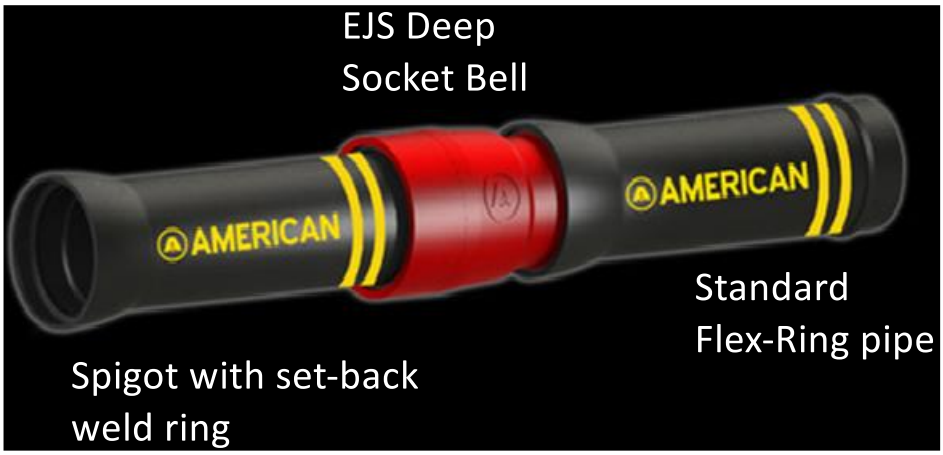

a) External View

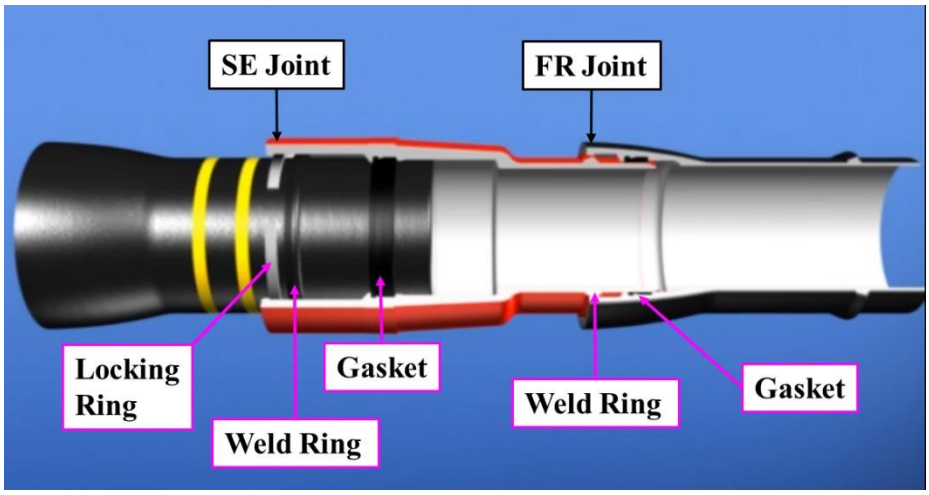

b) Cut-away View

Figure 1.1. Three-dimensional views of an AMERICAN Earthquake Joint System (EJS)

The deep socket (SE) joint is designed to accommodate a large axial slip, but can only accommodate a small amount of rotation. In contrast, the Flex-Ring (FR) joint can accommodate rotation, but allows very little axial displacement.

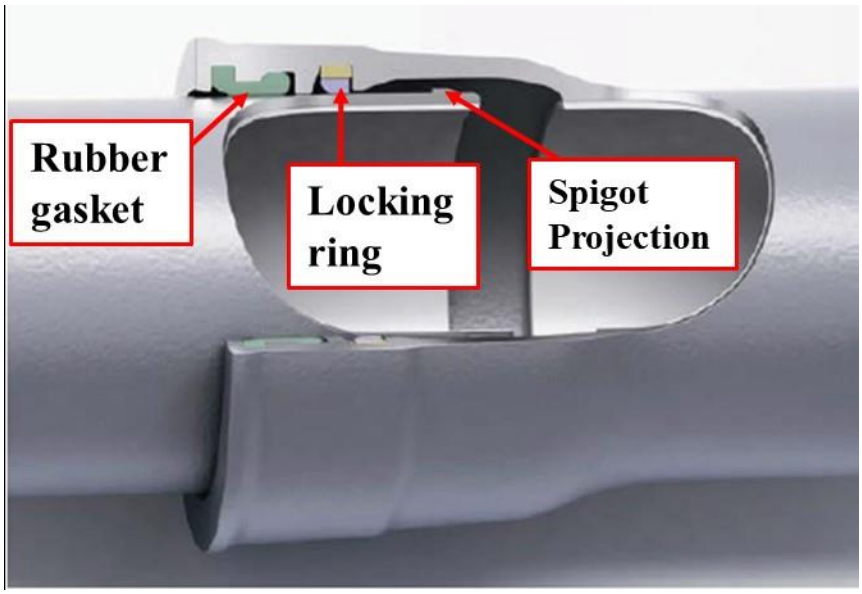

Figure 1.2. Cut-away View of ERDIP GENEX Joint (courtesy Kubota Corp.)

1.3.2 Kubota Earthquake Resistant Ductile Iron Pipe (ERDIP)

Figure 1.2 presents a cut-away view of a Kubota earthquake resistant ductile iron pipe (ERDIP), referred to as GENEX. The ERDIP has an extended bell that allows axial slip and rotation of the spigot inside the bell. The bell is equipped with a rubber gasket and a locking ring. The spigot has an indentation, which is about 1/16 in. (1.6 mm) deep and 0.15 in. (3.8 mm) wide, around its circumference at 1 in. (25.4 mm) from its end into which a ductile iron ring is either welded or connected by screws. This special feature is called a spigot projection. The thickness of the spigot projection is 0.12 in. (3 mm). The spigot is inserted into the bell past the rubber gasket and the locking ring. When the joint is pulled, the spigot projection bears against the locking ring, generating the locking mechanism.

1.3.3 McWane Seismic Flex Coupling (SFC)

The McWane Seismic Flex Coupling (SFC), shown in Figure 1.3, consists of plain and bell end adaptors that connect to standard TR Flex® joints. The complete assembly has a total of three joints: B, X, and P. A TR Flex® spigot is inserted into a plain end adapter, making the B joint. An X joint is referred to a joint between plain and bell end adapters. Lastly, a bell end adapter is inserted into a TR Flex® bell, making the P joint. Each joint is equipped with two locking segments and a rubber gasket to prevent leakage. Each spigot has a 0.5-in. (13-mm)-diameter weld bead that bears against two locking segments to resist joint pullout. The majority of axial slip is accommodated by the X joint, which is limited with respect to rotation. In contrast, the TR Flex®, B and P, joints are able to rotate significantly, but have limited capacity for axial displacement.

1.3.4 US Pipe TR-XTREME™

US Pipe manufactures pipe with a ductile iron joint, under the commercial name TR-XTREME™. The joint has an elongated bell, which allows axial movement and rotation of the spigot inside the bell, but also is restrained against pullout of the spigot. A 3D view of the joint is provided in Figure 1.4. The joint is equipped with a rubber gasket to prevent leakage. The spigot end has a 0.5-in. (13-mm)-diameter weld bead. Locking segments [two for 6-in. (150-mm) and four for 12 in. (300 mm) joint specimens] are inserted at two locations. The locking segments provide resistance to pullout when the weld bead moves axially into contact with them.

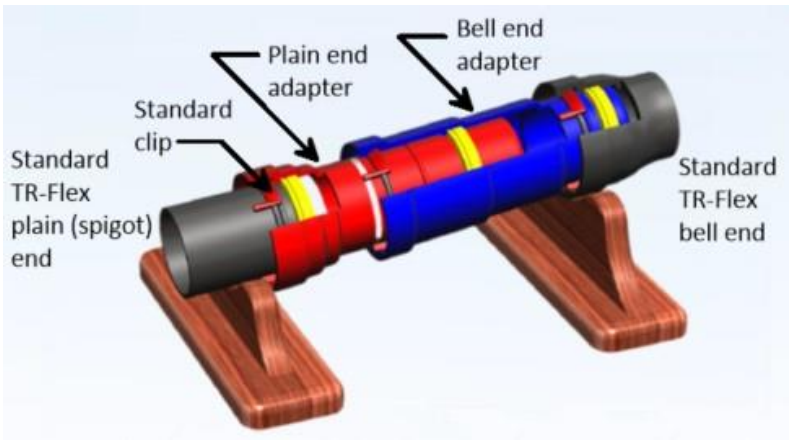

a) Three-dimension View

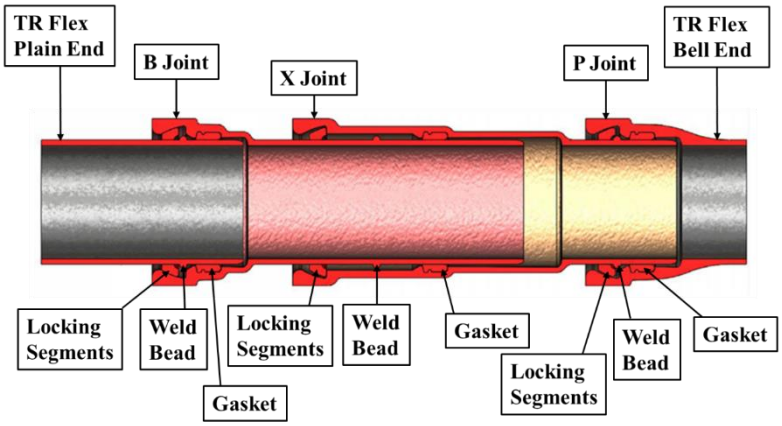

b) Cut-away View

Figure 1.3. Three-dimensional and Cut-away Views of a Seismic Flex Coupling (courtesy McWane)

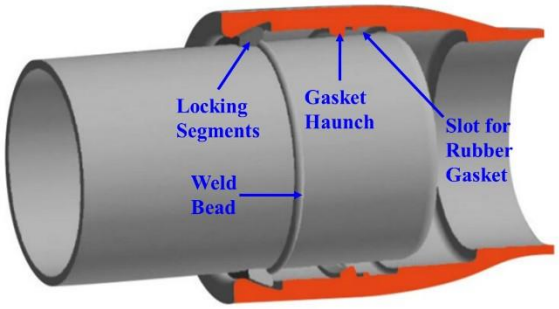

Figure 1.4. Cut-away View of US Pipe TR-XTREME™

1.4 Objectives

The overall goal of this work is to evaluate the key mechanical factors affecting the performance of DI pipelines with restrained axial slip joints under earthquake-induced ground deformation. This evaluation is based on large-scale laboratory tests on four different commercially available jointed DI pipelines with nominal 6-in. (150-mm) diameters. Each pipeline system was investigated with the same testing protocol involving 1) tensile coupon tests, 2) direct compression and tension tests, 3) four-point bending tests, 4) soil axial resistance tests in which a buried DI pipeline with a restrained axial joint is displaced axially through the soil, and 5) fault rupture tests on a jointed DI pipeline of approximately 34 ft. (10 m) in length. Similar conditions apply for the testing of each pipeline system, including pipe diameter, test setup and configuration, burial depth, and properties of the partially saturated sand used in the soil axial resistance and fault rupture tests. Thus, a consistent and repeatable framework was established with which to measure and characterize jointed DI pipeline response to

imposed deformation that is similar to that caused by earthquake-induced ground movements.

The research described in this dissertation is focused on four principal objectives:

- Evaluate and summarize the results of large-scale tests on four pipe and restrained axial slip joint systems with respect to DI tensile strength properties, direct axial compression and tension, moment vs rotation characteristics, soil axial restraint, and performance in response to fault rupture.
- Summarize the test results for the four jointed DI pipeline systems to help understand their mechanical characteristics on a comparative basis.
- Clarify key mechanical characteristics of the jointed DI pipeline systems so that load and deformation response is better understood, and quantifiable limit states are set for ultimate capacity and serviceability.
- Develop force vs. displacement and moment vs. rotation relationships from the test data for application in numerical and analytical models.

1.5 Organization

This dissertation is divided into eight chapters. The first chapter provides introductory comments, objectives, and scope of the work. The second chapter presents the results of tensile coupon tests to characterize the basic stress-strain-strength

characteristics of the DI pipe. The third chapter presents the test results for direct compression tests on nominal 6-in. (150-mm) joint specimens and tension tests on nominal 6-in. (150-mm) and 12-in. (300-mm) joint specimens. The force vs. displacement relationships are established, and limit state conditions for pipe leakage are also provided. The fourth chapter presents a summary of the four-point bending test procedures and laboratory results for nominal 6-in. (150-mm), 12-in. (300-mm), and 16-in. (400-mm) DI pipes. The failure modes and moment vs. rotation relationships are discussed. The fifth chapter presents the results of axial soil resistance tests. This chapter covers DI pipe frictional resistance, as well as the load drop across the joints and its relationship with the direction of movement. Fault rupture tests on nominal 6-in. (150-mm) DI pipelines with restrained axial slip joints are described in Chapter 6. Joint extension and rotation, as well as pipe forces and moments, during fault rupture tests are reported and compared to the test results in previous chapters. The seventh chapter presents analytical models that evaluates load drop across enlarged joints under axial displacement through soil, as well as axial load distributions for DI pipelines in the fault rupture tests. The last chapter summarizes key features of the investigation, and recommends future directions for research.

CHAPTER 2

TENSILE COUPON TESTS

2.1 Introduction

This chapter describes the uniaxial tension testing that was performed to determine key material properties of ductile iron (DI) pipe used in water distribution systems, including restrained axial slip pipelines. Ductile iron pipes are manufactured in the U.S. to meet standards, such as ANSI/AWWA C151/A21.51-17 (AWWA, 2017) [60 ksi (420 MPa) ultimate tensile strength, 42 ksi (290 MPa) yield, and 10% elongation]. In Japan, DI pipes are manufactured to meet standards, such as JWWA G113, 114-2010 (JWWA, 2010) [60 ksi (420 MPa) ultimate tensile strength and 10% elongation]. There is no minimum yield strength requirement in the Japanese standard. Although the standards set minimum stress and tensile strain requirements, testing is required to determine explicit stress vs strain characteristics for limit state thresholds and numerical modeling. Testing also provides data to evaluate the variability of properties in commercially available pipe and thus understand how this variability affects analytical modeling and design.

The test results reported herein represent pipe from several manufacturers, including AMERICAN, Kubota, McWane, and US Pipe. The testing was performed to obtain stress vs strain data for elastic and plastic characterization of DI pipe in numerical models and to determine the proportional limit, yield stress, ultimate tensile strength, and elongation at failure.

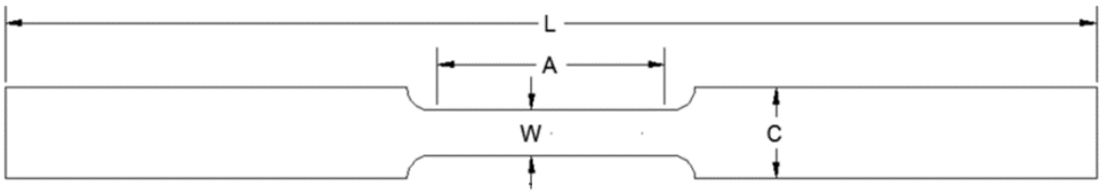

Figure 2.1. Schematic of Tensile Coupon Specimen

Table 2.1. Dimensions of Tensile Coupon Specimen

Dimensions	Length (in.)
W – Width	0.50
R – Radius	0.50
L – Overall Length	8.00
A – Length of Reduced Section	2.25
C – Width of Grip Section	1.00

2.2 Tensile Coupon Testing and Procedure

The tensile coupons were machined from DI pipes to obtain the nominal dimensions shown in Figure 2.1 and Table 2.1, and tested according to ASTM-E8 2016 (ASTM, 2013). A Baldwin Hamilton 60 BTE Universal Testing Machine, fitted with a pressure sensor, was used to apply and measure tensile loads. Axial and transverse strain gages were instrumented at the center of the reduced area of the specimens. Strain gages were used for smaller strains, typically less than 2%, because they are considerably more accurate at these levels. Because strain gages generally de-bond at strains between 0.6 and 5.8%, a laser extensometer was used to measure larger axial strain to material failure. A typical test setup is shown in Figure 2.2, in which a tensile test specimen is held by the grips of the Baldwin testing device.

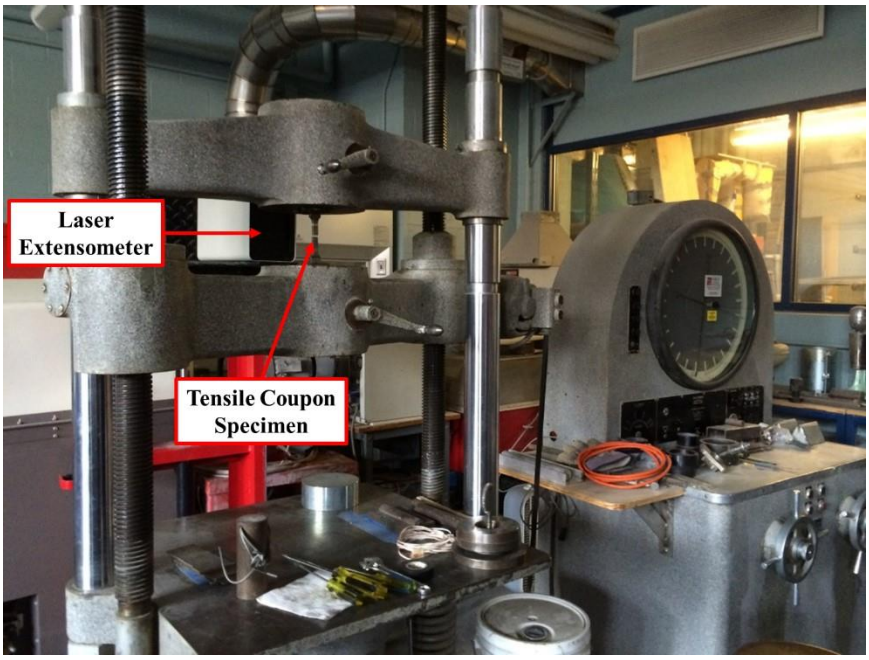

a) Baldwin Testing Apparatus

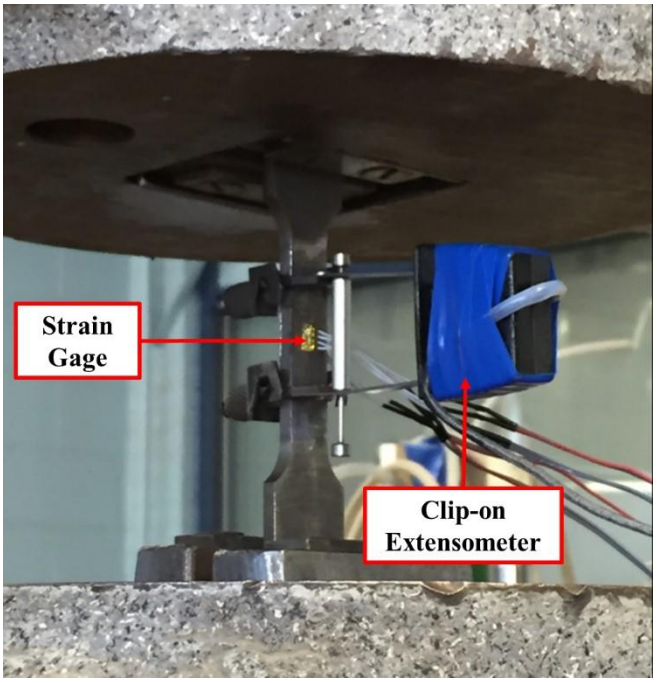

b) Tensile Coupon Specimen

Figure 2.2. Tensile Coupon Test Setup

2.3 Stress vs. Strain Relationships

The stress, referred as engineering stress, was computed by dividing the measured force by the original cross-sectional area of the specimen. The strain was measured from strain gages as discussed in Section 2.2. The uniaxial stress vs. axial strain plots for all specimens are shown in Figure 2.3 and Figure 2.4.

Figure 2.5 presents plots of the transverse vs axial strain in the elastic range for all specimens tested. The slope of each plot provides the average Poisson's ratio for the test specimen. Poisson's ratio, ν, is the negative ratio of transverse strain to axial strain for uniaxial loading. Poisson's ratio was measured in a very narrow range of 0.27 – 0.29, which agrees well with other reported values of Poisson's ration for ductile iron (Ductile Iron Group, 1990).

2.4 Young's Modulus, Yield Strength, and Proportional Limit

Young's modulus was determined by performing a linear regression for the stress vs. strain curve in the elastic region. The yield strength, σ_y, was computed using the offset method, in which a line parallel to the linear part of the stress vs. strain plot is projected from 0.2% strain (ASTM, 2013). The intersection of this line and the stress vs. strain curve provides an estimate of the yield stress for each specimen. The proportional limit is the stress at the end of the range where stress is proportional to strain. Beyond the proportional limit, the relationship between stress and strain becomes increasingly nonlinear.

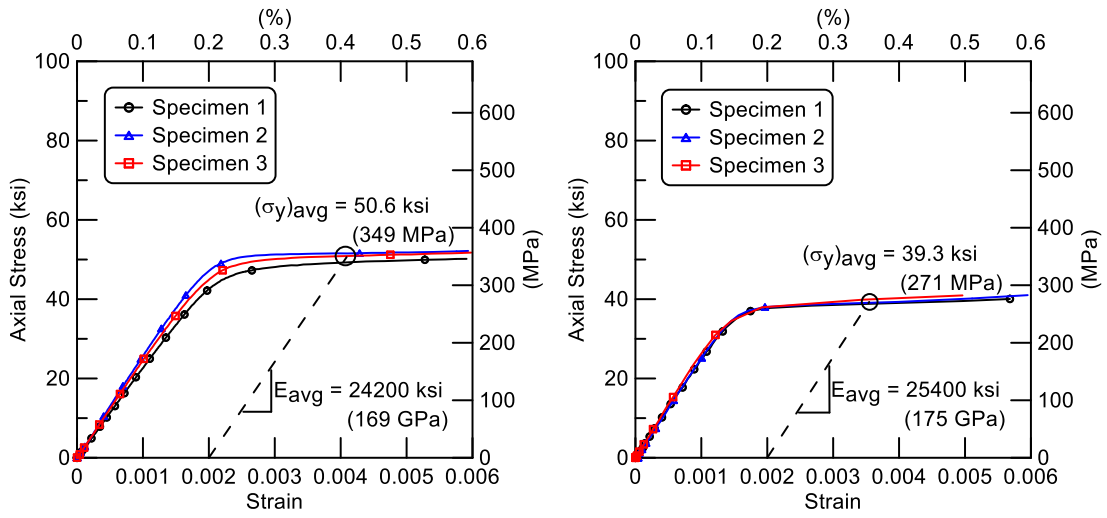

a) AMERICAN

b) Kubota

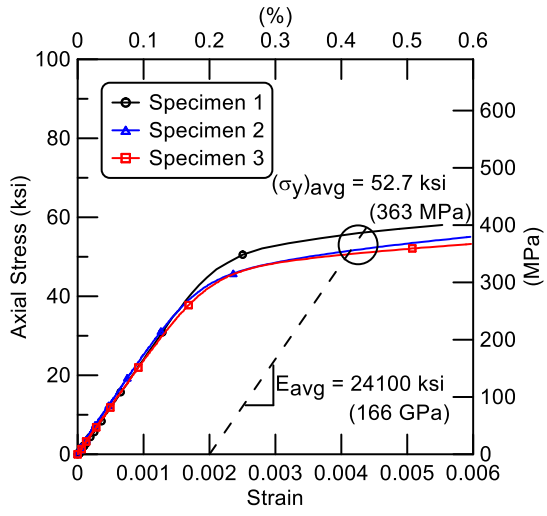

c) McWane

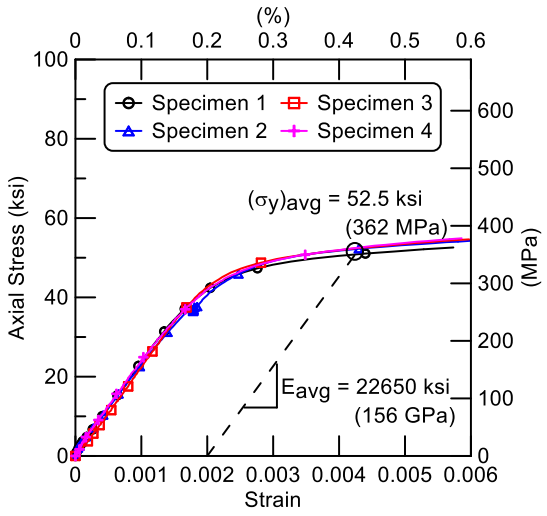

d) US Pipe

Figure 2.3. Stress vs. Strain Relationships at Maximum Stain of 0.6%

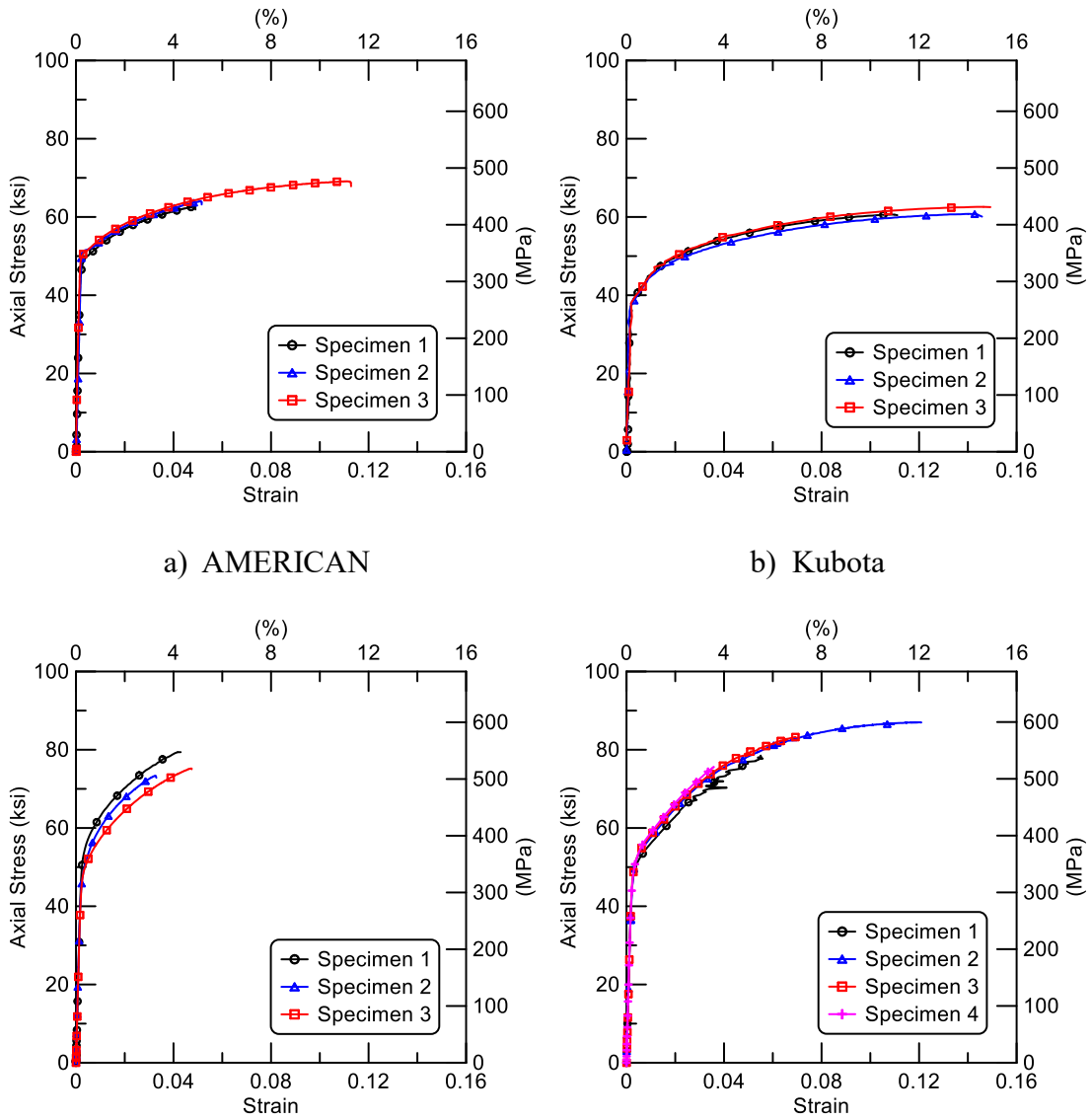

a) AMERICAN

b) Kubota

c) McWane

d) US Pipe

Figure 2.4. Stress vs. Strain Relationships to Failure

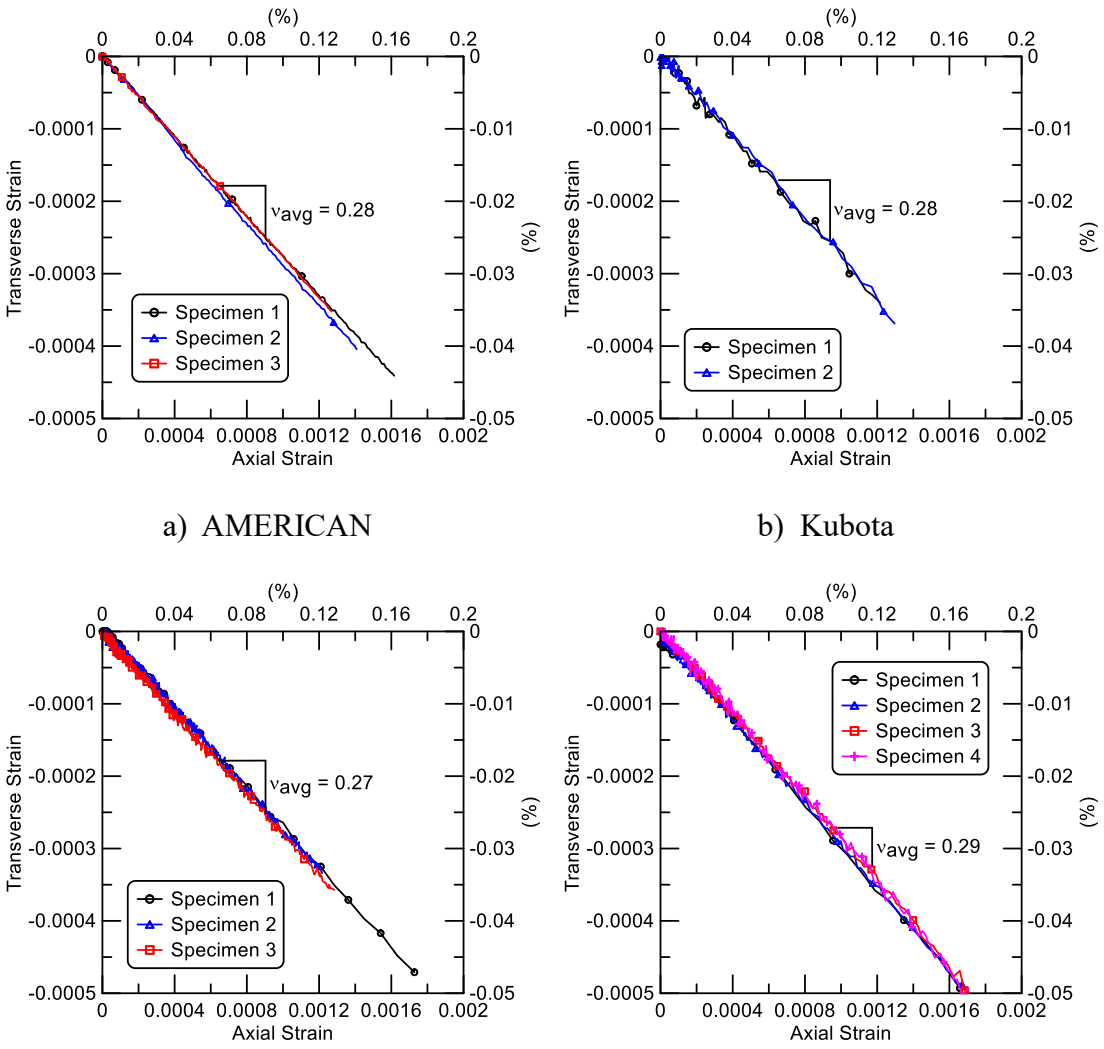

Figure 2.5. Transverse vs. Axial Strain in Elastic Range and Poisson's Ratio

Table 2.2. Summary of Average Young's Modulus, Proportional Limit Stress, and Yield Stress for DI Specimens

Specimen	Young's Modulus, E (ksi)	Proportional Limit Stress, σ_{prop} (ksi)	Yield Stress, σ_y (ksi)	σ_{prop}/σ_y Ratio
AMERICAN	24,200	34.1	50.6	0.67
Kubota	25,400	26.9	39.3	0.68
McWane	24,100	32.8	52.7	0.62
US Pipe Restrained Axial Slip Joint [a]	22,700	32.3	52.5	0.61
US Pipe Push-on Joint [b]	27,000	21.0	45.1	0.47

1 ksi = 6.89 MPa
[a] Prototype of restrained axial slip joint specimen
[b] Commercially available push-on joint (Wham et al., 2017)

Table 2.3. Summary of Average Ultimate Strength, Ultimate Strain, and Poisson's Ratio for DI Specimens

Specimen	Ultimate Stress, σ_{ult} (ksi)	Ultimate Strain, ε_{ult} (%)	Poisson's Ratio, ν
AMERICAN	65.3	7.4	0.28
Kubota	61.3	13.5	0.28
McWane	76.0	4.1	0.27
US Pipe Restrained Axial Slip Joint [a]	81.1	7.1	0.29
US Pipe Push-on Joint [b]	66.7	10.4 [c]	N/A

1 ksi = 6.89 MPa
[a] Prototype of restrained axial slip joint specimen
[b] Commercially available push-on joint (Wham et al., 2017)
[c] Based on one test result

Table 2.2 summarizes the average Young's modulus, yield strength, and proportional limit stress derived from tensile coupon tests for each of the DI pipe with restrained axial slip joint. The proportional limit stress represents the elastic limit for ductile iron. It should be noted that the strains at yield are more than double those at the proportional limit for all DI specimens. The ratio of proportional limit to yield stress, σ_{prop}/σ_y, is also shown in Table 2.2. σ_{prop}/σ_y ratios for restrained axial slip joints range from 0.61 to 0.68. These values agree with the σ_{prop}/σ_y ratio for steel pipes of 0.60 as reported by Mason (2006).

Also included in Table 2.2 are the average Young's modulus, yield strength, and proportional limit stress derived from tensile coupons that were machined from commercially available DI pipe manufactured by US Pipe (Wham et al., 2017). The Young's modulus for the push-on joints is higher than the modulus measured for the other pipe specimens, but the yield stress for the push-on joints is generally lower than that of the other DI pipes manufactured in the U.S. The σ_{prop}/σ_y ratio for the push-on joints is also significantly lower than that of the other DI pipes.

2.5 Ultimate Strength and Strain, and Poisson's Ratio

Ultimate strength, σ_{ult}, and strain, ε_{ult}, are defined as the maximum stress and strain measured during tensile coupon testing, respectively. Table 2.3 summarizes the average ultimate strength, ultimate strain and Poisson's ratio derived from tensile coupon tests for the DI pipes with restrained axial slip and push-on joints.

2.6 Summary

This chapter summarizes material properties obtained from tensile coupons representing the ductile iron in most DI pipelines commercially available in the U.S. Young's modulus of all four DI pipes range from 21,800 ksi (150 GPa) to 26,700 ksi (184 GPa) with a mean value of 24,000 ksi (165 GPa) and standard deviation of 1,400 ksi (9.65 GPa). The proportional limit stresses vary between 26.0 ksi (179 MPa) and 35.9 ksi (248MPa), and are more narrowly grouped between 30.0 ksi (207 MPa) and 35.9 ksi (248 MPa) for pipe manufactured in the U.S. The mean proportional limit and yield strengths for U.S. manufactured DI pipe, representing 10 tests, are 33.0 ksi (228 MPa) and 52.0 ksi (359 MPa), respectively, with standard deviations of 2.3 ksi (19 MPa) and 1.8 ksi (12 MPa), respectively. In contrast, the mean of the proportional limit and yield strengths for pipe manufactured according to JWWA standards, representing 3 tests, are 26.9 ksi (185 MPa) and 39.3 ksi (271 MPa), respectively, with standard deviations of 0.9 ksi (6 MPa) and 0.6 ksi (4 MPa), respectively. The ratio of proportional limit to yield strength, $\sigma_{prop}/\sigma_{y,}$ varies from 0.61 to 0.68.

The ultimate strengths of all DI specimens exceeded the ANSI/AWWA and JWWA standards of 60 ksi (420 MPa). The yield strengths of all U.S. manufactured ductile iron exceeded the ANSI/AWWA standard, whereas the yield strength of Japanese manufactured pipe specimens was slightly below this value. There was a wide range in ultimate strain between 4.1% and 13.5%, with only the Japanese manufactured pipe specimens exceeding the standard for 10% elongation.

CHAPTER 3

DIRECT COMPRESSION AND TENSION TESTS

3.1 Introduction

As explained in Chapter 1 detailed data and information in the general literature are scarce with respect to the compressive capacity of DI push-on and restrained joints. This situation also applies to the tensile capacity of restrained DI joints. Maragakis et al. (1990) and Meis et al. (2001, 2003) provide test data on the compressive and tensile capacity of DI joints, but the test results are for low internal water pressure of 3 - 4 psi (21 to 28 kPa) that is well below the operating pressure of water distribution pipelines. The testing did not include tensile stress vs strain data to characterize the strength and modulus of the DI pipe.

This chapter provides detailed information about direct compression and tension tests on nominal 6-in. (150-mm) diameter restrained axial slip DI pipe joints. All tests were performed on DI joints at water pressures of 75 to 85 psi (520 to 590 kPa). A description of the general set up used for all tests is provided, and the key mechanical characteristics of each joint type are described. The test results are plotted as force vs axial joint displacement, and interpreted for compression relative to the yield and proportional limit loads of the pipe barrel.

3.2 Joint Characteristics

Restrained axial slip joints are described in Chapter 1. They are available as a single bell and spigot assembly or a series of pipe, spigot, and bell components. The Kubota and US Pipe joints involve an enlarged bell that allows for axial movement of the spigot until either the spigot makes contact with the back of the bell in compression or meets resistance against pullout through spigot engagement with either a locking ring or locking segments. The AMERICAN and McWane joints involve a series of pipe and bell components that allow for axial displacement until either the end of a spigot component makes contact with the back of a bell in compression or resists pullout through spigot engagement with either a locking ring or locking segments. Resistance to compression and tension occurs due to compressive contact and restraint against pullout, respectively, among several bell-and-spigot components.

3.2.1 Locking Segments

Locking segments are used with McWane and US Pipe joints. A restrained 6-in. (150-mm) diameter joint has a weld bead on the spigot end and employs two locking segments to resist pullout under tension. As shown in Figure 3.1, with respect a US Pipe restrained axial joint, there is a separation between the gasket haunch and locking segment. If the restrained axial joint is set at a position midway between them, the joint can accommodate 1.2 in. (30 mm) of axial displacement for both tension and compression before weld bead contact with the gasket haunch or locking segment.

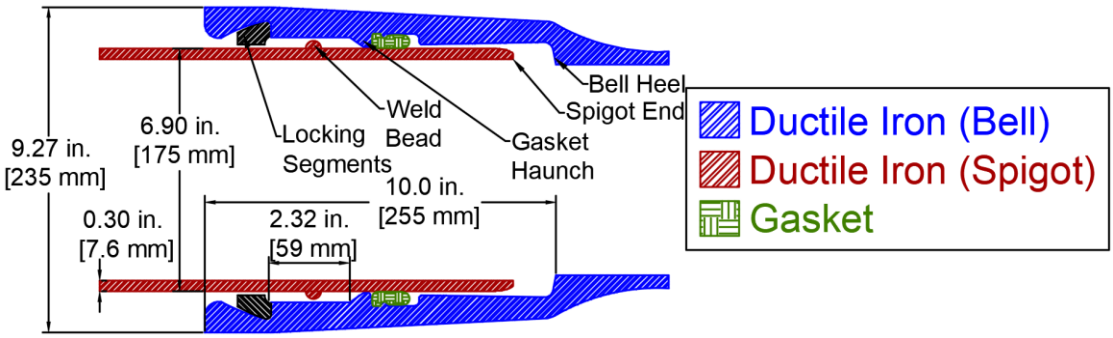

Figure 3.1. Cross-Sectional View of US Pipe Restrained Axial Slip DI Pipe Joint

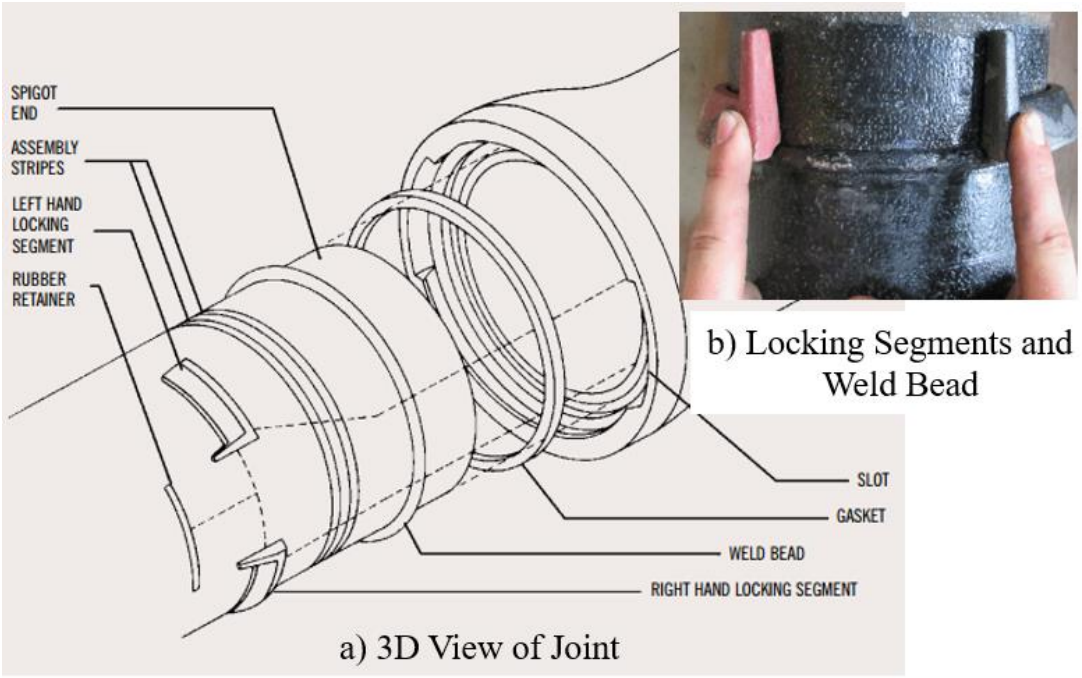

Figure 3.2. 3D View of Axial Joint Restraint with Locking Segments

The three dimensional (3D) view in Figure 3.2 shows that locking segments are typically inserted into slots in the bell and rotated into the 3 and 9 o'clock positions around the pipe circumference. Under full pullout the weld bead on the spigot makes

contact with the two locking segments, which provide resistance to further axial slip. Figure 3.2 b) is a photo, looking down, of the locking segments in contact with the weld bead at their approximate circumferential positions in a typical field installation.

3.2.2 Locking Ring

Locking rings are employed with AMERICAN and Kubota joints. Figure 3.3 shows the cross-section of a 6-in. (150-mm) AMERICAN restrained axial joint. The length of the socket, or bell, of the center EJS deep socket is 15.28 in. (388 mm). The spigot of the adjoining pipe is inserted into the deep bell so that the weld ring is located between the gasket haunch and locking ring. The available distance between the gasket haunch and locking ring for axial slip in the deep socket is 5.48 in. (139 mm). Figure 3.4 shows that after the spigot is inserted into the deep socket past the gasket, a split locking ring is installed into the socket locking groove. During installation the locking ring springs open from a contracted position to fit tightly in the locking groove. Under full pullout the weld ring on the spigot makes contact with the locking ring, which provides resistance to further axial slip.

3.3 Instrumentation and Test Procedures

A detailed description of the direct compression and tension tests performed on the commercially available restrained axial slip DI pipe joints covered in this work is provided in reports by Pariya-Ekkasut et al. (2015, 2016, 2017, 2018) and Stewart et al. (2015). Only the salient features of the tests are addressed herein.

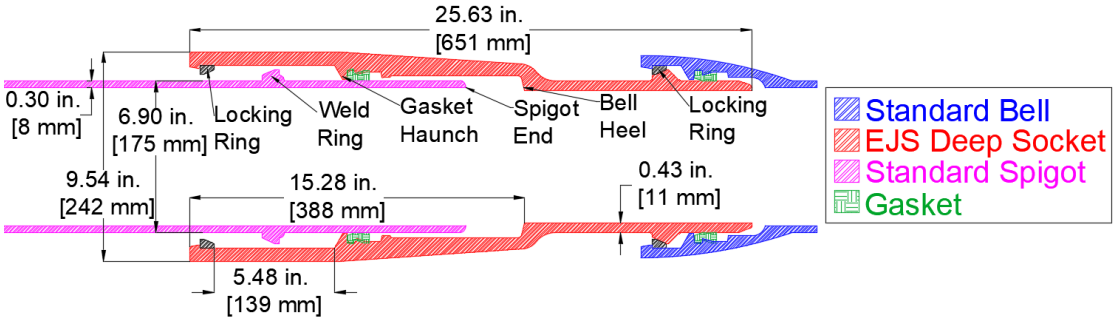

Figure 3.3. Cross-Sectional View of AMERICAN Restrained Axial Slip DI Pipe Joint

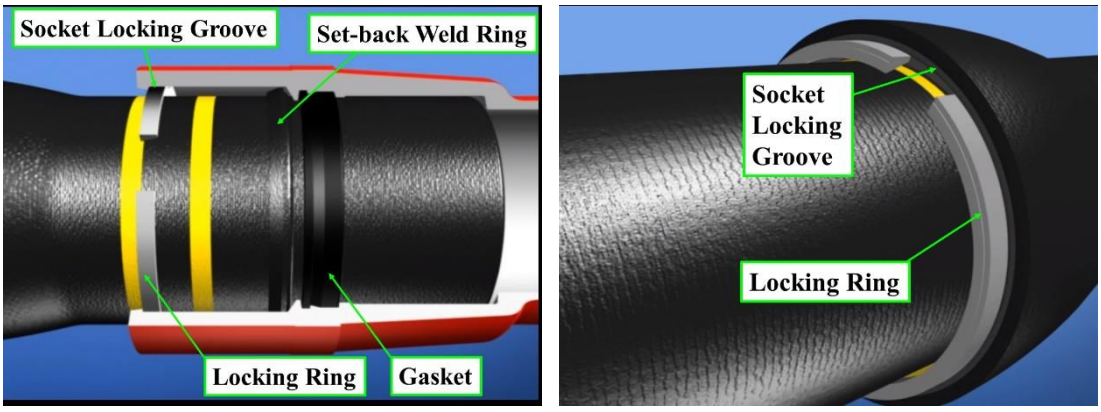

a) Cut-away View b) 3D View

Figure 3.4. Axial Joint Restraint with Locking Ring

A loading frame designed specifically for large-scale direct compression and tension tests was used. Figure 3.5 a) is a photo of the loading frame. An actuator and load cell were installed on the load frame to apply and measure axial force at the spigot end. The maximum axial capacity of the actuator is 400 kips (1,800 kN). An electronic pressure transducer, located at the end cap, measured internal water pressure during the test.

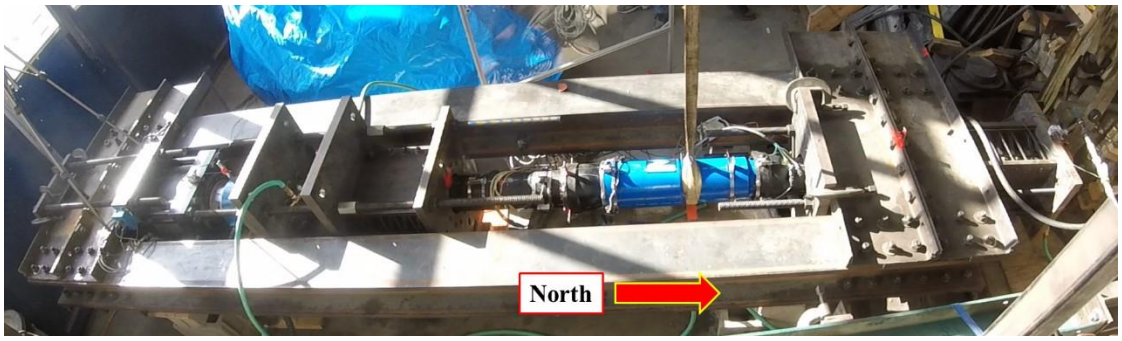

a) Photo

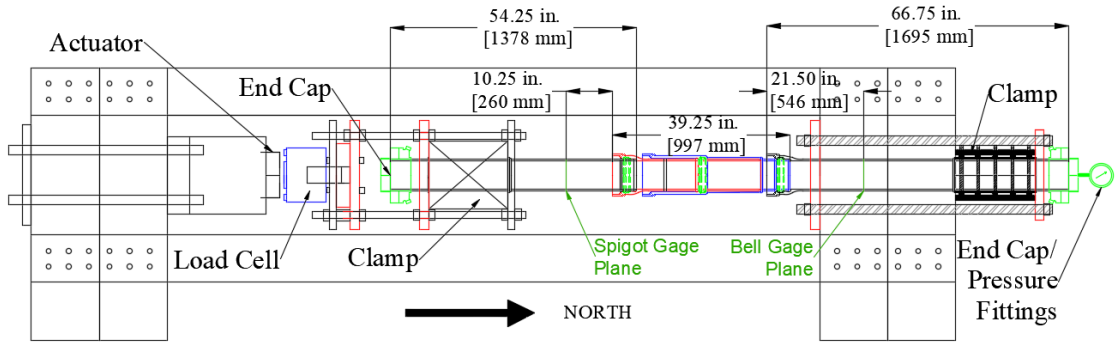

b) Schematic of Instrumentation for Direct Compression Test

Figure 3.5. General Compression Test Setup

To support the self-weight of the pipe, the bell either was supported on a steel roller or by a strap attached to an overhead crane, and the spigot was supported on a wheeled wooden dolly. The pipe lengths in these experiments ranged from 13 to 15 ft (4.0 to 4.6 m). A schematic of the instrumentation used in the McWane restrained axial slip joint compression test is presented in Figure 3.5 b), and used to describe the typical test setup and instrumentation of all the tests. Strain gages were mounted generally between 21 in. (0.53 m) and 40 in. (1.0 m) north of the bell face on the bell side of the pipe at the positions of 12, 3, 6, and 9 o´clock (crown, east, invert, and west,

respectively). Each location had a pair of axial and circumferential gages. Eight other gages (axial and circumferential pairs) were mounted approximately 10 in. (0.3 m) to 51 in. (1.3 m) south of the bell face on the spigot side at the same positions around the pipe. Four string potentiometers (pots) were installed near the bell face to measure the displacement of each joint. The stroke of the string pots varied from 10 in. (250 mm) to 20 in. (500 mm), depending on the expected displacement of the joint.

After the specimen was instrumented and centered in the test frame, the test was initiated by starting the data acquisition system and laboratory hydraulic systems. The pipe was then filled with water and pressurized to approximately 80 psi (550 kPa). The internal water pressure applied axial forces on the end caps and to expand the joint components to their fully extended positions. The water pressure line remained open to maintain a nearly constant pressure during the test. Axial displacement was applied to the pipe with the servo-hydraulic actuator under displacement control at a rate of 1 in. (25.4 mm) per minute until pipe failure. Failure is defined as the inability for the pipe to maintain 80 psi (550 kPa) of internal water pressure or observation of significant buckling at the joint.

3.4 Compression Tests

Compression test results for 6-in. (150-mm) restrained axial slip DI pipe joints are summarized under the subheadings that follow.

3.4.1 AMERICAN

The joints were initially installed at the fully-extended position. Figure 3.6 shows the relationship between force vs. total joint displacement. Also shown in Figure 3.6 are the proportional limit force, P_{prop}, of 212 kips (943 kN) and yield force, $P_{y,}$ of 315 kips (1,400 kN), which are the products of the respective proportional limit and yield stresses of 34.1 ksi (235 MPa) and 50.6 ksi (349 MPa) and the pipe cross-sectional area of 6.22 in.^{2} (40.1 cm^2). When the joint was fully engaged at 5.3 in. (135 mm) of displacement, there was a significant increase of compressive load. When the compressive force in the specimen exceeded the proportional limit and reached a maximum of 256 kips (1,140 kN) at a corresponding displacement of 5.9 in. (150 mm), irrecoverable deformation in the joint occurred, resulting in leakage of about 10 gal/min (38 l/min).

3.4.2 McWane

The joints were installed at the fully-inserted position at the beginning of the test. Internal water pressure caused the joints to open approximately 0.2 in. (50 mm). Figure 3.7 shows the compressive force vs. total joint displacement. The compressive force also caused rotation at the B joint (see Figure 1.3). Joint rotation was related in part to the orientation of the weld bead, which did not line up for an evenly distributed contact with the gasket haunch during compression. At a total joint closure of 0.66 in. (16.7 mm), the pipe compressive force was 210 kips (934 kN), which is close to the

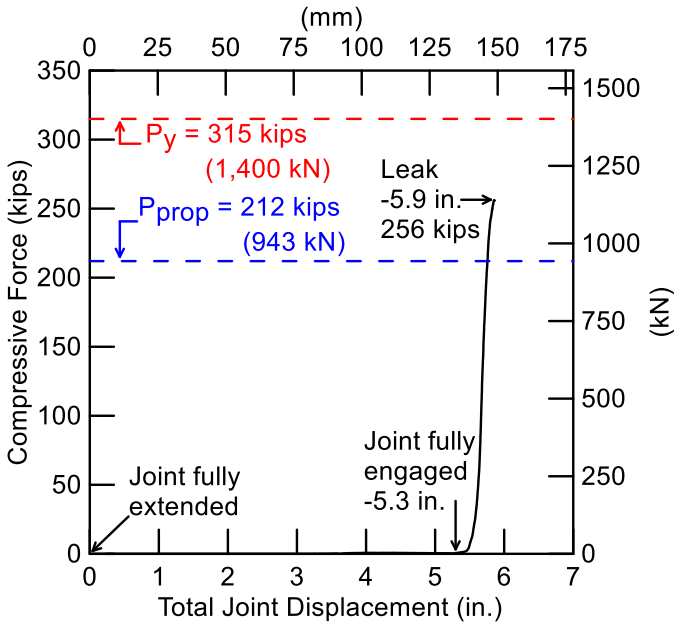

Figure 3.6. AMERICAN Compressive Force vs. Joint Closure

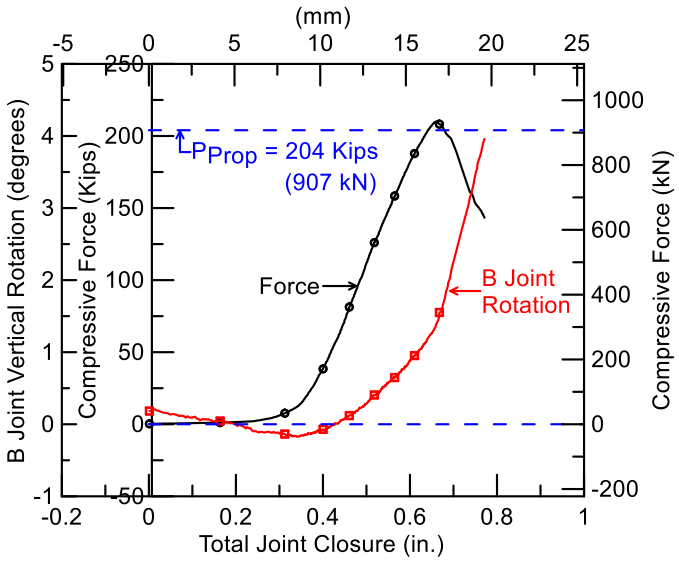

Figure 3.7. McWane Compressive Force and Lateral Joint Rotation vs. Joint Closure

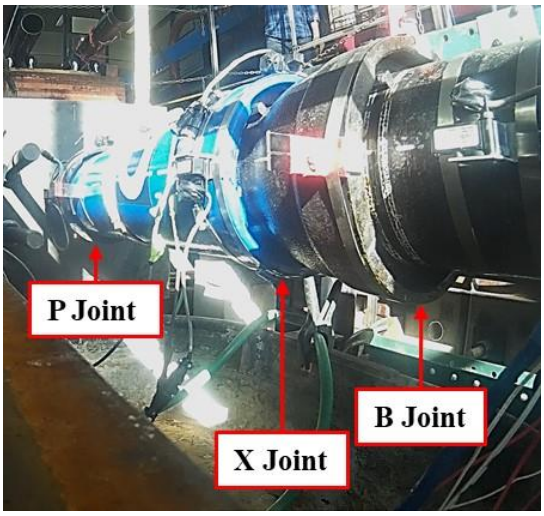

a) Side View Before Test

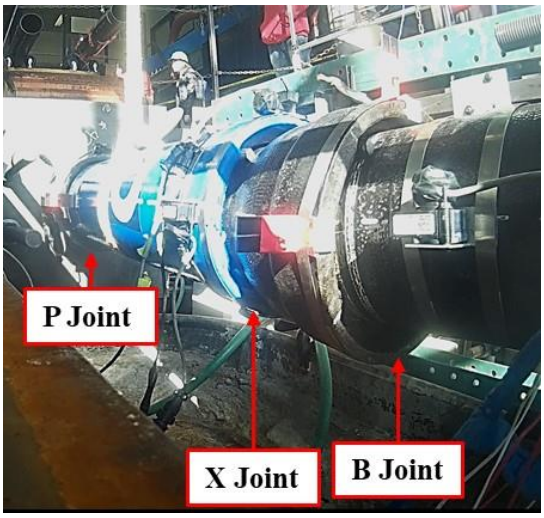

b) Side View After Test

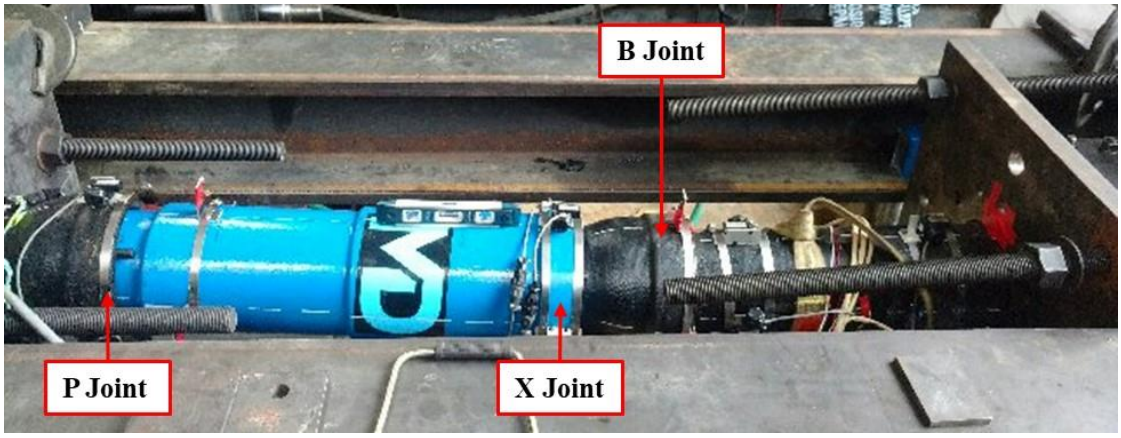

c) Overall View After Test

Figure 3.8. McWane Vertical Joint Rotation after Compression Test

proportional limit force of 204 kips (907 kN). After this maximum compressive force was achieved, the load dropped, and vertical rotation of the B joint increased rapidly. Downward movement at the B joint caused the vertical support for the pipe to deform at a total joint closure of 0.77 in. (19.6 mm) and actuator force of 143 kips (636 kN). At this point, the joint sustained significant rotation, and could not be returned to its original

alignment as illustrated in Figure 3.8. Although the rotation was severe, no leakage was observed in this test.

3.4.3 US Pipe

The joint was installed so that the weld bead was located partway between the gasket haunch and locking segments (see Figure 1.4 and Figure 3.1) to allow about 1.0 in. (25 mm) of axial movement before the weld bead contacted with the gasket haunch. Figure 3.9 shows the force and joint rotation vs. joint closure. At 1.0 in. (25 mm) of joint closure, the joint was fully seated, and the compressive force increased rapidly. Also shown in Figure 3.9 is the proportional limit force of 201 kips (894 kN). When the specimen reached the proportional limit force at a joint closure of 1.1 in. (28 mm), irrecoverable deformation occurred such that the joint rotated significantly in the lateral direction as shown in Figure 3.10. Although the test was terminated due to severe rotation, no leakage was observed.

3.5 Tension Tests

This section presents tension test results for restrained axial slip DI pipe joints. Seven tension tests were performed on 6-in. (150-mm) diameter joint specimens. One additional tension test was conducted on a 12-in. (300-mm) US Pipe restrained axial slip DI pipe joint. All tension test specimens were installed with the spigot fully inserted into the bell at the beginning of the tests.

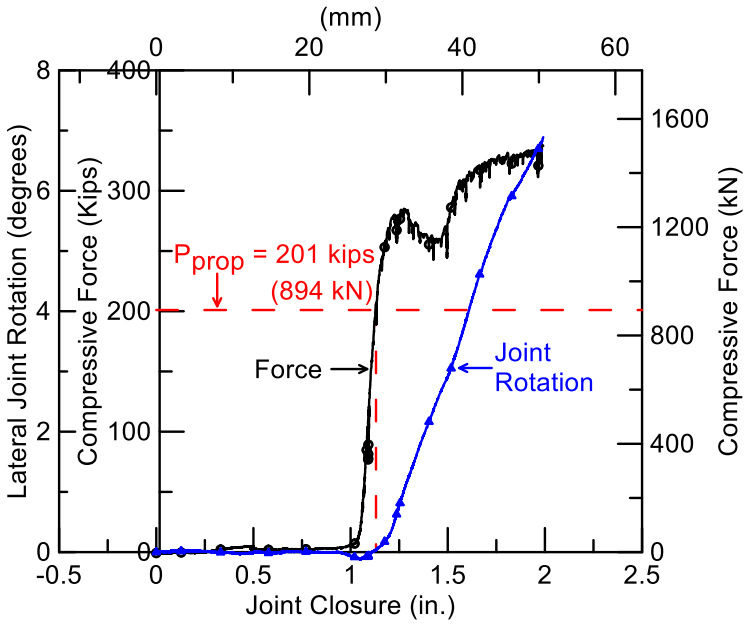

Figure 3.9. US Pipe Compressive Force and Lateral Joint Rotation vs. Joint Closure

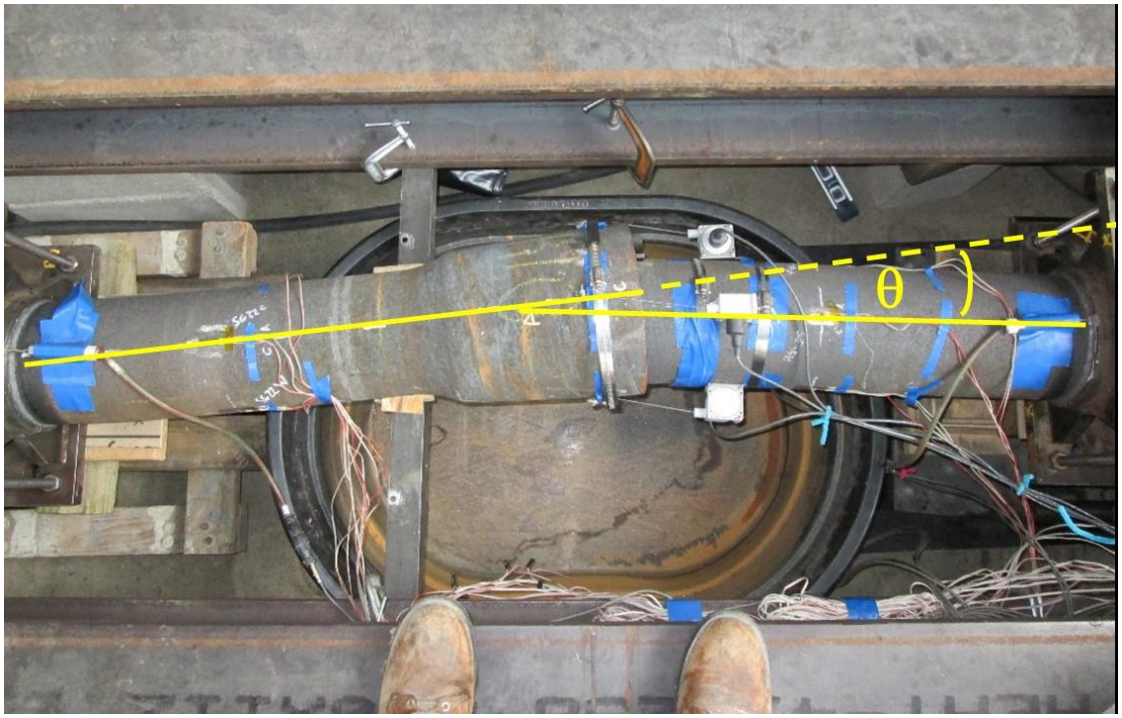

Figure 3.10. US Pipe Lateral Joint Rotation after Compression Test

3.5.1 6-in. (150-mm) Specimens

3.5.1.1 AMERICAN

Figure 3.11 presents two tensile force vs. displacement plots for AMERICAN restrained axial slip DI pipe joints. Initially, the joints were extended to 5.3 in. (135 mm) under pressurization to 80 psi (550 kPa). For each test the spigot was then pulled to bear against the locking ring and bell lip. The load increased rapidly with very little additional joint opening. In both tests the FR bell (see Figure 1.1) cracked circumferentially resulting in loss of pressure. Before failure the Tests 1 and 2 reached respective peak loads of 155 kips (689 kN) and 144 kips (641 kN) at the same joint displacement of 5.5 in. (140 mm). A photo of bell fracture in the tension test is shown in Figure 3.12.

3.5.1.2 Kubota

One tension test was conducted on the Kubota restrained axial slip DI pipe joint. Figure 3.13 shows the tensile force plotted against joint opening. The joint was extended to 4.5 in. (115 mm) so there was spigot projection/locking ring contact under internal water pressure of 30 psi (210 kPa). The pressure was then raised to 80 psi (550 kPa) before an application of axial movement by the actuator. The load increased rapidly with very little additional joint opening. A peak load of 115 kips (516 kN) was attained at 4.5 in. (115 mm) of joint opening. Immediately after the maximum load had been achieved, the spigot projection was sheared off, causing the spigot to slip suddenly from the bell, resulting in loss of pressure.

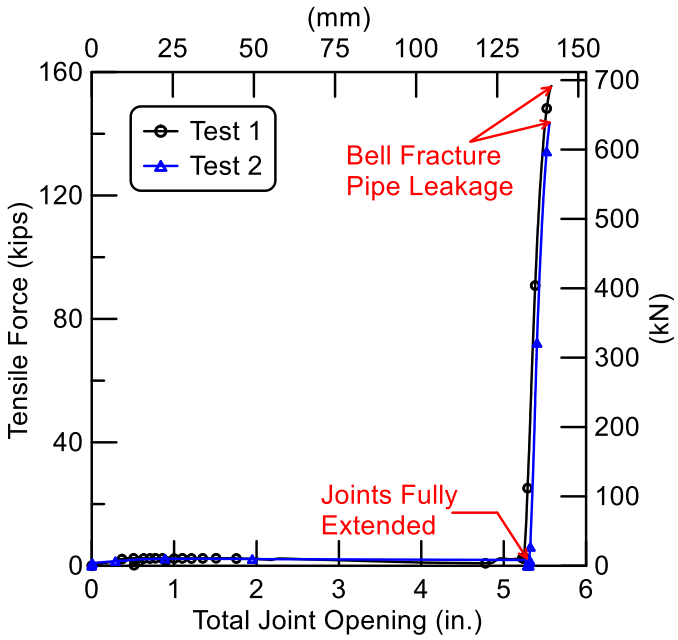

Figure 3.11. AMERICAN Tensile Force vs. Displacement Relationships

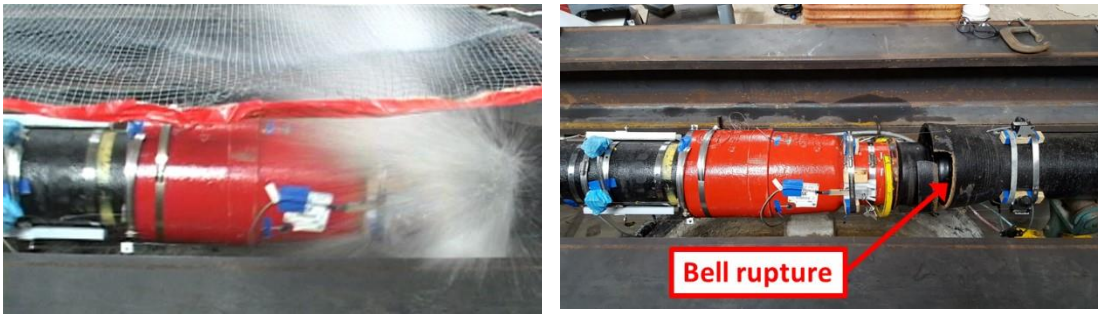

a) During Test

b) After Test

Figure 3.12. Bell Fracture in AMERICAN Tension Test Specimen

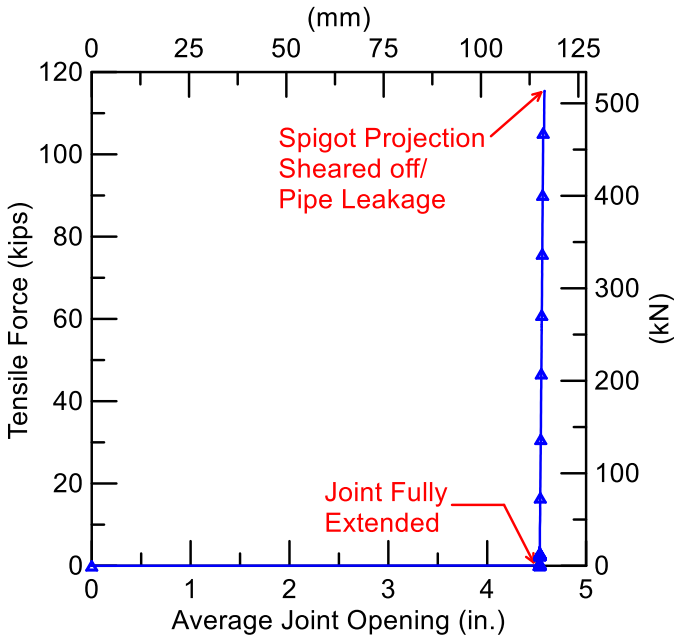

Figure 3.13. Kubota Tensile Force vs. Displacement Relationship

3.5.1.3 McWane

Two tension tests were performed on McWane restrained axial slip DI pipe joint systems. The locking segments were located at the east and west springlines. The tensile force vs. total joint displacement relationships of the two tension tests are provided in Figure 3.14. Internal water pressure of approximately 20 psi (140 kPa) was applied to open the SFC joints so that there was contact between the weld bead and locking segments at 10.8 in. (274 mm) and 11.1 in. (282 mm) of axial movement for Tests 1 and 2, respectively. The pressure was then raised to 80 psi (550 kPa) before an application of axial movement by the actuator. Test 1 reached the maximum tensile force of 70.7 kips (314 kN) at 11.9 in. (302 mm) of total joint opening. The peak load

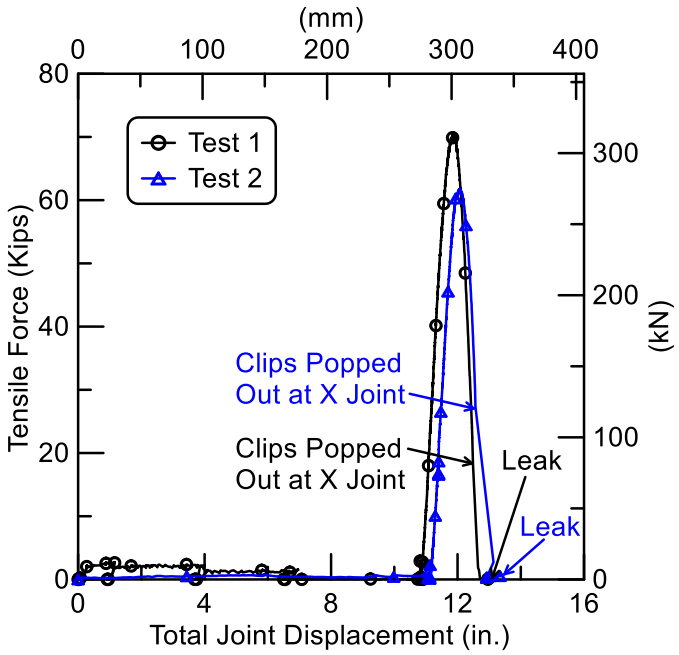

Figure 3.14. McWane Tensile Force vs. Displacement Relationships

of 61.8 kips (275 kN) was measured at a corresponding total joint displacement of 12.1 in. (307 mm) in Test 2. After the maximum loads had been achieved, the loads in both tests declined substantially because load concentration caused by the locking segments at the springline of the pipe deform the spigot inward from a circular to an oval shape. This inward deformation at the springline allowed the locking segments to slide past the weld bead so that the spigot pulled from the bell. Similar deformation was observed during the US Pipe tension test. A detailed description of spigot ovaling of the US Pipe joint is provided in Section 3.5.1.4.

The McWane locking segments slipped from the X joints (see Figure 1.3) in both tests at 12.5 in. (318 mm) of total joint displacement, but the pipes were still able to

a) Joint Fully Inserted

b) Joint Fully Extended and Locking Segments Rotated Inward

c) Locking Segments Popped out

d) Pipe Leaked

Figure 3.15. Photos of Successive Axial Displacement for a Tension Test of the McWane Joint

maintain full water pressure. Both SFC specimens were able to carry additional displacement until significant leakage of approximately 10 gal/min (38 l/min) was observed at the X joint at 13.0 in. (330 mm) and 13.4 in. (340 mm) of displacement in Tests 1 and 2, respectively. The progressive movements of the joint and locking segments are provided in Figure 3.15.

3.5.1.4 US Pipe

Two tension tests were performed on the US Pipe restrained axial slip DI pipe joints. The locking segments were located at the east and west springlines in both tests. Figure 3.16 presents tensile force vs. joint displacement relationships of the two tension tests. Internal water pressure of 31 psi (214 kPa) fully extended the joints in both tests to 2.3 in. (58 mm) of displacement. The pressure was then raised to 80 psi (550 kPa) in preparation for axial loading. Tests 1 and 2 reached a maximum force of 83 kips (369 kN) at 2.8 in. (71 mm) of joint displacement and a maximum axial load of 78 kips (347 kN) at 2.7 in. (69 mm) of displacement, respectively. After the maximum load had been achieved, load concentration at the east and west springlines caused the spigot to deform from a circular to an oval shape. This inward deformation at the locking segment locations allowed the weld bead to slip past the locking segments, causing leakage at 3.3 in. (84 mm) and 3.6 in. (91 mm) of joint displacement, for Tests 1 and 2, respectively.

The locking segment movement is shown in Figure 3.17. Once the joint was fully extended, weld bead on the spigot engaged the locking segments. The locking segments made contact with the bell lip, began rotating, and deformed the spigot inward a sufficient distance to allow the weld bead to slip past the locking segments. The deformed area of the spigot at the locking segment locations is shown in Figure 3.18.

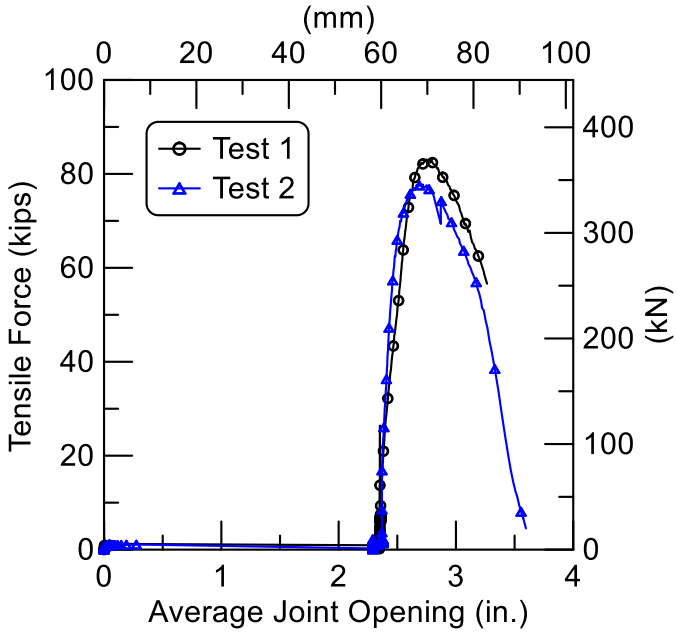

Figure 3.16. US Pipe Tensile Force vs. Displacement Relationships

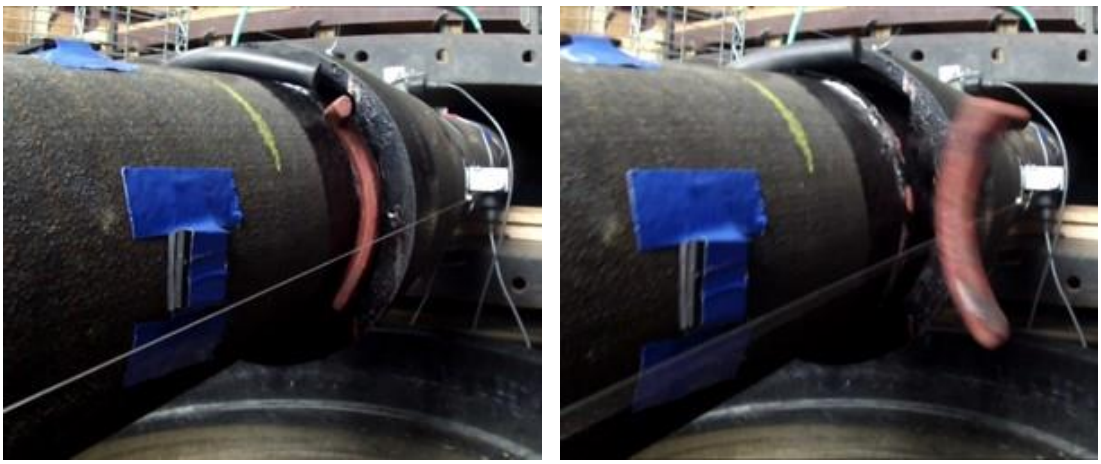

a) Outward Movement and Rotation of Locking Segment

b) Full Locking Segment Displacement and Joint Pull Out

Figure 3.17. US Pipe Locking Segment Movement

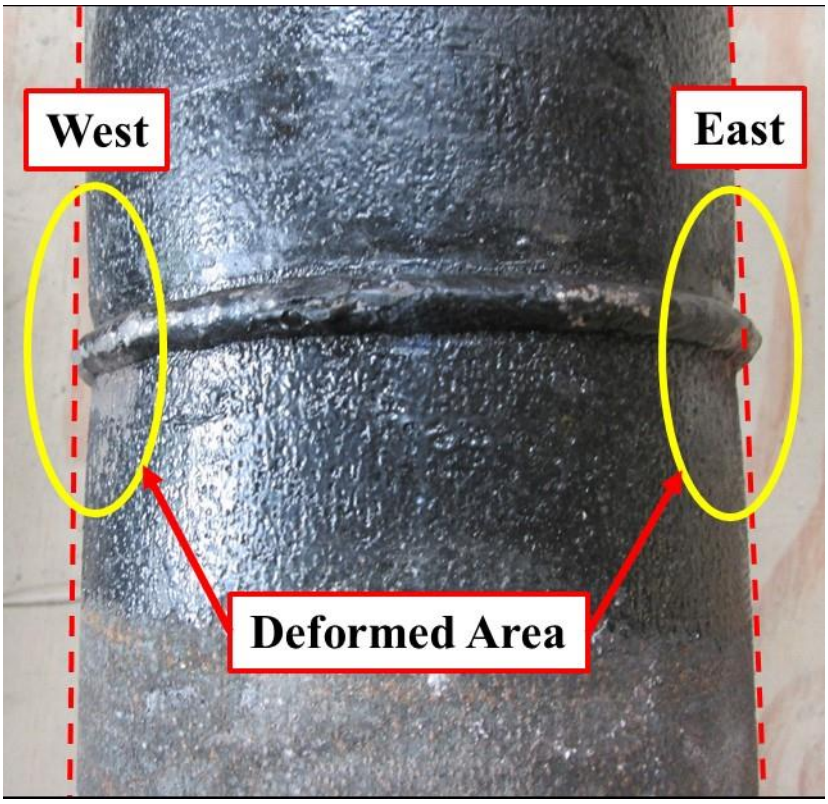

Figure 3.18. Deformed Area of Spigot Caused by Load Transferred from Locking Segments

The outer diameter of the spigot was measured before the tension test. The diameter of the spigot was measured at 4 different locations: Crown to Invert (C to I), Crown East to Invert West (CE to IW), East to West (E to W) and Invert East to Crown West (IE to CW) as shown in Figure 3.19. The measurements showed that initially the spigot had a circular cross-section with a 6.9-in. (175-mm) diameter.

Post-test spigot diameter measurements were taken at 5 different locations along the length of the spigot: at the spigot end, 2 in. (51 mm), 5 in. (127 mm) (close to weld bead locations), and 6 in. (152 mm) (locking segment bearing areas). The measurements

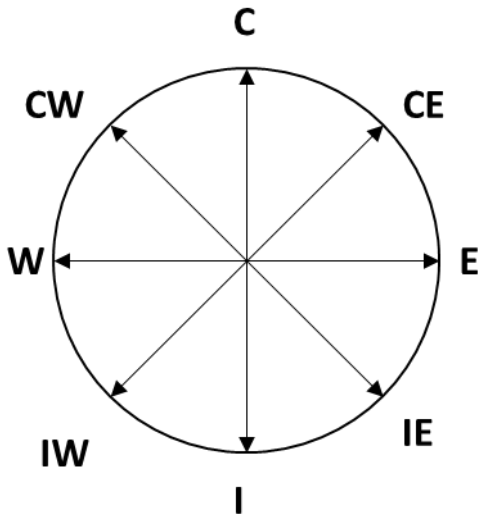

Figure 3.19. Spigot Measurement Locations

Table 3.1. Diameter Measurements on Spigot Section

Pre-Test				
Locations	C-I (in.)	CE-IW (in.)	E-W (in.)	CW-IE (in.)
Spigot End	6.907	6.905	6.896	6.902
Post-Test				
Locations	C-I (in.)	CE-IW (in.)	E-W (in.)	CW-IE (in.)
Spigot End	6.865	6.903	6.910	6.907
2 in. from End	6.919	6.905	6.832	6.878
5 in. from End	7.145	6.752	6.543	6.739
6 in. from End	7.184	6.602	6.570	6.585

1 in. = 25.4 mm

Table 3.2. Relative Changes in Spigot Diameter near Locking Segment Locations

Locations	C-I [in. (mm)]	E-W [in. (mm)]
2 in. from End	0.012 (0.30)	-0.064 (-1.63)
5 in. from End	0.238 (6.05)	-0.353 (-8.97)
6 in. from End	0.277 (7.04)	-0.326 (-8.28)

Positive represents lengthening, and negative represents shortening.

are presented in Table 3.1. At the 5-in. (127-mm) and 6-in. (152-mm) locations where weld bead and locking segment contact was made, there is a notable decrease in horizontal diameter and a corresponding increase in vertical diameter. Reduction in the horizontal diameter allowed the weld bead to slip past the locking segments.

3.5.2 US Pipe 12-in. (300-mm) Specimens

Figure 3.20 shows the tensile force vs. joint displacement relationship of the US Pipe 12-in. (300-mm) restrained axial slip DI pipe joint. The tests began with the spigot fully inserted into the bell. As the pipe was pressurized, the spigot was displaced from the bell seat at approximately 6 psi (41 kPa) internal pressure. The slip was 2.3 in. (58 mm) before the weld bead became engaged with the locking segments. A maximum force of 259 kips (1,150 kN) was attained at 2.9 in. (74 mm) of joint displacement. At 3.0 in. (76 mm) of joint displacement the bell cracked as shown in Figure 3.21, resulting in leakage.

3.6 Summary

This chapter provides detailed information about direct compression and tension tests performed on nominal 6-in. (150-mm) diameter restrained axial slip DI pipe joints at water pressures of 75 to 85 psi (520 to 590 kPa). The general set up used for all tests and the mechanical characteristics of each joint type are described.

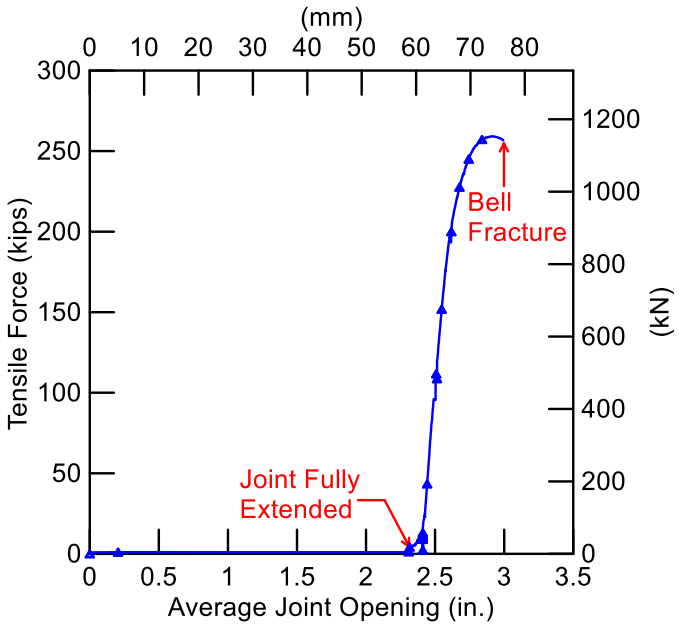

Figure 3.20. US Pipe 12-in. (300-mm) Tensile Force vs. Displacement Relationship

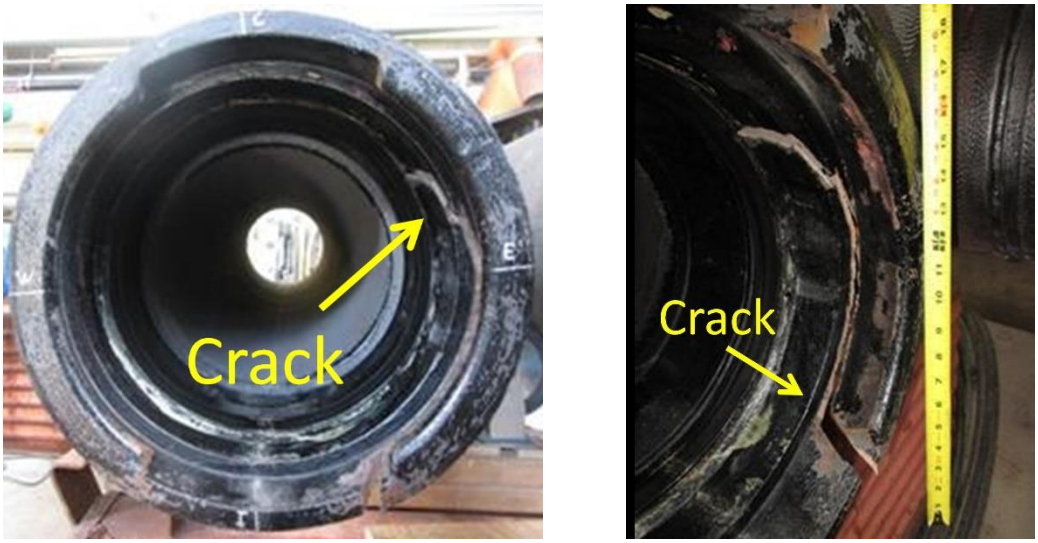

a) Bell Face

b) East Springline

Figure 3.21. Circumferential Crack on 12-in. (300-mm) US Pipe Bell Section

Table 3.3. Summary of Joint Direct Tension Test Results for 6-in. (150-mm)-diameter DI Pipes with Restrained Axial Slip Joint Systems

Types of DI Pipes	Maximum Tensile Force	Joint Travel Distance [a]	Joint Travel Distance at Leakage [b]	Failure Mode
AMERICAN	150 kips (667 kN)	5.3 in. (135 mm)	5.5 in. (140 mm)	Bell fracture
Kubota	115 kips (516 kN)	4.5 in. (115 mm)	4.5 in. (115 mm)	Shear at spigot projection
McWane	66.3 kips (295 kN)	11.0 in. (280 mm)	13.2 in. (335 mm)	Spigot ovaling
US Pipe	80.5 kips (358 kN)	2.3 in. (58 mm)	3.5 in. (89 mm)	Spigot ovaling

[a] Maximum travel distance from gasket haunch to locking segments or ring

[b] Maximum travel distance from gasket haunch until leakage

Axial force vs. displacement plots are presented for direct compression tests, and interpreted relative to the yield and proportional limit loads of the pipe barrel. The compression tests show that either leakage or irrecoverable deformation in the form of large rotation occurred at loads equal to or slightly higher than the proportional limit load.

Axial load vs. displacement plots are also presented for direct tension tests. Table 3.3 summarizes the direct tension test results for 6-in. (150-mm)-diameter DI pipes with restrained axial slip joint systems. The table lists the maximum tensile force sustained by each joint type, maximum travel distances from gasket haunch to locking segments or ring, maximum travel distance from gasket haunch until leakage, and failure mode.

Locking rings are full circumferential split rings that are used for axial pullout resistance in AMERICAN and Kubota joints. Under full pullout a DI ring, which is welded on the spigot, makes contact with the locking ring and provides resistance to further axial slip. Failure and leakage under tension with these features occurred as DI ring shear fracture (Kubota) and bell fracture (AMERICAN). For this type of restraint, the maximum joint travel distance equals the joint travel distance at leakage because there is little or no capacity for additional axial movement once the weld rings engage the locking rings.

In contrast, locking segments, which are employed with the US Pipe and McWane joints, only cover part of spigot circumference. As the spigot is pulled from the bell, the weld bead on the spigot engages the locking segments. The locking segments bear against the bell lip and begin rotating onto the spigot. Load concentration at the locking segment locations causes the spigot to deform from a circular to an oval shape. This plastic inward deformation at the locking segment locations allows the weld bead to slip past the locking segments, causing leakage.

It should be noted that additional axial slip occurs once the locking segments have been contacted by the spigot weld bead. Joints with locking segments are not as stiff as joints with locking rings once the locking mechanism is engaged. Although joints with locking segments can accommodate additional axial movement, the maximum axial load they carry is less the maximum axial force that can be sustained by joints with locking rings.

Tensile failure of the 12-in. (300-mm)-diameter US Pipe joint occurred as bell fracture. There are four locking segments as opposed to two for the 6-in. (150-mm) joint, which cover most of the spigot circumference. The load at the locking segments is more evenly distributed to confine the spigot, thus preventing ovaling of the pipe.

CHAPTER 4

FOUR-POINT BENDING TESTS

4.1 Introduction

Test data are scarce with respect to the bending response and moment vs rotation relationships associated with these types of joints. Four-point (Singhal and Benavides, 1984) and three-point (Yang et al., 2011) bending tests were conducted on DI push-on joints, and the results in terms of moment vs rotation relationships published in the technical literature. These tests, however, were conducted with little or no internal water pressure, which is not representative of practice. Three-point bending test results are reported by Oda et al. (2016), who used the results for numerical simulation of CI restrained axial slip joint response in large-scale fault rupture tests. Again, these tests were run with no internal water pressure, and thus inconsistent with actual operating pressures.

This chapter provides detailed information about four-point bending tests on nominal 6-in. (150-mm) diameter restrained axial slip joints. All tests were performed at water pressures of 75 to 85 psi (520 to 590 kPa). A description of the general set up and instrumentation used in all tests is provided. The test results are plotted as moment vs rotation relationships, and interpreted with respect to the moment that imposes yield and proportional limit stress in the pipe barrel.

4.2 Test Setup and Instrumentation

A detailed description of the moment vs rotation tests performed on restrained axial slip joints covered in this work is provided in reports by Pariya-Ekkasut et al. (2015, 2016, 2017, 2018) and Stewart et al. (2015). Only the salient features of these tests are addressed herein with specific reference to the four-point bending test performed for 6-in. (150-mm)-diameter DI pipe.

A four-post steel frame with a movable crosshead was used for the four-point bending tests. Figure 4.1 is a photograph of the bending test setup showing the two supports of the pipe. An actuator and load cell were installed on the crosshead in the vertical direction to apply and measure force onto the pipe. The maximum axial capacity of the actuator is 220 kips (980 kN) with a 6-in. (150-mm)-stroke displacement. The central load was applied through a steel spreader beam that was attached to the actuator and load cell. Although the center of rotation for the complex inner geometry of the joint is not well defined, the joint was positioned such that the vertical load was applied at the nominal center of the bell and spigot specimen. The spigot end was inserted fully into the bell. An electronic pressure transducer, located at the end cap, measured internal water pressure during the test. There were two temporary supports beneath the central loading points. The supports are used to level the test specimen and to support the self-weight of the pipe (including water for pressurized pipe) before vertical loading.

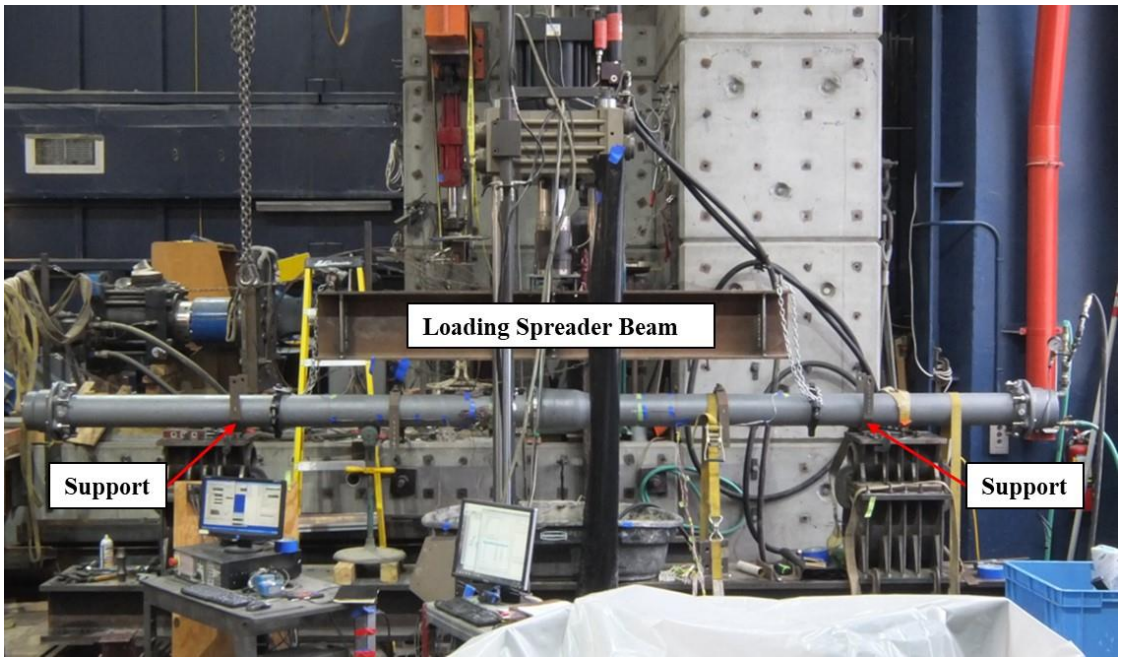

a) Photo of Test Setup

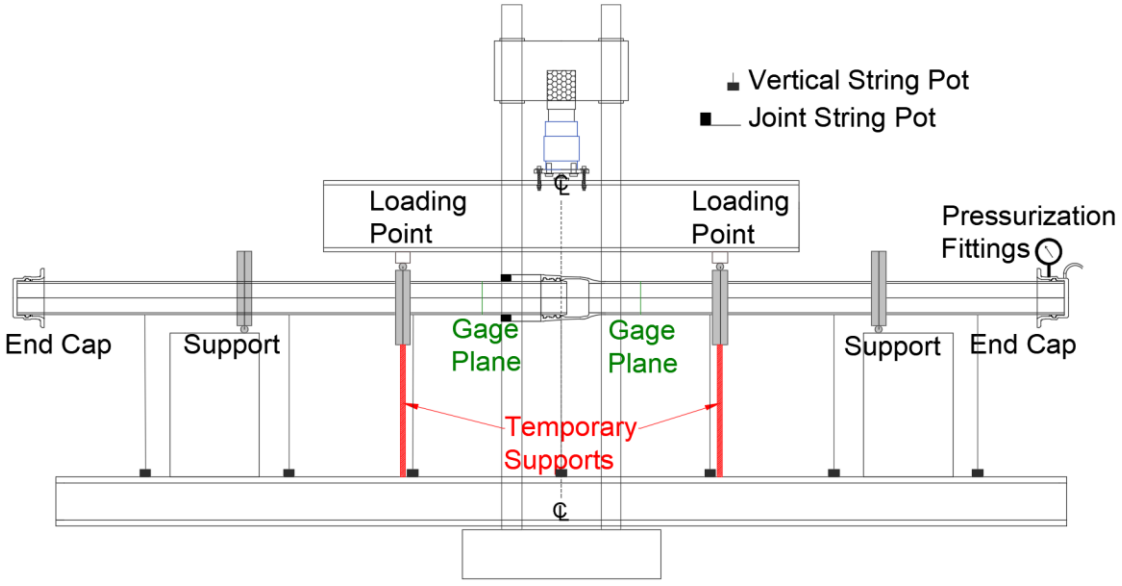

b) Schematic of Instrumentation

Figure 4.1. Four-Point Bending Test Setup

A schematic of the instrumentation used in the Kubota restrained axial slip joint four-point bending test is presented in Figure 4.1 b), and used to describe the typical test setup and instrumentation of all the tests. The instrumentation consisted of string potentiometers (pots) to measure horizontal displacements at the crown and invert of the joint, which were used to measure the bell rotation. Vertical displacements along the length of the specimen were measured using vertical string pots. The VSPs were used to determine the vertical displacement of the test specimen and to calculate the rotation at various locations along the pipe. Strain gage planes were located at the bell and spigot within the central portion and halfway between the joint and loading point to avoid local deformation effects on the measurements. Each strain gage plane had a pair of axial and circumferential gages at the crown and invert positions. These measurements provided a means for calculating bending strains of the pipe in the central portion.

4.3 Test Procedures

The pipe for the bending test was installed in the loading frame, leveled, and all instrumentation and data acquisitions systems were checked. The pipe was filled with water and pressurized, providing axial force sufficient to extend the joint. A nominal internal pressure of 80 psi (550 kPa) was supplied throughout the bending test. The temporary supports were removed, and the spreader beam was lowered by the crosshead onto the pipe. Vertical displacement was applied to the pipe with hydraulic force under displacement control at a rate of approximately 1 in. (25.4 mm) per minute until pipe

failure. Limit state is defined as either structural or serviceability failure when leakage exceeding 10 gal/min (38 l/min).

4.4 6-in. (150-mm)-Diameter Bending Test Specimens

4.4.1 AMERICAN

The moment vs. rotation test results are shown in Figure 4.2. Also shown in Figure 4.2 are moments, M, at different limits calculated as

$$M = \frac{\sigma I}{c} \tag{4.1}$$

where σ is either proportional limit, yield, or ultimate stress, c is distance to outer fiber, and I is moment of inertia. The EJS rotated about 7° before metal binding, referred to as internal joint metal-to metal contact. At 7° there was a significant increase in joint rotational stiffnesss. A leak first was observed at the FR joint (see Figure 1.1) at an EJS rotation of 12.7° at 323 kips-in. (37 kN-m) of applied moment, which was very close to the moment at proportional limit. The leak rate was approximately 10 drops/sec (25 ml/min). As the test continued, leakage rate at the FR joint increased. When the EJS reached a rotation of 16.6° with an associated moment of 491 kips-in. (56 kN-m) near the yield moment, the FR bell barrel fractured and caused pipe failure as shown in Figure 4.3.

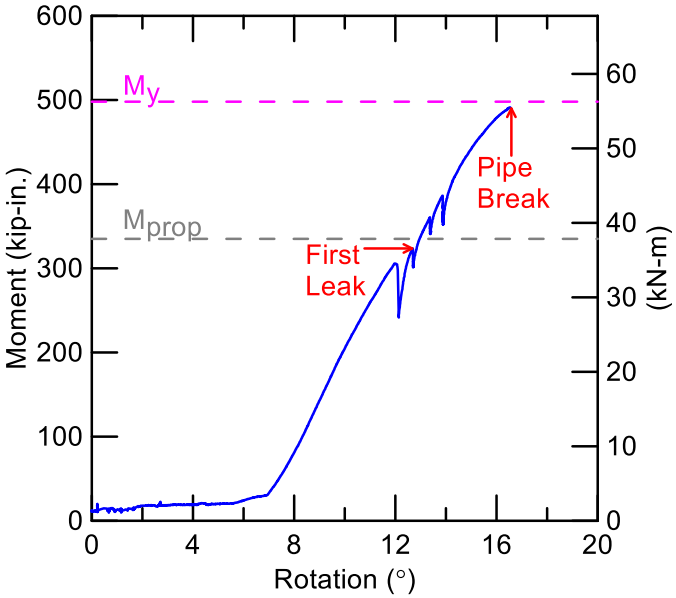

Figure 4.2. Moment vs. Rotation of 6-in. (150-mm) AMERICAN Restrained Axial Slip DI Pipe

Figure 4.3. Pipe Failure of 6-in. (150-mm) AMERICAN Restrained Axial Slip DI Bending Specimen

4.4.2 Kubota

The moment vs. rotation relationship is shown in Figure 4.4. At approximately 5.5° of joint rotation, the metal binding occurred, and the moment began to increase rapidly. The first leakage of approximately 0.1 gal/min (0.4 l/min) developed at a rotation of 12.2° with an applied moment of 520 kip-in. (59 kN-m). The leakage rate grew larger with increasing moment and joint rotation. At 14.3° of joint rotation with an associated moment of 580 kip-in. (66 kN-m), the pipe experienced significant leakage on the order of 10 gal/min (38 l/min). When the pipe reached the maximum moment near the ultimate yield moment of 630 kip-in. (71 kN-m) at 16.6° of rotation, the moment dropped rapidly, and the leakage stopped. The test was continued until the rotation reached 20.9° of joint rotation without leakage, when the actuator reached the limit of its stroke.

As the pipe was unloaded to reset the actuator, it rebounded to 18.0°. The actuator and crosshead were readjusted. The pipe was reloaded until it reached 32.0° of rotation. No leakage was observed during the second stroke of actuator movement. The test was then stopped, and the pipe was unloaded. There was a residual joint rotation of 27.8° after unloading. A photograph of the bending specimen after the test is shown in Figure 4.5. Investigation after the test showed that the spigot had substantial deformation and broke at the crown corresponding with the rapid moment drop at 16.6° of rotation during the first stroke of actuator movement.

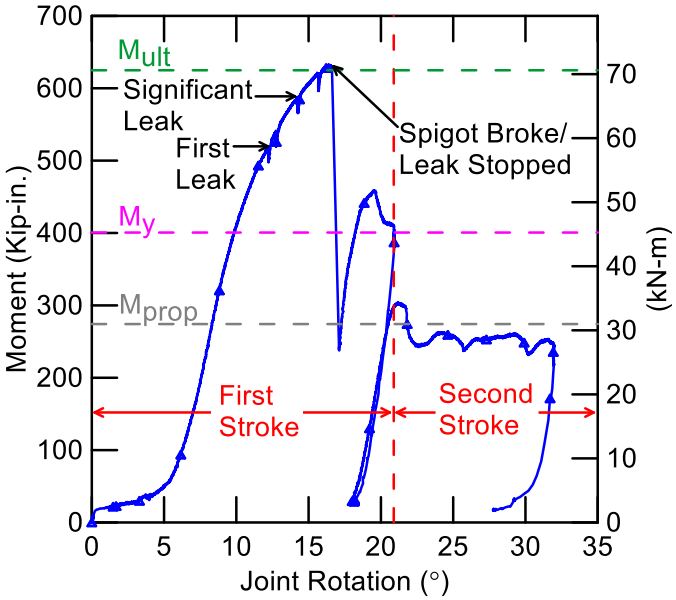

Figure 4.4. Moment vs. Rotation of 6-in. (150-mm) Kubota Restrained Axial Slip DI Pipe

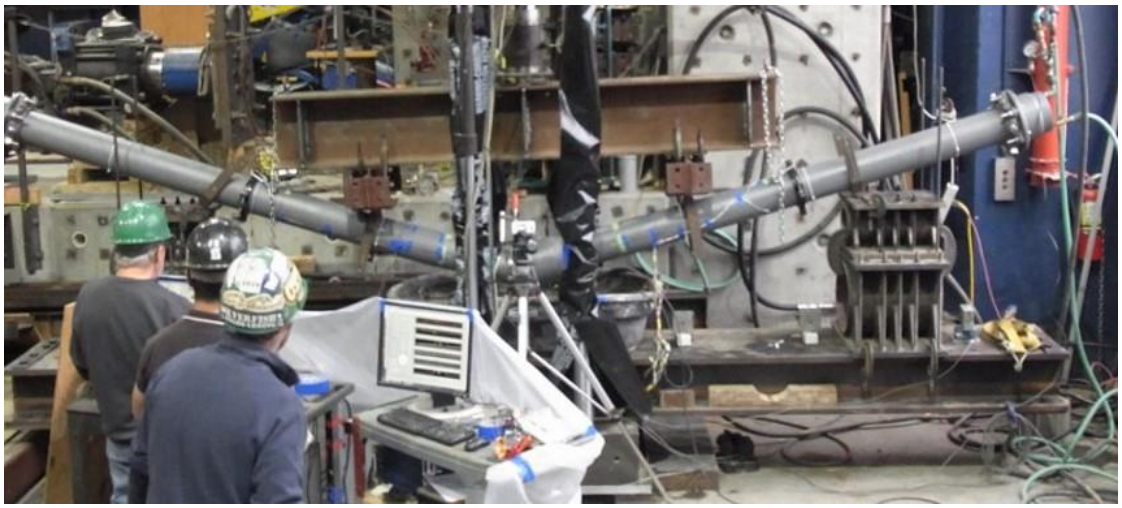

Figure 4.5. Photo of 6-in. (150-mm) Kubota Restrained Axial Slip DI Bending Specimen after Test

4.4.3 McWane

During the four-point bending test the load, P, is applied vertically. This vertical load represents horizontal differential soil displacement, which is typically associated with the most severe conditions of soil-pipe interaction during earthquake-induced ground deformation. Under the assumption that the slots [see Figure 3.2 a)] are at the pipe crown, the locking segments are inserted such that they are located near the springline (3 and 9 o'clock) positions of the pipe during regular pipeline installation as illustrated in Figure 4.6 a). In order to simulate the joint rotational response to the horizontal differential soil displacement in the fault rupture test, the slots of the McWane four-point bending specimen were located at the springline of the pipe, and The locking segments were inserted into one slot and pushed up and down such that they were at approximate crown and invert positions as seen in Figure 4.6 b).

The moment vs. pipe rotation relationships of the McWane four-point bending test are shown in Figure 4.7. First leakage of approximately 0.8 fl. oz./min (25 ml/min) was observed at the X joint (see Figure 1.3) at the beginning of the test. The metal binding was observed at about 6.5° of SFC rotation. The leakage at the X joint stopped when moment reached 202 kip-in. (23 kN-m) at 20.5° of pipe rotation. The applied moment and pipe rotation continued to increase until the pipe reached a rotation of 23.5° when the moment began to decline. When the moment dropped to 203 kip-in. (23 kN-m), the invert locking segment of the P joint fell out at 25.6° of pipe rotation. The test

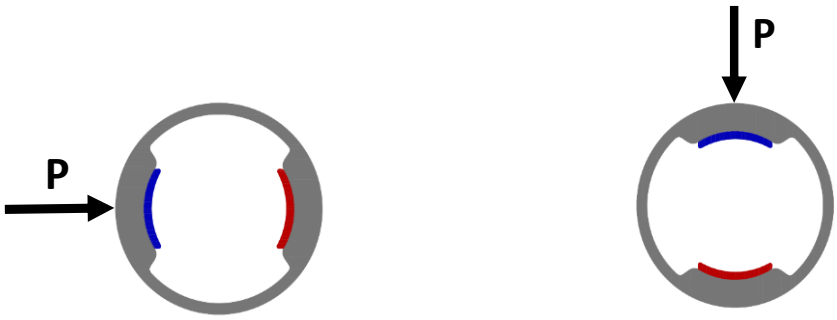

a) Horizontal Soil Movement with Locking Segments at Springline for Fault Rupture Test

b) Vertical Loading with Locking Segments at Crown and Invert for Bending Test

Figure 4.6. Locking Segment Orientations for 6-in. (150-mm)-Restrained Axial Slip DI Bending Specimens

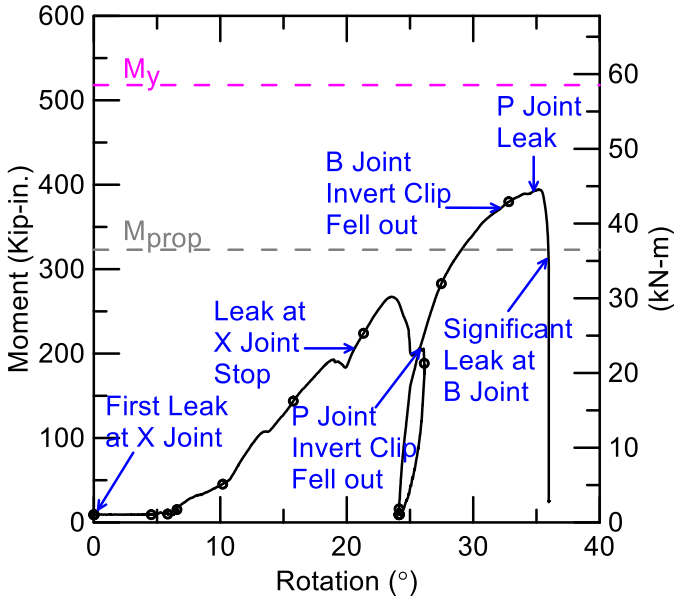

Figure 4.7. Moment vs. Rotation of 6-in. (150-mm) McWane Restrained Axial Slip DI Pipe

Figure 4.8. Significant Leakage of 6-in. (150-mm) McWane Restrained Axial Slip DI Bending Specimen

Figure 4.9. Photo of 6-in. (150-mm) McWane Restrained Axial Slip DI Bending Specimen after Test

was continued until the rotation reached 26.1° of rotation when the actuator reached the end of its stroke.

As the pipe was unloaded to reset the actuator, it rebounded to 24.1° of overall rotation. The actuator and crosshead were readjusted. The pipe was then reloaded. Another invert locking segment fell out of the B joint at applied moment and pipe rotation of 373 kip-in. (42 kN-m) and 32.2°, respectively.

When the pipe achieved a maximum moment of 393 kip-in. (44 kN-m), leakage of approximately 2.5 fl. oz./min (75 ml/min) was detected at the P joint at 34.9° of overall rotation. This maximum moment was close the average of proportional limit and yield moments. The applied moment then rapidly decreased, and the pipe failed and leaked at the B joint with a significant rate greater than 10 gal/min (38 l/min) at 36.0° of pipe rotation. Figure 4.8 shows the significant leakage at the B joint. Figure 4.9 shows a photograph of the McWane SFC bending specimen after the test.

4.4.4 US Pipe

The locking segment orientation of the US Pipe bending specimen was similar to the McWane test such that they were located at the crown and invert positions, as discussed in Section 4.4.3. Figure 4.10 presents the moment vs. rotation relationship of the US Pipe four-point bending test. The metal binding occurred at about 2.2° of rotation. The pipe exceeded the proportional limit moment with no indication of leakage. The test was stopped when a steady stream of leakage of approximately 4

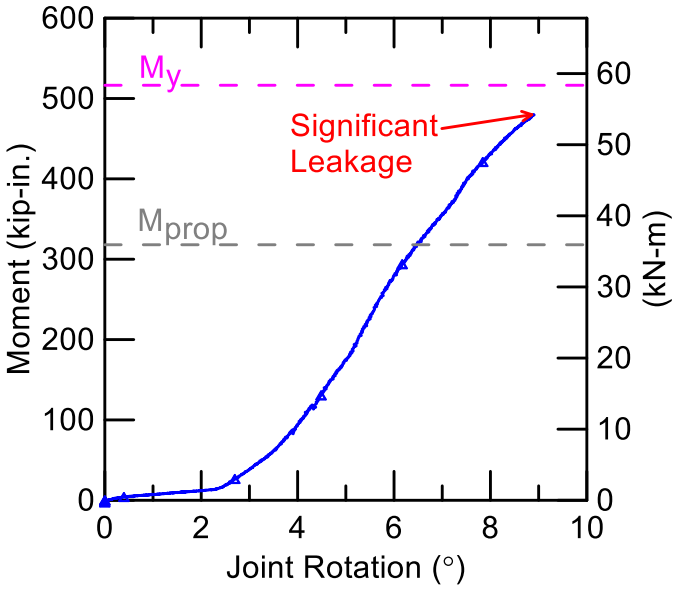

Figure 4.10. Moment vs. Rotation of 6-in. (150-mm) US Pipe Restrained Axial Slip DI Pipe

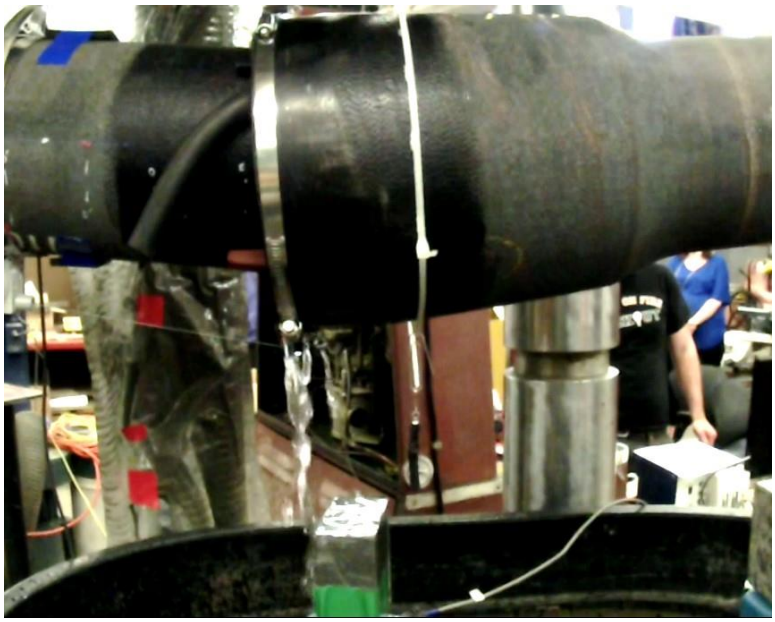

Figure 4.11. Final Leakage of 6-in. (150-mm) US Pipe Restrained Axial Slip DI Bending Specimen

gal/min (15 l/min) was observed at a rotation of 9.1° with an applied moment of 480 kip-in. (54 kN-m), which was close to the yield moment of 516 kip-in. (58 kN-m). Figure 4.11 shows the leakage at the end of the test.

4.5 12-in. (300-mm)-Diameter Bending Test Specimens

4.5.1 Kubota

The moment vs. rotation test results are shown in Figure 4.12. Metal binding was detected at about 4.8° of joint rotation. The pipe reached a maximum moment of 1,560 kip-in. (176 kN-m), which was very close to the yield moment, at a joint rotation at 12.4°. The moment rapidly dropped to approximately 480 kip-in. (54 kN-m) with no indication of leakage. The test was continued until the pipe reached 20.5° of joint rotation when the actuator reached the limit of its stroke. While the pipe was being unloaded, the first and significant leakage of more than 10 gal/min (38 l/min) occurred at 19.3° of joint rotation. There was a residual joint rotation of 16.8° after unloading. A photograph of the bending specimen after the test is shown in Figure 4.13. Investigation after the test shows that the pipe broke at the spigot crown corresponding to the rotation of 12.4° at which there was a rapid drop in moment.

4.5.2 US Pipe

Figure 4.14 a) shows locking segment orientation for typical installation for a 12 in.-(150-mm)-diameter restrained axial slip pipeline, which is constructed with the

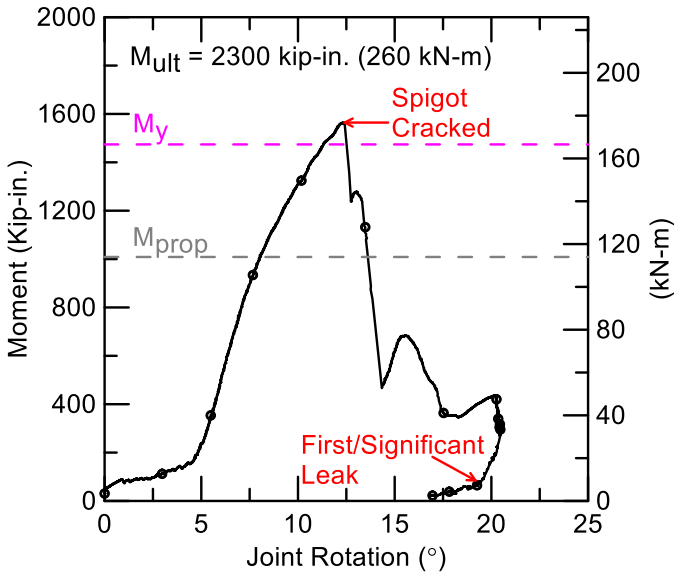

Figure 4.12. Moment vs. Rotation of 12-in. (300-mm) Kubota Restrained Axial Slip DI Pipe

Figure 4.13. Photo of 12-in. (300-mm) Kubota Restrained Axial Slip DI Bending Specimen after Test

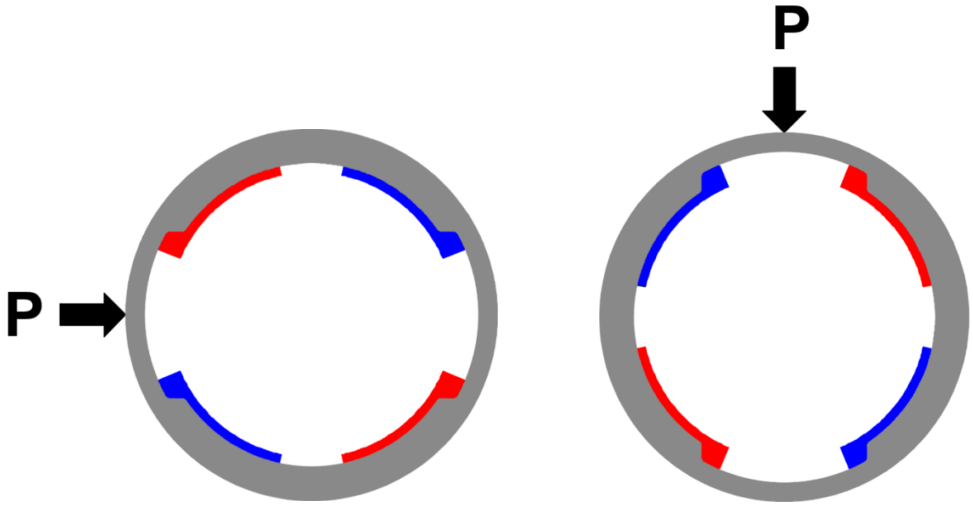

a) Horizontal Soil Movement with Locking Segments at Crown and Invert for Fault Rupture Test

b) Vertical Loading with Locking Segments at Springline for Bending Test

Figure 4.14. Locking Segment Orientations for 12-in. (300-mm)-Restrained Axial Slip DI Bending Specimens

slots at the springline. Two locking segments were inserted into each slot and pushed up and down. Therefore, two locking segments were located near the crown (12 o´clock) position, and the other two were positioned near the invert (6 o´clock). In addition, the pipeline is subjected to the most severe ground deformation in the horizontal direction.

To simulate the rotational response of the joint to the horizontal differential soil displacement in the fault rupture test, the slots of the 12-in. (300-mm)-diameter US Pipe bending specimen were located at the crown and invert, and the load, P, is applied vertically. Four locking segments were inserted into the two slots such that they were located near the springline as shown in Figure 4.14 b).

Figure 4.15 shows the moment vs. rotation relationship of the specimen. Metal binding was detected at 5.5° of joint rotation, at which the moment began increasing rapidly. First leakage of 5 fl. oz./min (150 ml/min) was observed at a moment of 565 kip-in. (64 kN-m) and an associated joint rotation of 6.5°. The leakage rate slowed down to approximately 0.1 fl. oz./min (3 ml/min) as the test continued. The test was paused when the load transfer plate at one of the loading points broke. The pipe was unloaded, causing the leakage to stop. The broken plate was then replaced with a new one. After the test was resumed, leakage of 0.1 fl. oz./min (3 ml/min) was observed at 635 kip-in. (72 kN-m) and a rotation of 10.1°. The leakage rate grew larger with increasing moment and rotation. Leakage of 8.7 gal/min (33 l/min), shown in Figure 4.16, was observed at the maximum moment of 1770 kip-in. (200 kN-m) and a rotation of 15.9°. The maximum moment was close to the average of the proportional limit and yield moments.

4.6 16-in. (400-mm)-Diameter Bending Test Specimens

Two bending tests were conducted on 16-in. (400-mm) Kubota restrained axial slip joints. Full operating pressure of 75 to 85 psi (520 to 590 kPa) was supplied during the first test. An additional test was performed to investigate the effect of pressurization following an initial 8° of rotation under zero internal pressure.

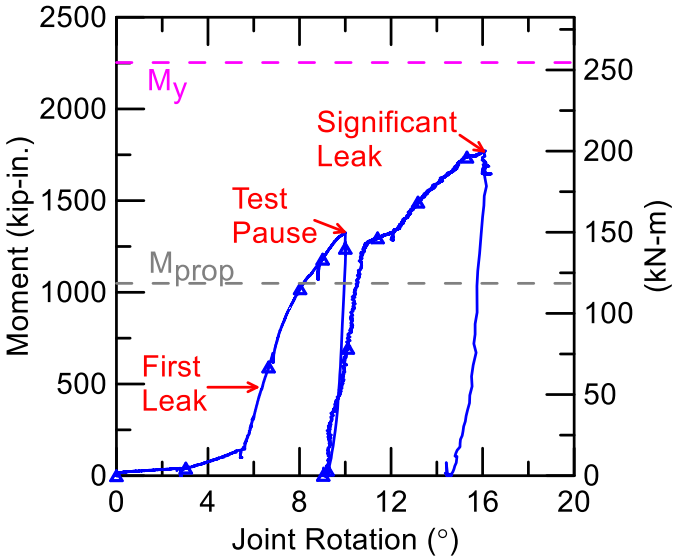

Figure 4.15. Moment vs. Rotation of 12-in. (300-mm) US Pipe Restrained Axial Slip DI Pipe

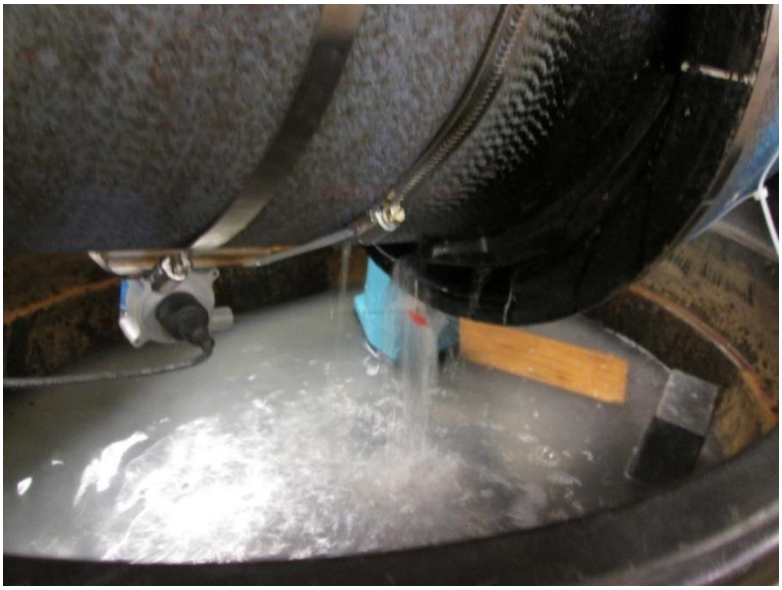

Figure 4.16. Final Leakage of 12-in. (300-mm) US Pipe Restrained Axial Slip DI Bending Specimen

4.6.1 Kubota Test 1

The moment vs. rotation relationship is shown in Figure 4.17. Metal binding occurred at about 5.2° of joint rotation. First leakage of approximately 0.7 gal/min (2.6 l/min) was detected at the yield moment of 2,700 kip-in. (305 kN-m) and an associated rotation of 17.5°. At the same joint rotation, the moment dropped slightly to 2,500 kip-in. (282 kN-m), and leakage of at least 8.3 gal/min (31 l/min) was observed. At 18.9° of rotation, the pipe broke and the moment dropped rapidly from 2,420 to 307 kip-in. (273 to 35 kN-m). A photograph of the bending specimen 1 after the test is shown in Figure 4.18.

4.6.2 Kubota Test 2

An additional test was performed on a pressurized 16-in. (400-mm)-diameter pipe specimen after an initial 8° of rotation under zero internal pressure. The joint was initially set at the neutral position, referring as a location that allows equal displacement for both tension and compression before internal contact in the pipe joint. The moment vs. rotation relationship is shown in Figure 4.19. The weight of the pipe plus water caused a joint rotation of 5.6°. Additional moment was applied past metal binding at 5.6° of rotation and until 8° of rotation was achieved at 358 kip-in. (41 kN-m). The test was paused, and the pipe was pressurized to 80 psi (550 kPa). There was no joint displacement during pressurization. The test was then continued. The pipe reached a maximum applied moment of 2,400 kip-in. (271 kN-m) at a joint rotation of 13.6°. This

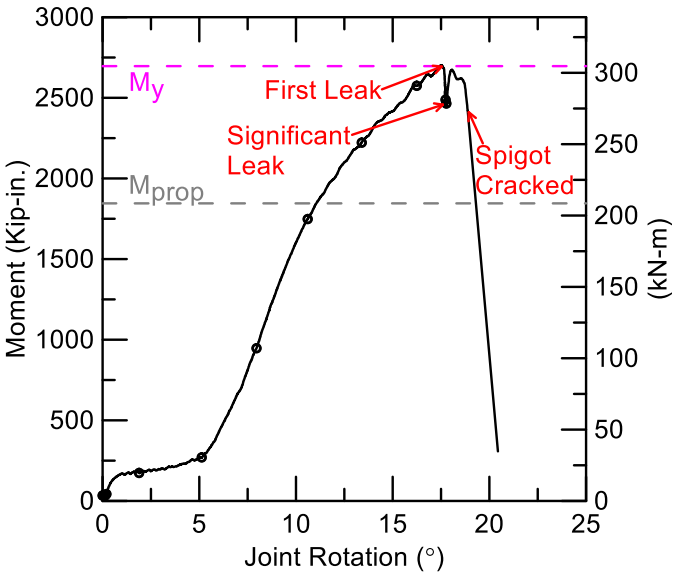

Figure 4.17. Moment vs. Rotation of 16-in. (400-mm) Kubota Restrained Axial Slip DI Pipe 1

Figure 4.18. Photo of 16-in. (400-mm) Kubota Restrained Axial Slip DI Bending Specimen 1 after Test

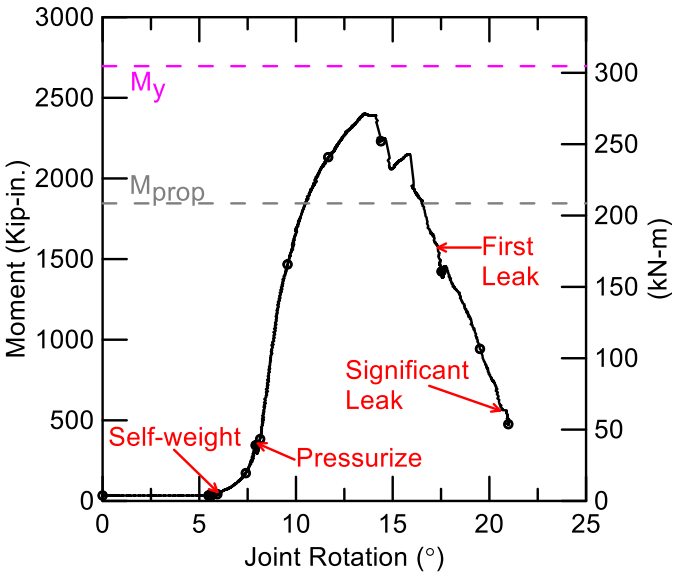

Figure 4.19. Moment vs. Rotation of 16-in. (400-mm) Kubota Restrained Axial Slip DI Pipe 2

Figure 4.20. Photo of 16-in. (400-mm) Kubota Restrained Axial Slip DI Bending Specimen 2 after Test

maximum moment was close the average of proportional limit and yield moments. The moment steadily decreased to 1,580 kip-in. (178 kN-m) when the first leakage of about 6.4 fl. oz./min (190 ml/min) was observed at a joint rotation of 17.3°. The pipe continued to leak until significant leakage of approximately 15 gal/min (57 l/min) suddenly occurred at a moment of 563 kip-in. (64 kN-m) and a joint rotation of 20.7°. A photograph of the 16-in. (400-mm) bending specimen 2 after the test is shown in Figure 4.20. Investigation after the test shows that the pipe fractured at the crown of the spigot, corresponding to the drop in moment shown in Figure 4.19.

4.6.3 Comparisons of 16-in. (400-mm) Kubota Restrained Axial Slip Joint

The moment vs. rotation comparisons for the 16-in. (400-mm) Kubota joints are shown in Figure 4.21. The unpressurized pipe, Test 2, rotated approximately 5° under its own weight. In contrast, a moment of about 270 kip-in. (31 kN-m) was required to apply the same amount of rotation for the pressurized pipe, Test 1. The maximum moments of bending tests 1 and 2 were on the order of 2,500 kip-in. (280 kN-m). The first leakage of both tests was observed at approximately 17.5°. Significant leakage from Test 1 occurred immediately after first leakage occurred. Specimen 1 failure occurred when the moment dropped rapidly at 19°. Test 2 moment declined steadily after the maximum moment had been achieved at 13.6° of joint rotation. After the first leakage was observed, specimen 2 continued to leak and reached a state of significant leakage at a joint rotation of 20.7 °.

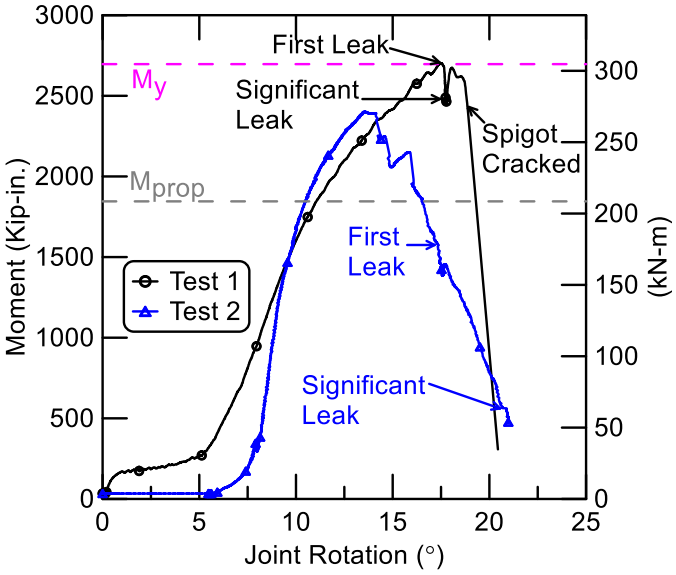

Figure 4.21. Moment vs. Rotation Comparisons for 16-in. (400-mm) Kubota Restrained Axial Slip Joints

Table 4.1. Summary of Four-Point Bending Test Results

Pipe Nominal Diameters	Types of DI Pipes	Metal Binding	Maximum Moment	Rotation at Significant Leakage [a]
6 in. (150 mm)	AMERICAN	7.0°	491 kips-in. (56 kN-m)	16.6°
	Kubota	5.5°	630 kip-in. (71 kN-m)	32.2°
	McWane	6.5°	393 kip-in. (44 kN-m)	36.0°
	US Pipe	2.2°	480 kip-in. (54 kN-m)	9.1°
12 in. (300 mm)	Kubota	4.8°	1,560 kip-in. (176 kN-m)	20.5°
	US Pipe	5.5°	1770 kip-in. (200 kN-m)	15.9°
16 in. (400 mm)	Kubota Test 1	5.2°	2,700 kip-in. (305 kN-m)	17.5°
	Kubota Test 2	5.6°	2,400 kip-in. (271 kN-m)	20.7°

[a] Significant leakage is referred as leakage exceeding 10 gal/min (38 l/min).

4.7 Summary

This chapter provides detailed information about four-point bending tests on nominal 6-in. (150-mm) diameter restrained axial slip joints. All tests were performed at water pressures of 75 to 85 psi (520 to 590 kPa). The general set up and instrumentation used in all tests is described.

The test results are plotted as moment vs rotation relationships, and interpreted with respect to the moment that imposes yield and proportional limit stress in the pipe barrel. Table 4.1 summarizes the four-point bending results for DI pipes with restrained axial slip joint systems. The table lists the rotation at metal binding, maximum moment sustained by each joint type, and maximum rotation at significant leakage, which is referred as leakage exceeding 10 gal/min (38 l/min). The maximum moments of most pipes in these investigations were within the upper half of the range between the proportional limit and yield moments. An exception was observed for the 6 in. (150 mm) Kubota bending test, for which the maximum moment was equal to at the ultimate moment.

When the maximum moment was attained, the DI joint either noticeably deformed or cracked at the spigot end or bell barrel, with significant leakage observed for the AMERICAN, McWane, and US Pipe joints. However, the Kubota pipe was able to maintain the internal water pressure and accommodate more rotation after the spigot end cracked because the gasket, which was located near the bell end opening (bell face), prevented leakage at the joint.

CHAPTER 5

SOIL AXIAL RESISTANCE TESTS

5.1 Introduction

This chapter reports on the soil-structure interaction associated with relative axial movement of DI pipe with a restrained axial slip joint through soil. While there are procedures for estimating the axial resistance along straight underground pipelines and conduits (e.g., ASCE 1984, Honegger & Nyman 2004, Wijewickreme et al. 2009, Weerasekara 2011), there is little information available to address the increased resistance associated with the enlarged cross-section and length of a restrained axial slip joint. The results of large-scale soil axial resistance tests are reported herein to quantify the axial force vs. displacement performance of a restrained axial slip joint and pipe system. A 6-in. (150-mm) US Pipe DI pipe with a restrained axial slip joint was used in this investigation.

5.2 Test Layouts and Instrumentation

Figure 5.1 provides a plan view of the general experimental setup for the four soil axial resistance tests of restrained axial slip joints. A detailed description of the tests is provided by Stewart et al. (2015). The total length of the specimens buried in soil was 12.4 ft. (3.78 m). Four strain gages were installed at quarter points around the circumferences of the bell and spigot sections. Two string potentiometers (pots) were

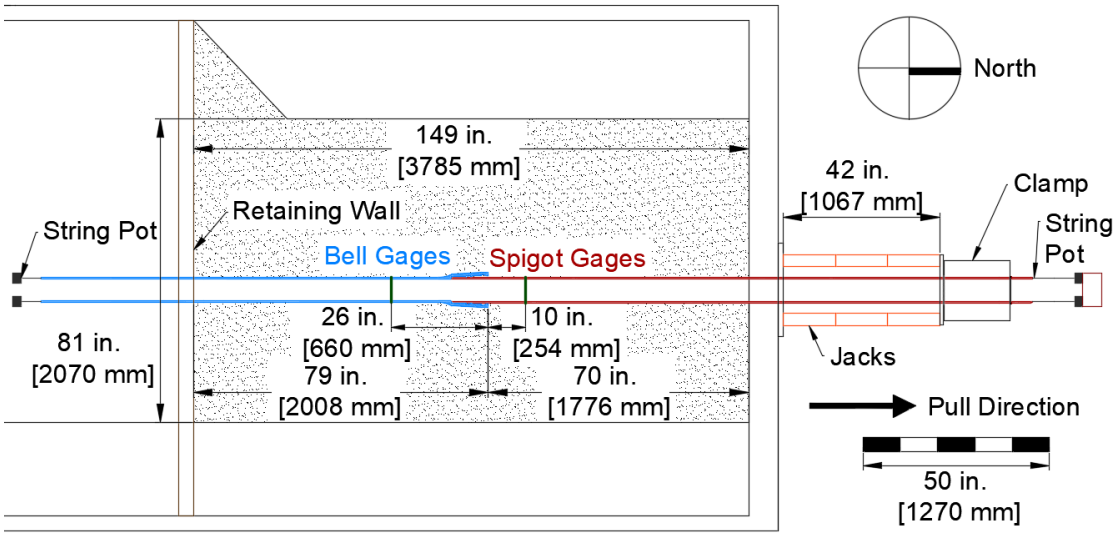

(a) Detailed Plan View of Test 1 and 2

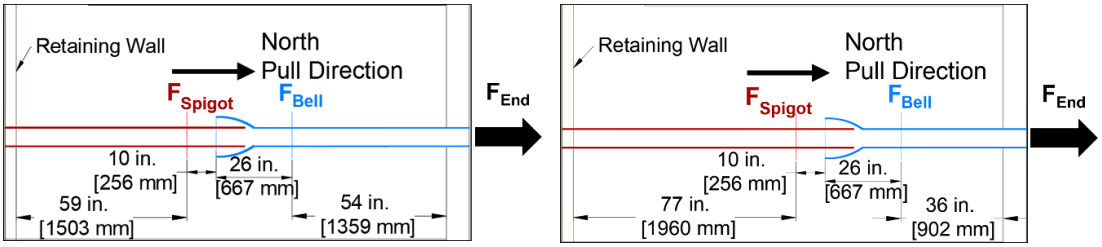

(b) Test 3 (c) Test 4

Figure 5.1. Setup of Restrained Axial Slip Joint in Soil Axial Resistance Tests

fixed to both the north (leading) and south (trailing) ends of the specimen to measure axial displacements. Jack hydraulic pressure was measured in all tests to determine applied axial force.

The orientations and locations of the pipes and joints in all four tests are shown in Figure 5.1. Test 1 was set up such that the pipe was pulled from the spigot end. Thus, the flat face of the bell was pulled against the soil. The setup for Test 2 was identical to the first, except that the pipe was covered in a hand-fastened low density polyethylene

wrap intended to reduce friction along the soil-pipeline interface. Figure 5.1 b) and c) show that the Test 3 and 4 pipes were pulled from the bell ends of the specimens. Thus, the rounded ends of the bells were pulled through the soil. Test 4 pipe was positioned 18 in. (0.46 m) closer to the north wall than the Test 3 pipe, and the soil in Test 4 was denser. The alterations to Test 4 were intended to increase the frictional resistance along the trailing section of pipe (spigot) in an effort to promote joint opening. During each test the specimen was pulled from the north end about 18 in. (0.46 m).

5.3 Soil Placement and Compaction Data

The specimen was buried in partially saturated sand that was compacted to have an average friction angle of approximately 42˚, equivalent in strength to that of a typical medium dense to dense granular backfill (O'Rourke, 2010). The pipeline was placed on 8 in. (200 mm) of soil and covered in approximately 8 in. (200 mm) lifts with a depth of burial to the pipe crown of 30 in. (760 mm). The average dry unit weight and moisture content of Tests 1 to 3 were 106.2 lb/ft^3 (16.7 kN/m^3) and 4.6%, respectively, and for Test 4 were 107.4 lb/ft^3 (16.9 kN/m^3) and 4.2%, respectively.

5.4 Axial Pull Forces and Displacements

Figures 5.2 and 5.3 show the pull force and joint opening versus north end displacement for the four tests, respectively. Tests 1 and 2 were designed so that pullout forces and displacements applied from the north end of the specimen caused the spigot

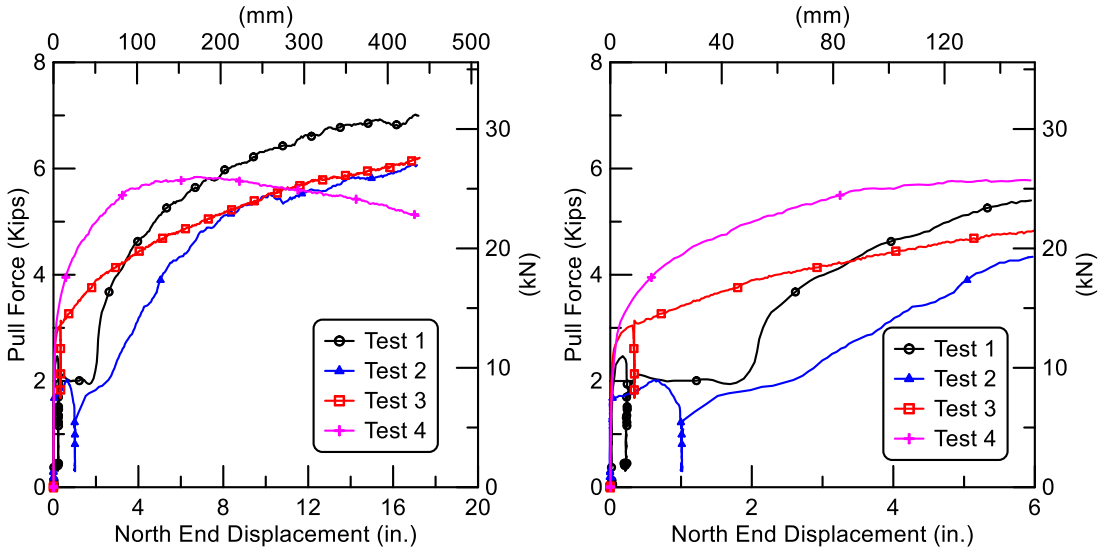

a) Full Range b) First 6 in. (152 mm) of Displacement

Figure 5.2. Axial Pull Force vs. North End Displacement

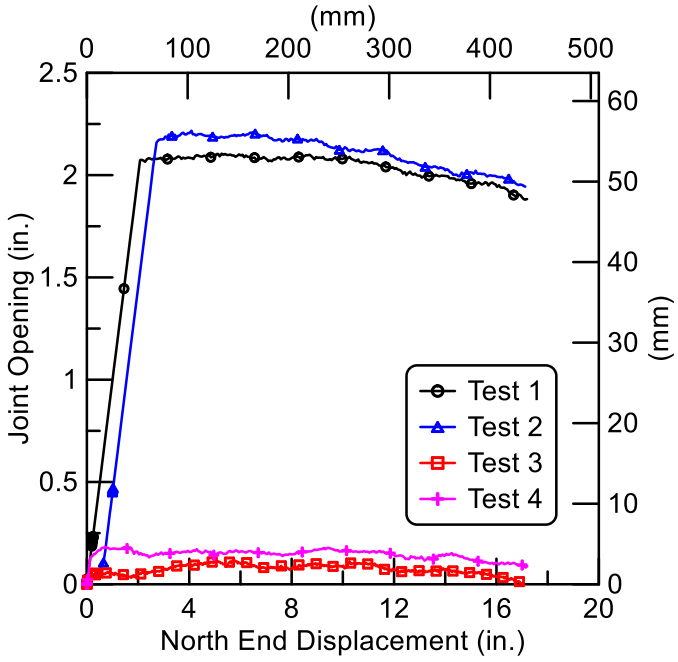

Figure 5.3. Joint Opening vs. North End Displacements

to pull from the bell until the weld bead on the spigot was engaged with the locking segments and bell mouth, after which both sections of pipe were pulled through the soil. Tests 3 and 4 were designed so that pullout forces and displacements caused the bell end to pull through the soil. As indicated in Figure 5.3, there is a notable difference in the joint opening vs. north end displacement for the two sets of tests. During Tests 1 and 2, axial displacement initially caused the joints to open as the spigot was pulled from the bell, and the weld bead engaged the locking segments at approximately 2.1 to 2.2 in, (53 to 56 mm) of joint opening. In Tests 3 and 4, the axial pull forces were accompanied by axial displacement of the bell without opening of the joint. This is shown in Figure 5.3 by the negligible levels of joint opening measured for Tests 3 and 4.

Figure 5.4 compares the results of Tests 1 and 2. During the first 2.0 in. (50 mm) of displacement the joint in each test opened under a relatively constant pull force of 2.0 kips (8.9 kN), after which the bell and spigot moved together as increasingly larger pullout forces were mobilized. The increased pullout force was generated by soil reaction at the bell face as it was pulled through the soil. A direct comparison between Tests 1 and 2 shows that the polyethylene wrap reduced the axial pullout force by about 15% or more at displacements exceeding 4.0 in. (100 mm).

The test results show that the initial pull force for Test 2 was comparable to that of Test 1. The main difference in axial force occurred after the spigot locked into the bell, and the flat face of the bell was pulled forward. The reduction in axial force for

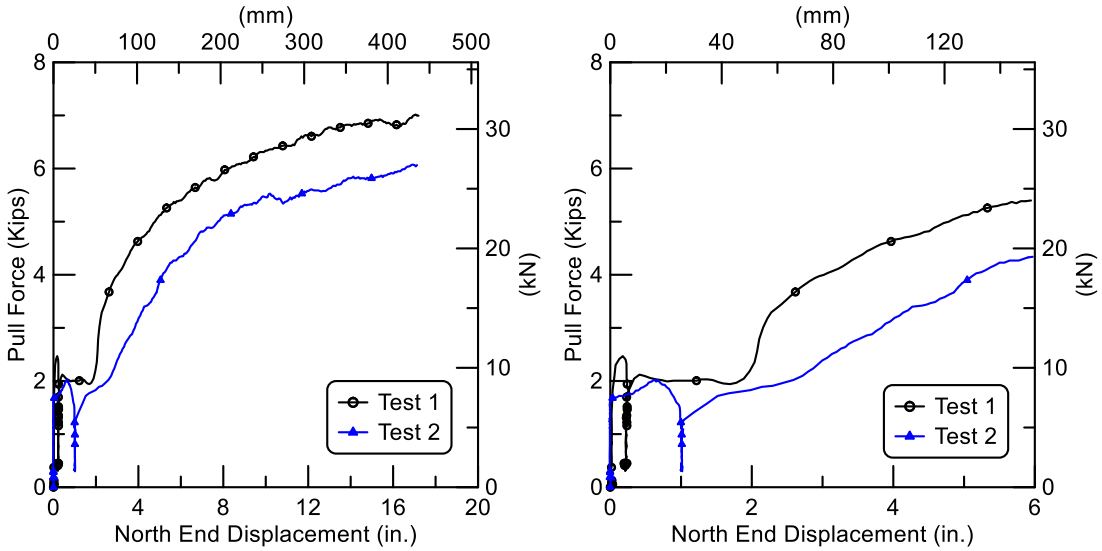

a) Full Range b) First 6 in. (152 mm) of Displacement

Figure 5.4. Axial Pull Force vs. North End Displacement for Tests 1 and 2

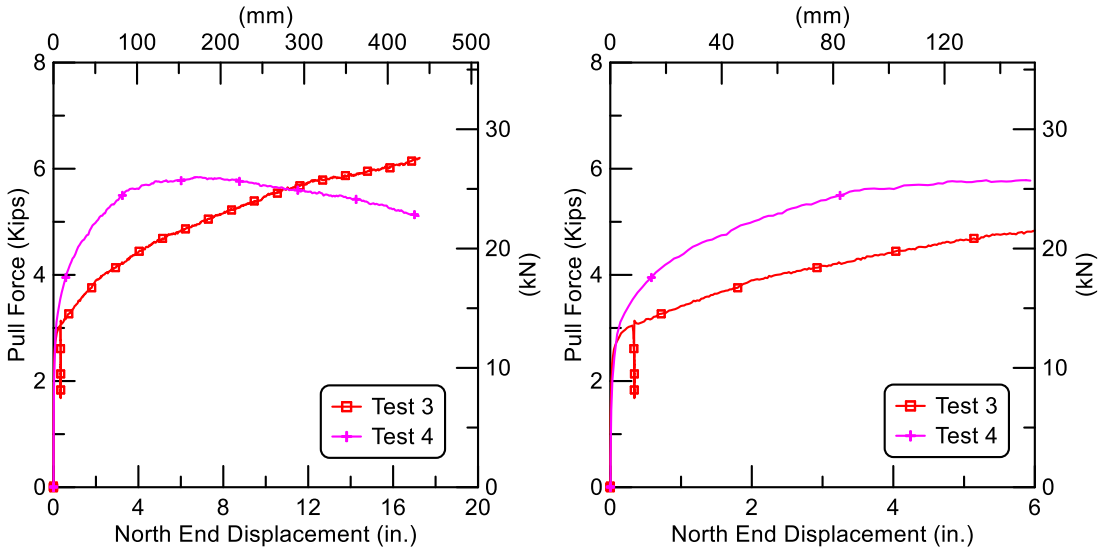

a) Full Range b) First 6 in. (152 mm) of Displacement

Figure 5.5. Axial Pull Force vs. North End Displacement for Tests 3 and 4

the polyethylene wrap appears to be related primarily to a decrease in bell resistance. The pull out force for the bell wrapped in polyethylene compares more closely with force mobilized in Test 3 for pullout of the curved end of the bell. Further discussion of this comparison is provided in Section 5.6.

Figure 5.5 compares the results of Tests 3 and 4 when displacement was applied to the bell end of the pipe such that axial resistance to pullout was generated at all times by the bell pulling through the soil in combination with frictional resistance mobilized between the soil and pipe surface. The force in Test 4 increased at a faster rate than that of Test 3, and reached its peak of about 5.9 kips (26 kN) at 5.0 in. (130 mm) of north end displacement. As the pipe was pulled further north, the force decreased.

5.5 Joint Axial Resistance

The axial loads, F, on the spigot and bell sections are calculated from the product of the average strain measured by four axial gages positioned circumferentially around the pipe, cross-sectional area of the pipe, and Young's modulus of the DI. The cross-sectional area of the pipe is A = 6.22 in.^{2} (40.1 cm^2). Figure 5.1 illustrates the locations of the measured hydraulic jack load, F_{End}, and the calculated loads from strain gages at both the bell, F_{Bell}, and spigot, F_{Spigot}.

Axial loads were calculated from strain gage measurements in front of (leading section) and behind (trailing section) the joints. Load drops across joints were calculated by subtracting the trailing section axial force from the measured leading

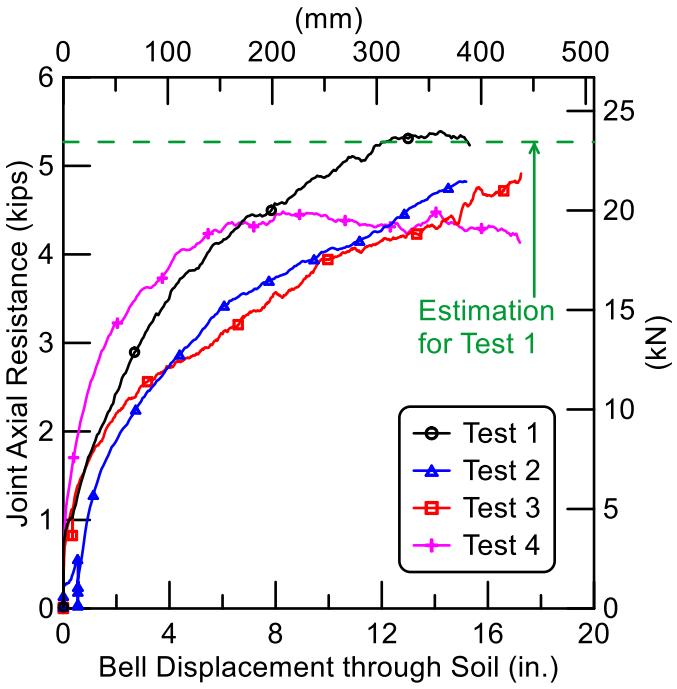

Figure 5.6. Joint Axial Resistance

section axial force. Figure 5.6 shows load drops across the joints for all four tests plotted against relative bell displacement through soil.

In Test 1, the spigot was a leading section, and the bell mouth faced north. The bell began displacing after about 0.74 kips (3.3 kN) of joint axial resistance and continued to increase with further displacement until reaching a peak resistance of 5.4 kips (24 kN) at 14.2 in. (360 mm) of bell displacement. Comparison of Tests 1 and 3 indicates that the orientation of the bell with respect to relative soil movement affects the load drop across the bell. The maximum measured load drop across the bell was approximately 15% larger when the flat face of the bell was oriented in the direction of pipe movement. There was also a stiffer response with this orientation.

The load drop at a joint can be estimated from the expression for face resistance of the leading edge of a jacked pipe proposed by Meskele and Stuedlein (2015) from the work of Weber and Hurtz (1981) whereby the axial resistance of the joint, R_f, is given by

$$R_f = r_f \frac{\pi}{4}\left[D_B{}^2 - D_S{}^2\right] \tag{1}$$

where D_B and D_S are the respective outside diameter of bell and spigot, and the unit face resistance, r_f, is expressed as

$$r_f = \lambda \cdot \sigma'_v \cdot \tan\phi' \tag{2}$$

where ϕ' is an effective soil friction angle, σ'_v is an effective overburden stress at the springline of the pipe, and λ is a carrying capacity coefficient. For $\phi' \leq 45°$, λ can be approximated as

$$\lambda = \frac{3\pi}{2} e^{\pi \tan\phi'} \tag{3}$$

The calculated axial resistance of the joint compares favorably with the data for Test 1, as shown in Figure 5.6. The axial resistance coincides with the maximum load drop at the joint for Test 1 and is greater than the maximum load drop for Test 3 by about 15%. The load drops for Tests 1 and 3 are for flat face and curved end bell movements, respectively, for which the curved end axial resistance is lower than that mobilized by the flat face.

5.6 Effect of Polyethylene Wrap

Of particular interest are the plots in Figure 5.6 for Tests 2 (polyethylene wrap) and 3 (curved end facing north), which show very similar axial force vs. displacement behavior. As discussed previously, a comparison between Tests 1 and 2 show that the reduction in load for the polyethylene wrap was not primarily related to reduction in shear resistance along the pipe barrel, but related to a reduction in load drop across the joint. Post-test excavation showed that the polyethylene wrap was torn and bunched up near the joint. It appears that the wrinkled and deformable polyethylene wrap reduced the bearing resistance of the bell flat face in response to axial joint movement. The joint resistance reduction from the deformable polyethylene wrap appears to have resulted in an axial force vs. displacement relationship very close to that for Test 3, where the curved bell was facing the direction of movement.

The experimental evidence shows that the polyethylene wrap in Test 2 reduced the pullout force by approximately 15% compared to the results of Test 1. This reduction of 15% is comparable to the load reduction of 15% for the curved end of the bell (Test 3) relative to the flat end of the bell (Test 1) facing the direction of axial movement. Moreover, the reduction of force for polyethylene wrap was related primarily to a reduction of load drop across the joint, which in turn was likely caused by the deformable polyethylene wrap reducing the resisting stresses acting on the bell. The test results show that the reduction in axial soil resistance with polyethylene wrap is affected by complex shear transfer between the joint and surrounding soil as the

polyethylene wrap compresses, folds, and tears. Additional testing and research are required to understand the mechanism for load transfer.

5.7 Soil/Pipeline Frictional Resistance

The difference between the measured end load (measured by load cell), F_{End}, and the load in the leading end section (measured by strain gages) provides the soil/pipeline frictional resistance, F, along a length of pipe spanning the north end of the box to the gage plane. Following the ASCE (1984) design guidelines, the frictional resistance per length of straight pipe, f, can also be calculated as:

$$f = \left(\frac{1 + K_o}{2}\right) \tan(\delta)\, \gamma H \pi D \tag{4}$$

where K_o is the lateral at-rest earth pressure coefficient and assumed to be 0.45 (O'Rourke et al., 1989), H is the depth to pipe springline, D is pipe outer diameter, γ is soil total unit weight, and δ is the pipe/soil interface friction angle. The frictional force per unit length for the leading section of each of the four pull tests is provided in Figure 5.7. The results from a similar axial resistance test performed on a straight section of DI pipe under similar test conditions (Stewart et al., 2012). The frictional force per length for the test setup ranges between approximately 278 lb/ft (4.1 kN/m) and 377 lb/ft (5.5 kN/m), which are equivalent to δ/ϕ values between 0.8 and 1.0. These values are shown in the plots for comparison with the measurements. For pipe in direct contact with soil (Tests 1, 3, and 4), the δ/ϕ value ranges from about 0.8 to 1.0 during the first

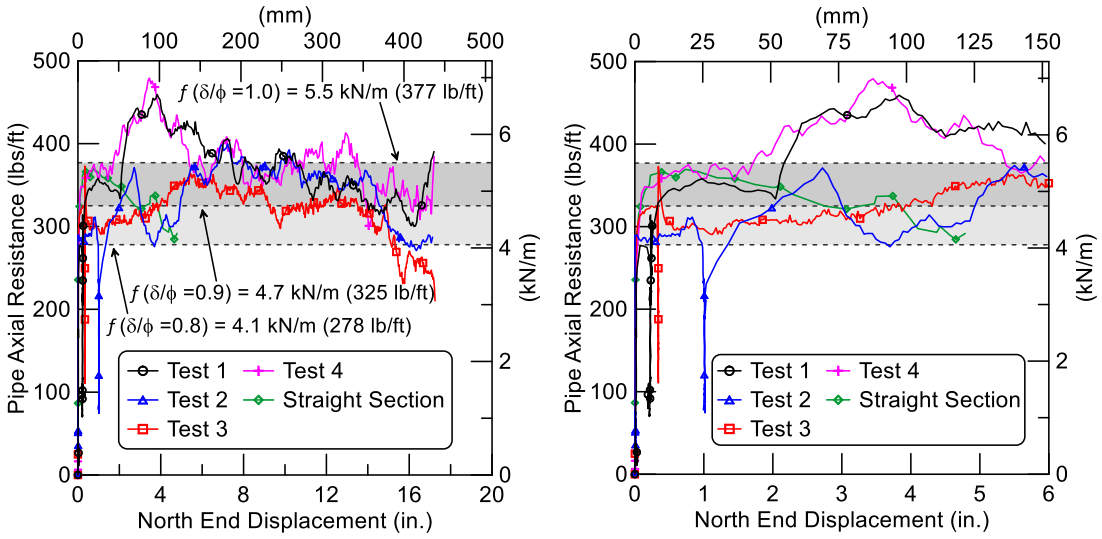

a) Full Displacement Range b) First 6 in. (150 mm) of Displacement

Figure 5.7. Frictional Resistance along Leading Section of Pipe

2.0 in. (50 mm) of displacement. At larger displacements the majority of results fall within the δ/ϕ range of 0.9 and 1.0, as shown in the Figure 5.7.

5.8 Summary

The axial soil resistance tests report on the soil-structure interaction associated with relative axial movement of DI pipe with the restrained axial slip joint through soil. The axial resistances created by the enlarged axial slip joints and soil/pipe friction are quantified, as well as the effect of the polyethylene wrap on the DI pipe with a restrained axial slip joint.

The maximum measured load drop across the bell was approximately 15% larger when the flat face of the bell was oriented in the direction of pipe movement. There

was also a stiffer response with this orientation. Ratio of interface to soil friction angle, δ/ϕ, estimated from these experiments ranges from about 0.8-1.0 at small axial displacements less than 2.0 in. (50 mm) and 0.9-1.0 for larger displacements. The application of polyethylene wrap did not result in a significant reduction in shear resistance along the pipe barrel, but related to a reduction in load drop across the joint. The deformable polyethylene wrap reduced the bearing resistance of the bell flat face such that joint resistance with polyethylene wrap over the flat face is very close to the joint resistance of the curved bell facing the direction of movement.

CHAPTER 6

FAULT RUPTURE TESTS

6.1 Introduction

One of the most significant trends in geotechnical earthquake engineering has been the implementation of large-scale testing facilities for soil-structure interaction, such as those at the Japanese National Research Institute for Earth Science and Disaster Prevention that have been used to characterize soil-pile interaction during liquefaction (Tokomatsu and Suzuki, 2004). In addition, large-scale fault rupture experiments at the Cornell Large-Scale Lifelines Testing Laboratory allow for soil-structure interaction at full scale so that conditions in the field can be simulated reliably under laboratory control, with detailed characterization and response measurements of soil and structure (O'Rourke et al., 2008). Fault rupture testing has the capability of imposing abrupt soil displacements on buried pipelines consistent with permanent ground deformation effects at fault crossings and the margins of lateral spreads and landslides. These sources of ground deformation impose the most severe conditions of soil-structure interaction that are experienced by underground pipelines and conduits in the field, and provide the basis for qualifying next generation of seismic resistant pipeline products as well as validating the numerical models for the analysis and design of such facilities.

The split-box test basin at Cornell can generate strike-slip fault rupture in over 99 tons (90 metric tons) of partially saturated sand per test with 4 ft. (1.2 m) of strike-slip displacement. In this chapter the results of large-scale fault rupture tests performed

at Cornell are presented for DI pipelines four different types of restrained axial slip joints. Each fault rupture test was designed to understand how the DI pipelines and specialized joints are able to accommodate the simultaneous axial movement and lateral offset that accompanies strike slip fault rupture at oblique angles of pipeline/fault intersection. Measuring simultaneous performance of multiple joints allows for confirmation that the pipeline will respond to ground failure as intended, understand the complex interaction among the different joints, and determine the maximum ground deformation and axial pipeline load that can be sustained before joint leakage.

6.2 Experimental Setup

A detailed description of the fault rupture tests performed on restrained axial slip joints covered in this work is provided in reports by Pariya-Ekkasut et al. (2015, 2016, 2017, 2018) and Stewart et al. (2015). Only the salient features of the tests are addressed herein.

Figure 6.1 is the plan view of the AMERICAN pipeline layout which shows the fault rupture plane and approximate locations of the four actuators generating basin movement. The pipeline consisted of five DI pipe segments with four restrained axial slip couplings. The intersection angle between the pipe and fault was 50°.

The pipeline was buried in the Cornell large-scale test basin in partially saturated sand that was compacted to have an average friction angle of $\phi' = 42^{o}$, equivalent in strength to that of a medium dense to dense granular backfill (O'Rourke, 2010). During

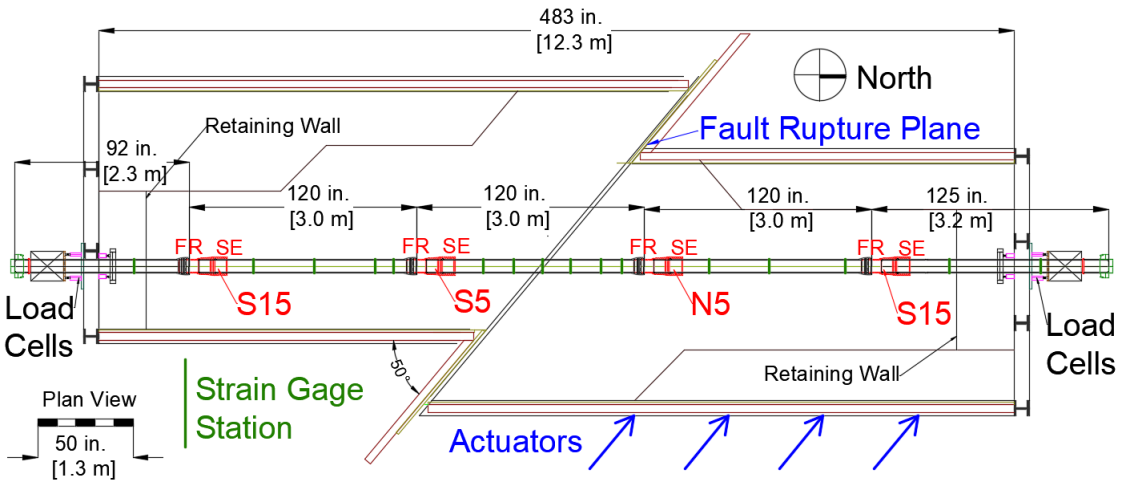

a) Overall Test Configurations

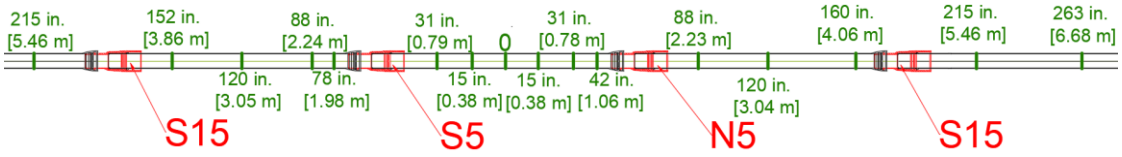

b) Strain Gage Layout

Figure 6.1. Plan View of Pipe Centered AMERICAN Restrained Axial Slip DI Pipeline in Test Basin

the test, the south part of the basin remained stationary, whereas the north part was displaced to the north and west by large-stroke actuators to cause soil rupture and slip at the interface between the two parts of the test basin.

The depth of burial to top of pipe was 30.0 in. (762 mm), resulting in the total soil depth of 48 in. (1.2 m). The length of the pipeline buried in soil was approximately 34 ft. (10 m). The pipe was pressurized with water to approximately 80 psi (550 kPa). The north (movable) portion of the test basin was connected to four MTS hydraulic actuators with load cells controlled by a MTS Flextest GT controller. Two short-stroke

actuators (SSAs) and two long-stoke actuators (LSAs) are connected between the movable portion of the test basin and the modular reaction wall in the laboratory. Each SSA has a displacement range of ± 2 ft (± 0.61 m) for a total stroke of 4 ft (1.22 m) and load capacity of 100 kips (445 kN) tension and 145 kips (645 kN) compression. Each LSA has a displacement range of ± 3 ft (0.91 m) for a total stroke of 6 ft (1.83 m) and load capacity of 63 kips (280 kN) tension and 110 kips (489 kN) compression. All actuators were operated in synchronized displacement control.

6.2.1 Test Procedure

The general test procedure followed for this test is similar to that followed for the other fault ruptures tests covered in this chapter. After all instruments were installed, soil placed, and pipe filled and initially pressurized with water to 80 psi (550 kPa), the test procedure was as follows:

a) Begin data acquisition and start the servo-controlled hydraulic system,
b) Verify constant internal water pressure of 80 psi (550 kPa),
c) Move the test basin at a rate of 1 ft./minute (305 mm/minute) until pipe failure (full pressure loss),
d) Stop basin movement but maintain hydraulic actuator pressure,
e) Verify data acquisition, and
f) Excavate.

6.2.2 Instrumentation

Figure 6.1 shows the location of the instrumentation along the AMERICAN pipeline. The instrumentation consisted of sixteen strain gage planes along the pipeline,

four load cells at the ends of the pipeline, and string pots to measure joint displacements and rotations. Strain gages were installed at the crown, invert, and springline of the pipe at different locations along the pipeline to measure strains and to evaluate axial forces and bending moments. Strain gage locations were chosen on the basis of the expected deformed shape and axial behavior of the pipeline as determined from direct tension and four-point bending tests as well as the results of finite element analyses used to design the test. The strain gage locations in the AMERICAN pipeline are presented in Figure 6.1 b).

6.2.3 Soil Preparation

The soil used during the tests was crushed, washed, glacio-fluvial sand obtained from RMS Gravel, Dryden, NY, consisting of particles mostly passing the ¼ in. (6.35 mm) sieve. Figure 6.2 is the grain size distribution of the RMS graded sand. Approximately 6-in. (152-mm)-thick lifts of soil were placed and compacted until there was approximately 30 in. (760 mm) cover of compacted sand above the pipe crown. Every layer was compacted to the same extent and moistened with water in a similar way to achieve uniformity. Dry density measurements were taken for each layer using a Troxler Model 3440 densitometer. Moisture content measurements were obtained using both soil samples and the densitometer at the same locations.

The target value of dry density was γ_{dry} = 106 lb/ft^3 (16.7 kN/m^3), and the target value of moisture content was w = 4.0%, corresponding to an angle of shearing resistance (friction angle) of the sand of approximately 42º. Eight measurements of dry

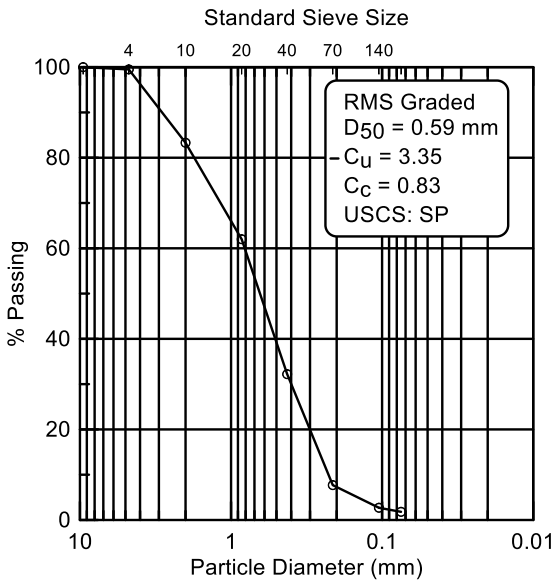

Figure 6.2. Particle Size Distribution of RMS Graded Sand

unit weight and moisture content were made for each soil lift. The soil strength properties are representative of a well-compacted dense sand.

6.3 Experimental Results of AMERICAN Restrained Axial Slip DI Pipeline

As shown in Figure 6.1, the AMERICAN restrained axial slip DI pipeline consisted of five DI pipe segments and four EJS castings. The designations of the four EJS castings from south to north are S15, S5, N5, and N15 where S and N stands for the south and north direction of an EJS from the fault rupture plane, respectively, and the following number refers to the distance from an EJS to the fault in feet. A 115-in. (2.92-m)-long pipe section was placed directly over the fault. Two identical pipes with EJS castings were installed to the north and the south of the center pipe. A 120-in. (3.05-m)-long pipe with an EJS casting was connected at the north end of the pipeline. Lastly,

a 95.8-in. (2.43-m)-long pipe with an EJS casting was connected at the south end of the pipeline. All joints were installed at fully-inserted positions. The average and standard deviation of all dry unit weight measurements were 108.4 lb/ft^3 (17.0 kN/m^3) and 1.1 lb/ft^3 (0.17 kN/m^3), respectively. Moisture content measurement had an average of 4.4% and standard deviation of 0.6%.

The pipeline was able to accommodate 36.0 in. (914 mm) of fault displacement before the pipe lost pressure. This fault displacement corresponds to 23.1 in. (587 mm) of axial pipeline displacement and an average tensile strain of 4.8% along the pipeline. After verification of total pressure lost, the test was then stopped at 38.5 in. (978 mm) of fault displacement. The failure mode for this test was ductile iron breakage at the FR bell of joint S15 as shown in Figure 6.3.

6.3.1 Deformed Shape of Pipeline

Figure 6.4 a) shows a photo of the pipeline before backfilling and burial of the pipe. After fault rupture, the pipeline was excavated carefully in a manner that preserved its deformed shape as shown in Figure 6.4 b). Angles of S5 and N5 EJS rotations are also illustrated in Figure 6.4 b). These rotation angles were obtained from the survey data as discussed in the next section.

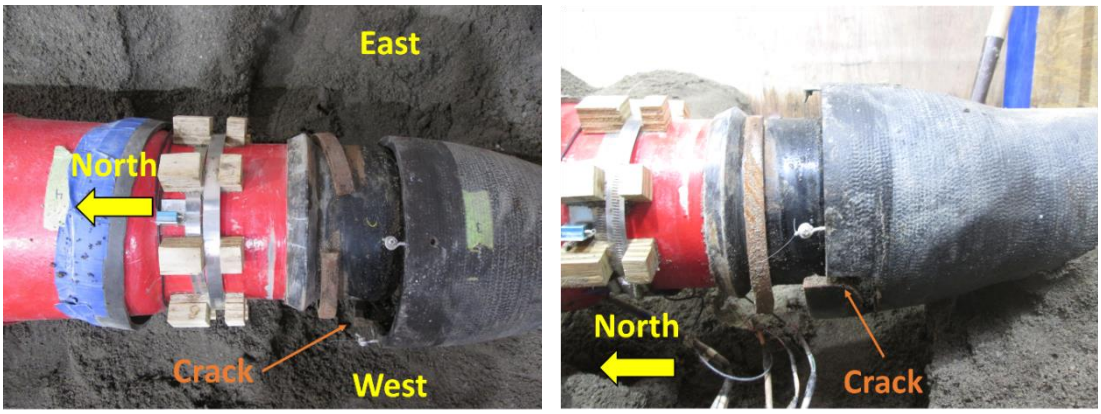

a) Plan View of S15 FR Bell

b) Elevation View of S15 FR Bell from West Springline

Figure 6.3. AMERICAN Pipe Rupture at S15 FR Bell following Test

6.3.2 Survey Data

The Bovay Laboratory uses a general coordinate system established in 2012 as part of Cornell's participation in the George E. Brown, Jr. Network for Earthquake Engineering Simulation (NEES). The coordinate system was developed with a Leica Flexline TS02 reflectorless total station to identify baseline positions within the laboratory. When the AMERICAN pipe was placed in the basin and backfilled to approximately the springline depth, survey measurements were taken at marked locations every 12 in. (25 mm) along the pipe crown. These data provide a baseline of the initial pipeline position, albeit prior to complete backfill. Following careful pipe excavation with minimal disturbance, the pipeline was re-surveyed. The actuator loads were maintained as the pipeline was excavated and exposed for survey measurements to minimize relaxation and sustain the pipeline deformation that was experienced immediately after pipeline failure.

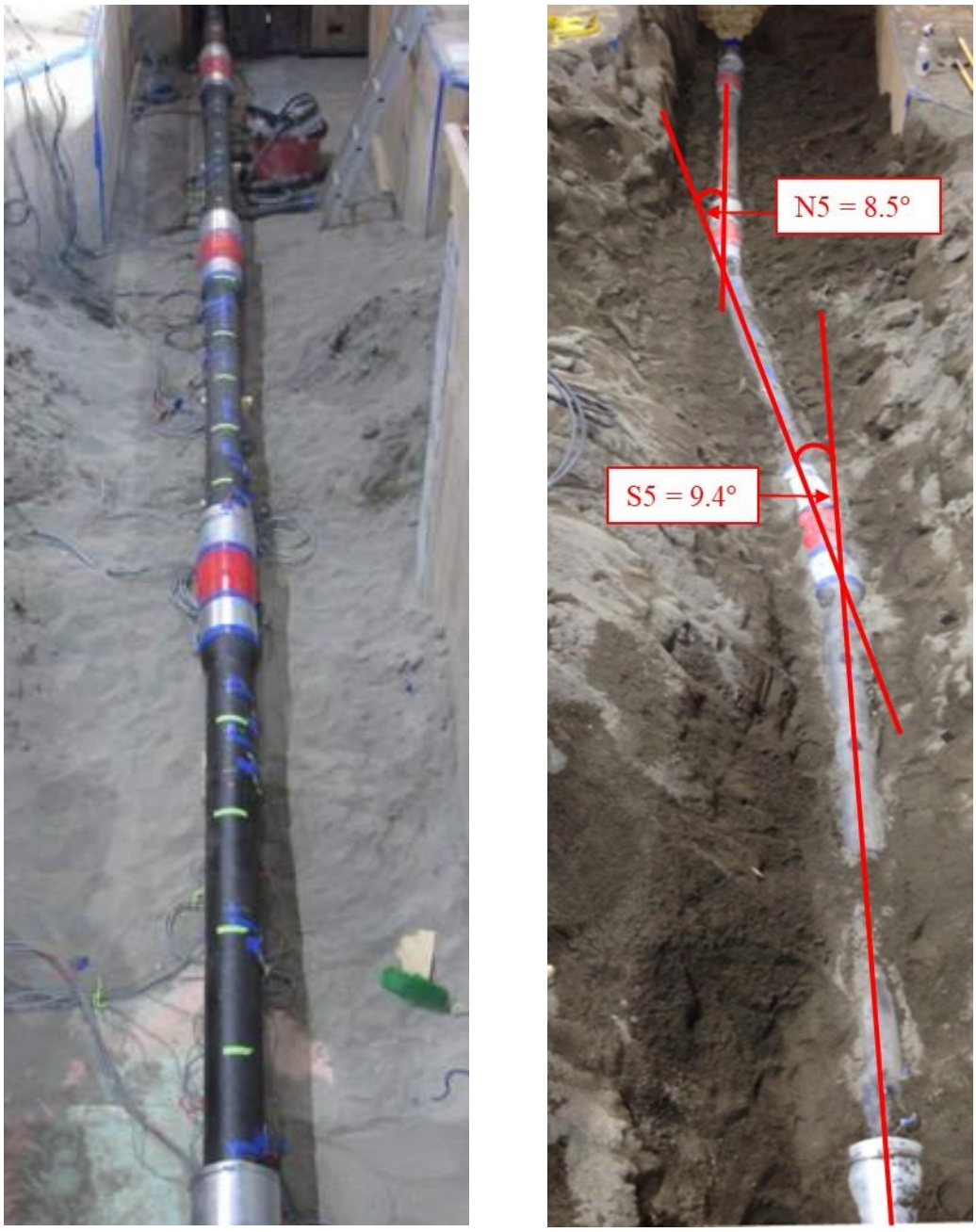

a) Before Burial b) After Excavation

Figure 6.4. Images of AMERICAN Pipeline Positions (angles shown from total station surveying measurements)

Figure 6.5 shows, on a greatly exaggerated scale, the survey data for the initial and final pipeline positions. It should be noted that the pipeline lost pressure at 36.0 in. (914 mm) of fault displacement, whereas the final pipeline position was surveyed after excavation at 38.5 in. (978 mm) of fault displacement. The survey data suggest that, at 38.5 in. (978 mm) of fault displacement, the pipeline moved 23.6 in. (599 mm) axially with 27.5 in. (699 mm) of lateral offset. The S15, S5, N5, and N15 EJS displacements were 9.9 in. (251 mm), 4.0 in. (102 mm), 4.6 in. (117 mm), and 4.7 in. (119 mm), respectively. The displacement at the S15 EJS was largest because the pipeline failed and was pulled out at the S15 FR joint.

The S5 EJS displacement was smaller than those of the other EJSs. Figure 6.1 shows that the SE joint of the S5 EJS is closest to the fault, resulting high rotation at the S5 SE joint. As illustrated in Figure 1.1 and discussed in Section 1.3.1, the SE joint is designed to accommodate a large axial slip, but can only accommodate a small amount of rotation. The high rotation caused the S5 SE spigot to be stuck inside the deep socket, and thus the S5 EJS could not be pulled out to the full range of displacement. In addition, the rotations of the S5 EJS and N5 EJS were 9.4° and 8.5°, respectively. The rotation measurements at the other two EJSs were, however, too small to provide useful information.

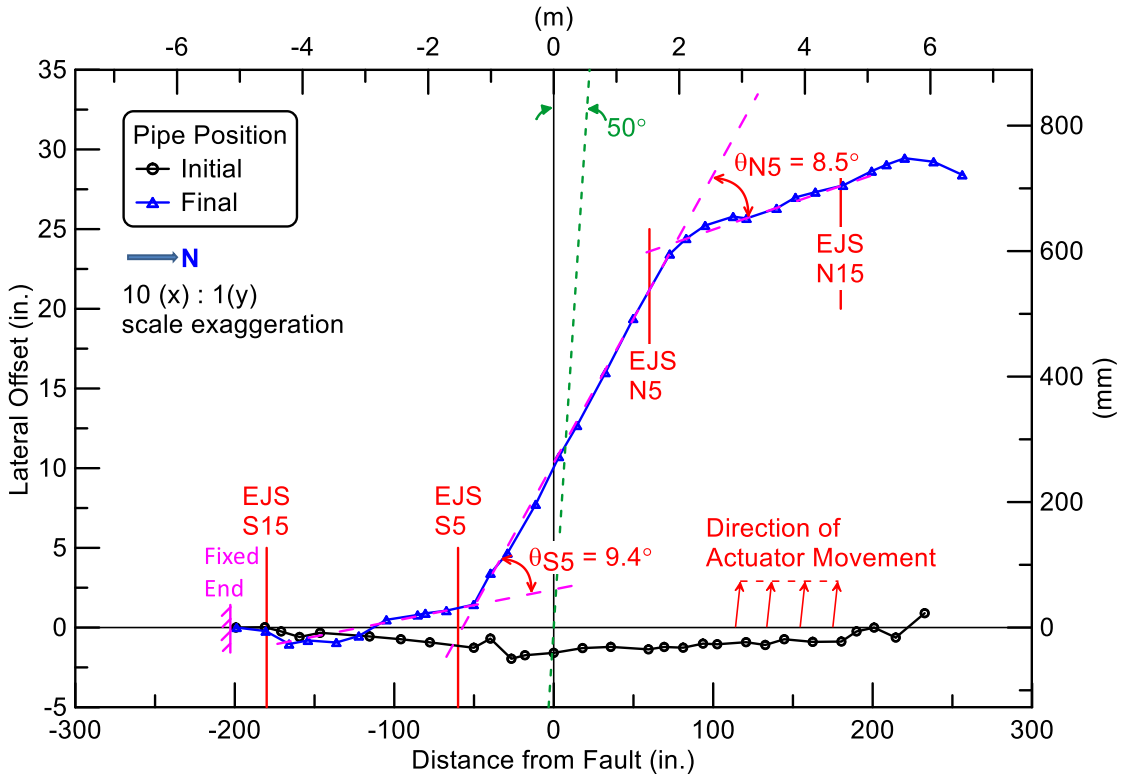

Figure 6.5. Initial and Final AMERICAN Pipeline Positions from Surveying Measurements

6.3.3 Joint Pullout

The joint pullout movements were measured by string potentiometers (string pots) and compared with survey measurements. The axial movements of the S15, S5, N5, and N15 EJSs vs. fault displacement are shown in Figure 6.6. Joint slip initiated at the north joint closest to the fault plane, N5 EJS, and continued until slip was resisted at 13 in. (330 mm) of fault displacement by the spigot weld ring contact with the locking ring. Axial slip was initiated next at the south joint closest to the fault, S5 EJS. It also moved until slip was resisted. Similar slip initiation and movement occurred in the

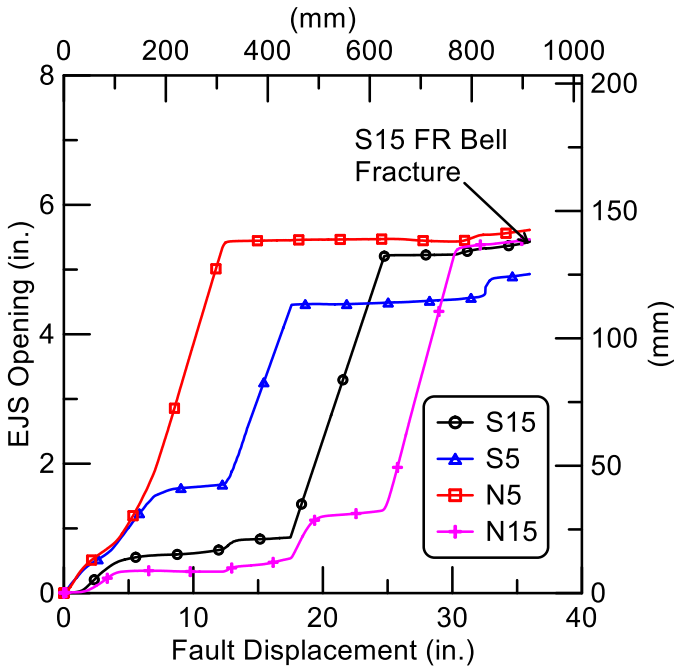

Figure 6.6. EJS Displacements vs. Fault Displacement

Table 6.1. Maximum AMERICAN EJS Displacement

EJS Location	EJS Displacement (in.)	
	String Pot Data [a]	Survey Data [b]
S15	5.4	9.9
S5	4.9	4.0
N5	5.6	4.6
N15	5.5	4.7
Average	5.4	5.8
All four EJS joints	∑ = **21.5**	∑ = **23.2**
Axial Basin Extension (in.)	(36.0 in.) cos 50° = **23.1**	
Direct Tension Tests	Three fully extended EJS = 5.3 in. × 3 = 15.9 in. One failed EJS = 5.5 in.	∑ = **21.4**

1 in. = 25.4 mm

[a] EJS displacement when pipe failure at 36.0 in. (914 mm) of fault displacement

[b] EJS displacement after test end at 38.5 in. (978 mm) of fault displacement

remaining joints until all joints had moved through their maximum range of movement. Failure occurred at a fault displacement of approximately 36.0 in. (914 mm) at the south joint farthest the fault, S15 EJS, by cracking and leaking of the S15 FR bell.

The movement of each EJS at the end of the test is presented in Table 6.1. String pot and survey measurements of the EJS movements are different because they were recorded at different fault displacements. The string pot data correspond to EJS movements immediately before the S15 EJS failed at 36.0 in. (914 mm) of fault displacement. The test was stopped at a fault displacement of 38.5 in. (978 mm), after which the pipeline was exposed, and the survey measurements were taken.

6.3.4 Joint Rotations

Joint rotations were measured with the string pots at each joint and compared with survey measurements. As illustrated in Figure 1.1, rotation across the AMERICAN EJS involves rotation of both the FR and SE joints within the joint system. During the fault rupture test the S5 SE and N5 FR joints were closest to the fault rupture plane. Figures 6.7 and 6.8 show the FR and SE joint rotations vs. fault displacement. The S5 SE joint reached a maximum rotation of 3.6° at 9.0 in. (229 mm) of fault displacement. At approximately the same fault movement, rotation of the S5 FR joint started as the EJS rotation shifted from the SE to FR joint. For the remainder of the test, rotation increased in the S5 FR joint, whereas rotation declined by a small amount in the S5 SE joint. The data indicate that the S5 SE joint had limited capacity for joint rotation under

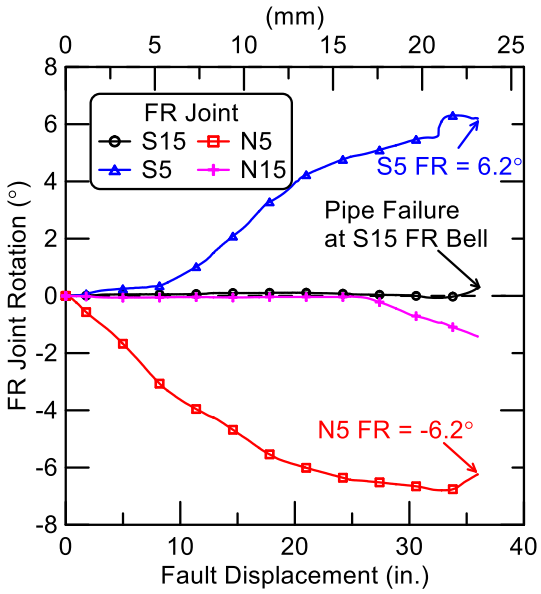

Figure 6.7. FR Joint Rotations vs. Fault Displacement

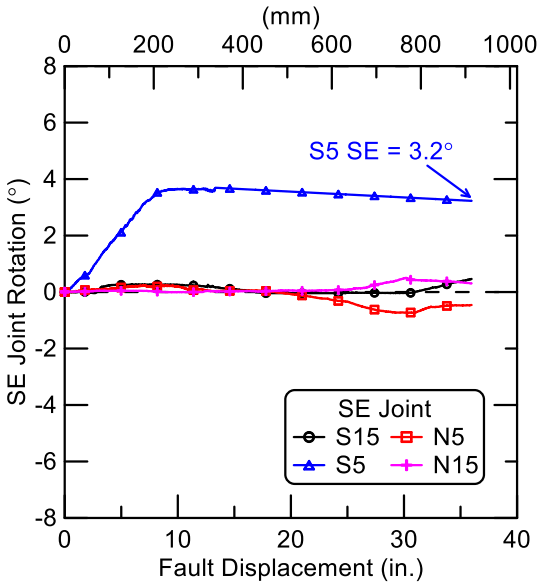

Figure 6.8. SE Joint Rotations vs. Fault Displacement

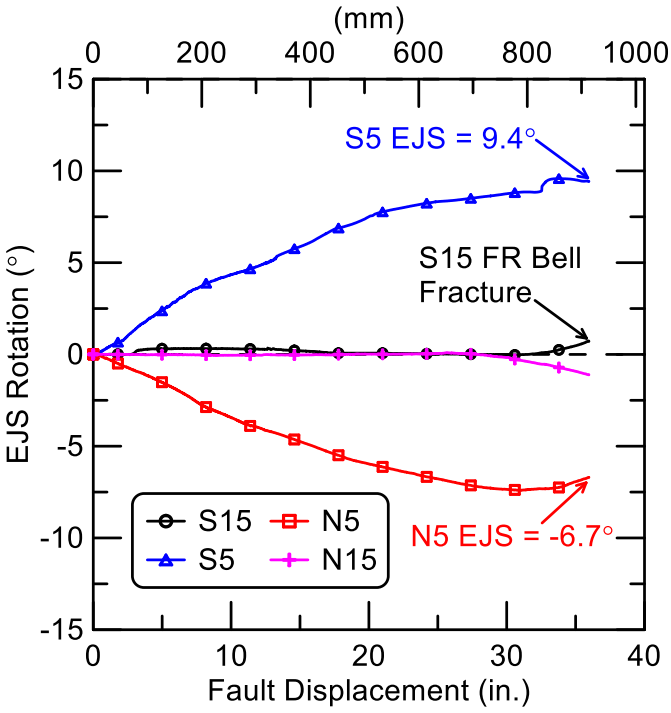

Figure 6.9. EJS Rotations vs. Fault Displacement

Table 6.2. Maximum AMERICAN EJS Rotation

EJS Location	EJS Rotation (°)	
	String Pot Data [a]	Survey Data [b]
S15	0.7	N/A
S5	9.4	9.4
N5	-6.7	-8.5
N15	-1.1	N/A

Positive refers to rotation in counter-clockwise direction
[a] Rotation when pipe failure at 36.0 in. (914 mm) of fault displacement
[b] Rotation after test end at 38.5 in. (978 mm) of fault displacement

the combined axial slip and rotation imposed by fault movement for joint rotation under the combined axial slip and rotation imposed by fault movement. In contrast, the S5 FR joint had greater capacity for rotation. The greater rotational capacity of the FR joint is also shown by the 6.2° rotation of the N5 FR joint, whereas negligible to small rotations were recorded at the N5 SE joint.

EJS rotations are the sums of FR and SE joint rotations. They are plotted relative to fault displacement in Figure 6.9. As the test basin was displaced, the south joint closest to the fault, S5 EJS, accommodated most of the fault offset with maximum rotation of nearly 9.4° in a counter-clockwise rotation without failure. The N5 EJS, which was the joint closest to the fault on the north side, rotated in a clockwise direction of 6.7°. The joints located farthest from the fault show maximum rotations of approximately 1°.

The maximum rotations of each EJS obtained from string pot measurements and survey data are presented in Table 6.2. As discussed in the previous section, string pot

and survey measurements of the EJS rotations are different because the string pot data correspond to the EJS rotations at 36.0 in. (914 mm) of fault displacement, whereas the survey data were taken at 38.5 in. (978 mm) of fault movement.

6.3.5 Pipe Axial Forces

The test basin end loads were measured with four load cells at the south end of the test basin and four load cells at the north end. Figure 6.10 shows the total load at the south and north ends of the test basin vs. fault displacement. The end loads were near zero during the beginning part of the test, and then increased sharply at a fault displacement of approximately 30.0 in. (762 mm). At 36.0 in. (914 mm) of fault displacement, maximum loads of 95.0 kips (423 kN) and 90.3 kips (402 kN) were measured at the south and north ends, respectively.

Also included in Figure 6.10 are loads calculated with the axial strain gage measurements at the stations 215 in. (5.46 m) south and 263 in. (6.68 m) north of the fault, which were close to the south and north ends of the test basins, respectively. The axial force from strain gage measurements was calculated as $F = \varepsilon AE$. The outside diameter of the pipe was OD = 6.9 in. (175 mm) and the average measured wall thickness was t_W = 0.3 in. (7.6 mm). This gives a pipe wall cross-sectional area, A = 6.22 in.^{2} (4,013 mm^2). The Young's modulus of the DI was E = 24,200 ksi (169 GPa), which was determined from tensile coupon tests. The maximum load calculated from the north gages was 84.6 kips (376 kN), which is about 6% lower than the maximum

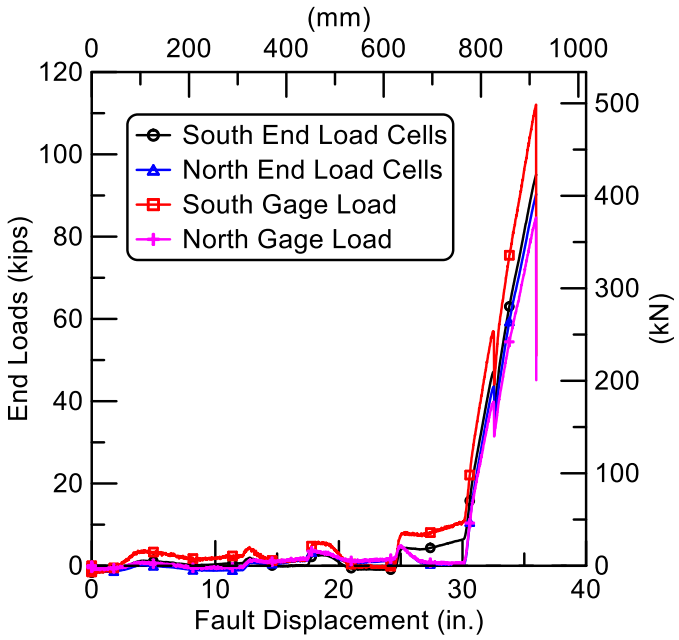

Figure 6.10. Comparisons of End Forces from Load Cells and Strain Gages for AMERICAN Pipe Fault Rupture Test

load of 90.3 kips (402 kN) measured by the north load cells. The maximum load attained at the south gage station was 112 kips (498 kN), which was noticeably higher than the measured south end load. This load, however, agrees well with 112 kips (498 kN) maximum axial load measured at the station on the north side of the S15 joint [station 152 in. (3.86 m) south of the fault].

The loads at each gage plane along the pipeline, determined from the axial gage measurements, are presented in Figure 6.11 for various levels of fault displacement. The EJS locations are shown by red shaded areas. Figure 6.11 a) shows the tensile forces up to 15 in. (380 mm) of fault movement. Relatively low tensile forces were measured along the pipeline during these initial increments of displacement. The highest axial

force was detected near the fault location, and the loads were lower at locations further away from the fault.

Figure 6.11 b) (note change in scale for load) shows that tensile forces were generally higher with increasing fault displacement. The highest axial force was detected near the S5 SE joint. However, a rapid increase in tensile force was observed at the -152 plane, which was located near the S15 SE joint.

Figure 6.11 c) shows that the loads increased rapidly from 30 in. (762 mm) to 36 in. (914 mm) of fault displacement. All joints attained contact between the spigot weld rings and the locking rings at 30 in. (762 mm) of fault displacement. About the same levels of maximum tensile loads were measured along the pipeline during these displacements, with the loads slightly higher towards the south end of the test basin. The peak forces of approximately 112 kips (498 kN) were found near S15 joints at -215 and -152 planes.

Figure 6.12 shows the force vs. displacement plots of EJSs in the fault rupture test compared to the force vs. displacement relationship from the direct tension tests. The force at each EJS was taken from the average calculated load of the south and north gage stations closest to the EJS. The S5 displacement was smaller than the other EJS displacements. As discussed in Sections 0 and 6.3.4, the S5 SE joint experienced high initial rotation after which rotation was transferred to the S5 FR joint. It appears that rotation of the S5 SE joint restricted axial slip so that the EJS opening was

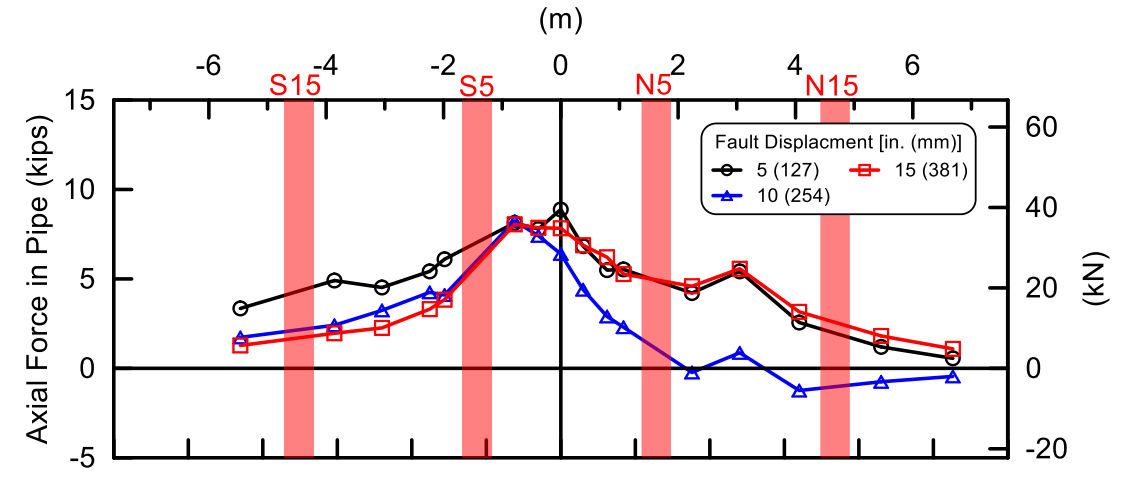

(a) 5 to 15 in. (127 to 381 mm) of Fault Displacement

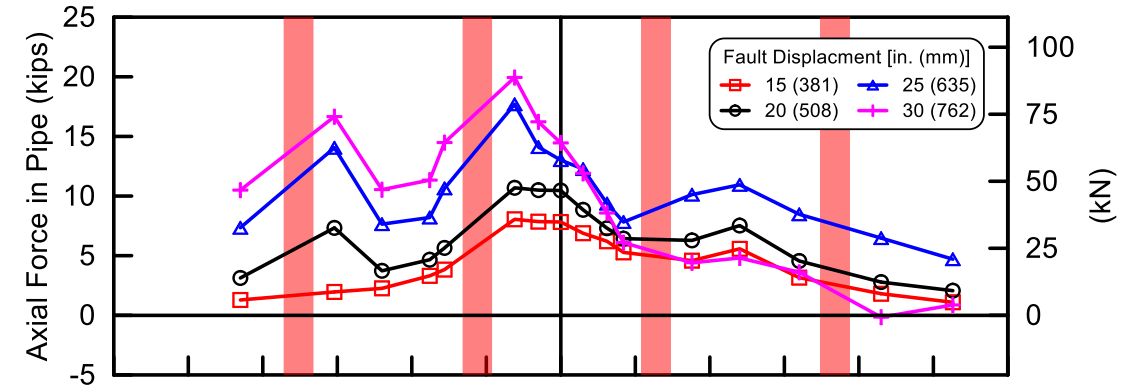

(b) 15 to 30 in. (381 to 762 mm) of Fault Displacement

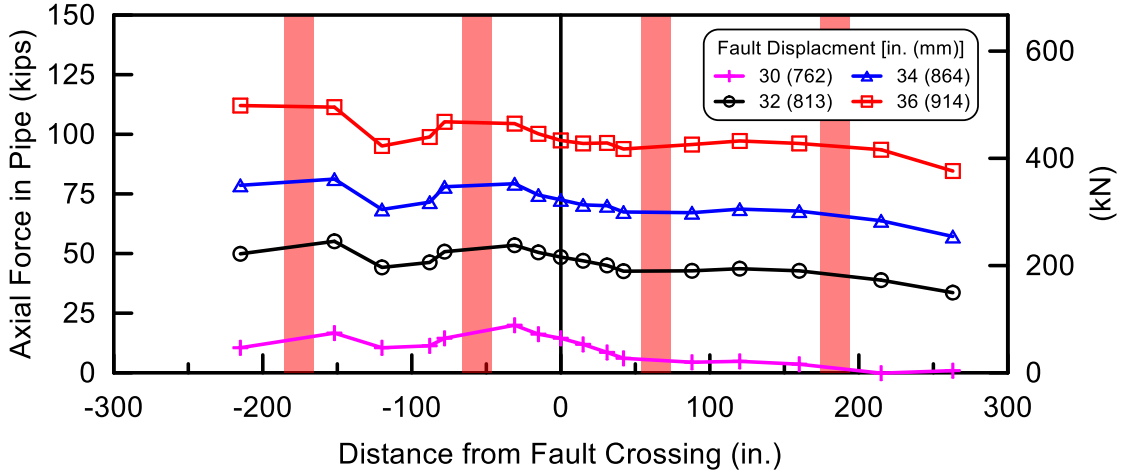

(c) 30 to 36 in. (762 to 914 mm) of Fault Displacement

Figure 6.11. Axial Forces in AMERICAN Pipeline vs. Distance from Fault

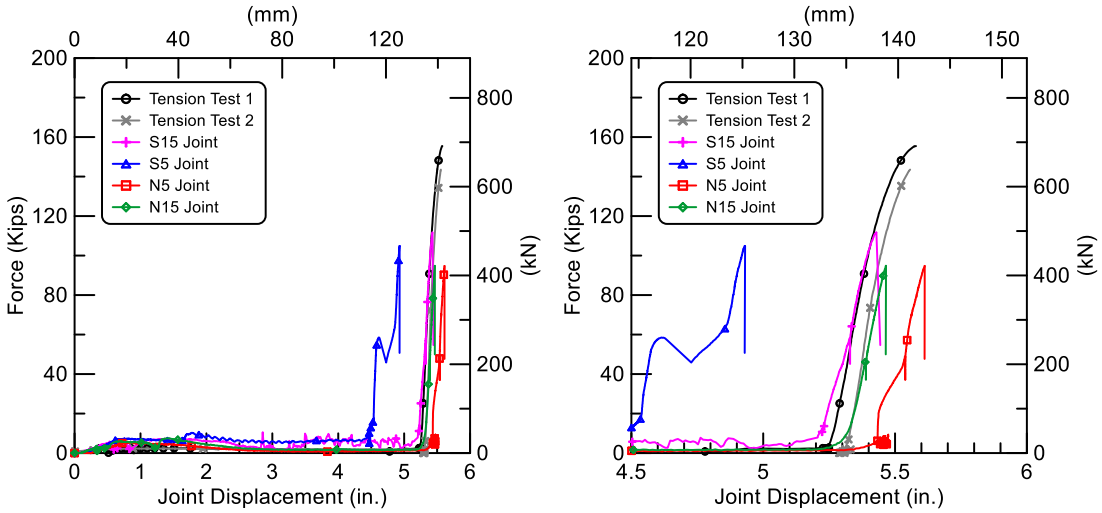

a) Full Displacement Range b) Between 4.5 in. and 6 in. (114 mm and 152 mm)

Figure 6.12. Joint Axial Force vs. Displacement Comparisons for AMERICAN Pipes

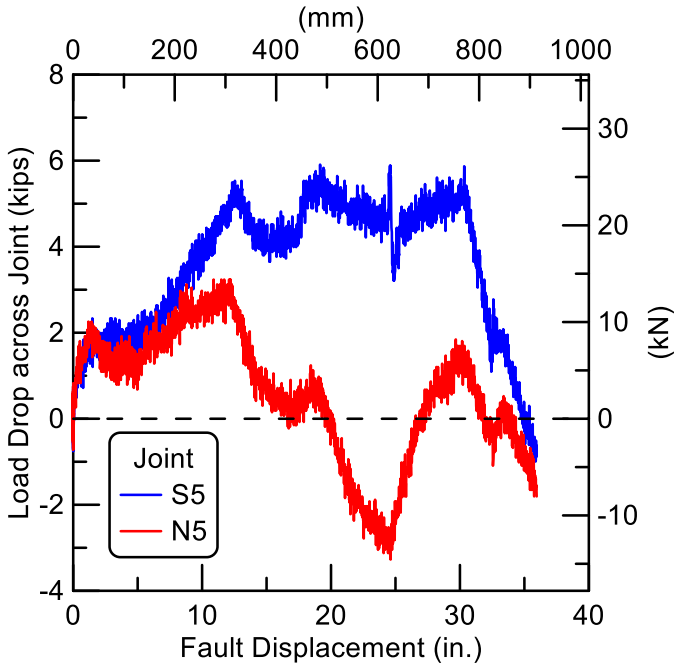

Figure 6.13. Load Drop across AMERICAN Joint vs. Fault Displacement

approximately 1 in. (25 mm) less than the other three EJSs. A maximum load of 112 kips (498 kN) was observed at the S15 EJS in the fault rupture test. This load is 25% lower than the direct tension load reported in Section 3.5.1.1. Axial loads at the other joints were 25 to 35% lower than the direct tension test load.

Figure 6.13 shows the load drops across the closest joints south, S5, and north, N5, of the fault plane. The load drop across the S5 joint is calculated by subtracting the load at the station 31 in. (0.79 m) south of the fault with the load at the station on the south side of the joint [station 78 in. (1.98 m) south of the fault]. Similarly, the load drop across the N5 joint is calculated by subtracting the load at the 42 in. (1.06 m) north of the fault with the load at the station on the north side of the joint [station 88 in. (2.23 m) north of the fault]. The load drop across the S5 joint initiated at the beginning of the test, and continued to increase until it reached 5.5 kips (24 kN) at about 11 in. (279 mm) of fault displacement. The load drop then varied between approximately 4 and 6 kips (18 and 27 kN) until about 30 in. (762 mm), at which time all joints were fully extended. The load drop across the S5 joint decreased rapidly for the remainder of the test. There was virtually no load drop across the S5 joint at the end of the test. The load drop across the N5 joint also initiated at the beginning of the test, and continued to increase until it reached 3.2 kips (14 kN) at about 11 in. (279 mm) of fault displacement. The N5 load drop then decreased rapidly, became negative, and reached -3.3 kips (15 kN). Negative values of load drop indicate that the N5 joint moved north and away from the fault plane during this part of the test. The N5 load drop varied between about 2 and -2 kips (9 and -9 kN) for the remainder of the test.

6.3.6 Bending Moments

Bending moments, M, were calculated at each strain gage station along the pipeline as:

$$M = \frac{\varepsilon_{bend} EI}{c} \tag{5.2}$$

where the bending strain, $\varepsilon_{bend,}$ is one half the difference between the springline strains; E is the DI Young's modulus of 24,200 ksi (169 GPa); I is moment of inertia of 33.9 in^4 (1,410 cm^4); and c is distance to outer fiber of 3.45 in (87.6 mm). Figure 6.14 presents the moments measured along the pipeline at various levels of fault displacement. The EJS locations are also shown by red shaded areas. Figure 6.14 a) shows that, during the first 15 in. (381 mm) of fault displacement, moments along the pipeline were relatively low. The measurements disclose an anti-symmetric pattern of moment distribution centered on the fault. Figure 6.14 b) (note change in scale for moment) shows that the moments were higher as the fault movement increased. The peak moments were detected near S5 and N5 locations. Figure 6.14 c) shows a similar pattern of bending moment distribution for fault movements of 30 in. (762 mm) to 36 in. (914 mm). At a fault displacement of 30 in. (726 mm) the maximum moments are on the order of 200 kip-in. (22.6 kN-m) in the vicinity of the S5 and N5 EJSs. Low moments were measured at the fault location because it was close to the inflection point of the pipeline.

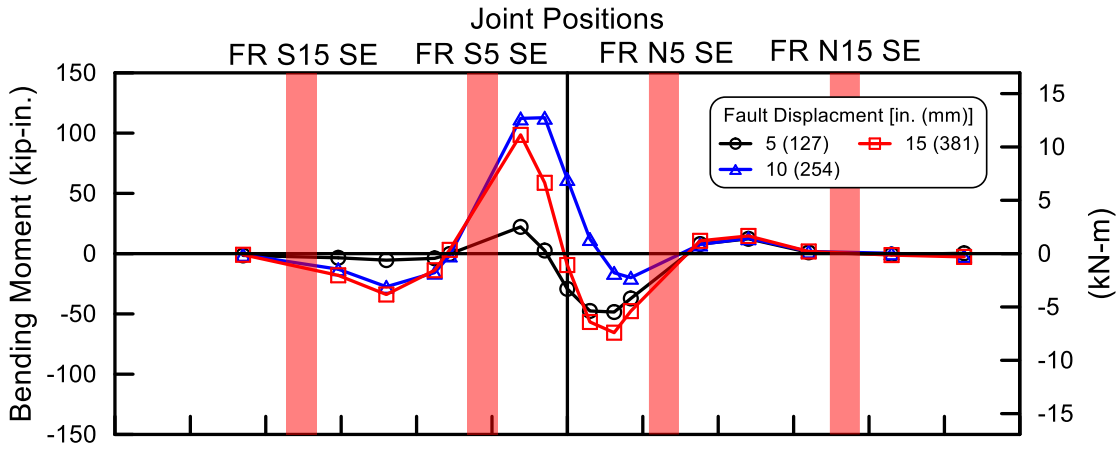

(a) 5 to 15 in. (127 to 381 mm) of Fault Displacement

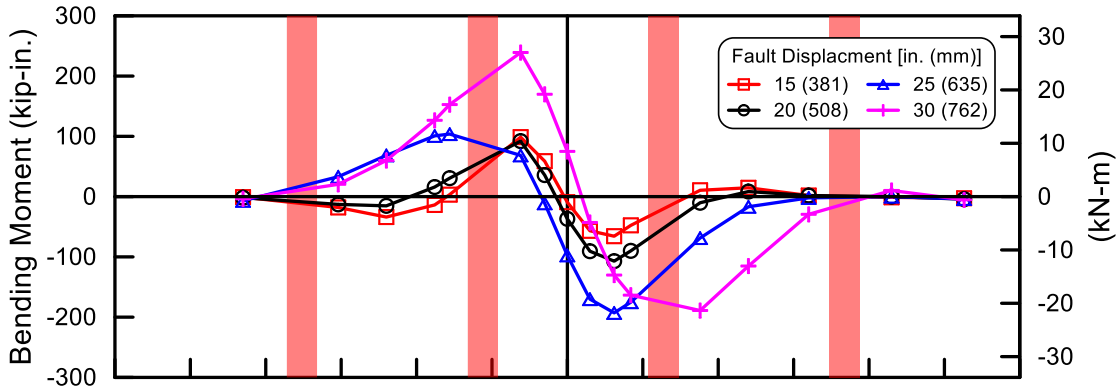

(b) 15 to 30 in. (381 to 762 mm) of Fault Displacement

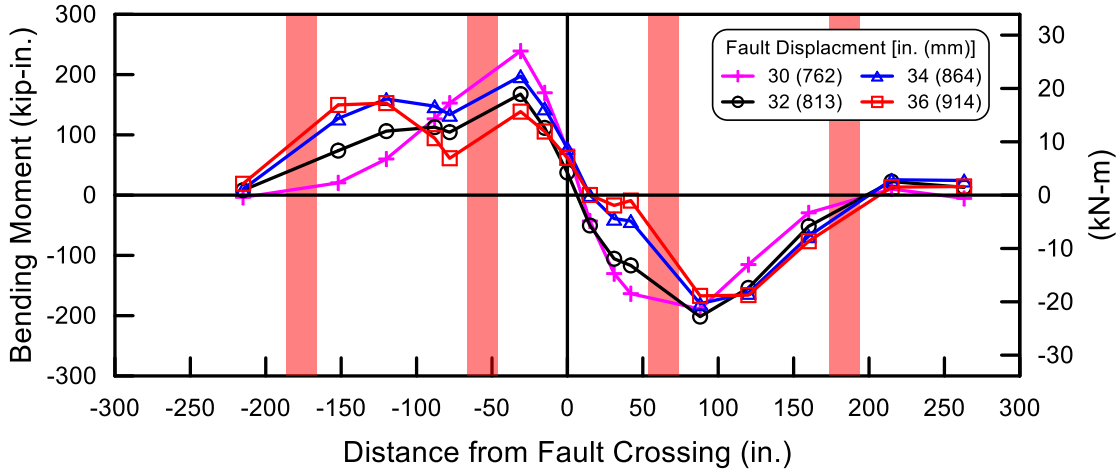

(c) 30 to 36 in. (762 to 914 mm) of Fault Displacement

Figure 6.14. Bending Moments in AMERICAN Pipeline vs. Distance from Fault

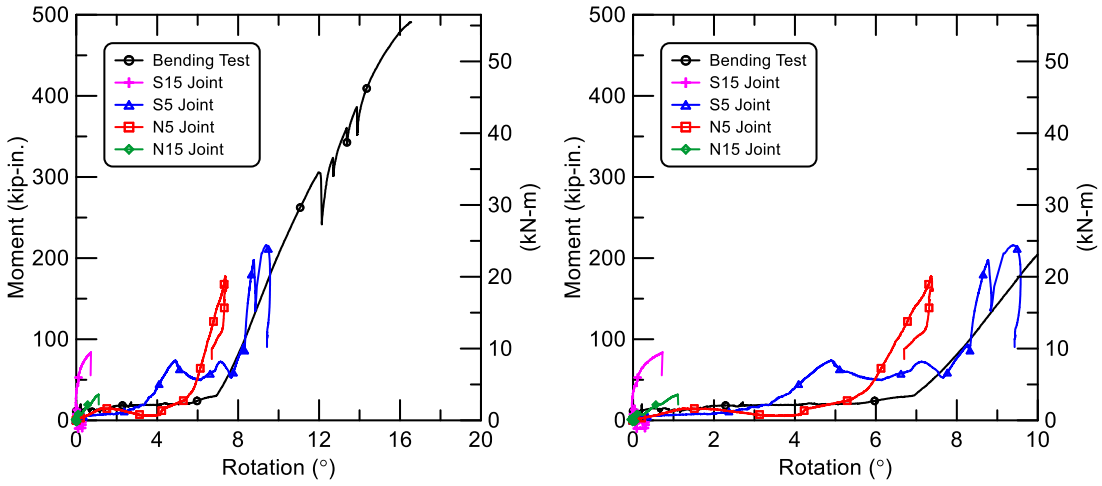

a) Full Range b) First 10° of Rotation

Figure 6.15. Joint Moment vs. Rotation Comparisons for AMERICAN Pipes

Figure 6.15 shows the moment vs. rotation plots for the EJSs derived from fault rupture test measurements in comparison with the moment vs. rotation relationship from the four-point bending test. The moment of each EJS in the fault rupture test was taken from the average calculated moments of the south and north gage stations closest to the joint. The rotations at the S15 and N15 EJSs are small and may be neglected. The moment vs. rotation plots of the S5 and N5 EJSs are in reasonable agreement with the four-point bending test results.

6.4 Experimental Results of Kubota Restrained Axial Slip DI Pipeline

The test procedure, soil placement method, and soil density and strength characteristics associated with the Kubota fault rupture test are very similar to those for the AMERICAN fault rupture test. The reader should refer to Sections 6.2.1 and 6.2.3 for information about the general test procedure and soil characteristics. There are some

small differences in the soil properties. The average and standard deviation of all dry unit weight measurements were 105.6 lb/ft^3 (16.6 kN/m3) and 1.5 lb/ft^3 (0.24 kN/m3), respectively. Moisture content measurements showed an average of 3.7% and standard deviation of 0.5%.

Figure 6.16 shows the layout and the location of the instrumentation along the Kubota DI pipeline with restrained axial slip joints. The Kubota pipeline consisted of seven DI pipe segments with six restrained axial slip joints. The designations of the six joints from south to north are S18, S15, S5, N5, N15, and N18, where S and N stands for the south and north direction of a joint from the fault rupture plane, respectively, and the following number refers to the distance from a joint to the fault in feet. A spigot projection (DI ring) was screwed onto each spigot in the fault rupture test, whereas the spigots in the direct tension and four-point bending tests had welded spigot projections, as shown in Figure 6.17. It was expected that a screw-on spigot projection would have a lower tensile capacity than a welded spigot projection.

A 128-in. (3.25-m)-long pipe section was placed directly over the fault. Two identical 128-in. (3.25 m)-long pipes were installed to the north and the south of the center pipe. Two 36-in. (0.91 m)-long pipes were assembled to the north and the south of the three identical 128-in. (3.25 m)-long pipes. A 87-in. (2.2-m)-long pipe was connected at the north end of the pipeline and had 36 in. (0.91 m) of its portion buried in the soil. Lastly, a 71-in. (1.8-m)-long pipe was connected at the south end of the pipeline with 25 in. (0.64 m) of its portion in the test basin. All joints were fully inserted.

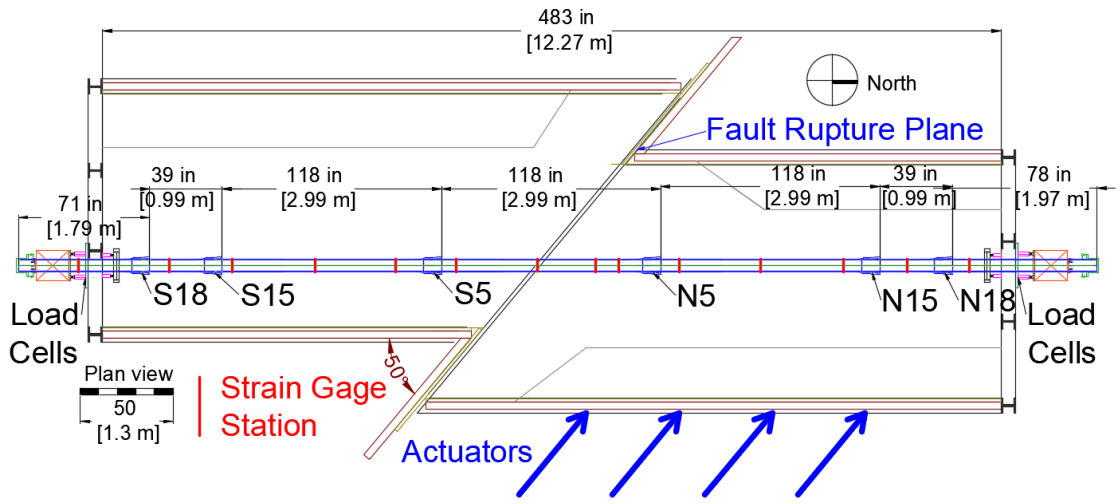

a) Overall Test Configurations

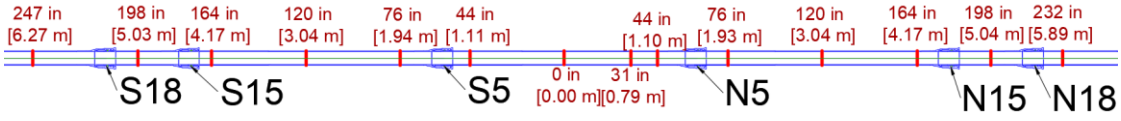

b) Strain Gage Layout

Figure 6.16. Plan View of Pipe Centered Kubota Restrained Axial Slip DI Pipeline in Test Basin

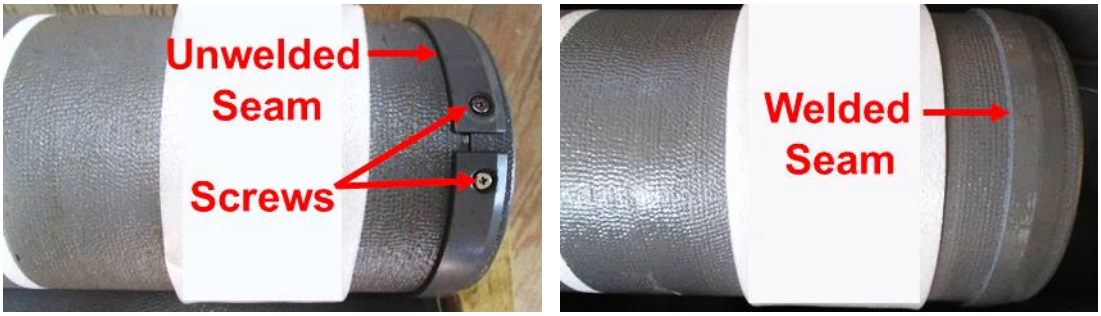

a) Fault Rupture Test

b) Direct Tension and Four-Point Bending Tests

Figure 6.17. Welded and Screw-on Spigot Projections

The pipeline was able to accommodate 44.4 in. (1.13 m) of fault displacement before the pipe lost pressure. This fault displacement corresponds to 28.5 in. (0.72 m) of axial pipeline displacement and an average tensile strain of 5.9% along the pipeline. After verification of total pressure lost, the test was then stopped at 46.0 in. (1.17 m) of fault displacement. The failure mode for this test was a fracture of the spigot projection at the west springline of the S5 joint.

6.4.1 Deformed Shape of Pipeline

Figure 6.18 a) shows a photo of the pipeline before backfilling and burial of the pipe. After fault rupture, the pipeline was excavated carefully in a manner that preserved its deformed shape as shown in Figure 6.18 b). Angles of S5 and N5 rotations are also illustrated in Figure 6.18 b). These rotation angles were obtained from the survey data as discussed in the next section.

6.4.2 Survey Data

Figure 6.19 shows, on a greatly exaggerated scale, the survey data for the initial and final pipeline positions. It should be noted that the pipeline lost pressure at 44.4 in. (1.13 m) of fault displacement, whereas the final pipeline position was surveyed after excavation at 46.0 in. (1.17 m) of fault displacement. The survey data suggest that, at 46.0 in. (1.17 m) of fault displacement the pipeline moved 28.7 in. (729 mm) axially with 35.7 in. (907 mm) of lateral offset. The S18, S15, S5, N5, N15, and N18 joint displacements were 4.9 in. (124 mm), 4.0 in. (102 mm), 7.8 in. (198 mm), 3.5 in. (89

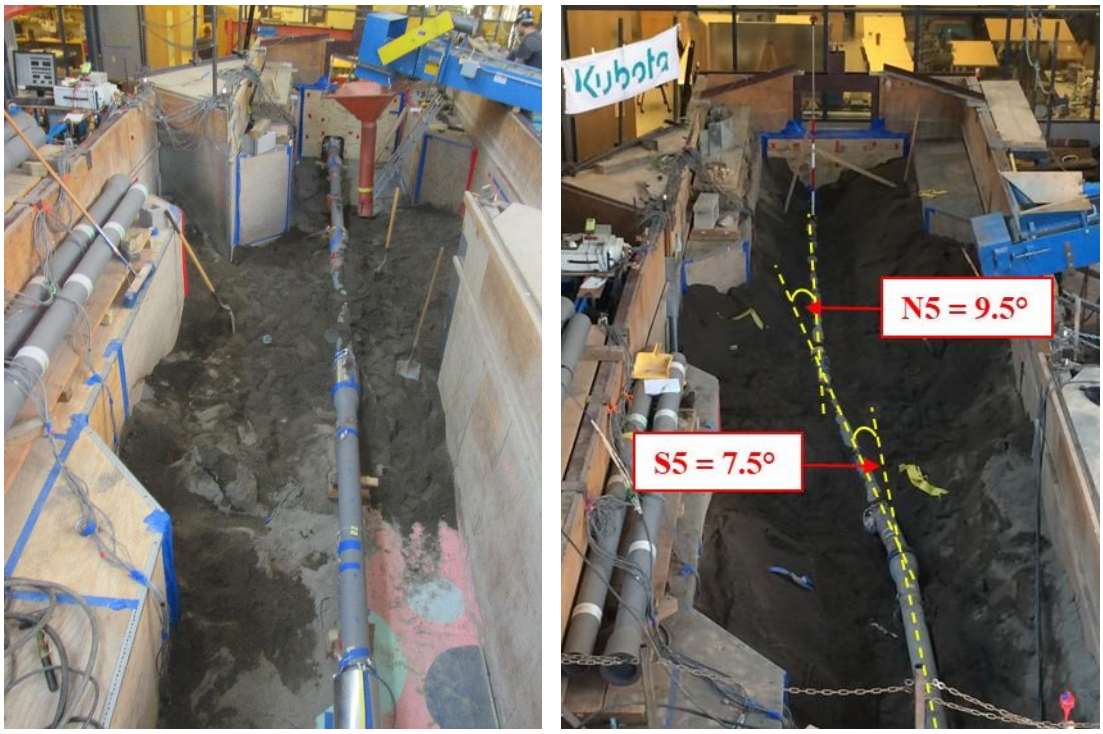

a) Before Burial b) After Excavation

Figure 6.18. Images of Kubota Pipeline Positions (angles shown from total station surveying measurements)

mm), 4.3 in. (109 mm), and 4.7 in. (119 mm), respectively. The displacement at the S5 joint was largest because the pipeline failed and was pulled out at the S5 joint. In addition, the rotations of the S5 and N5 were 7.5° and 9.5°, respectively. The rotation measurements at the other four joints were, however, too small to provide useful information.

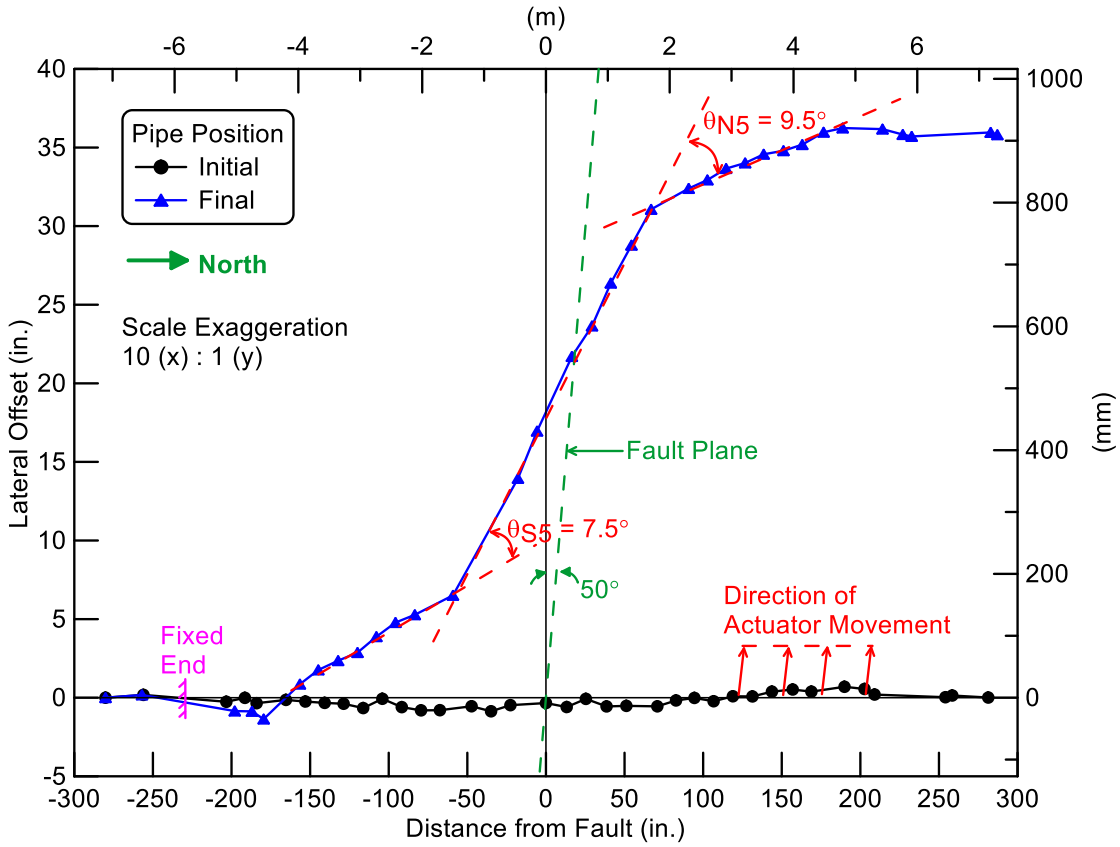

Figure 6.19. Initial and Final Kubota Pipeline Positions from Surveying Measurements

6.4.3 Joint Pullout

The joint pullout movements were measured by string potentiometers (string pots) and compared with survey measurements. Figure 6.20 shows the joint opening of all six joints vs. fault displacement. Joint slip initiated at the south joint closest to the fault plane, S5, and continued until slip was resisted at 8.0 in. (203 mm) of fault displacement by the spigot projection contact with the locking ring. Axial slip was initiated next at the north joint closest to the fault, N5. It also moved until slip was resisted. Similar slip initiation and movement occurred in the remaining joints until all

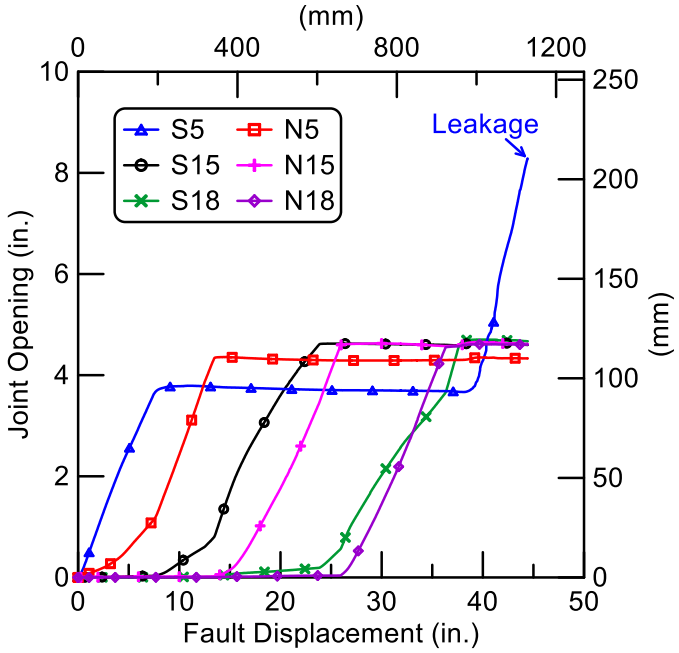

Figure 6.20. Kubota Joint Openings vs. Fault Displacement

Table 6.3. Maximum Kubota Joint Displacement

Joint Location	Joint Displacement (in.)	
	String Pot Data [a]	Survey Data [b]
S18	4.7	4.9
S15	4.6	4.0
S5	8.3	7.8
N5	4.3	3.5
N15	4.6	4.3
N18	4.6	4.7
Average	5.2	4.9
All Six Joints	∑ = **31.1**	∑ = **29.2**
Axial Basin Extension (in.)	(44.4 in.) cos 50° = **28.5**	
Direct Tension Test	Six joint travel distance = 4.5 in. × 6 joints	∑ = **27.0**

1 in. = 25.4 mm

[a] Joint displacement when pipe failure at 44.4 in. (1.13 m) of fault displacement

[b] Joint displacement after test end at 46.0 in. (1.17 m) of fault displacement

joints had moved through their maximum range of movement. All six joints were fully extended when the fault displacement reached 38.0 in. (965 mm). Failure occurred at a fault displacement of approximately 44.4 in. (1.13 m) by shearing at the spigot projection and leaking of the south joint closest to the fault, S5.

The displacement of each joint at the end of test is presented in Table 6.3. String pot and survey measurements of the joint movements are different because they were recorded at different fault displacements. The string pot data correspond to joint displacements immediately before the S5 joint failed at 44.4 in. (1.13 m) of fault displacement. The test was stopped at a fault displacement of 46.0 in. (1.17 m), after which the pipeline was exposed, and the survey measurements were taken.

6.4.4 Joint Rotations

Joint rotations were measured with the string pots at each joint and compared with survey measurements. Joint rotations vs. fault displacement are provided in Figure 6.21. The N5 and S5 joints, closest to the fault, had opposite joint rotations and accommodated most of the fault offset with maximum rotations of nearly 8.5°. The other joint rotations were relatively small. The S15 and N15 joint rotations were approximately 2.5°, whereas the rotations at the S18 and N18 joints were about 1°.

The maximum rotation of each joint obtained from string pot and survey data is presented in Table 6.4. As discussed in the previous section, the joint rotations measured by the string pots and the survey data are different because the string pot data correspond

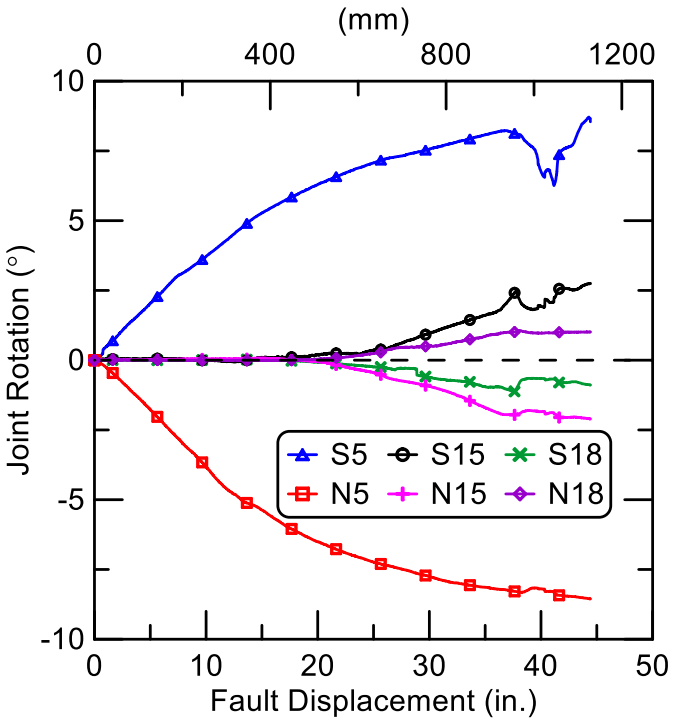

Figure 6.21. Kubota Joint Rotations vs. Fault Displacement

Table 6.4. Maximum Kubota Joint Rotation

Joint Location	Joint Rotation (°)	
	String Pot Data [a]	Survey Data [b]
S18	-0.9	N/A
S15	2.8	N/A
S5	8.5	7.5
N5	-8.6	-9.5
N15	-2.1	N/A
N18	1.0	N/A

Positive refers to rotation in counter-clockwise direction
[a] Rotation when pipe failure at 44.4 in. (1.13 m) of fault displacement
[b] Rotation after test end at 46.0 in. (1.17 m) of fault displacement

to the joint rotations at 44.4 in. (1.13 m) of fault displacement, whereas the survey data were taken at 46.0 in. (1.17 m) of fault movement.

6.4.5 Pipe Axial Forces

The test basin end loads were measured with four load cells at the south end of the test basin and four load cells at the north end. Figure 6.22 shows the total load at the south and north ends of the test basin vs fault displacement. The end loads were near zero during the beginning part of the test, and then increased sharply at a fault displacement of approximately 38.0 in. (965 mm), corresponding to an axial basin displacement of 24.4 in. (620 mm). At 39.5 in. (1.03 m) of fault displacement, maximum loads of 31.7 kips (141 kN) and 32.5 kips (145 kN) were measured at the south and north ends, respectively. The loads then declined substantially until the pipeline lost pressure at 44.4 in. (1.13 m) of fault displacement.

Also included in Figure 6.22 are loads calculated with the axial strain gage measurements at the stations 247 in. (6.27 m) south and 232 in. (5.89 m) north of the fault, which were close to the south and north ends of the test basins, respectively. The axial force in the pipeline was derived from average strain gage measurements and calculated as $F = \varepsilon AE$. The outside diameter of the pipe was OD = 6.65 in. (169 mm) and the average measured wall thickness was $t_W = 0.34$ in. (8.64 mm). This gives a pipe wall cross-sectional area, $A = 6.74$ in.^{2} (4348 mm^2). The Young's modulus of the DI was E = 25,400 ksi (175 GPa), which was determined from tensile coupon tests. The

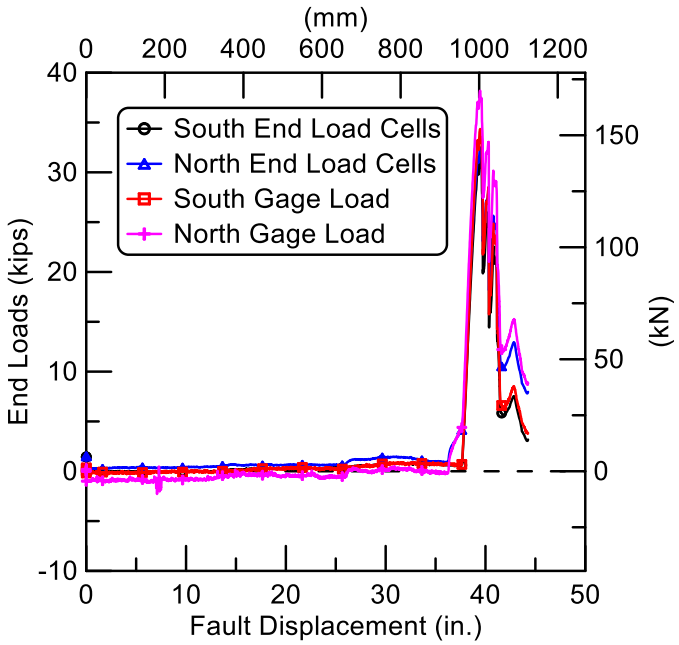

Figure 6.22. Comparisons of End Forces from Load Cells and Strain Gages for Kubota Pipe Fault Rupture Test

maximum loads at the south and north gage stations were 34.4 kips (153 kN) and 38.2 kips (170 kN), respectively, which are larger by about 10-15% of maximum loads measured by the south and north end load cells of 31.7 kips (141 kN) and 32.5 kips (145 kN), respectively.

The loads at each gage plane along the pipeline, determined from the axial gage measurements, are presented in Figure 6.23 for various levels of fault displacement. The joint locations are shown by green dashed lines. Figure 6.23 a) shows the tensile forces up to 15 in. (380 mm) of fault movement. The tensile forces were generally higher with increasing fault displacement. High axial force was detected near the fault between the S5 and N5 joints, and the loads were lower at locations further away from the fault. Figure 6.23 b) (note change in scale for load) shows the pipeline axial forces

between 20 in. (508 mm) and 30 in. (762 mm) of fault displacement, which are similar in pattern to those during smaller fault displacements.

Figure 6.23 c) shows that the loads increased rapidly from 30.0 in. (762 mm) to 39.5 in. (1,003 mm) of fault displacement. The strain gages at the fault plane did not function properly after 30 in. (762 mm) of fault displacement, and therefore the axial loads at this location are not shown. The maximum tensile load in the pipeline was measured at 39.5 in. (1,003 mm) of fault displacement, at which the axial force of 89 kips (396 kN) was largest at 76 in. (1.93 m) north of the fault. The axial forces in the pipeline dropped after 39.5 in. (1,003 mm) until the pipeline lost pressure at 44.4 in. (1.13 m) of fault displacement.

Figure 6.24 shows the force vs. displacement plots of at the S5 and N5 joints in the fault rupture test compared to the force vs. displacement relationship from the direct tension test. The force at each joint was taken from the average calculated load of the south and north gage stations closest to the joint. The maximum forces at the S5 and N5 joints were 59 kips (262 kN) and 79 kips (351 kN), respectively, which are approximately 29-47% lower than the maximum force in the direct tension test. The lower axial failure load is likely related to the effects of combined loading in tension and bending at the joints. It should be noted that the spigot projections in the fault rupture test were screwed onto the spigots, whereas the spigot projection was welded onto the spigot for the direct tension test. Lower tensile capacity may also be related to lower load at failure of the spigot projection.

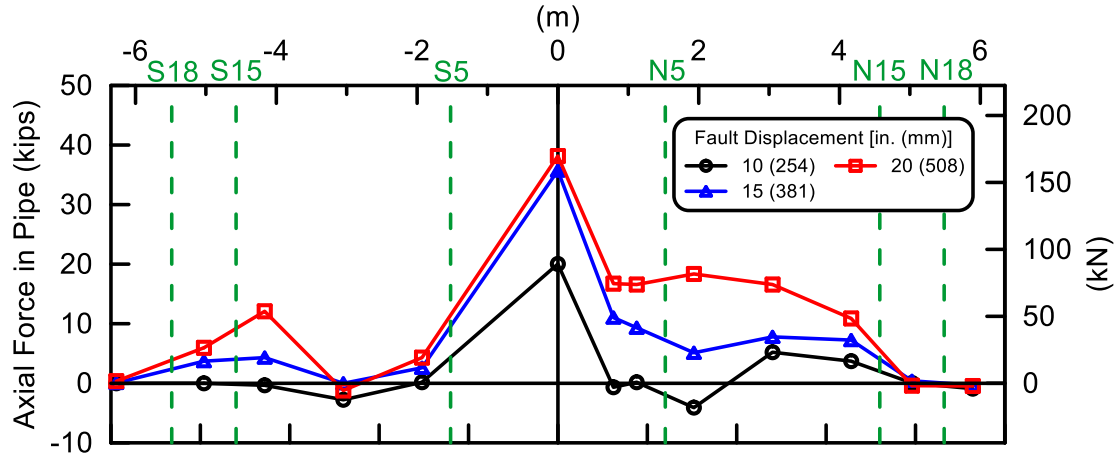

(a) 10 to 20 in. (254 to 508 mm) of Fault Displacement

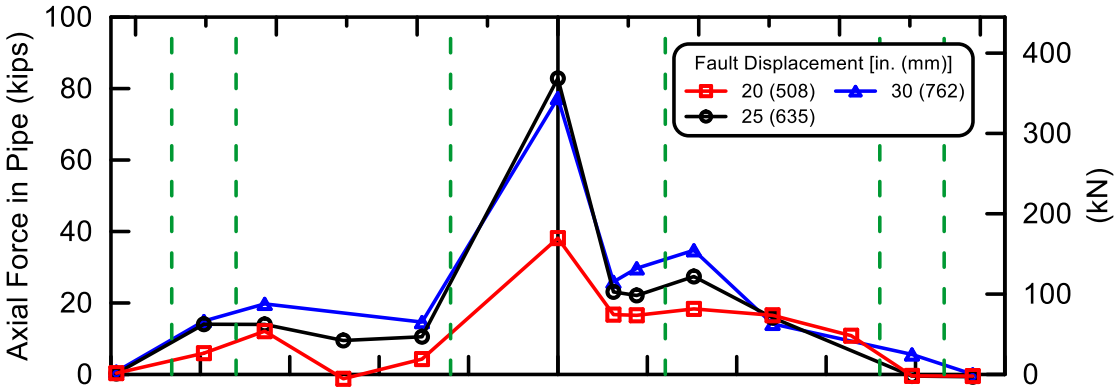

(b) 20 to 30 in. (508 to 762 mm) of Fault Displacement

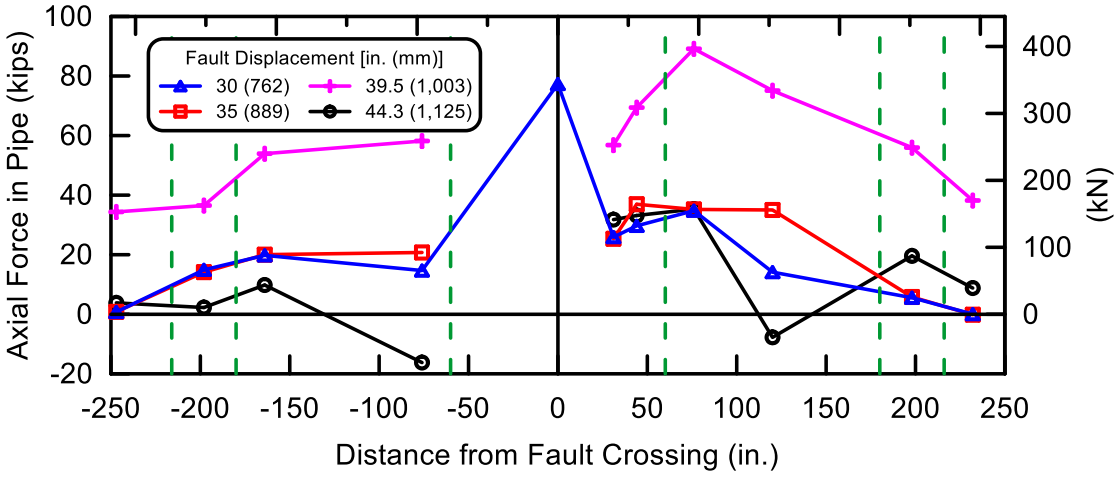

(c) 30 to 44.3 in. (762 to 1,125 mm) of Fault Displacement

Figure 6.23. Axial Force in Kubota Pipeline vs. Distance from Fault

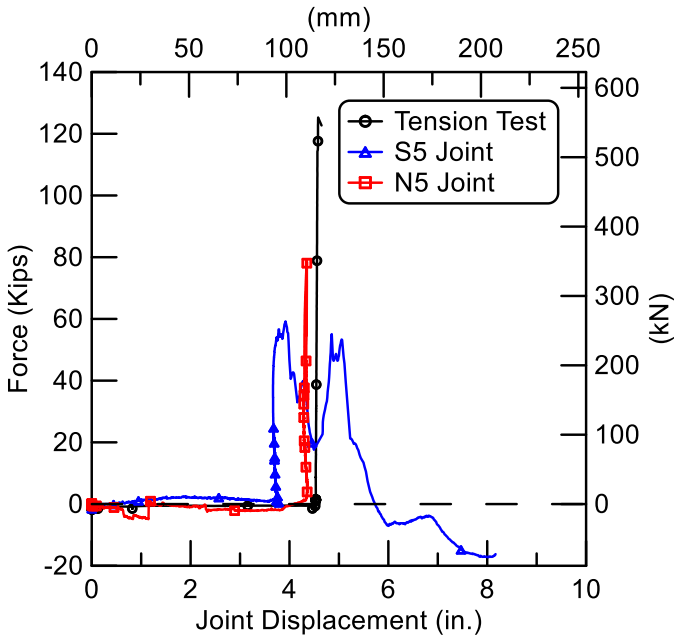

Figure 6.24. Kubota Joint Axial Force vs. Displacement Comparisons

After the maximum load at the S5 joint was achieved, the spigot projection was sheared off, resulting in the load fluctuation shown in Figure 6.24. However, the S5 joint was still able to maintain water pressure and accommodate additional displacement because the gasket, which was located near the bell end opening (bell face), prevented leakage at the joint until the S5 spigot was completely pulled out at 8.3 in. (211 mm) of joint displacement.

Figure 6.25 shows the load drops across the closest joints south, S5, and north, N5, of the fault plane. The load drop across the N5 joint is calculated by subtracting the load at the 44 in. (1.12 m) north of the fault with the load at the station on the north side of the joint [station 76 in. (1.93 m) north of the fault]. The strain gages at the 44 in. (1.12 m) south of the fault were damaged. The load at the south side of the fault is

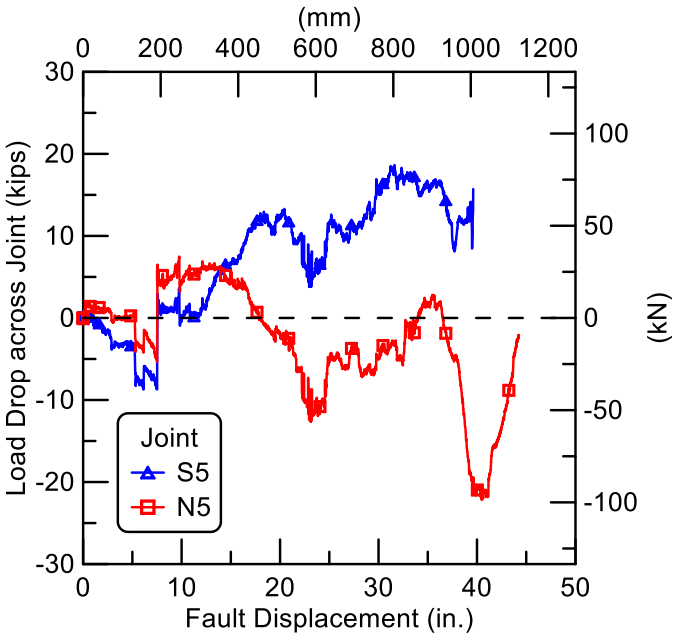

Figure 6.25. Load Drop across Kubota Joint vs. Fault Displacement

assumed to be symmetric with respect to the north side, and load at the north 44 in. (1.12 m) station is assumed to equal to that at the south 44 in. (1.12 m) station. The S5 joint load drop is therefore calculated by subtracting the load at the station 44 in. (1.12 m) north of the fault with the load at the station on the south side of the joint [station 76 in. (1.93 m) south of the fault]. Negative values of load drop indicate that the S5 joint was moving south and away from the fault. The load drop across the S5 joint increased rapidly after 12 in. (305 mm) and reached a maximum of 18.6 kips (83 kN) at 31.6 in. (806 mm) of fault displacement. The load drop across the S5 joint is not shown after 39.6 in. (1.01 m) because the strain gages at the station 76 in. (1.93 m) south of the fault were too damaged to provide useful information. The load drop across the N5 joint varied between about 5 and -5 kips (22 and -22 kN) during the first 8 in. (203 mm) of

fault displacement. The load drop fluctuation became larger during the remainder of the test.

6.4.6 Bending Moments

Figure 6.26 presents the bending moments measured along the pipeline, corresponding to various levels of fault displacement. The joint locations are shown by green dashed lines. Figure 6.26 a) shows that, during the first 15.0 in. (381 mm) of fault displacement, bending moments along the pipeline were very low. The measurements disclose an anti-symmetric pattern of moment distribution centered on the fault. Figure 6.26 b) shows the pipeline bending moments between 20.0 in. (508 mm) and 30.0 in. (762 mm) of fault displacement, similar in pattern to those developed during smaller fault displacements. The peak moments were detected near the S5 and N5 joints. Figure 6.26 c) shows a similar pattern of bending moment distribution for fault movements of 30.0 in. (762 mm) to 39.5 in. (1,003 mm). At a fault displacement of 39.5 in. (1,003 mm), the maximum moments are on the order of 300 kip-in. (33.9 kN-m) near the S5 and N5 joints. When the pipeline lost pressure at 44.4 in. (1.13 m) of fault displacement, the moment near the S5 joint dropped to about 69 kip-in. (7.8 kN-m), whereas the moment near the S5 joint increased to 372 kip-in. (42.0 kN-m)

Figure 6.27 shows the moment vs. rotation plots for the S5 and N5 joints derived from the fault rupture test measurements in comparison with the moment vs. rotation relationship from the four-point bending test. The moment of each joint in the fault

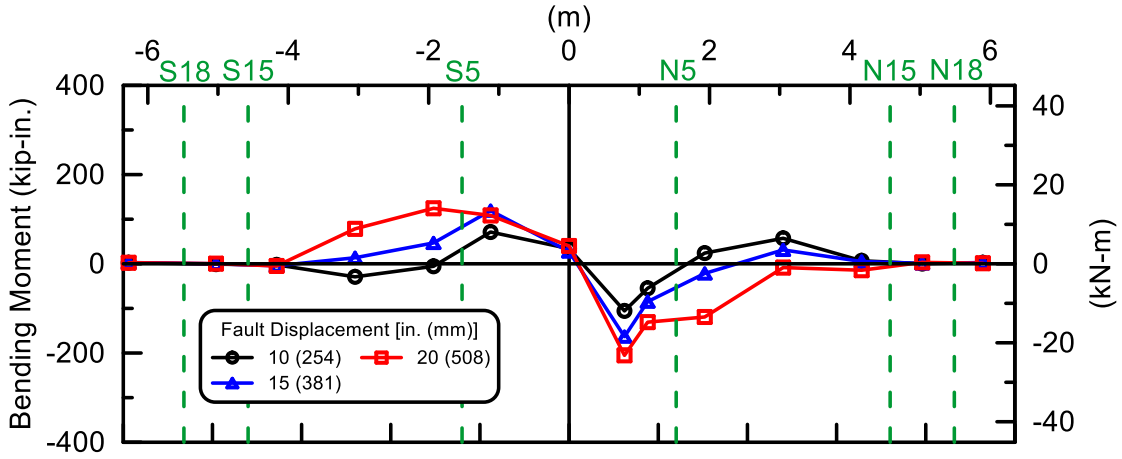

(a) 10 to 20 in. (254 to 508 mm) of Fault Displacement

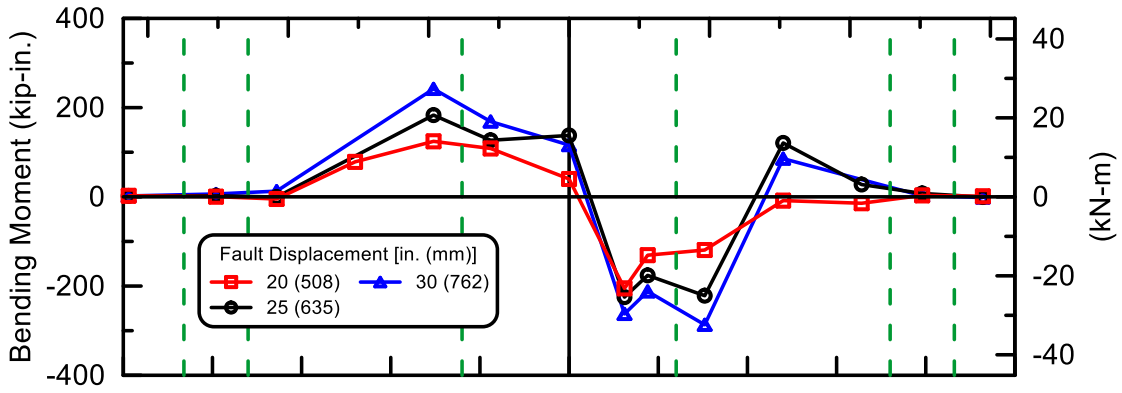

(b) 20 to 30 in. (508 to 762 mm) of Fault Displacement

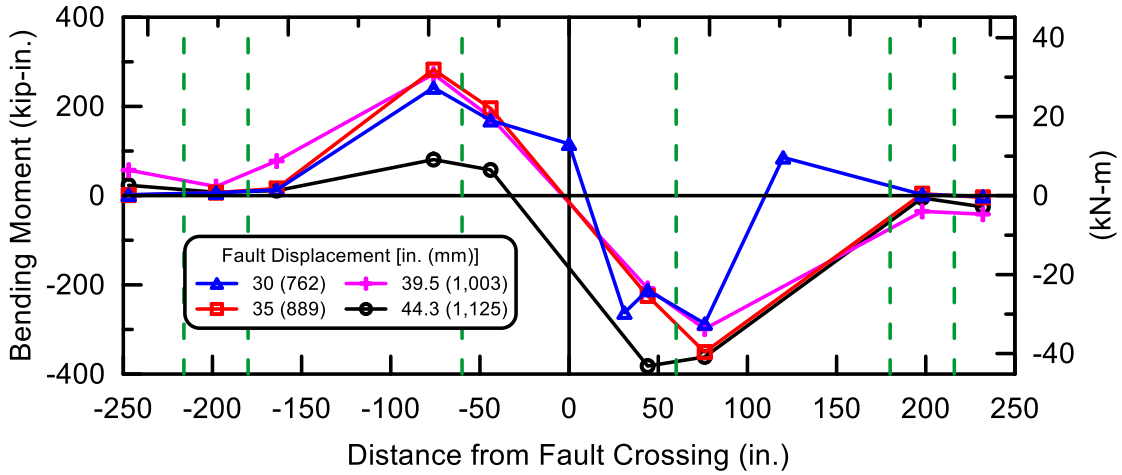

(c) 30 to 44.3 in. (762 to 1,125 mm) of Fault Displacement

Figure 6.26. Bending Moment in Kubota Pipeline vs. Distance from Fault

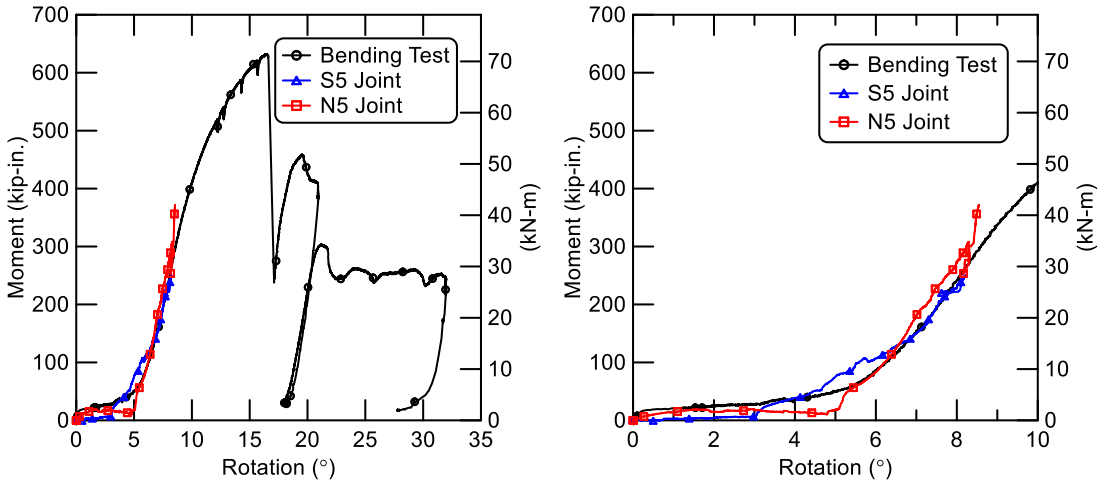

a) Full Range b) First 10° of Rotation

Figure 6.27. Kubota Joint Moment vs. Rotation Comparisons

rupture test was taken from the average calculated moment of the south and north gage stations closest to the joint. The moment vs. rotation plots of the S5 and N5 joints are in an excellent agreement with the four-point bending test results.

6.5 Experimental Results of McWane Restrained Axial Slip DI Pipeline

The test procedure, soil placement method, and soil density and strength characteristics associated with the McWane fault rupture test are very similar to those for the AMERICAN fault rupture test. The reader should refer to Sections 6.2.1 and 6.2.3 for information about the general test procedure and soil characteristics. There are some small differences in the soil properties. The average and standard deviation of all dry unit weight measurements were 106.7 lb/ft^3 (16.8 kN/m^3) and 1.7 lb/ft^3 (0.17

kN/m^3), respectively. Moisture content measurement had an average of 4.9% and standard deviation of 0.5%.

Figure 6.28 shows the layout and the location of the instrumentation along the McWane DI pipeline with restrained axial slip joints. The McWane DI pipeline consisted of three DI pipe segments and two SFC couplings, which were designated as south (S) and north (N) SFCs. Each SFC was located 60 in. (1.5 m) away from the fault plane. A 125-in. (3.18 m)-long pipe section was placed directly over the fault, with an intersection angle of 50^o. A 207-in. (5.26-m)-long pipe with an SFC was connected at the north end of the pipeline. Lastly, a 178-in. (4.52-m)-long pipe with an SFC was connected at the south end of the pipeline. The B and P joints were installed at the fully-inserted positions. The X joints were positioned at 1.5 in. (38 mm) from the fully-inserted position in order to provide adequate space for string pot installation.

The pipeline was able to accommodate 33.4 in. (848 mm) of fault displacement before the pipe lost pressure. This fault displacement corresponds to 21.5 in. (546 mm) of axial pipeline displacement and an average tensile strain of 4.5% along the pipeline. After verification of total pressure lost, the test was then stopped at 33.7 in. (856 mm) of fault displacement. The failure mode for this test was the B joint pullout at the south SFC as shown in Figure 6.29.

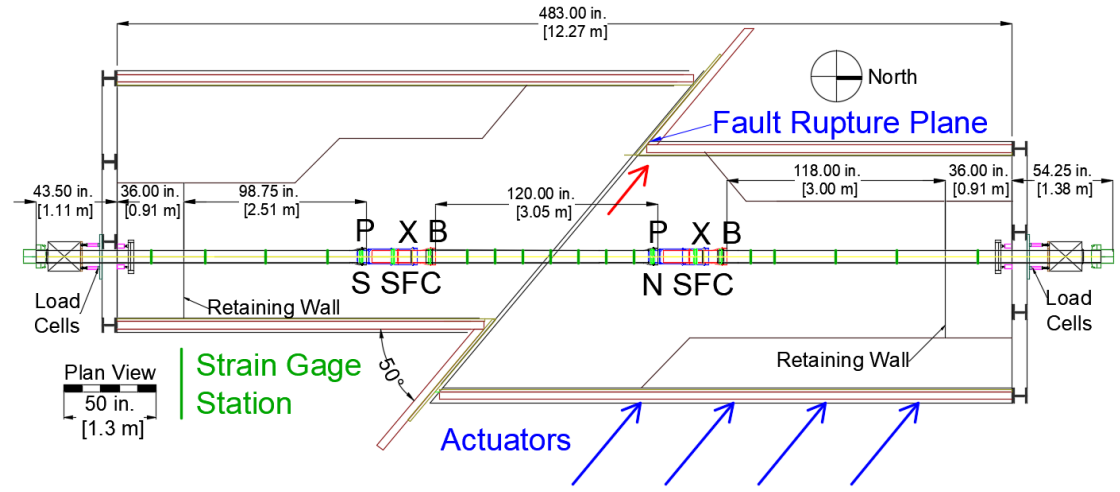

a) Overall Test Configurations

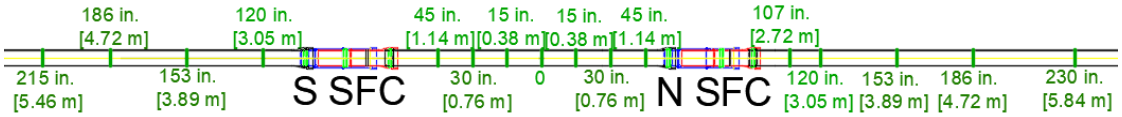

b) Strain Gage Layout

Figure 6.28. Plan View of Pipe Centered McWane SFC Specimen in Test Basin

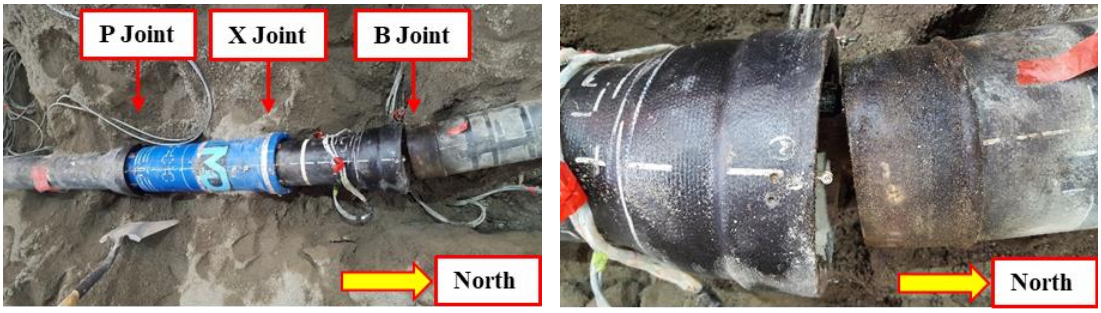

a) Plan View of South SFC b) Close-up View of South SFC B Joint

Figure 6.29. B Joint Pullout at South SFC following Test

a) Before Burial

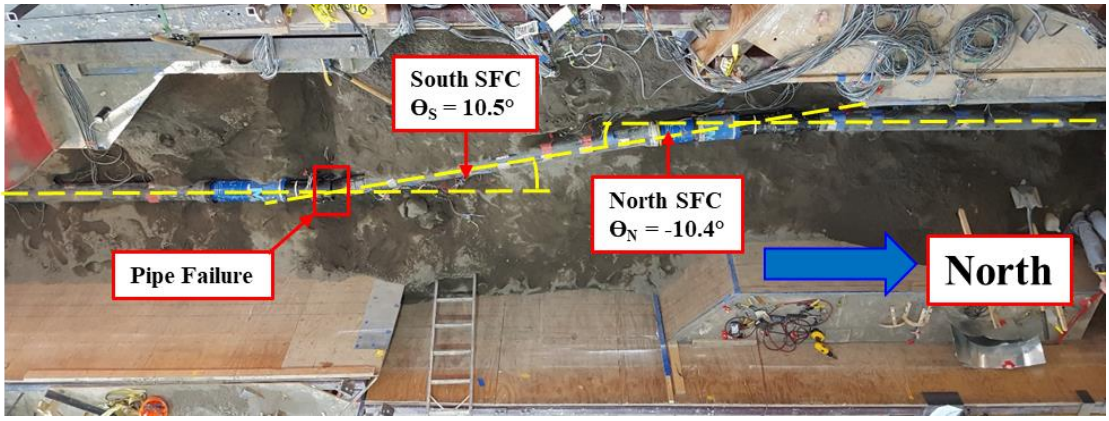

b) After Excavation

Figure 6.30. Images of McWane Pipeline Positions (angles shown from total station surveying measurements)

6.5.1 Deformed Shape of Pipeline

Figure 6.30 a) shows a photo of the pipeline before backfilling and burial of the pipe. After fault rupture, the pipeline was excavated carefully in a manner that preserved its deformed shape as shown in Figure 6.30 b). Angles of S and N SFC rotations are also illustrated in Figure 6.30 b). These rotation angles were obtained from the survey data as discussed in the next section.

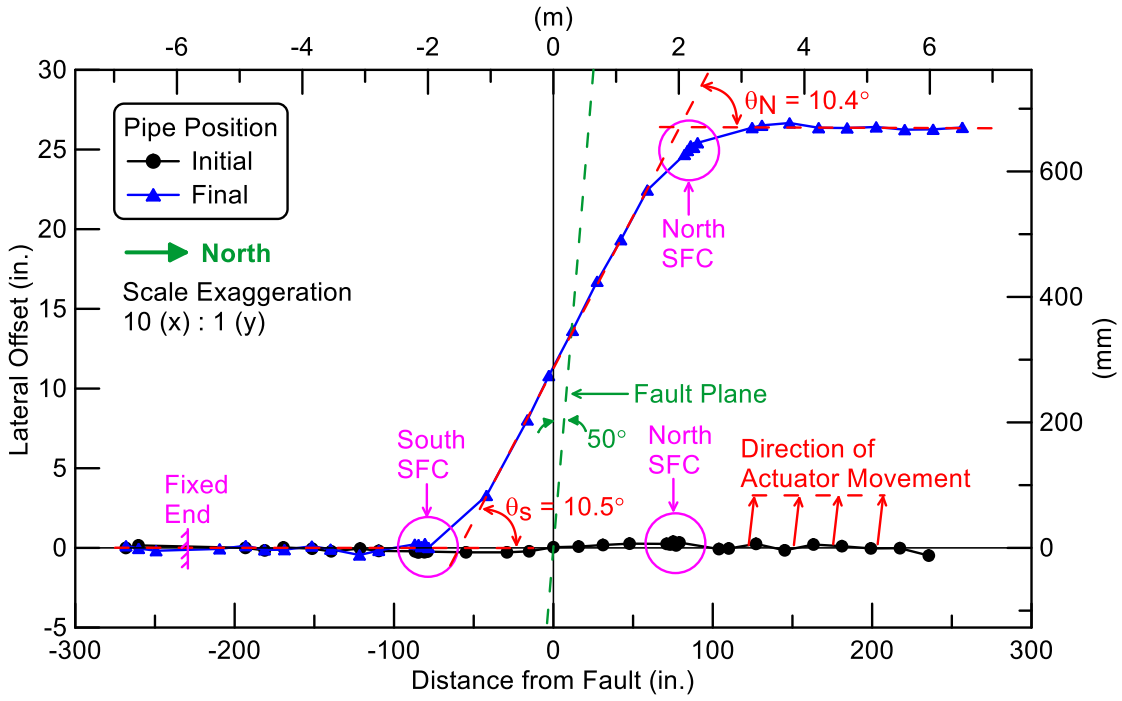

Figure 6.31. Initial and Final McWane Pipeline Positions from Surveying Measurements

6.5.2 Survey Data

Figure 6.31 shows, on a greatly exaggerated scale, the survey data for the initial and final pipeline positions. It should be noted that the pipeline lost pressure at 33.4 in. (848 mm) of fault displacement, whereas the final pipeline position was surveyed after excavation at 33.7 in. (856 mm) of fault displacement. The survey data suggest that, at 33.7 in. (856 mm) of fault displacement, the pipeline moved 21.1 in. (536 mm) axially with 26.7 in. (678 mm) of lateral offset. The S and N SFC displacements were 11.6 in. (295 mm) and 9.4 in. (239 mm), respectively. The displacement at the S SFC was larger than the N SFC displacement because the pipeline failed and was pulled out at the S SFC. In addition, the rotations of the S5 and N5 were 10.5° and 10.4°, respectively.

6.5.3 Joint Pullout

Figure 6.32 shows the total movements of the S and N SFCs. The test basin movement was accommodated by the SFC displacements. The S and N SFC joint slips were resisted by the spigot weld bead contacts with the locking segments at 17.4 in. (442 mm) and 28.0 in. (711 mm) of fault displacements, respectively. Failure occurred at a fault displacement of approximately 33.4 in. (848 mm) by the B joint pullout at the S SFC.

The movements of the SFCs at the end of test is presented in Table 6.5. String pot and survey measurements of the SFC movements are different because they were recorded at different fault displacements. The string pot data correspond to the SFC movements immediately before the B joint of the S SFC failed at 33.4 in. (848 mm) of fault displacement. The test was stopped at a fault displacement of 33.7 in. (856 mm), after which the pipeline was exposed, and the survey measurements were taken.

However, it must be noted that the X joint was installed at 1.5 in. (38 mm) from fully inserted position for string pot instrumentation. Had the X joints been set at the fully inserted positions, each SFC in the fault rupture test would have been able to accommodate an additional 1.5 in. (38 mm) of displacement. Therefore, the pipeline would have been able to accommodate a total [3 in. (78 mm) + 21.5 in. (546 mm)]/ cos 50° = 38.1 in. (968 mm) of fault displacement, which is equivalent to 5.0% of average tensile strain along the pipeline.

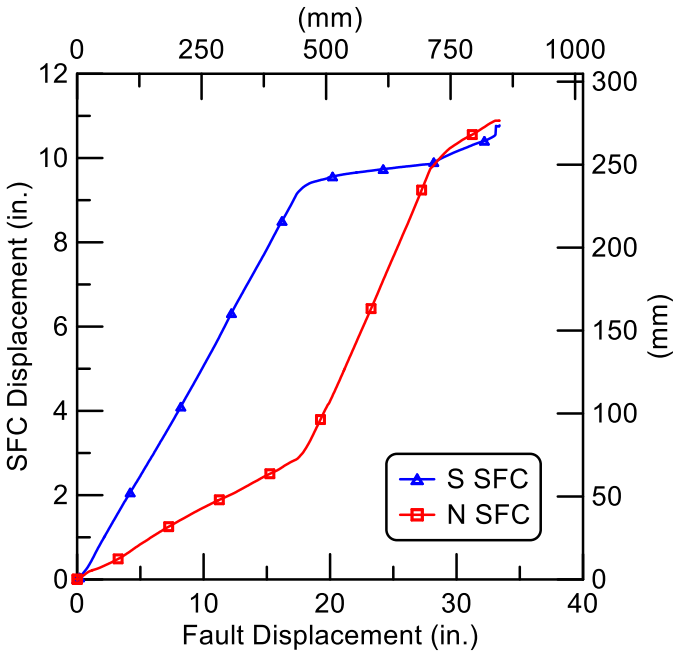

Figure 6.32. McWane SFC Displacements vs. Fault Displacement

Table 6.5. Maximum McWane SFC Displacement

Direction from Fault	SFC Displacement (in.) [a]	
	String Pot Data [b]	Survey Data [c]
South	10.8	11.6
North	10.9	9.4
Average	10.9	10.6
Two SFC joints	∑ = **21.7**	∑ = **21.1**
Axial Basin Extension (in.)	(33.4 in.) cos 50°	**21.5**
Direct Tension Tests	One fully extended SFC = 11.0 in.-1.5 in.= 9.5 in. One leaked SFC = 13.2 in.-1.5 in.= 11.7 in.	∑ = **21.2**

1 in. = 25.4 mm

[a] X joint was set at 1.5 in. (38 mm) from fully inserted position for string pot instrumentation

[b] SFC displacement when pipe failure at 33.4 in. (848 mm) of fault displacement

[c] SFC displacement after test end at 33.7 in. (856 mm) of fault displacement

6.5.4 Joint Rotations

Joint rotations were measured with the string pots at each joint and compared with survey measurements. As illustrated in Figure 1.3, rotation across the McWane SFC involves rotation of B, X, and P joints within the coupling. Figures 6.33 and 6.34 show the south and north joint rotations vs. fault displacement, respectively. During the fault rupture test the south B and north P joints were closest to the fault rupture plane. The highest rotation of 11.6° occurred at the south B joint at the end of the test.

SFC rotations are the sums of B, X, and P joint rotations. They are plotted relative to fault displacement in Figure 6.35. The south SFC accommodated most of the fault offset with maximum rotation of nearly 13.7° in a counter-clockwise rotation. The N SFC rotated in a clockwise direction of 11.6°.

The maximum rotations of each SFC obtained from string pot measurements and survey data are presented in Figure 6.6. As discussed in the previous section, string pot and survey measurements of the SFC rotations are different because the string pot data correspond to the SFC rotations at 33.4 in. (848 mm) of fault displacement, whereas the survey data were taken at 33.7 in. (856 mm) of fault movement.

6.5.5 Pipe Axial Forces

The test basin end loads were measured with four load cells at the south end of the test basin and four load cells at the north end. Figure 6.36 shows the total load at the south and north ends of the test basin vs. fault displacement. The end loads were

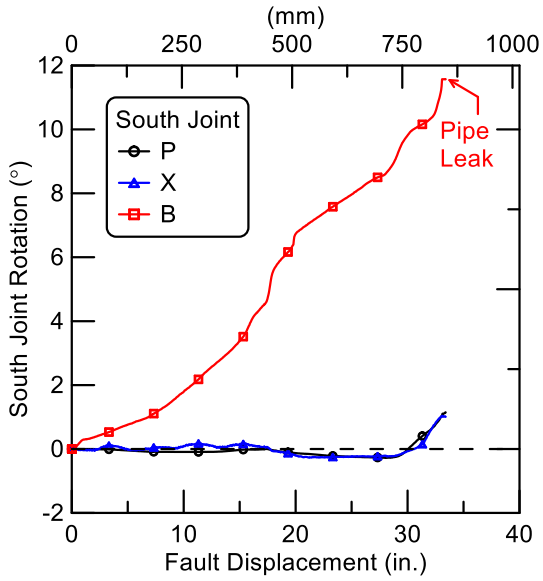

Figure 6.33. South SFC Joint Rotations vs. Fault Displacement

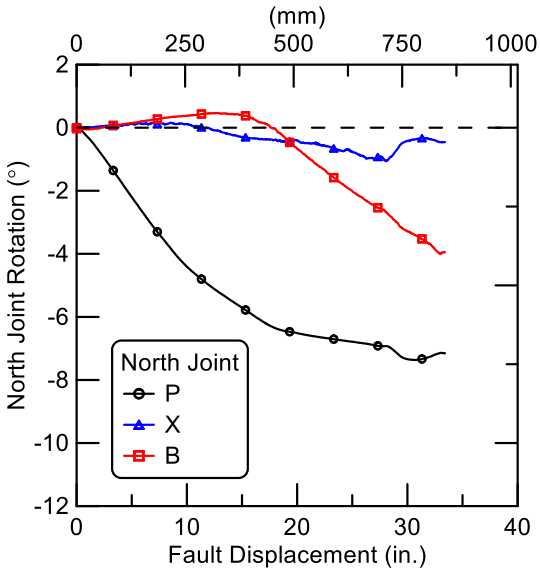

Figure 6.34. North SFC Joint Rotations vs. Fault Displacement

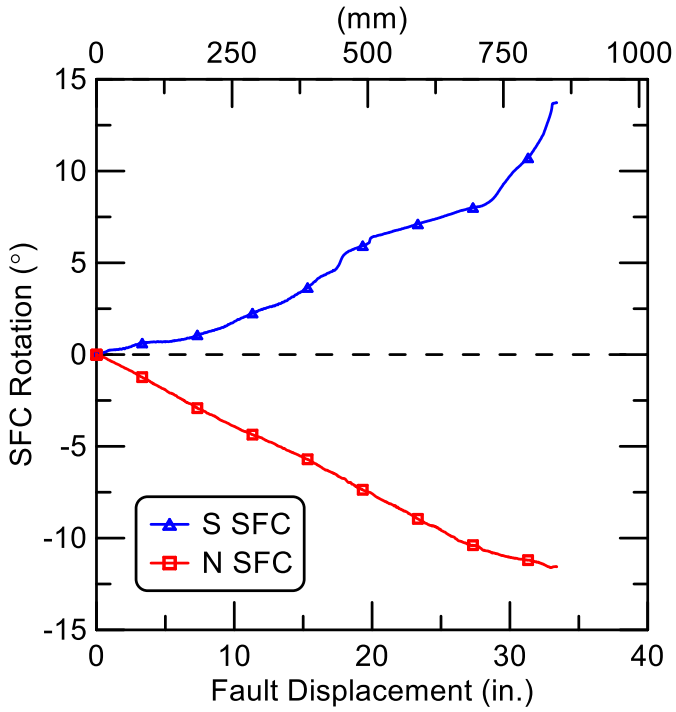

Figure 6.35. McWane SFC Rotations vs. Fault Displacement

Table 6.6. Maximum McWane SFC Rotation

SFC	SFC Rotation (°)	
	String Potentiometers Data [a]	Survey Data [b]
South	13.7	10.5
North	-11.6	-10.4

Positive refers to rotation in counter-clockwise direction
[a] Rotation when pipe failure at 33.4 in. (848 mm) of fault displacement
[b] Rotation after test end at 33.7 in. (856 mm) of fault displacement

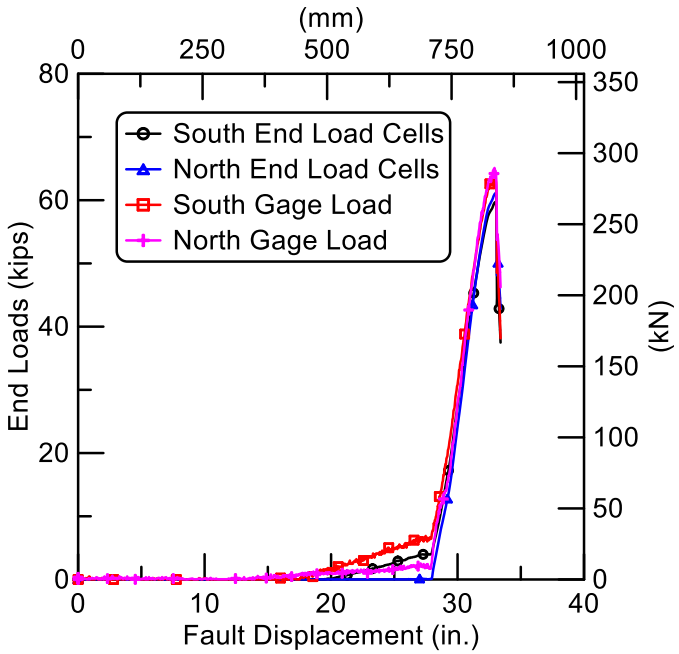

Figure 6.36. Comparisons of End Forces from Load Cells and Strain Gages for McWane Pipe Fault Rupture Test

near zero during the beginning part of the test, and then increased sharply at a fault displacement of approximately 28.0 in. (711 mm). At 33.0 in. (838 mm) of fault displacement, maximum loads of 59.7 kips (266 kN) and 61.1 kips (272 kN) were measured at the south and north ends, respectively.

Also included in Figure 6.36 are axial loads calculated with the axial strain gages at planes close to the end of the test specimen. The axial force from average strain gage measurements was calculated as $F = \varepsilon AE$. The outside diameter of the pipe was OD = 6.9 in. (175 mm) and the average measured wall thickness was t_W = 0.3 in. (7.6 mm). This gives a pipe wall cross-sectional area, A = 6.22 in.^{2} (4013 mm^2). The Young's modulus of the DI was E = 24,100 ksi (166 GPa), which was determined from tensile coupon tests. The maximum loads at the south and north gage stations were 63.9 kips (284 kN) and 65.1 kips (290 kN), respectively, which are larger by about 7% of with maximum loads measured by the south and north end load cells of 59.7 kips (266 kN) and 61.1 kips (272 kN), respectively.

The loads at each gage plane along the pipeline, determined from the axial gage measurements, are presented in Figure 6.37 for various levels of fault displacement. The SFC locations are shown by blue shaded areas. Figure 6.37 a) shows the tensile forces up to 20 in. (508 mm) of fault movement. Relatively low tensile forces were measured along the pipeline during these initial increments of displacement. High axial force was detected near the fault between the S and N SFCs, and the loads were lower at locations further away from the fault.

Figure 6.37 b) (note change in scale for load) shows that tensile forces were generally higher with increasing fault displacement. The highest axial force was detected at the fault location. The forces increased rapidly after 28 in. (711 mm) of fault

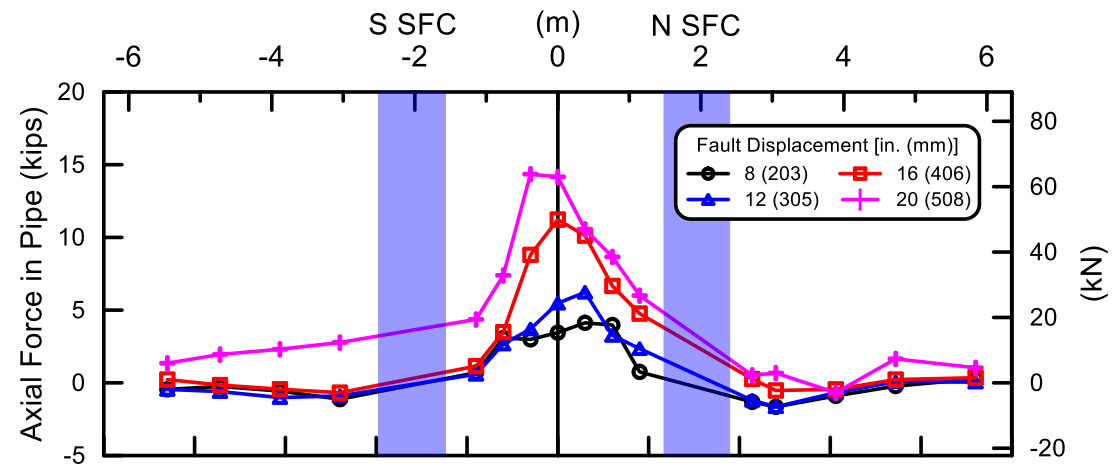

(a) 8 to 20 in. (203 to 508 mm) of Fault Displacement

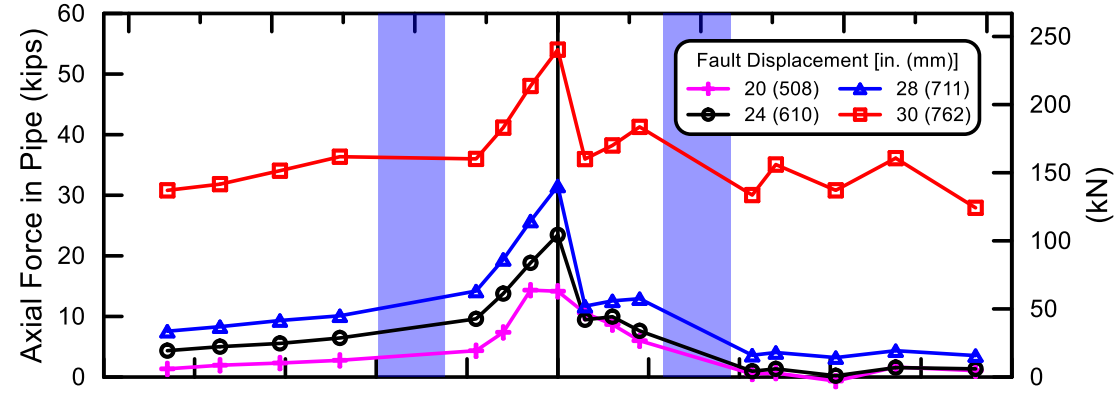

(b) 20 to 30 in. (508 to 762 mm) of Fault Displacement

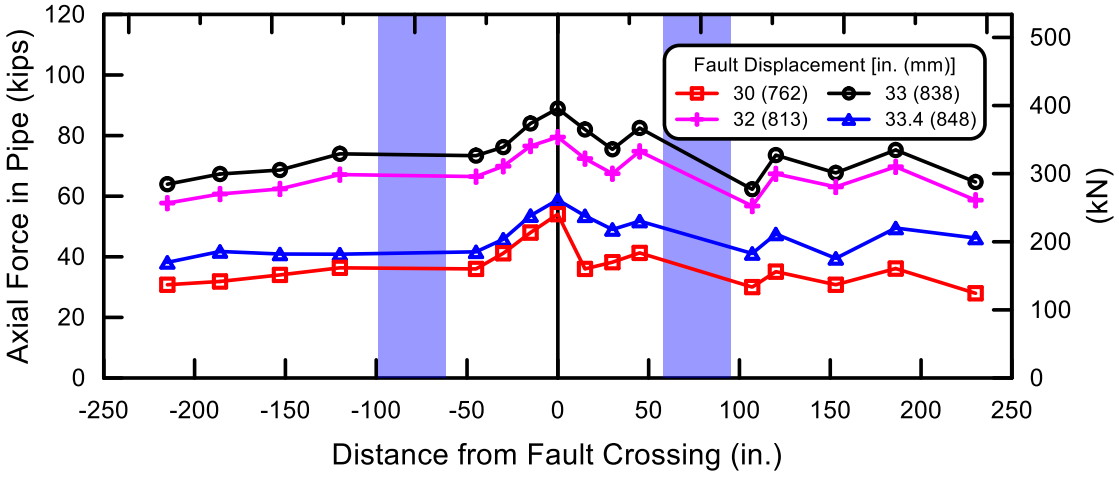

(c) 30 to 33.4 in. (762 to 848 mm) of Fault Displacement

Figure 6.37. Axial Forces in McWane Pipeline vs. Distance from Fault

displacement, indicating that all joint had been fully extended. Figure 6.37 c) (note change in scale for load) shows the evolutions of the pipe axial loads from 30 in. (762 mm) to the end of test at 33.4 in. (848 mm) of fault displacement. At 33.0 in. (838 mm) of fault movement, the peak force of 88.9 kips (395 kN) was detected at the fault location. The axial forces then decreased, yielding similar behaviors as the joint axial tension tests. The highest force of 58.8 kips (262 kN) was also found at the fault before the pipe lost pressure at 33.4 in. (848 mm) of fault displacement.

Figure 6.38 shows the force vs. displacement plots of at the S and N SFCs in the fault rupture test compared to the force vs. displacement relationship from the direct tension tests. The force at each SFC was taken from the average calculated load of the south and north gage stations closest to the SFC. The maximum forces at the S and N SFCs were 73.7 kips (328 kN) and 72.6 kips (323 kN), respectively, which is approximately 10% higher than the average maximum forces of 66.3 kips (295 kN) in the SFC direct tension tests. It should be noted that the tension tests failed at the X joint whereas the pipeline in the fault rupture test failed at the B joint of the S SFC. An axial test on only the B joint of the McWane SFC resulted in failure at 96.5 kips (429 kN) (Pariya-Ekkasut, 2018), which is approximately 25% higher than the failure load in the fault rupture test.

Figure 6.39 shows the load drops across the south and north joints of the fault plane. The load drop across the S SFC is calculated by subtracting the load at the station 45 in. (1.14 m) south of the fault with the load at the station on the south side of the joint

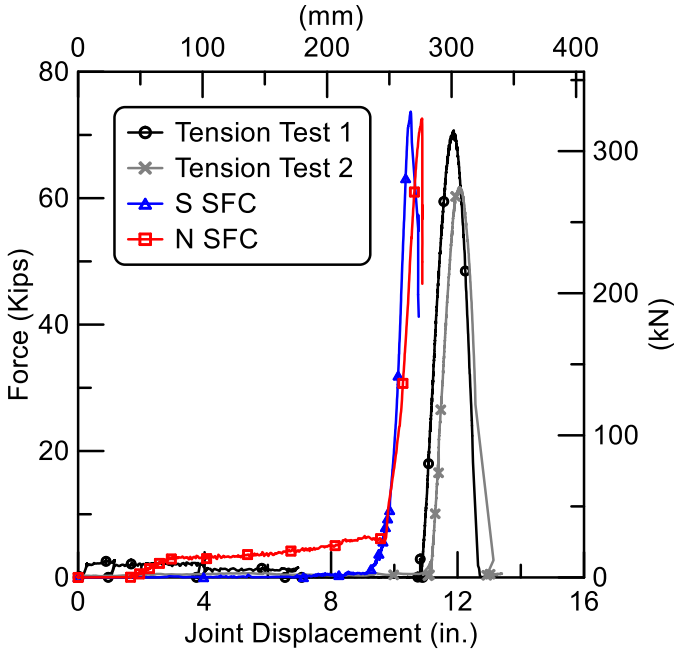

Figure 6.38. McWane Joint Axial Force vs. Displacement Comparisons

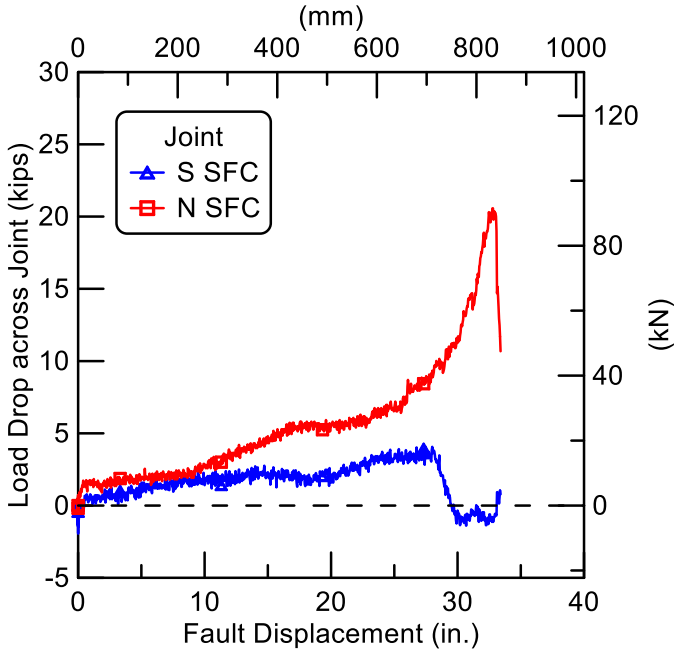

Figure 6.39. Load Drop across McWane Joint vs. Fault Displacement

[station 120 in. (3.05 m) south of the fault]. Similarly, the load drop across the N SFC is calculated by subtracting the load at 45 in. (1.14 m) north of the fault with the load at the station on the north side of the joint [station 107 in. (2.23 m) north of the fault]. The load drop across the S SFC increased steadily from the beginning of the test and reached a maximum of 4.0 kips (18 kN) at 29 in. (737 mm) of fault displacement. The load drop then decreased rapidly and stayed near zero until the end of the test. The load drop across the N SFC steadily increased from the beginning of the test and reached 5.5 kips (24 kN) at 16.5 in. (419 mm) of fault displacement. The load drop across the N SFC remained constant between 16.5 in. (419 mm) and 22.5 in. (572 mm), after which the load drop increased rapidly and reached a maximum of 20.6 kips (92 kN) at 32.8 in. (146 mm) of fault displacement. The load drop then declined rapidly to 10.7 kips (48 kN) at the end of the test.

6.5.6 Bending Moments

Figure 6.40 presents the bending moments measured along the pipeline, corresponding to various levels of fault displacement. The SFC locations are shown by blue shaded areas. Figure 6.40 a) shows that during the first 20 in. (508 mm) of fault displacement, high moments were observed in the area between the fault and the N SFC. Figure 6.40 b) shows that the moments were higher with increasing the fault movement. The measurements disclose an anti-symmetric pattern of moment distribution centered on the fault. Figure 6.40 c) shows a similar pattern of bending moment distribution for

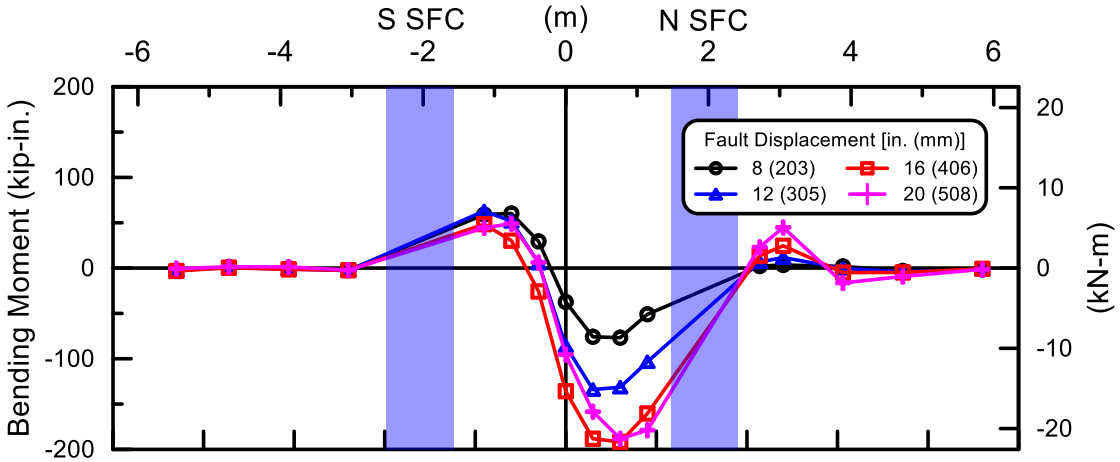

(a) 8 to 20 in. (203 to 508 mm) of Fault Displacement

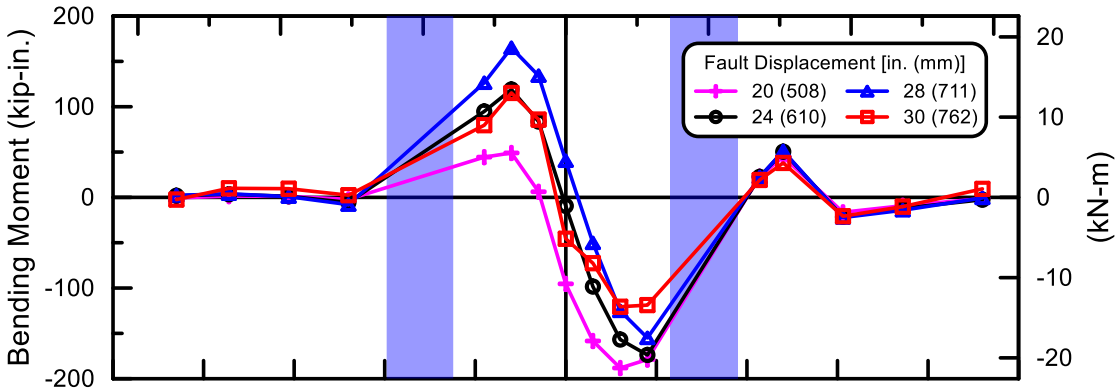

(b) 20 to 30 in. (508 to 762 mm) of Fault Displacement

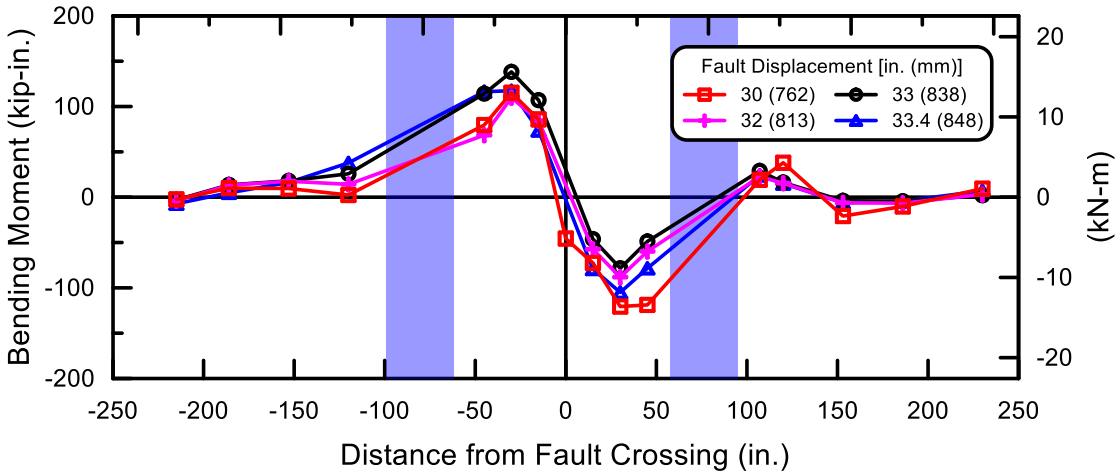

(c) 30 to 33.4 in. (762 to 848 mm) of Fault Displacement

Figure 6.40. Bending Moments in McWane Pipeline vs. Distance from Fault

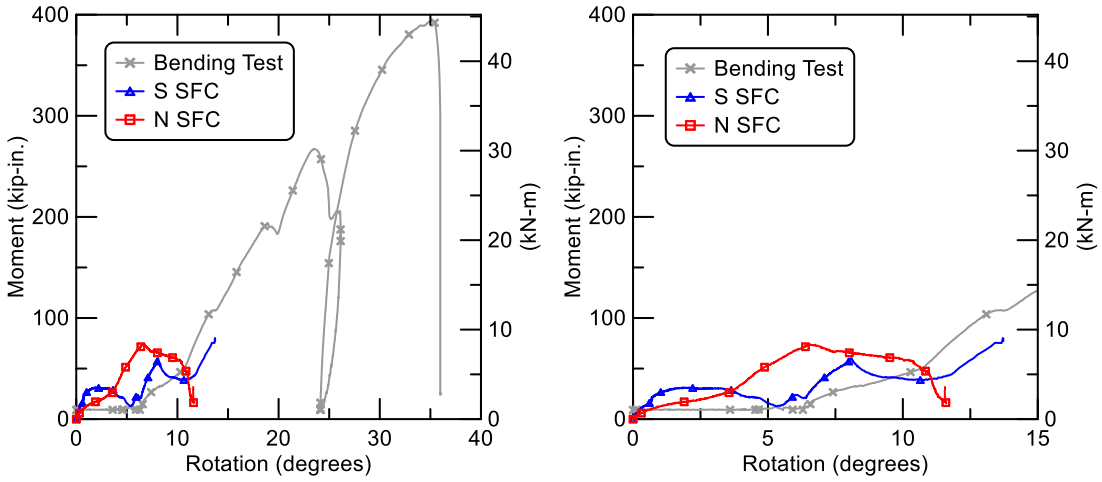

a) Full Range b) First 15° of Rotation

Figure 6.41. McWane Joint Moment vs. Rotation Comparisons

fault movements of 30 in. (762 mm) to 33.4 in. (848 mm). The highest moments of about 110 kip-in. (12.4 kN-m) were detected at 30 in. (762 mm) from the fault. Low moments were measured at the fault location because it was close to the inflection point of the pipeline.

Figure 6.41 shows the moment vs. rotation plots for the S and N SFCs derived from fault rupture test measurements in comparison with the moment vs. rotation relationship from the four-point bending test. The moment of each joint in the fault rupture test was taken from the average calculated moment of the south and north gage stations closest to the joint. The moments and rotations of the S and N SFC were relatively low compared to those from the four-point bending test. However, the moment vs. rotation plots of the S5 and N5 SFCs are in reasonable agreement with the four-point bending test results.

6.6 Experimental Results of US Pipe Restrained Axial Slip DI Pipeline

The test procedure, soil placement method, and soil density and strength characteristics associated with the US Pipe fault rupture test are very similar to those for the AMERICAN fault rupture test. The reader should refer to Sections 6.2.1 and 6.2.3 for information about the general test procedure and soil characteristics. There are some small differences in joint displacement measurements and soil properties. Three direct current differential transformers (DCDTs), instead of string pots, were installed at each joint to measure its displacement. The average and standard deviation of all dry unit weight measurements were 106.7 lb/ft^3 (16.8 kN/m^3) and 2.5 lb/ft^3 (0.4 kN/m^3), respectively. Moisture content measurement had an average of 3.9% and standard deviation of 1.1%.

Figure 6.42 shows the layout and the location of the instrumentation along the US Pipe DI pipeline with restrained axial slip joints. The US Pipe DI pipeline consisted of five DI pipe segments with four restrained axial slip joints. The designations of the six joints from south to north are S15, S5, N5, and N15 where S and N stands for the south and north direction of a joint from the fault rupture plane, respectively, and the following number refers to the distance from a joint to the fault in feet.

A 120.5-in. (3.06-m)-long pipe section was placed directly over the fault. Two identical 120.5-in. (3.06 m) pipes were installed to the north and the south of the center pipe. A 120.5-in. (3.06 m)-long pipe was connected at the north end of the pipeline and

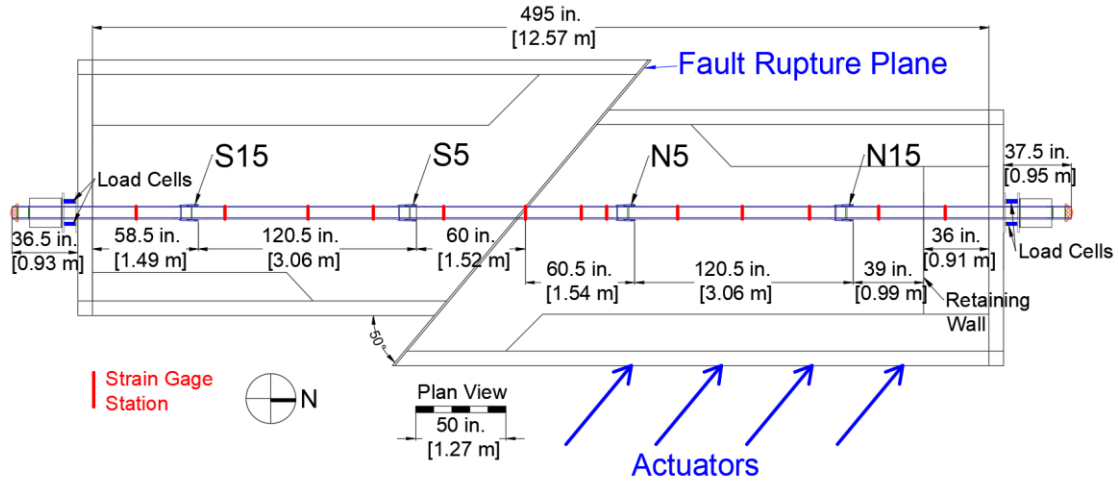

a) Overall Test Configurations

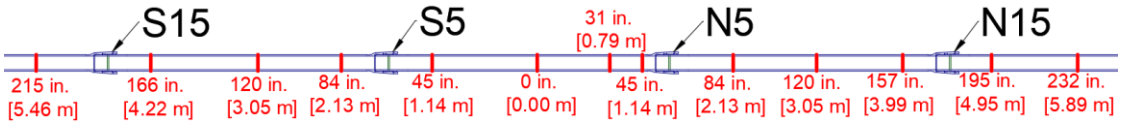

b) Strain Gage Layout

Figure 6.42. Plan View of Pipe Centered US Pipe Restrained Axial Slip DI Pipeline in Test Basin

a) Plan View b) Elevation View from West Springline

Figure 6.43. Bell Rupture at S5 Joint Following Test

had 39 in. (0.99 m) of its portion buried in the soil. Lastly, a 103-in. (2.6-m)-long pipe was connected at the south end of the pipeline with 58.5 in. (1.49 m) of its portion in the test basin. All spigots were fully inserted into the bells.

The pipeline was able to accommodate 19.0 in. (483 mm) of fault displacement before the pipe lost pressure. This fault displacement corresponds to 12.2 in. (310 mm) of axial pipeline displacement and an average tensile strain of 2.5% along the pipeline. After verification of total pressure lost, the test was then stopped at 20.2 in. (513 mm) of fault displacement. The failure mode for this test was DI breakage at the bell of the S5 joint as shown in Figure 6.43.

6.6.1 Deformed Shape of Pipeline

Figure 6.44 a) shows a photo of the pipeline before backfilling and burial of the pipe. After fault rupture, the pipeline was excavated carefully in a manner that preserved its deformed shape as shown in Figure 6.44 b). Angles of S5 and N5 EJS rotations are also illustrated in Figure 6.44 b). These rotation angles were obtained from the survey data as discussed in the next section.

6.6.2 Survey Data

Figure 6.45 shows, on a greatly exaggerated scale, the survey data for the initial and final pipeline positions. It should be noted that the pipeline lost pressure at 19.0 in. (483 mm) of fault displacement, whereas the final pipeline position was surveyed after excavation at 20.2 in. (513 mm) of fault displacement. The survey data suggest that, at

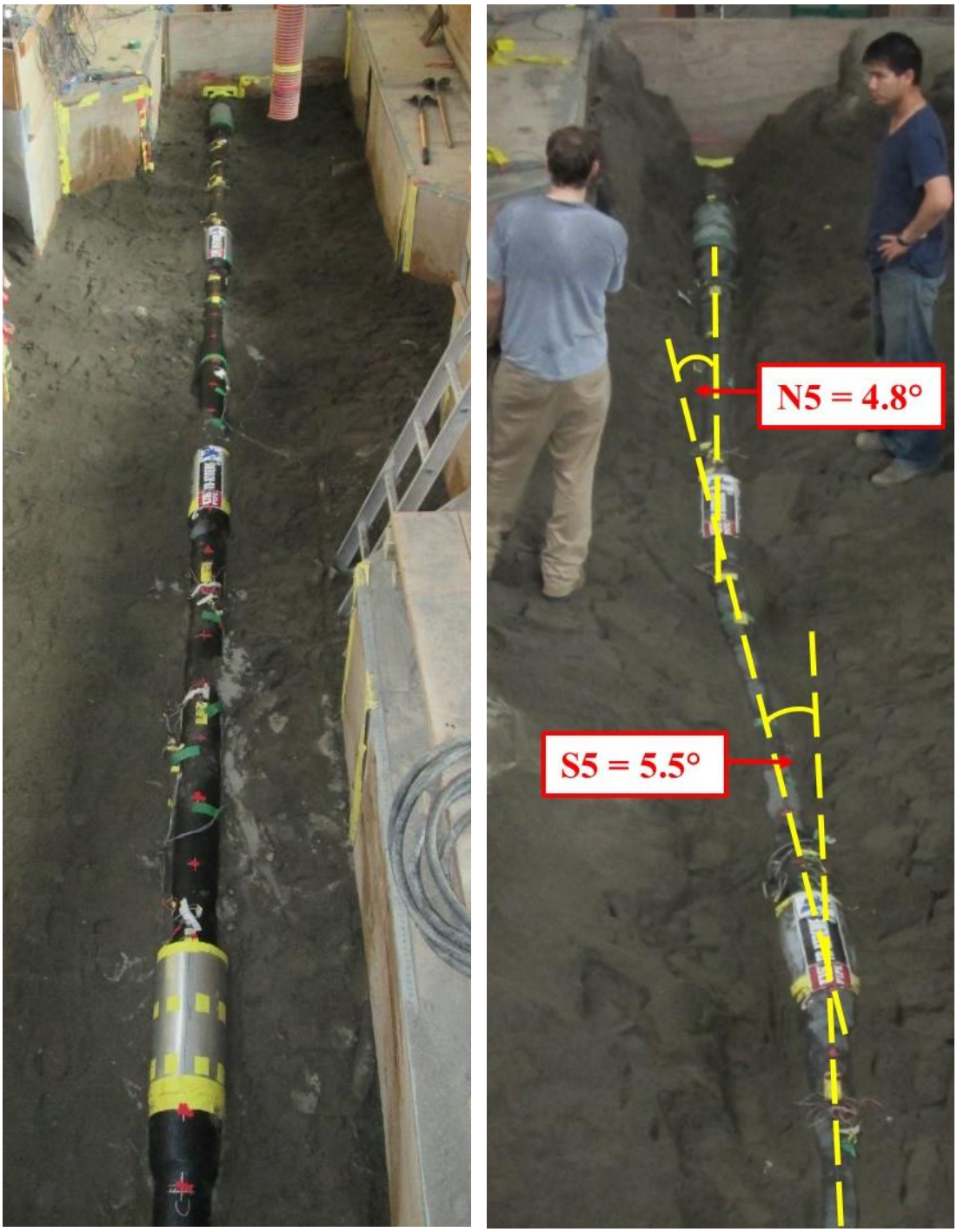

a) Before Burial b) After Excavation

Figure 6.44. Images of US Pipe Pipeline Positions (angles shown from total station surveying measurements)

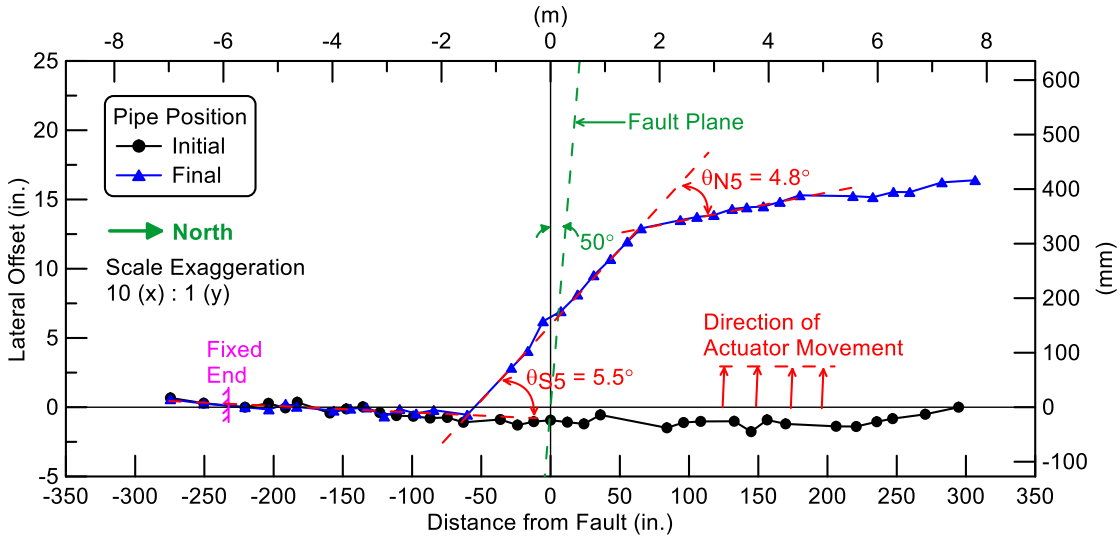

Figure 6.45. Initial and Final US Pipe Pipeline Positions from Surveying Measurements

20.2 in. (513 mm) of fault displacement, the pipeline moved 12.1 in. (307 mm) axially with 16.5 in. (419 mm) of lateral offset. The S15, S5, N5, and N15 joint displacements were 2.7 in. (69 mm), 4.6 in. (117 mm), 2.1 in. (53 mm), and 2.6 in. (66 mm), respectively. The displacement at the S5 joint was largest because the pipeline failed and cracked at the S5 bell. In addition, the rotations of the S5 and N5 were 5.5° and 4.8°, respectively. Small rotations of 0.4° and 1.1° were measured at the S15 and N15 joints, respectively.

6.6.3 Joint Pullout

The movements of all joints vs. fault displacement are presented in Figure 6.46. Joint slip initiated at the south and north joint closest to the fault plane, S5 and N5, followed by movement until slip was resisted by the spigot weld bead contacts with the

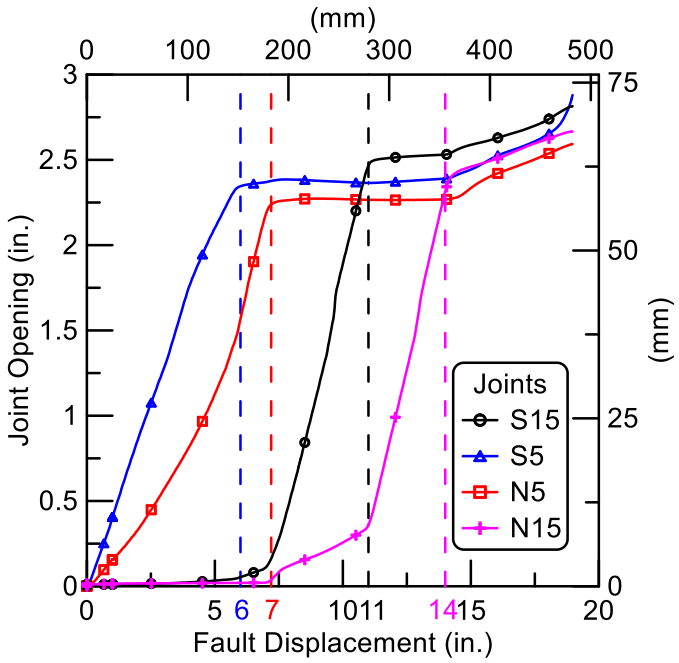

Figure 6.46. US Pipe Joint Displacement vs. Fault Displacement

Table 6.7. Maximum US Pipe Joint Displacement

Joint Location	Joint Displacement (in.)	
	DCDT Data [a]	Survey Data [b]
S15	2.8	2.7
S5	2.9	4.6
N5	2.6	2.1
N15	2.7	2.6
Average	2.7	3.0
All Four Joints	∑ = **11.0**	∑ = **12.0**
Axial Basin Extension (in.)	(19.0 in.) cos 50° = **12.2**	
Direct Tension Test	Three fully extended joints = 2.3 in. × 3 = 6.9 in. One failed joint = 3.5 in.	∑ = **10.4**

1 in. = 25.4 mm

[a] Joint displacement when pipe failure at 19.0 in. (483 mm) of fault displacement

[b] Joint displacement after test end at 20.2 in. (513 mm) of fault displacement

locking segments at 6 in. (152 mm) and 7 in. (178 mm) of fault movement, respectively. Similar slip initiation and movement occurred in the remaining joints until all joints had moved through their maximum range of movement. All four joints were fully engaged at 14 in. (356 mm) of fault displacement. Failure occurred at a fault displacement of approximately 19.0 in. (483 mm) by cracking and leaking of the S5 bell.

The movement of each joint at the end of test is presented in Table 6.7. DCDT and survey measurements of the joint movements are different because these measurements were taken at different fault displacements. The DCDT data correspond to the joint movements immediately before the S5 joint failed at 19.0 in. (483 mm) of fault displacement. The test was stopped at a fault displacement of 20.2 in. (513 mm), after which the pipeline was exposed, and the survey measurements were taken.

6.6.4 Joint Rotations

Joint rotations were determined with the DCDTs at each joint and compared with survey measurements. Joint rotations vs. fault displacement are provided in Figure 6.47. The N5 and S5 joints had opposite joint rotations and accommodated most of the fault offset with maximum rotations of 5.7° and 5.3°, respectively. Small rotations of 1.9° and 1.1° were measured at the S15 and N15 joints, respectively.

The maximum rotation of each joint obtained from DCDT and survey data is presented in Table 6.8. As discussed in the previous section, the joint rotations measured by the string pots and the survey data are different because the DCDT data correspond

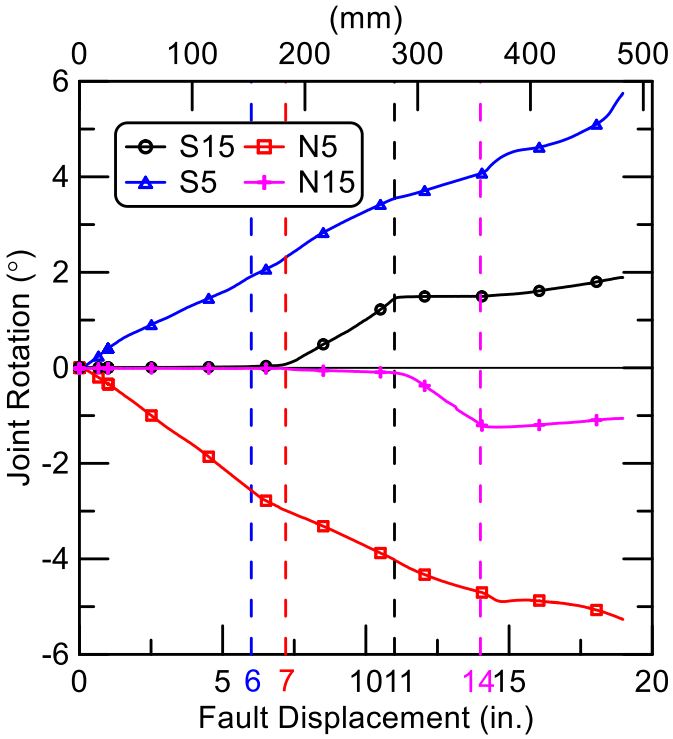

Figure 6.47. US Pipe Joint Rotations vs. Fault Displacement

Table 6.8. Maximum US Pipe Joint Rotation

Joint Location	Joint Rotation (°)	
	DCDT Data [a]	Survey Data [b]
S15	1.9	0.4
S5	5.7	5.5
N5	-5.3	-4.8
N15	-1.1	-1.1

Positive refers to rotation in counter-clockwise direction

[a] Rotation when pipe failure at 19.0 in. (483 mm) of fault displacement

[b] Rotation after test end at 20.2 in. (513 mm) of fault displacement

to the joint rotations at 19.0 in. (483 mm) of fault displacement, whereas the survey data were taken at 20.2 in. (513 mm) of fault movement.

6.6.5 Pipe Axial Forces

The test basin end loads were measured with four load cells at the south end of the test basin and four load cells at the north end. Figure 6.48 shows the total load at the south and north ends of the test basin vs fault displacement. The end loads were near zero during the beginning part of the test, and then increased sharply at a fault displacement of approximately 14.0 in. (356 mm). At 18.8 in. (1.03 m) of fault displacement, maximum loads of 61.9 kips (275 kN) and 61.3 kips (273 kN) were measured at the south and north ends, respectively.

Also included in Figure 6.48 are axial loads calculated with the axial strain gages at planes close to the end of the test specimen. The axial force in the pipeline was derived from average strain gage measurements and calculated as $F = \varepsilon AE$. The outside diameter of the pipe was OD = 6.9 in. (175 mm) and the average measured wall thickness was t_W = 0.3 in. (7.6 mm). This gives a pipe wall cross-sectional area, A = 6.22 in.^{2} (4,013 mm^2). The Young's modulus of the DI was E = 22,700 ksi (156 GPa), which was determined from tensile coupon tests. The maximum loads at the south and north gage stations were 54.6 kips (243 kN) and 60.4 kips (269 kN), respectively, which are within 12% lower than maximum loads measured by the south and north end load cells of 61.9 kips (275 kN) and 61.3 kips (273 kN), respectively.

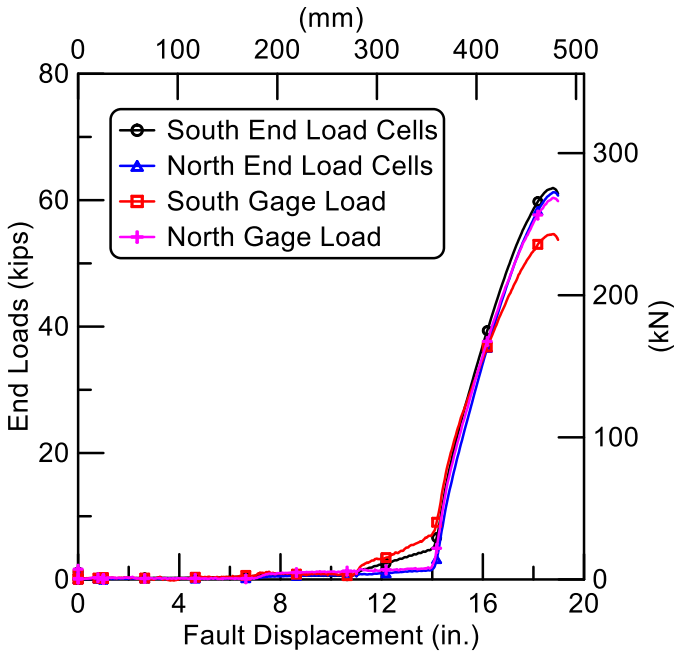

Figure 6.48. Comparisons of End Forces from Load Cells and Strain Gages for US Pipe Fault Rupture Test

The calculated axial loads at each gage plane along the pipeline are presented in Figure 6.49 for various levels of fault displacement. The joint locations are shown by green dashed lines. Figure 6.49 a) shows the tensile forces at 6 in. (152 mm), 7 in. (178 mm), 11 in. (279 mm), and 14 in. (356 mm) of fault movement where the S5, N5, S15, and N15 joints were fully extended, respectively. The tensile forces were generally higher with increasing fault displacement. High axial force was detected near the fault between the S5 and N5 joints, and the loads were lower at locations further away from the fault.

Figure 6.49 b) (note change in scale for load) shows the pipeline axial forces from 14 in. (356 mm) to the end of test at 19 in. (483 mm) of fault displacement. The

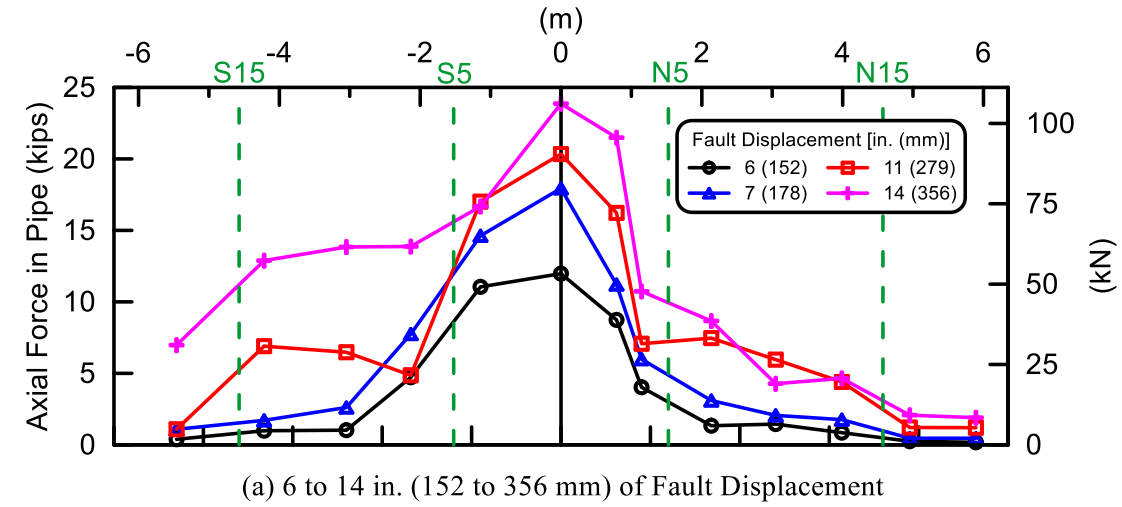

(a) 6 to 14 in. (152 to 356 mm) of Fault Displacement

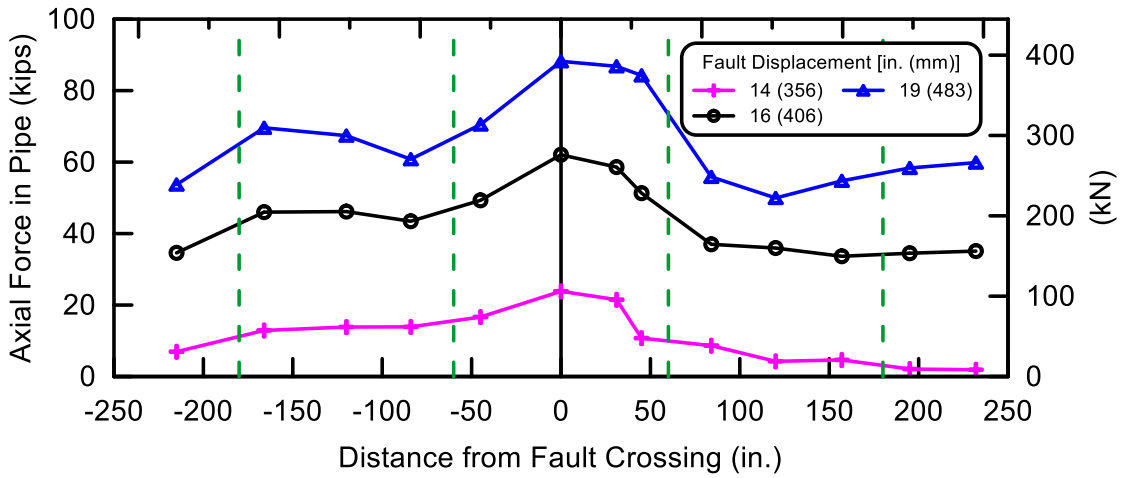

(b) 14 to 19 in. (356 to 483 mm) of Fault Displacement

Figure 6.49. Axial Forces in US Pipe Pipeline vs. Distance from Fault

forces increased rapidly after 14 in. (356 mm) of fault displacement. At 19 in. (483 mm) of fault movement, the peak force of 88.2 kips (392 kN) was detected at the fault location.

Figure 6.50 shows the force vs. displacement plots of at the S5 and N5 joints in the fault rupture test compared to the force vs. displacement relationship from the direct

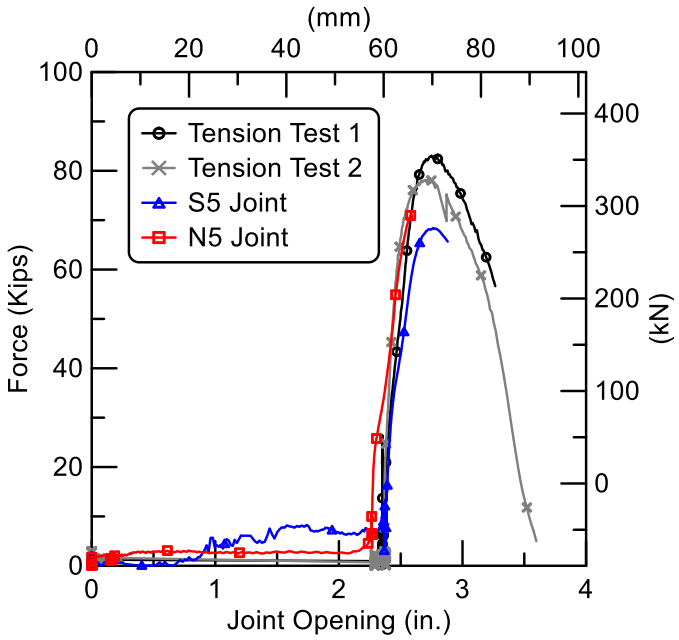

Figure 6.50. US Pipe Joint Axial Force vs. Displacement Comparisons

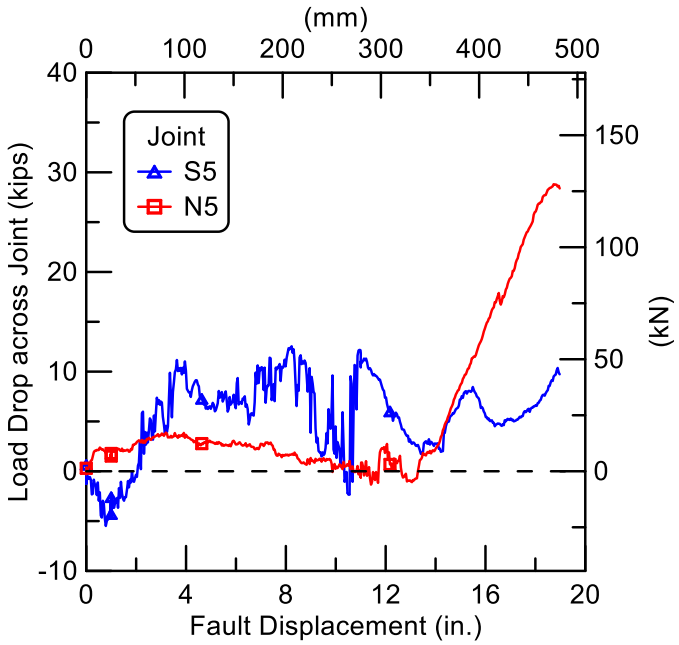

Figure 6.51. Load Drop across US Pipe Joint vs. Fault Displacement

tension tests. The force at each joint was taken from the average calculated load of the south and north gage stations closest to the joint. The maximum forces at the S5 and N5 joints were 68.4 kips (304 kN) and 71.1 kips (316 kN), respectively, which are approximately 12-15% lower than the maximum force in the direct tension test because the fault rupture imposed combined loading in tension and bending at the joints.

Figure 6.51 shows the load drops across the closest joints south, S5, and north, N5, of the fault plane. The load drop across the S5 joint is calculated by subtracting the load at the station 45 in. (1.14 m) south of the fault with the load at the station on the south side of the joint [station 84 in. (2.13 m) south of the fault]. Similarly, the load drop across the N5 joint is calculated by subtracting the load at the station 45 in. (1.14 m) north of the fault with the load at the station on the north side of the joint [station 84 in. (2.13 m) north of the fault]. The load drop across the S5 joint fluctuated between about 5 and 10 kips (22 and 44 kN) during most of the test, related primarily to fluctuation in measurements at station 45 in. (1.14 m) south of the fault. The maximum load drop across the N5 joint of 28.8 kips (128 kN) was observed near the end of the test at 18.8 in. of fault displacement.

6.6.6 Bending Moments

Figure 6.52 presents the bending moments measured along the pipeline, corresponding to various levels of fault displacement. The joint locations are shown by green dashed lines. Figure 6.52 a) shows the bending moments at to 6 in. (152 mm), 7

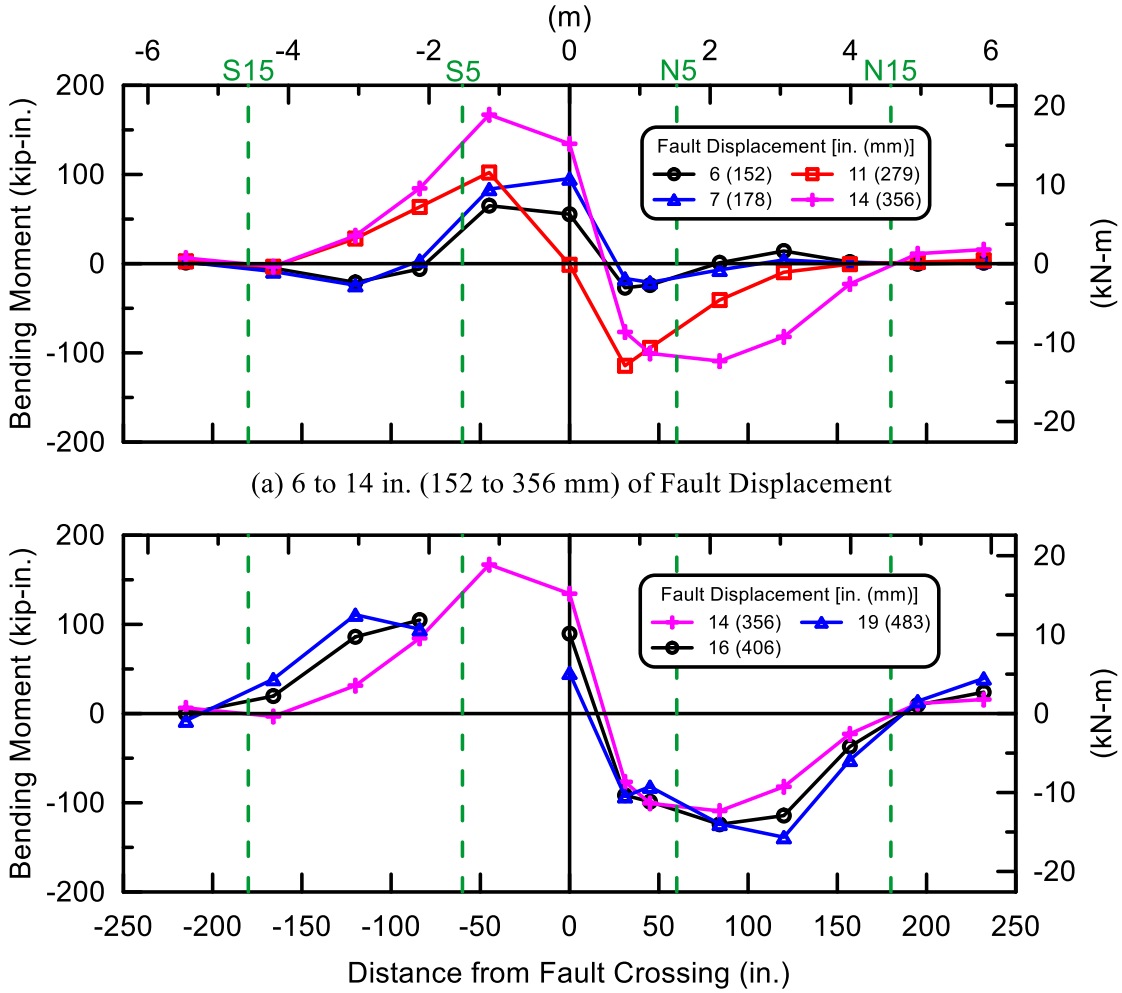

(a) 6 to 14 in. (152 to 356 mm) of Fault Displacement

(b) 14 to 19 in. (356 to 483 mm) of Fault Displacement

Figure 6.52. Bending Moments in US Pipe Pipeline vs. Distance from Fault

in. (178 mm), 11 in. (279 mm), and 14 in. (356 mm) of fault movement where the S5, N5, S15, and N15 joints were fully extended, respectively. The measurements disclose an anti-symmetric pattern of moment distribution centered on the fault. Figure 6.52 b) shows a similar pattern of bending moment distribution for fault movements of 14 in. (356 mm) to 19 in. (483 mm). The springline strain gages at the station 45 in. (1.14 m)

south of the fault did not function properly after 14 in. (356 mm) of fault displacement, and therefore the bending moments at this location are not shown.

Figure 6.53 shows the moment vs. rotation plots for the S5 and N5 joints derived from fault rupture test measurements in comparison with the moment vs. rotation relationship from the four-point bending test. The moment of each joint in the fault rupture test was taken from the average calculated moment of the south and north gage stations closest to the joint. The moment vs. rotation plots of the S5 and N5 joints are in a reasonable agreement with the four-point bending test results. It should be recognized that the moment vs. rotation relationship of the S5 joint is shown until 14 in. (356 mm), after which the springline strain gages at the station 45 in. (1.14 m) south of the fault did not function properly.

6.7 Significance of Fault Rupture Test Results

The amount of tensile strain of all four DI pipelines with restrained axial slip joints are large enough to accommodate the great majority (over 90%) of liquefaction-induced lateral ground strains measured by high resolution LiDAR after each of four major earthquakes during the recent Canterbury Earthquake Sequence (CES) in Christchurch, NZ (Bouziou et al., 2015). These high resolution LiDAR measurements for the first time provide a comprehensive basis for quantifying the ground strains caused by liquefaction on a regional basis. To put the CES ground strains in perspective, the levels of liquefaction-induced ground deformation measured in Christchurch exceed

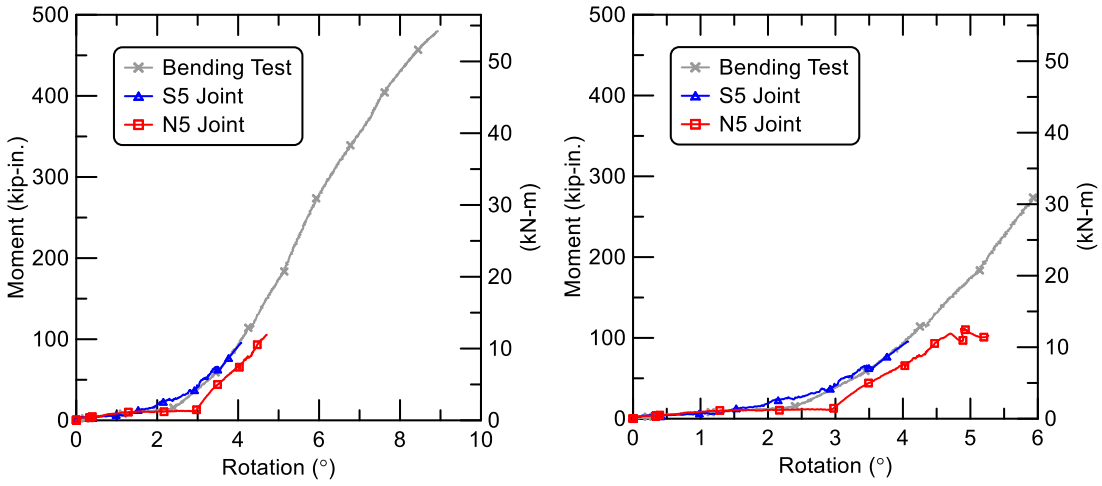

a) Full Range b) First 6° of Rotation

Figure 6.53. US Pipe Joint Moment vs. Rotation Comparisons

those documented in San Francisco during the 1989 Loma Prieta earthquake and in the San Fernando Valley during the 1994 Northridge earthquake. They are comparable to the levels of most severe liquefaction-induced ground deformation documented for the 1906 San Francisco earthquake, which caused extensive damage to the San Francisco water distribution system.

6.8 Summary

Fault rupture tests were performed on four nominal 6-in. (150-mm) diameter DI pipelines with restrained axial slip joints. These pipelines were able to accommodate significant fault movement through axial pullout and rotation of the joints with their sequence of movements. The amount of tensile strain that can be accommodated with

a DI pipeline will depend on the number and spacing of the joints or couplings and the positioning of the spigot within the bell at the pipeline joints.

Force vs. displacement and moment vs. rotation relationships of the joints closest to the fault were developed and compared to similar relationships obtained from the direct tension and four-point bending tests, respectively. The test measurements show that moment vs. rotation relationships of the joints for the fault rupture test are in close agreement with the results of the four-point bending tests. All four-point bending tests were performed with the joints fully extended, which is consistent with the full joint extension developed in the fault rupture test.

Although the force vs. displacement relationships from the fault rupture tests follow a pattern similar to those measured during the direct tension tests, the loads at failure are significantly lower than those measured in the direct tension tests. Reductions in the tensile capacity of 15% and 25% were measured in the US Pipe and McWane tests, respectively. The experimental evidence indicates that these reductions in joint tensile capacity were caused by combined rotation and axial expansion of the joints.

CHAPTER 7

SIMPLIFIED MODELS FOR PIPELINE RESPONSE TO FAULT RUPTURE

7.1 Introduction

This chapter explores the use of a simplified model to evaluate the resistances of pipeline joints and restraints against axial movement through soil. It provides an assessment of the axial load drop across DI pipeline joints during fault rupture tests. It applies the simplified analytical model presented in Appendix A to predict the axial load distribution in the McWane and US Pipe fault rupture tests, and compares the analytical results with the measured loads.

7.2 Joint Axial Resistance Model

As shown in Chapter 5, an enlarged axial slip joint increases axial resistance to DI pipeline longitudinal movement in soil. Soil axial resistance tests, similar to those described in Chapter 5, were conducted on nominal 6-in. (150-mm)-diameter seismic resistant, oriented polyvinyl chloride (PVCO) pipelines. A detailed description of these tests is provided by Wham et al. (2017). The PVCO pipelines were installed with mechanical restraints across bell-and-spigot push-on joints to resist axial pullout, and thus accommodate axial elongation imposed by earthquake-induced ground deformation. The joint restraint had an enlarged cross-section that also increased the axial resistance of the joint against movement in soil. Both the DI and PVCO pipelines were buried in partially saturated medium dense to dense sand with $\phi' = 42°$.

The joint axial resistance is predicted from the expression for face resistance of the leading edge of a jacked pipe proposed by Meskele and Stuedlein (2015) from the work of Weber and Hurtz (1981) whereby the joint axial resistance, R_f, is given by

$$R_f = r_f A = r_f \frac{\pi}{4}\left[D_B{}^2 - D_S{}^2\right] \tag{7.1}$$

where A is the cross-sectional area of the cutting edge, D_S is the outside diameter of a spigot, and D_B is the outside diameter of a DI bell. For a PVCO pipe, face resistance is mobilized by the cross-sectional bearing area of the restraint. Figure 7.1 shows a cross-section of a nominal 6-in. (150-mm)-diameter PVCO restraint. The estimated outside diameter of the restraint, D_B, is 11.1 in. (281 mm). The restraint is installed around a nominal 6-in. (150-mm)-diameter PVCO pipe that has an outside diameter, D_S, of 6.9 in. (175 mm). These outside diameter, D_B and D_S, are then substituted in Eqn. 7.1 to calculate the cross-sectional bearing area of the restraint, A.

The unit face resistance, r_f, is expressed as

$$r_f = \lambda \cdot \sigma'_v \cdot \tan\phi' \tag{7.2}$$

where ϕ' is the effective stress soil friction angle, σ'_v is the vertical effective stress at the springline of the pipe, and λ is a carrying capacity coefficient. For $\phi' \leq 45°$, λ can be approximated as

$$\lambda = \frac{3\pi}{2} e^{\pi \tan\phi'} \tag{7.3}$$

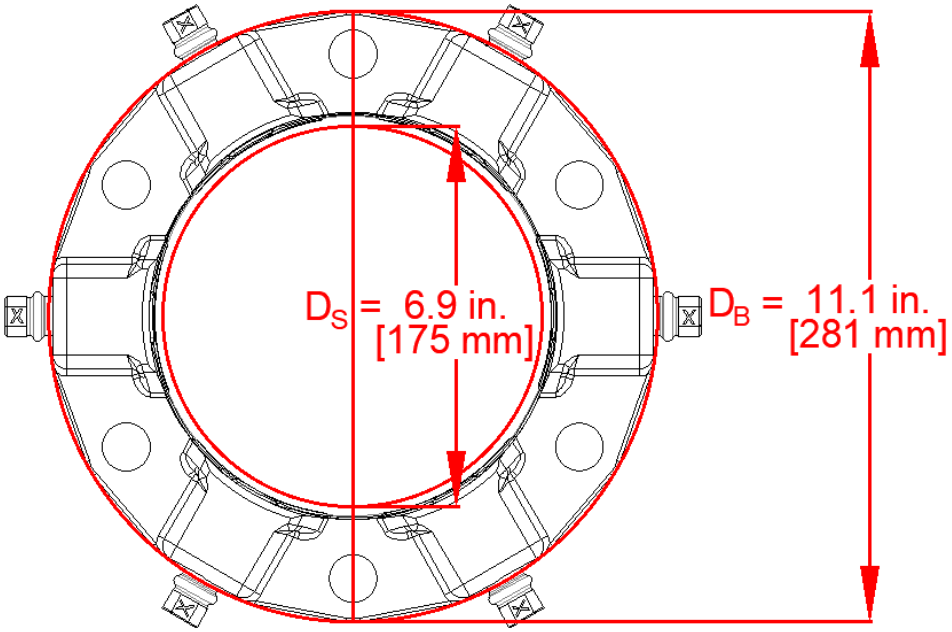

Figure 7.1. Transverse Cross-section of Nominal 6-in. (150-mm)-Diameter PVCO Restraint

It should be noted the predicted face resistance proposed by Weber and Hurtz (1981) applies to an orientation where the flat end of a bell restraint is facing the direction of axial movement. As discussed in Chapter 5, the curved bell resistance was approximately 15% lower than the flat bell, and thus the calculated joint axial resistance, R_f, must be reduced by 15% for predicting the curved bell resistance.

Table 7.1 lists the various joints and restraints used in the tests as well as their relevant dimensions. Figure 7.2 shows the peak measured joint axial resistances plotted against the predicted load from Eqns. 7.1 to 7.3 for DI pipe with a restrained axial slip joint and seismic resistant PVCO pipelines with restraints across the joints. The line with slope of 1H:1V defines the relationship where the measured load everywhere

Table 7.1. Summary of Joint Type, Pipe Dimensions, and Predicted and Measured Load Drops

Pipeline	D_S (in.)	D_B (in.)	H_c (in.)	Predicted Load Drop (kips)	Measured Load Drop (kips)
DI pipeline with restrained axial slip joint	6.9	9.3	38	5.3	5.4
PVCO pipeline with restrained bell and spigot joint (Wham et al., 2017)	6.9	11.1	33	8.9	7.4
	6.9	11.1	48	13.2	10.9
	6.9	11.1	63	17.1	15.5
PVC pipeline with restrained bell and spigot joint [a]	6.9	10.0	33	6.4	6.2
	6.9	10.0	48	9.2	9.6
	6.9	9.7	48	8.0	8.4

[a] Data reduced from axial pull tests. No final report available for these tests at the time of dissertation preparation.
1 in. = 25 mm
1 kip = 4.4 kN

equals the predicted one. In general, the experimental results plot within ±15% of the predicted loads. Eqns. 7.1 through 7.3 provide for relatively close prediction of the actual maximum load mobilized by axial movement of the joints under K_o conditions.

7.3 Axial Load Drops from Fault Rupture Tests

As explained in Appendix A, the axial resistance to joint movement during a fault rupture test can be evaluated by recognizing that longitudinal shear transfer from soil to pipe scales in direct proportion to the lateral soil forces mobilized during fault

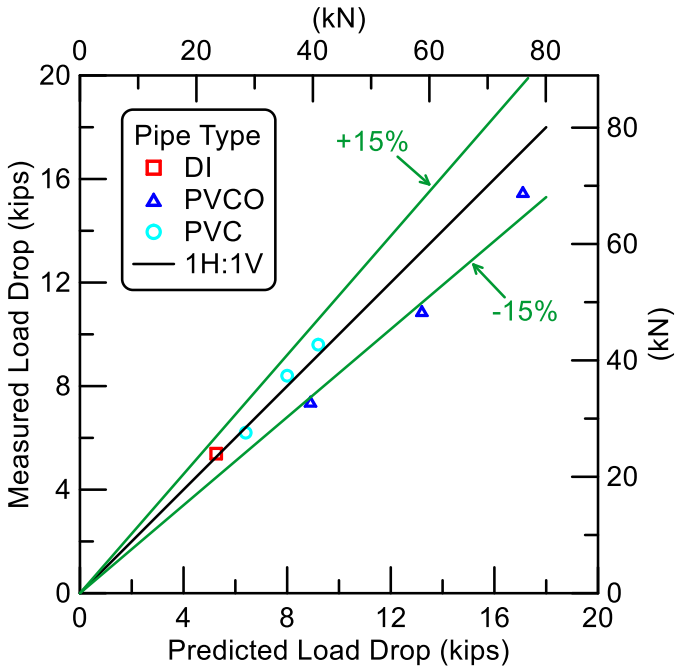

Figure 7.2. Comparison of Measured and Predicted Axial Load Drops

movement. Using the scaling relationship proposed by Argyrou (2018) and described in Section A.4, the maximum axial bell resisting force is calculated by Eqn. A.23. The axial bell resisting force for at-rest (K_o) conditions is calculated by Eqn. A.22. These estimated resisting forces are compared with the axial load drops measured for the joints closest to the fault during the AMERICAN, Kubota, McWane, and US Pipe fault rupture tests.

Figure 7.3 shows measured load drops across the AMERICAN joints vs. fault displacement, as well as the load predictions for K_o conditions. To understand the sequence of load drops, it is important to recognize that the fault rupture test with AMERICAN restrained axial slip joints followed a sequence of axial joint movement that differed from what was observed in the other fault rupture tests.

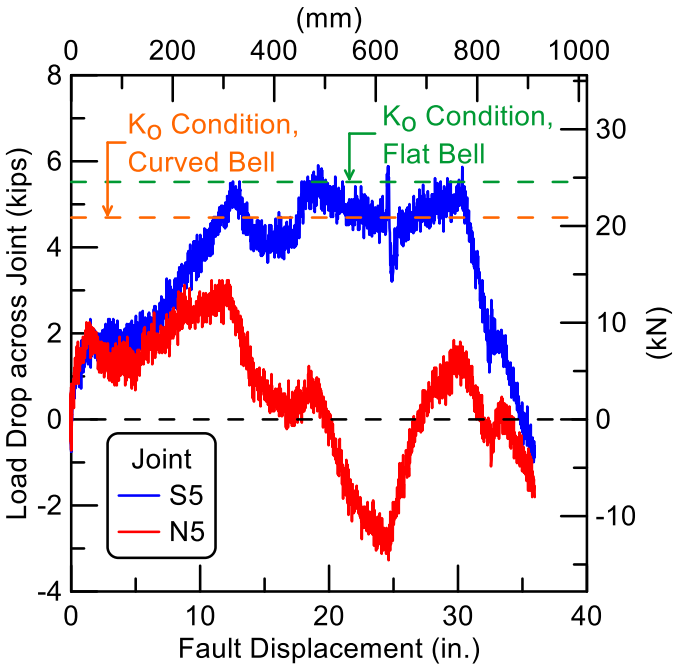

Figure 7.3. Load Drop across Joint in AMERICAN Fault Rupture Test

The south joint nearest to the fault was equipped with a deep socket SE component [see Figure 1.1 b)] closest to fault rupture. During initial fault movement the SE part of the joint was subject to metal binding at relatively low rotation, thereby generating axial resistance to movement that transferred pullout load to the north joint nearest the fault, which was equipped with an FR component [see Figure 1.1 b)] closest to fault rupture. This transfer of force resulted in the north joint moving first. Thus, the sequence of joint movements differed from that of the other tests, with the north joint closest to the fault undergoing full axial slip until its locking mechanism was engaged. This movement was followed by pullout of the south joint spigot nearest the fault to engage its locking mechanism, after which axial movement was transferred to the second joint south of the fault. The consecutive pullout of the two south joints caused

a reversal of direction at the north joint nearest the fault. This reversal of movement can be seen as a negative load drop between 20 and 25 in. (508 mm and 635 mm) of fault displacement in Figure 7.3.

Figure 7.3 also shows load drops across the joints that are the lowest measured for all the fault rupture tests. Apparently, the reversal of movement for the relatively long and large diameter joints caused soil disturbance and modification of the soil stress state to conditions for which axial joint resistance was more consistent with forces mobilized under K_o conditions. The predicted flat bell resistance for the K_o conditions compares favorably with the maximum load drop measured at the S5 joint of 5.9 kips (26 kN). In contrast, measured load drop across the N5 joint is significantly lower than that at the S5 joint, which reflects a reversal of joint movement as described above.

Figure 7.4 shows measured load drops across the Kubota joints vs. fault displacement, as well as the load predictions for K_o and maximum lateral soil force conditions. The load drop across the S5 joint was higher than that of the N5 joint. The maximum load drop across the S5 joint was halfway between the load drop predicted for K_o and maximum lateral soil force conditions. The data show negative load drops in the N5 joint for fault displacement exceeding approximately 20 in. (508 mm). As discussed previously for the AMERICAN fault rupture test, negative load drop implies a reversal of axial movement at the N5 joint. It should be recognized that due to the large fault offset and soil reaction condition, more than 40% of the strain gages were

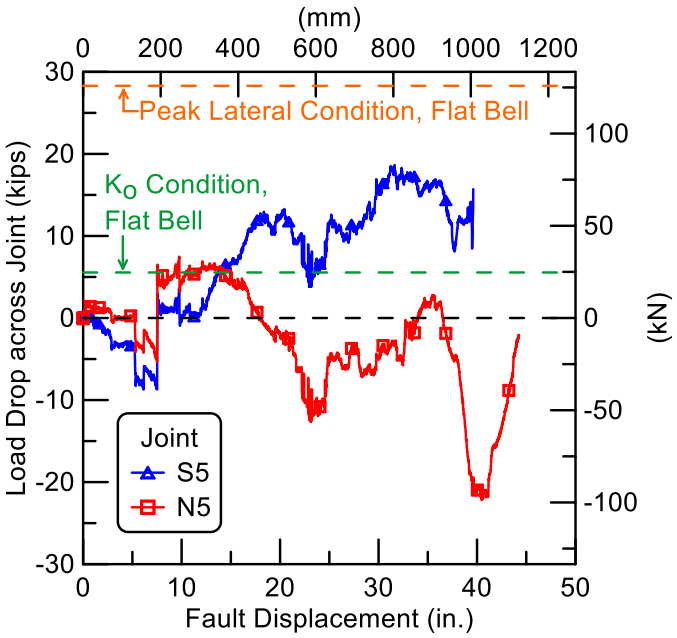

Figure 7.4. Load Drop across Joint in Kubota Fault Rupture Test

damaged at the end of the test. The lack of data makes it difficult to evaluate the load drops across the Kubota joints with the same detail and precision as for the other tests.

Figure 7.5 shows measured load drops across the McWane joints vs. fault displacement, as well as their peak predictions for K_o and maximum lateral soil force conditions. The S SFC joint had a small load drop of 4.0 kips (18 kN), which was close to the K_o conditions of 5.5 kips (23 kN). In contrast, a substantial load drop of 20.6 kips (92 kN) was measured at the N SFC joint. This load was approximately 12% lower than the predicted curved bell resistance for peak lateral soil force conditions.

Figure 7.6 shows measured load drops across the US Pipe joints vs. fault displacement, as well as their peak predictions for K_o and maximum lateral soil force

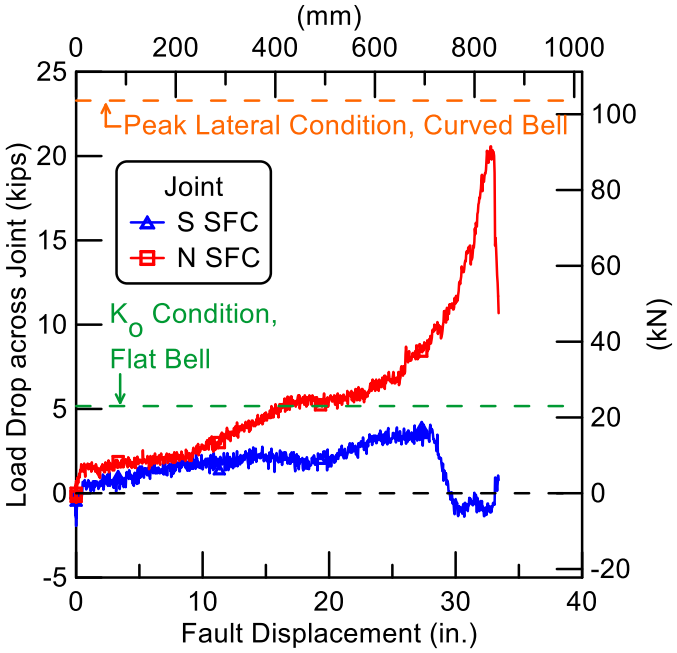

Figure 7.5. Load Drop across Joint in McWane Fault Rupture Test

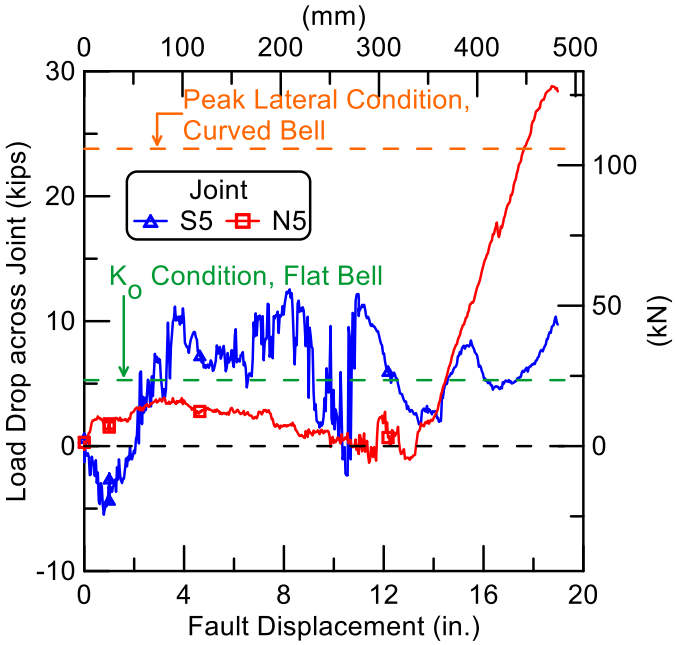

Figure 7.6. Load Drop across Joint in US Pipe Fault Rupture Test

conditions. The load drop across the S5 joint fluctuated between 5 and 10 kips (22 and 44 kN) during most of the test. In contrast, significant load drop of 28.8 kips (128 kN) was generated at the N5 joint. This load was approximately 21% higher than the predicted curved bell resistance for the peak lateral soil force conditions, but approximately equal to predicted flat face joint resistance for peak lateral soil force.

Load drop variations were caused by complex soil/pipe interactions and longitudinal shear transfer from soil to pipeline. In some cases, the load drops across the joints are higher than predicted for maximum lateral soil reaction. In other cases, the load drops across the joints are below K_o conditions. It appears that there is significant soil disturbance caused by reversal of axial movement of the relatively large AMERICAN joints. Reversal of movement disrupts the soil stress conditions, reducing the shear transfer from soil to pipeline.

In some cases, it appears that there is some out of plane deformation of the pipeline and the joints. Test data indicate that significant bending occurred both in the lateral and vertical planes for the US Pipe fault rupture experiment. Vertical bending would add to the bearing forces at the joint caused by lateral bending, thus increasing the maximum load drop across the joints.

7.4 Simplified Model for Axial Force Distribution during Fault Rupture Tests

A simplified model for axial force distribution along a DI pipeline with restrained axial slip joints is presented in Appendix A. The model is used to predict the axial force distributions in the McWane and US Pipe fault rupture tests for two

conditions. The first condition involves full slip of all joints with all locking mechanisms engaged to resist further axial slip. The second condition corresponds to the maximum axial force in the pipeline before failure. These two conditions bound the pipeline behavior of interest during fault rupture tests. The correction factor described in Appendix B was applied to evaluate the actual axial elongation of the test pipeline for the first condition with full slip of all joints. When this correction factor is applied, little to no axial anchor force is predicted using the simplified model. This absence of anchor forces is consistent with the accommodation of axial slip among all pipeline joints. Such slip is accompanied by very little axial force until the locking mechanism is engaged, as shown by the experimental results in Chapter 3. Once the locking mechanism is activated in all joints, there is a continuous tensile load path through all pipe segments with a buildup of anchor forces.

7.4.1 McWane

Figures 7.7 and 7.8 show the axial force distributions in the McWane pipeline for the condition of full slip at each joint and at the maximum axial load in the pipeline before failure, respectively. These plots show comparisons between the experimental data and the results of the simplified models. As presented in Figure 6.31, the survey data for the McWane fault rupture test show that there was large lateral movement at the N SFC joint, whereas the lateral displacement at the S SFC joint was very small at the end of the test. From the survey data, it appears that K_o conditions result in a more appropriate state of soil stress for the south joint.

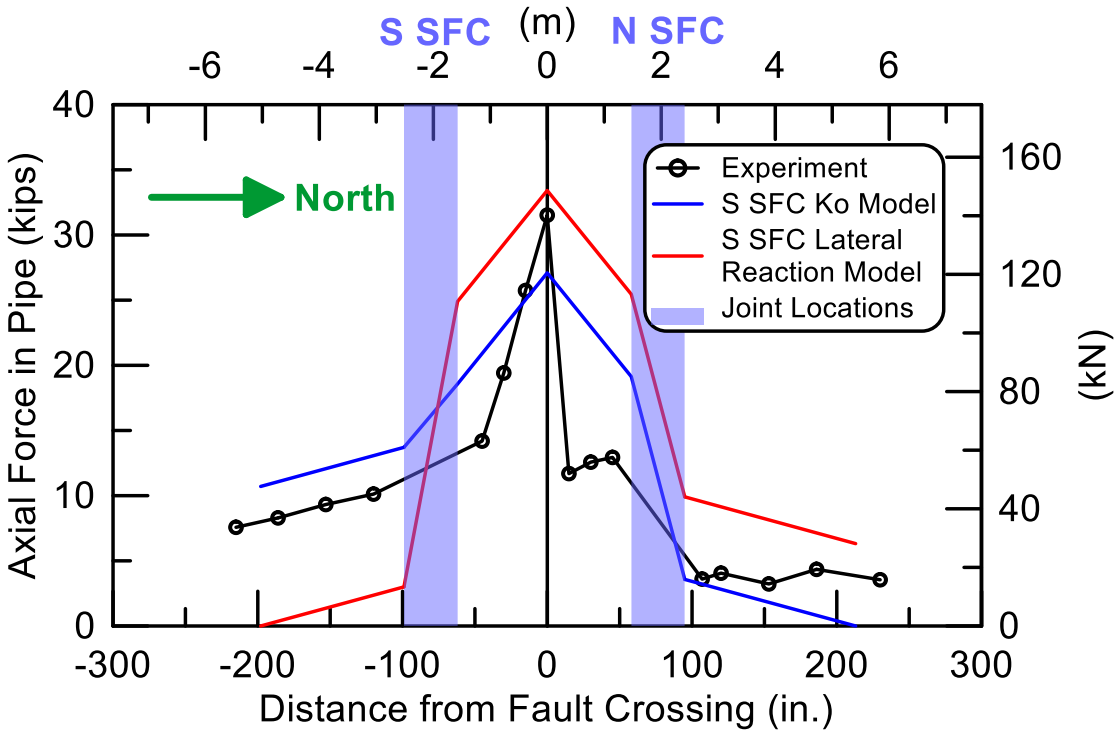

Figure 7.7. Axial Load Distributions in McWane DI Pipeline at Full Joint Slip

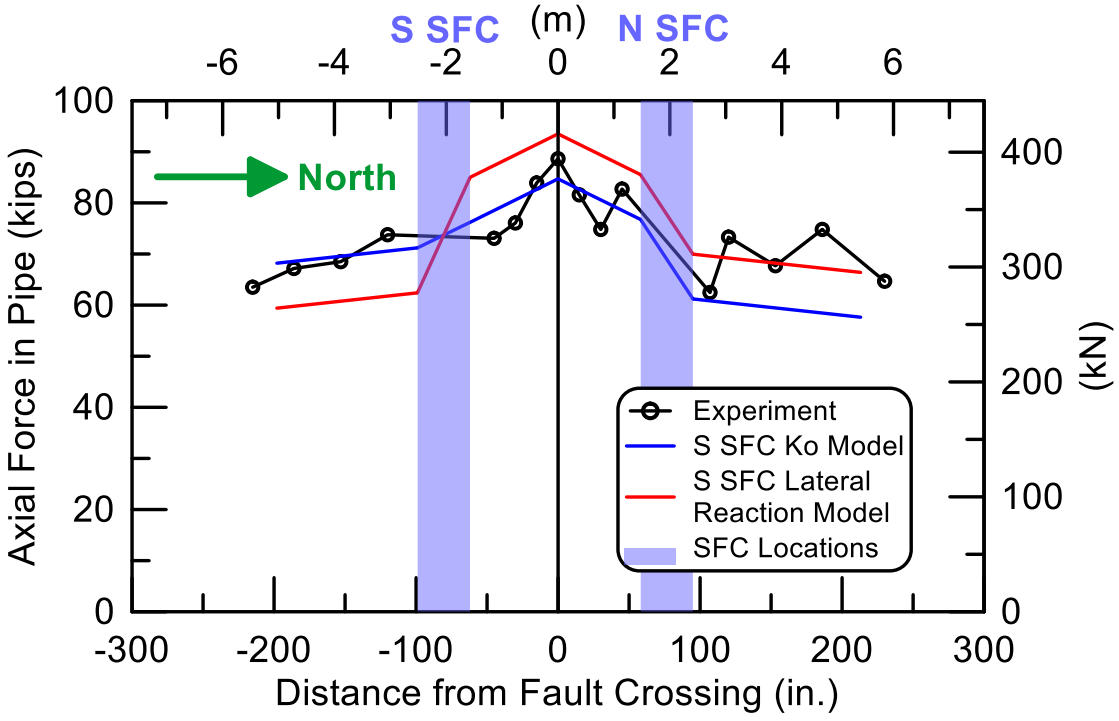

Figure 7.8. Maximum Axial Load Distributions in McWane DI Pipeline

Figure 7.7 compares the axial load measurements at full slip of all joints with the loads calculated for the same condition with the simplified model. Two cases using the simplified model are plotted, involving 1) load drop across both joints under maximum lateral soil reaction (S SFC lateral reaction model), and 2) load drop across the south and north joints under K_o and maximum lateral soil reaction conditions (S SFC K_o model), respectively. The S SFC K_o model results follow the trend of the measurements more closely, although they under predict the maximum axial force at the fault. In comparison, the S SFC lateral reaction model provides a close prediction of the maximum axial force, but shows load distributions away from the fault that do not closely match the experimental data.

Figure 7.8 compares the axial load measurements at maximum load before failure with the loads calculated for the same condition with the simplified model. The S SFC K_o model results agree well with the experimental data, especially for the south and central section of the test basin. The S SFC lateral reaction model results provide an upper bound for the data throughout the pipeline section closest to the fault.

7.4.2 US Pipe

Figures 7.9 and 7.10 show the axial force distributions in the US Pipe test pipeline for the condition of full slip at each joint and at the maximum axial load in the pipeline before failure, respectively. These plots show comparisons between the experimental data and the results of the simplified models. As presented in Figure 6.45,

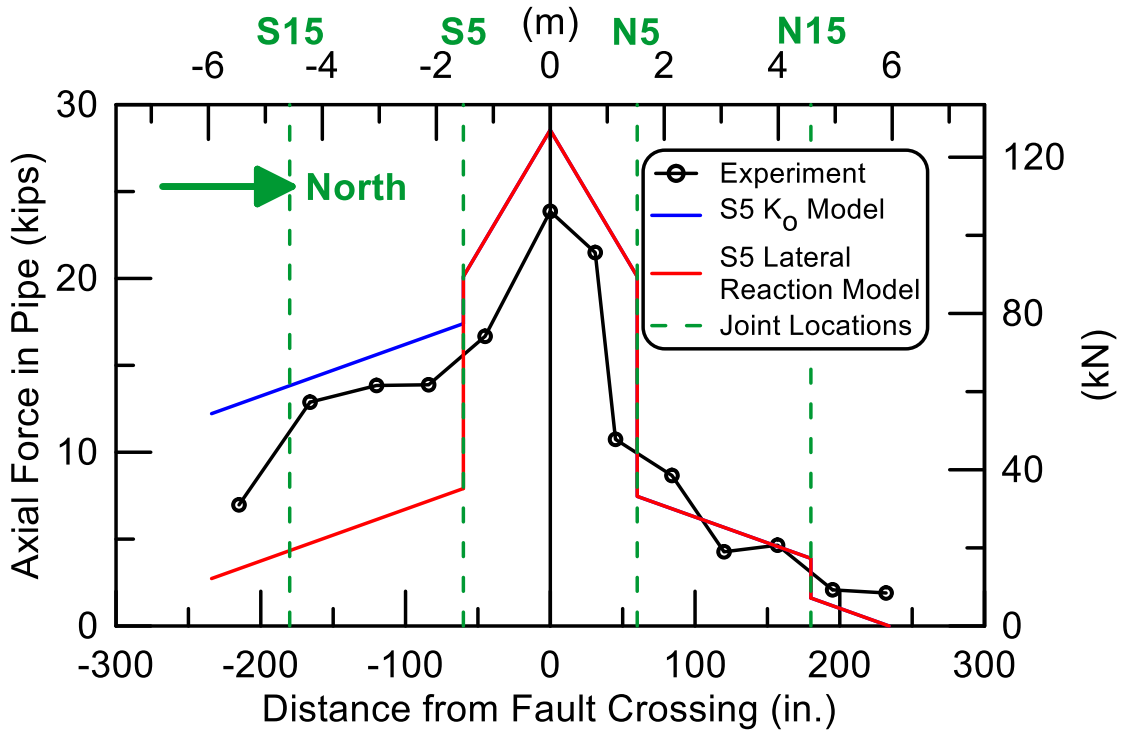

Figure 7.9. Axial Load Distributions in US Pipe DI Pipeline at Full Joint Slip

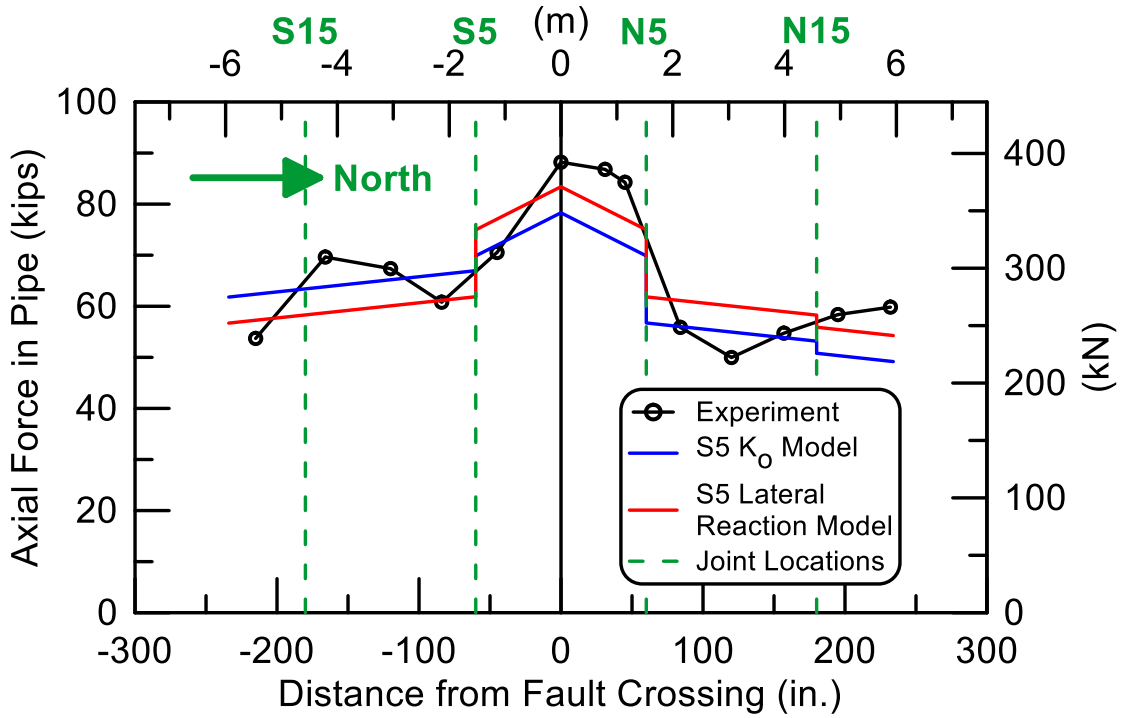

Figure 7.10. Maximum Axial Load Distributions in US Pipe DI Pipeline

the survey data for the US Pipe fault rupture test show that there was large lateral movement at the N5 joint, whereas the lateral displacement at the S5 joint was very small at the end of the test. From the survey data, it appears that K_o conditions result in a more appropriate state of soil stress for the south joint.

Figure 7.9 compares the axial load measurements at full slip of all joints with the loads calculated for the same condition with the simplified model. Two cases using the simplified model are plotted, involving 1) load drop across both joints under maximum lateral soil reaction (S5 lateral reaction model), and 2) load drop across the south and north joints under K_o and maximum lateral soil reaction conditions (S5 K_o model), respectively. Both models agree well with the experimental data north of the N5 joint, and over predict the maximum axial force by about 18% at the fault crossing. In the south section of the test basin, the S5 K_o model results agree well with the experimental data.

Figure 7.10 compares the axial load measurements at maximum load before failure with the loads calculated for the same condition with the simplified model. Both model results agree well with the experimental data at the south and north sections of the test basin. The maximum axial force at the fault crossing is under predicted by about 5%. The experimental data show a very large load drop across the N5 joint. Relatively large vertical bending movements were measured at the N5 joint. Vertical movement at the joint would add to the load drop generated by high lateral soil reaction.

7.5 Summary

This chapter explores the use of a simplified model to evaluate the resistances of pipeline joints and restraints against axial movement through soil. The joint axial resistance model provides for relatively close prediction within ±15% of the actual maximum load mobilized by axial movement of the joints under K_o conditions.

The predicted bell resisting forces are compared with the axial load drops measured for the joints closest to the fault during the AMERICAN, Kubota, McWane, and US Pipe fault rupture tests. Load drop variations were caused by complex soil/pipe interactions and longitudinal shear transfer from soil to pipeline. It appears that there is significant soil disturbance caused by reversal of axial movement of the relatively large AMERICAN joints. Reversal of movement disrupts the soil stress conditions, reducing the shear transfer from soil to pipeline. In some cases, significant bending occurred both in the lateral and vertical planes, which would increase the maximum load drop across the joints.

The simplified analytical model is used to predict the axial load distribution in the McWane and US Pipe fault rupture tests for two conditions. The first condition involves full slip of all joints with all locking mechanisms engaged to resist further axial slip. The second condition corresponds to the maximum axial force in the pipeline before failure. The simplified model provides range of axial load distributions in reasonable agreements with the McWane and US Pipe experimental results.

CHAPTER 8

SUMMARY AND CONCLUSIONS

8.1 General Objectives

The primary objectives of this work are to evaluate the key mechanical factors affecting the performance of DI pipelines with restrained axial slip joints under earthquake-induced ground deformation. This evaluation is based on large-scale laboratory tests on four different commercially available jointed DI pipelines with nominal 6-in. (150-mm) diameters. Each pipeline system was investigated with the same testing protocol involving 1) tensile coupon tests, 2) direct compression and tension tests, 3) four-point bending tests, 4) soil axial resistance tests in which a buried DI pipeline with restrained axial joint is displaced axially through the soil, and 5) fault rupture tests on a jointed DI pipeline of approximately 34 ft. (10 m) in length. Thus, a consistent and repeatable framework was established with which to measure and characterize jointed DI pipeline response to imposed deformation that is similar to that caused by earthquake-induced ground movements. Conclusions associated with these objectives are summarized in the sections that follow. Recommendations for future research are given at the end of the chapter.

8.2 Tensile Coupon Tests

Tensile coupon tests were performed on DI specimens taken from pipe supplied by AMERICAN, Kubota, McWane, and US Pipe. Tensile coupon tests were performed

in accordance with ASTM-E8 2016 (ASTM, 2013). The test data for AMERICAN, McWane, and US Pipe specimens show Young's modulus, E, between 21,800 ksi (150 GPa) and 26,700 ksi (184 GPa) with an average of 23,700 ksi (163 GPa). Average yield and ultimate stresses are 52.0 ksi (359 MPa) and 74.1 ksi (511 MPa), respectively. The average ultimate tensile strain for all DI pipe specimens tested is 6.2%. All tensile coupon test specimens for pipe manufactured in the U.S. comply with ANSI/AWWA C151/A21.51-17 (AWWA, 2017) with respect to yield and ultimate stresses, but are low with respect to ultimate strain.

In comparison, tensile coupon test specimens from pipe supplied by Kubota comply with JWWA G113, 114-2010 (JWWA, 2010) with respect to ultimate stress and strain. The standard does not cover yield stress. The average yield, ultimate stress, and ultimate strain from the tensile coupon tests are 39.3 ksi (271 MPa), 61.3 ksi (422 MPa), and 13.5%, respectively.

For all specimens, there is a narrow range of Poisson's ratio between 0.27 and 0.29. There is also a close agreement for all specimens regarding to the ratio of proportional limit to yield stress between 0.61 to 0.68 with an average of 0.65.

8.3 Direct Compression and Tension Tests

Direct compression and tension tests were performed on nominal 6-in. (150-mm) diameter restrained axial slip DI pipe joints at water pressures of 75 to 85 psi (520 to 590 kPa). The direct compression tests show either leakage or irrecoverable

deformation in the form of large rotation at loads equal to or slightly higher than load consistent with the proportional limit stress of DI pipe.

The direct tension tests show that tensile failure of the pipeline depends on the axial restraining mechanism of the joint. Joints that use full circumferential rings to resist axial pullout generate the highest resisting force, whereas those that use locking segments mobilized lower pullout force. Failure of the Kubota joint occurred as DI ring shear failure both in the direct tension test and fault rupture tests. Failure of the AMERICAN joint occurred as a bell fracture in both the direct tension and fault rupture tests.

Locking segments, which are employed with the US Pipe and McWane joints, cover only part of the spigot circumference, as shown in Figure 4.6. As the spigot is pulled from the bell, the weld bead on the spigot engages the locking segments. The locking segments bear against the bell lip and begin rotating onto the spigot. Load concentration at the locking segment locations causes the spigot to deform from a circular to an oval shape. This inward deformation at the locking segment locations allows the weld bead to slip past the locking segments, causing leakage.

The 12-in. (300-mm)-diameter US Pipe joint uses four locking segments as opposed to two for the 6-in. (150-mm) joint. The locking segments cover most of the spigot circumference, as shown in Figure 4.14. The circumferential loads from the locking segments are more evenly distributed to confine the spigot, thus preventing ovaling of the pipe. As a consequence, ovaling of the 12-in. (300-mm)-diameter pipe is

not the governing mechanism for failure. Tensile failure of the 12-in. (300-mm)-diameter occurred as bell fracture at an axial stress in the pipe barrel equivalent to 77% of the proportional limit stress.

DI pipelines with nominal diameters of 4-in. (100-mm) to 8-in. (200-mm) supplied by McWane and US Pipe are equipped with two locking segments so that spigot ovaling will control the pullout resistance. DI pipelines with a nominal diameter greater than or equal to 12 in. (300 mm) are able to sustain higher axial load without ovaling, resulting in higher stress concentration conveyed to the bell.

8.4 Four-Point Bending Tests

Four-point bending tests were performed on nominal 6-in. (150-mm) diameter restrained axial slip DI pipe joints at water pressures of 75 to 85 psi (520 to 590 kPa). The maximum moments of most pipes in these investigations were within the upper half of the range between the proportional limit and yield moments. An exception was observed for the 6 in. (150 mm) Kubota bending test, for which the maximum moment was equal to the ultimate moment.

When the maximum moment was attained, the DI joint either noticeably deformed or cracked at the spigot end or bell barrel, with significant leakage exceeding 10 gal/min (38 l/min) observed for the AMERICAN, McWane, and US Pipe joints. However, the Kubota pipe was able to maintain the water pressure and accommodate more rotation after the spigot end cracked because the gasket, which was located near

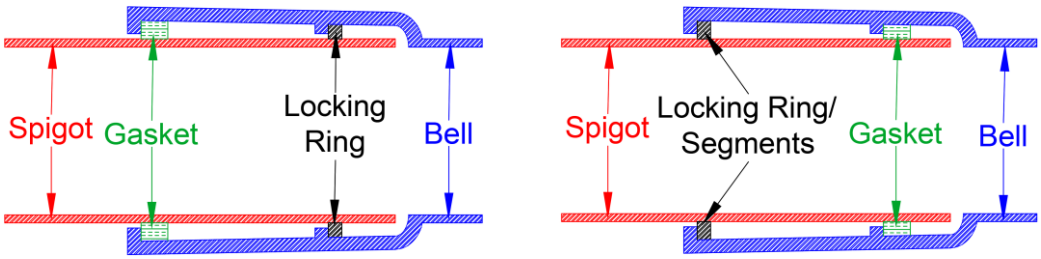

a) Gasket near Front of Bell Face b) Gasket near Back of Bell

Figure 8.1. Schematic of Restrained Axial Slip Joints

the bell end opening (bell face), prevented leakage at the joint. Figure 8.1 a) shows a joint cross-section in which the gasket is located near the front of the bell, consistent with the gasket location in the Kubota pipe. Figure 8.1 b) shows a joint cross-section in which the gasket is located near the back of the bell, consistent with the other pipes.

8.5 Soil Axial Resistance Tests

Soil axial resistance tests were performed to evaluate the soil-structure interaction associated with relative axial movement of DI pipe with the restrained axial slip joint through soil. The axial resistance created by the enlarged axial slip joints, and soil/pipe frictional resistance along the pipe barrel were measured. In addition, the effect of polyethylene wrap on the axial resistance of the DI restrained axial slip joint was investigated.

The ratio of pipe interface to soil friction angle, δ/ϕ, estimated from these experiments varies from 0.8-1.0 throughout the full range of 16 in. (400 mm) of axial

pipe movement applied during testing. For axial displacement in soil greater than 5 in. (150 mm), δ/ϕ varies in a narrower range of 0.9-1.0.

The maximum measured load drop across the bell was approximately 15% larger when the flat face of the bell was oriented in the direction of pipe movement. There was also a stiffer response in this orientation, with the ratio of axial load vs. displacement during the development of load between 15 and 30% higher than the corresponding ratio when the curved end was facing the direction of movement.

The application of polyethylene wrap did not result in significant reduction of shear resistance along the pipe barrel, but did result in a load drop reduction across the joint. The deformable polyethylene wrap reduced the bearing resistance of the bell flat face by 15%, which is very close to the joint resistance of the curved bell facing in the direction of movement.

8.6 Fault Rupture Tests

Full-scale fault rupture tests were performed on nominal 6-in. (150-mm) diameter DI pipelines with restrained axial slip joints manufactured by four different companies. The pipelines were buried at the same depths of 30 in. (762 mm) to top of pipe in dense, partially saturated sand with $\phi = 42°$ and water content of approximately 4.0%. All pipelines were under internal water pressure of approximately 80 psi (550 kPa). They were subjected to left lateral strike-slip fault movement at a pipeline/fault crossing angle 50°, following similar test procedures.

Large-scale fault rupture tests demonstrate the ability of the restrained axial slip joints to accommodate significant fault movement through axial pullout and rotation of the joints. Moreover, the measurements provide a comprehensive and detailed understanding of how the movement was accommodated at each joint, the sequence of movements, and combined axial pullout and rotation at each joint.

Fault rupture simulated in the large-scale tests is also representative of the most severe ground deformation that occurs along the margins of liquefaction-induced lateral spreads and landslides. The amount of tensile strain that can be accommodated with the restrained axial slip joints depends on the spacing of the pipeline joints. For the joint spacing used in the fault rupture tests, the pipeline extensions were large enough to accommodate the great majority (over 90%) of liquefaction-induced lateral ground strains measured by high resolution LiDAR after each of four major earthquakes during the recent Canterbury Earthquake Sequence (CES) in Christchurch, NZ (O'Rourke et al., 2014).

Key results of the fault rupture tests are summarized under the subheadings that follow.

8.6.1 Combined Axial Slip and Joint Rotation

Force vs. displacement and moment vs. rotation relationships of the joints closest to the fault were developed and compared to similar relationships obtained from the direct tension and four-point bending tests, respectively. The test measurements show that moment vs. rotation relationships of the joints for the fault rupture test are in

close agreement with the results of the four-point bending tests. All four-point bending tests were performed with the joints fully extended, which is consistent with the full joint extension developed in the fault rupture test.

Although the force vs. displacement relationships from the fault rupture tests follow a pattern similar to those measured during the direct tension tests, the loads at failure are significantly lower than those measured in the direct tension tests. Reductions in the tensile capacity of 15% and 25% were measured in the US Pipe and McWane tests, respectively. The experimental evidence indicates that these reductions in joint tensile capacity were caused by combined rotation and axial expansion of the joints.

During fault rupture and abrupt ground deformation, restrained axial slip joints are subjected to simultaneous axial slip and rotation. The experimental evidence shows that the moment vs. rotation response of the joints during strike-slip fault movement that causes pipeline extension is similar to the moment vs. rotation relationship during four-point bending tests performed with the joint at its fully extended position. The axial force vs. displacement relationship for the same fault rupture conditions is affected by a significantly lower axial pullout force ranging between 15 and 25% below those determined by direct tension tests. The test results show that, for the strike-slip fault conditions simulated in the laboratory, the combined application of axial slip and rotation do not affect significantly the moment vs. rotation relationship as measured directly by four-point bending tests. They do reduce significantly, however, the axial tensile failure load relative to the axial force capacity measured by direct tension tests.

8.6.2 Axial Slip of Joints

As mentioned previously the fault rupture tests provide a comprehensive picture of axial slip and the sequence of axial joint movements to accommodate fault displacement. The general sequence of joint slip response was for the south joint nearest the fault to move first. All test pipelines were installed with the flat face of the joints facing north so that axial resistance of the bell of the closest south joint was larger than the axial resistance of the curved end bell of the closest north joint. The spigot was pulled from the closest south joint first because bell movement at that joint was resisted by the highest axial reaction force. Once the spigot at the closest south joint had slipped to engage its locking mechanism, axial slip was transferred to the nearest north joint. Once the nearest north joint had slipped to engage its locking mechanism, axial force was transferred to the closest south joint, mobilizing movement that caused the spigot at the second joint south of the fault to slip and engage its locking mechanism. Axial slip was then transferred to the second joint north of the fault.

The same alternating pattern of spigot slip at the south joint nearest the fault followed by north joint movement and then south bell movement, as described above, was followed by six, four, and two joints in the Kubota, US Pipe, and McWane fault rupture tests, respectively, until tensile failure and pullout occurred at the south joint nearest the fault. Only the fault rupture test with the AMERICAN restrained axial slip joints followed a different sequence of axial joint movement as described in Chapter 7.

8.6.3 Axial Pipeline Loads

Axial pipeline forces are affected by the longitudinal frictional resistance mobilized along the pipe barrel and the load drop across pipeline joints. Both contribute to the maximum load imposed in the pipeline for a given amount of fault or ground rupture displacement, and thus influence the maximum ground deformation that can be sustained by the pipeline before axial joint failure.

The fault rupture tests provide an opportunity to evaluate at full scale the actual axial forces influenced by longitudinal frictional resistance and axial resistance to movement at the joints. The longitudinal frictional forces are controlled by at rest (K_o) conditions, which set the initial state of stress along the pipeline, and the conditions of maximum lateral soil reaction during fault rupture, which establish the maximum longitudinal frictional resistance for the pipeline in the vicinity of fault rupture.

As explained in Appendix A, the frictional resistance per length of straight pipe, f, is calculated as:

$$f = \left(\frac{1 + K_o}{2}\right) \tan(\delta)\, \gamma H_c \pi D_o \tag{8.1}$$

where K_o is the lateral at-rest earth pressure coefficient taken from full scale test measurements as 0.45 (O'Rourke et al., 1989), H_c is the depth to pipe springline, D_o is the pipe outer diameter, γ is soil unit weight, and δ is the pipe/soil interface friction angle of 0.9ϕ.

In the zone between pipeline joints closest to the fault plane, the pipeline is subjected to high horizontal soil reaction, and the at-rest conditions are disrupted. The frictional force per unit pipe length, f, is given as

$$f_t = p_H \tan\delta = \alpha N_{qH} \gamma H_c D_o \tan\delta \tag{8.2}$$

in which p_H is the horizontal soil reaction per unit distance, N_{qH} is the maximum dimensionless lateral force as described by Jung et al. (2016), and α is a correction factor to account for three-dimensional shear transfer, as explained in Appendix A.

Measurements during fault rupture tests confirm that the distribution of axial loads are consistent with K_o conditions near the north and south ends of the split basin where the pipeline is not affected by lateral movement between the soil and pipe. The slope of the axial force distribution at these locations compares favorably with the frictional force per unit distance calculated by Eqn. 8.1. Likewise, fault rupture test measurements show that the distribution of axial pipeline load in the vicinity of the fault rupture is consistent with the frictional force per unit pipe length, f_t, given by Eqn. 8.2. The length of the pipeline affected by elevated lateral soil forces extends from the closest joint south of the fault to the closest joint north of the fault.

As explained in Appendix A, Argyrou (2018) provides a scaling relationship for estimating the axial load drop across enlarged DI joints subject to lateral movement during fault displacement. The scaling relationship is given by:

$$\frac{F_{bell.fym}}{F_{bell.ref}} = \frac{N_{qH}}{\pi \frac{(1+K_o)}{2}} \tag{8.3}$$

where $F_{bell,fym}$ is the axial bell resisting force in the zone where maximum lateral soil forces are mobilized, and $F_{bell,ref}$ is the bell resistance measured at a reference burial depth, $H_{c,ref}$, under at-rest (K_o) conditions. For these conditions, the bell resisting force is directly proportional to N_{qH} in Eqn. A.21.

Axial load drops across the DI joints closest to the fault rupture plane during all fault rupture tests are plotted as a function of fault displacement in Chapter 7. The maximum axial load drops for the Kubota, McWane, and US Pipe fault rupture tests are high, ranging between 18 and 28 kips (80 and 125 kN). These values are substantially higher than those predicted from the soil axial resistance test results presented in Chapter 5, but mostly smaller than the load drop estimated by Eqn. 8.3. During the McWane and US Pipe fault rupture tests, the measured load drops were approximately 15% less and 20% greater than the load drop estimated with Eqn. 8.3.

It appears that Eqn. 8.3 provides a generally conservative estimate of the axial load drop across DI restrained axial slip joints. The test results, however, show a wide variation in axial load distribution that depends on the interaction among lateral soil reaction forces, reversal of joint movement, longitudinal shear transfer, and annular bearing forces generated by the enlarged DI joints as they move axially with respect to the soil. The axial pipeline forces also depend on the amount of disruption and alteration of the soil stress state that occurs as the enlarged joints move laterally and axially during fault rupture. Despite the uncertainties, the fault rupture test results provide for a substantially improved understanding of soil-pipeline interaction under the extreme conditions of fault rupture, and allow for estimates of longitudinal shear transfer to pipe

barrel as well as axial load drops across enlarged DI joints at locations both close to and distant from the fault rupture plane. These estimates compare favorably with the results of the fault rupture tests.

8.7 Simplified Models for Pipeline Response to Fault Rupture

8.7.1 Joint Axial Resistance Model

The joint axial resistance model proposed in this work is obtained from the expression for face resistance of the leading edge of a jacked pipe proposed by Meskele and Stuedlein (2015) from the work of Weber and Hurtz (1981). The model assumes that resistance to axial movement is mobilized by bearing capacity of the leading edge. For pipe jacking, the leading edge is the circumferential protrusion at the advancing face of the pipe, resulting in an annular bearing area that is pushed into the surrounding ground.

The model is used to predict the axial resistance from a restrained axial slip joint for DI pipe and the pullout restraints of PVCO and PVC pipelines. The proposed model provides for relatively close prediction under K_o conditions within ±15% of the actual maximum load measured during full scale soil axial resistance tests described in this work.

8.7.2 Simplified Model for Axial Force Distribution during Fault Rupture Tests

The simplified analytical model is developed to predict the axial load distribution in the McWane and US Pipe fault rupture tests for two conditions. The first

condition involves full slip of all joints with all locking mechanisms engaged to resist further axial slip. The second condition corresponds to the maximum axial force in the pipeline before failure. The simplified model provides estimates of axial load distributions in reasonable agreements with the McWane and US Pipe experimental results for both conditions.

8.8 Recommendations for Future Research

The experimental evidence shows that the reduction in axial soil resistance with polyethylene wrap is affected by complex shear transfer between the joint and surrounding soil as the polyethylene wrap compresses, folds, and tears. Experimental evidence from large-scale testing in this work suggests that the deformable polyethylene wrap reduces the bearing resistance of the bell flat face, thereby reducing soil axial resistance from the joint rather than the longitudinal frictional forces along the pipe barrel. Additional testing and research are required to understand the mechanisms for load transfer. It is important to understand what mechanisms control resistance with polyethylene wrap and what limitations apply to its use in the field.

Argyrou (2018) provides the scaling relationships for estimating the load drop across an enlarged joint under at-rest (K_o) and high horizontal soil reaction conditions. Additional experimental work is required to characterize these soil/pipe interactions and verify the scaling relationship from at-rest (K_o) to high horizontal soil reaction conditions. As explained previously, the fault rupture test measurements show that the axial load distribution in a jointed DI pipeline depends on the interaction among lateral

soil reaction forces, reversal of joint movement, longitudinal shear transfer, and annular bearing forces at the joints. It appears that the proposed scaling relationships establish upper bound condition for maximum load drops across DI joints. Conditions required to mobilize maximum axial resistance were not met in some fault rupture tests. Additional fault rupture tests would help clarify the load transfer mechanism associated with abrupt ground deformation imposed on jointed pipelines and identify the conditions under which maximum axial loads are developed.

Although the moment vs. rotation relationships from four-point bending and fault rupture tests are in favorable agreement, the joint pullout capacity in the fault rupture test is lower than that in the direct tension test. Experiments on combined axial and bending loading are required to characterize the tensile failure load and force vs. axial displacement relationships for DI pipelines subject to fault rupture and abrupt ground deformation.

Although DI pipelines are particularly vulnerable to joint pullout, compressive axial movement can cause local, irrecoverable deformation, which may lead to leakage in the pipelines. The strike-slip fault rupture test results reported in this work produced axial elongation in the pipelines. Additional tests, in which fault rupture imposes axial compression, are needed to understand and characterize in detail pipeline response under ground deformation that results in combined bending and thrust.

APPENDIX A

SIMPLIED MODEL FOR AXIAL FORCE DISTRIBUTION ALONG JOINTED PIPELINE AT FAULT CROSSING

This appendix describes a simplified model for axial force distribution along a pipeline with push-on, restrained, and restrained axial slip joints. It consists of four sections covering the simplified model, its application, estimation of soil shear transfer forces, and load drops across joints.

A.1. Simplified Model

It is assumed that the axial stress at all locations along the pipe barrel are within the linear elastic range. Figure A.1 a) is a schematic of a jointed pipeline crossing a left-lateral strike-slip fault at angle β. The pipeline is anchored at equal distances from the intersection of the pipeline and fault. It is assumed that the pipeline material, geometric properties, burial depth, and soil properties are identical either side of the pipeline/fault intersection.

The left-lateral fault displacement in the schematic causes the pipeline to elongate. If restrained axial slip joints are used, the joints will slip or pull out until the restraints resist further movement, causing axial force to increase in the pipeline.

As long as axial stress is everywhere in the elastic range the simplified model applies also to right-lateral strike-slip fault movement that imposes axial compression

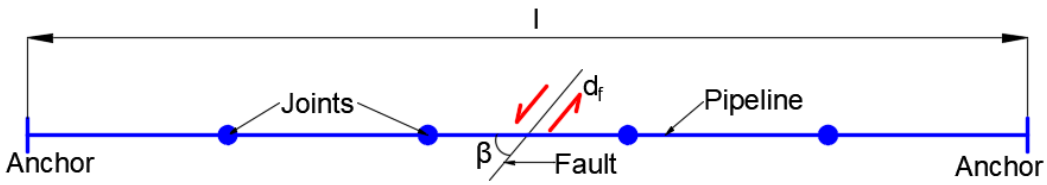

a) Pipeline Fault Crossing

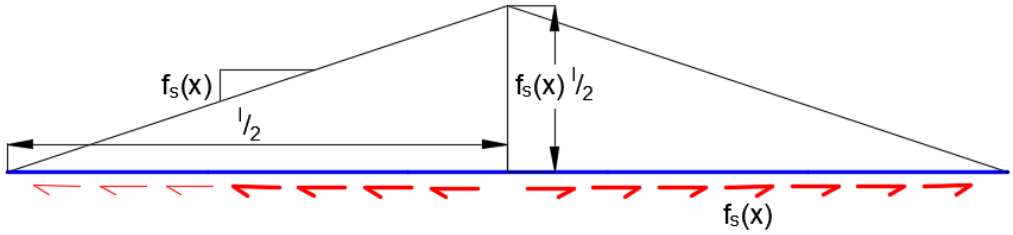

b) Axial Shear Transfer

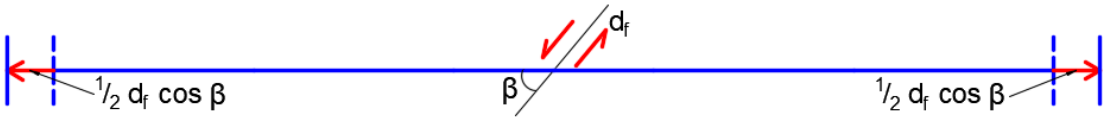

c) Axial Extension

Figure A.1. Jointed Pipeline Axial Elongation and Axial Shear Transfer at Fault Crossing

in the pipeline. Under these condition axial slip at the joints will cause them to close until there is resistance to further movement that results from contact between the spigot and back of the bell at each joint. For restrained axial slip joints, it is assumed that axial force mobilized by axial slip is negligible until restraint occurs.

The total axial slip, d_{jt}, of all joints across the length, l, between anchors is

$$d_{jt} = \sum_{i=1}^{n} d_{ji} \qquad (A.1)$$

where d_{ji} is the slip at the i^{th} joint, and n is the number of joints between the anchors.

After all joints slip to their full distances, the pipeline will elongate by elastic extension until maximum axial capacity of a joint is exceeded. The elastic extension can be calculated by superposition of the axial shear transfer, as illustrated in Figure A.1 b) and the axial elongation of the pipeline, $d_f \cos \beta$, depicted in Figure A.1 c), where d_f is the fault displacement for the angle of pipeline/fault intersection, β.

For the case where axial shear transfer between pipe and soil, $f_s(x)$, is constant and equal to f_s, the axial load distribution from f_s is triangular, as depicted in Figure A.1 b). The maximum axial load from f_s at the center of the pipeline, P_{fs}, is shown in Figure A.1 b) as follows

$$P_{fs} = \frac{f_s l}{2} \tag{A.2}$$

The average axial strain, ε_{avg}, in the pipeline is given by

$$\varepsilon_{avg} = \frac{f_s l}{2AE} \tag{A.3}$$

where A is the pipe cross-sectional area, and E is Young's modulus.

The shear-induced elastic extension of the pipeline, d_{fs}, is simply the product of ε_{avg} and l such that

$$d_{fs} = \frac{f_s l^2}{2AE} \tag{A.4}$$

The net axial elongation of the pipeline is given by

$$d_{Net} = d_f \cos \beta - d_{jt} - d_{fs} \tag{A.5}$$

To satisfy compatibility of axial displacement, the extension of the pipeline imposed by the anchor load, P_{ANCH}, must be equal to the net axial elongation of the pipeline as follows

$$P_{ANCH} = \frac{d_{Net} AE}{l} \tag{A.6}$$

Combining Eqns A.1, A.4, A.5, and A.6 results in

$$P_{ANCH} = \left(d_f \cos\beta - \frac{f_s l^2}{2AE} - \sum_{i=1}^{n} d_{ji} \right) \frac{AE}{l} \tag{A.7}$$

Given d_f, β, l, and AE, Eqn A.7 can be used to predict the anchor load, P_{ANCH}. The maximum axial load, $P_{A\,Max}$, at the pipeline/fault intersection is

$$P_{A\,Max} = P_{ANCH} + \frac{f_s l}{2} \tag{A.8}$$

For restrained joints with no axial slip, the anchor force is

$$P_{ANCH} = \left(d_f \cos\beta - \frac{f_s l^2}{2AE} \right) \frac{AE}{l} \tag{A.9}$$

and the maximum axial force is given by Eqn A.8.

For push-on joints with negligible resistance to axial slip and pullout displacement capacity, d_s, the maximum fault movement that can be accommodated is

$$d_f = \frac{d_s}{\cos\beta} \tag{A.10}$$

with negligible axial force in the pipeline.

For the above derivation, the effective frictional force, $f_s(x)$, was taken as a constant, f_s. In the field, $f_s(x)$, will result from variable $f_s(x)$ along the pipeline generated by maximum lateral soil reaction conditions near the fault, at rest (K_o) conditions further away from the fault, and axial load drops across pipeline joints.

A.2. Application of Simplified Model

Figure A.2 provides a simplified axial load distribution for a fault crossing of a pipeline with either restrained or restrained axial slip joints. The maximum lateral force and axial soil resistance, f_{s2}, are mobilized between the two joints, each of which has a load drop, F_j. At-rest (K_o) soil conditions result in f_{s1} between the joints and the anchors, each of which carries an axial force, P_{ANCH}.

The soil shear and axial joint induced elastic extension of the pipeline, d_{fs}, is associated with either the force or average force for the rectangular and triangular areas, respectively, numbered 2 to 4 in Figure A.2. Since the axial load distribution is symmetric about the center of the pipeline, the axial extension from each area needs to be doubled. The axial extensions d_2, d_3, and d_4, associated with their corresponding areas in Figure A.2 are given by the following equations:

$$d_2 = \frac{f_s l_1^{\,2}}{2AE} \tag{A.11}$$

$$d_3 = \frac{2(f_s l_1 + F_j)(\frac{l}{2} - l_1)}{AE} \tag{A.12}$$

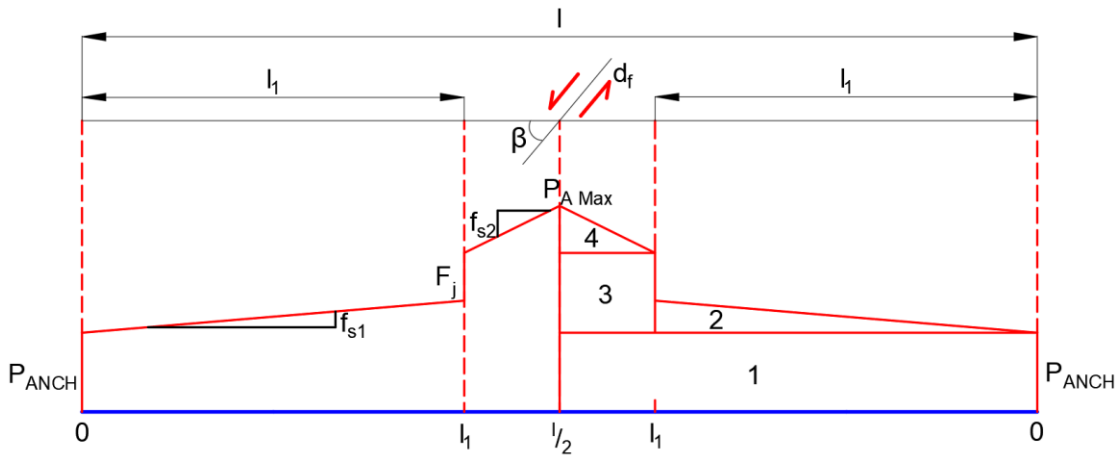

Figure A.2. Axial Force Distribution for Pipeline with Two Restrained Axial Slip Joints

$$d_4 = \frac{f_{s2}\left(\frac{l}{2} - l_1\right)^2}{AE} \tag{A.13}$$

The effective shear-induced elastic extension, d_{fs}, for this case is given by

$$d_{fs} = d_2 + d_3 + d_4 \tag{A.14}$$

For a pipeline with restrained axial slip joints, the anchor force, P_{ANCH}, is calculated by

$$P_{ANCH} = \left[d_f \cos\beta - (d_2 + d_3 + d_4) - 2d_j\right]\frac{AE}{l} \tag{A.15}$$

where d_j is the axial slip, assumed to be equal at each restrained axial slip joint.

The maximum axial load at the pipeline/fault intersection is given by

$$P_{A\,Max} = P_{ANCH} + f_s l_1 + F_j + f_{s2}\left(\frac{l}{2} - l_1\right) \tag{A.16}$$

If the pipeline has restrained joints with no axial slip capacity, the anchor force, P_{ANCH}, for this example is given by:

$$P_{ANCH} = \left[d_f \cos\beta - (d_2 + d_3 + d_4)\right] \frac{AE}{l} \quad (A.17)$$

and the maximum axial load is given by Eqn. A.16.

The preceding equations are valid as long as the pullout capacity of the joint is not exceeded in tension and the proportional limit stress is not exceeded in compression. Satisfying both of these conditions ensures that the pipe barrel stress remains within the elastic range.

A.3. Soil Pipe Axial Shear Transfer

Following the ASCE (1984) guidelines, the frictional resistance per length of straight pipe, f, is calculated as:

$$f = \left(\frac{1 + K_o}{2}\right) \tan(\delta)\, \gamma H_c \pi D_o \quad (A.18)$$

where K_o is the lateral at-rest earth pressure coefficient taken from full scale test measurements as 0.45 (O'Rourke et al., 1989), H_c is the depth to pipe springline, D_o is the pipe outer diameter, γ is soil unit weight, and δ is the pipe/soil interface friction angle of 0.9ϕ. As explained in Chapter 5, soil axial resistance tests on DI pipelines with restrained axial slip joints show that δ/ϕ varies from 0.8 to 1.0.

In the zone between pipeline joints closest to the fault plane, the pipeline is subjected to high horizontal soil reaction, and the at-rest conditions are disrupted. The apparent frictional force per unit pipe length, f_a, is given as

$$f_a = p_H \tan\delta = N_{qH} \gamma H_c D_o \tan\delta \quad (A.19)$$

in which p_H is the horizontal soil reaction per unit distance, and N_{qH} is the maximum dimensionless lateral force as described by Jung et al. (2016). Figure A.3 shows plots of N_{qh} vs dimensionless depth, H_c/D, for partially saturated medium dense sand and dry medium, dense, and very dense sand for $H_c/D \leq 11$. As explained by O'Rourke et al. (2016), the actual, or "true", longitudinal frictional force per unit length, f_t, is expressed as the ratio f_t/f_a which is a correction factor given by

$$\frac{f_t}{f_a} = \frac{1.652}{1.346 + 0.741\tan\delta} \tag{A.20}$$

Combining Eqns. A.19 and A.20 results in

$$f_t = \left(\frac{1.652}{1.346 + 0.741\tan\delta}\right) N_{qH}\gamma H_c D_o \tan\delta \tag{A.21}$$

A.4. Joint Axial Resistance

Argyrou (2018) describes a scaling relationship derived from experimental results (Wham et al., 2018a) given by the following expression

$$\frac{F_{bell.fym}}{F_{bell.ref}} = \frac{H_c}{H_{c,ref}} \tag{A.22}$$

where $F_{bell,ref}$ is the bell resistance measured at a reference depth to pipe center, $H_{c,ref}$, and $F_{bell,Hc}$ is the bell resisting force projected to a different depth of interest, H_c. The experimental data reported by Wham et al. (2018a) show that the resisting force scales to higher or lower values at approximately the same axial displacement when the bell resisting force is plotted against axial pipe movement.

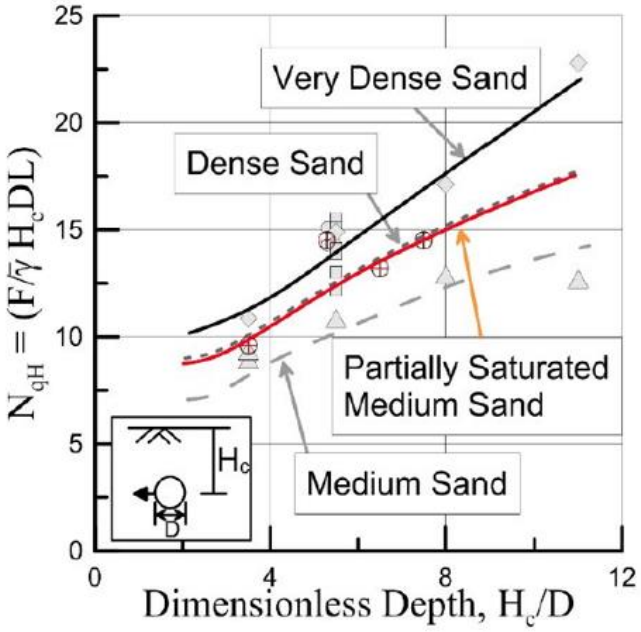

Figure A.3. Maximum Dimensionless Lateral Pipe Force after O'Rourke et al. (2016)

As discussed in the previous section, the longitudinal shear transfer from soil to pipe barrel scale in direct proportion to the lateral soil forces mobilized during fault movement. Following on this principle, Argyrou (2018) provides a similar scaling relationship for estimating the axial load drop across enlarged DI joints subject to transverse lateral movement during fault displacement. The scaling relationship is given by:

$$\frac{F_{bell.fym}}{F_{bell.ref}} = \frac{N_{qH}}{\pi\frac{(1+K_o)}{2}} \tag{A.23}$$

where $F_{bell,fym}$ is the axial bell resisting force in the zone where maximum lateral soil forces are mobilized. For these conditions, the bell resisting force is directly proportional to N_{qH} in Eqn. A.21. $F_{bell,ref}$ is the bell resistance measured at a reference

burial depth, $H_{c,ref}$, where the bell resisting force is directly proportional to $(1+K_o)/2$ for at-rest conditions. This scaling relationship requires the same soil and pipe material properties, depths of burial, and bell geometries for both K_o and the high lateral soil reaction condition.

APPENDIX B

CORRECTION FOR AXIAL EXTENSION

This appendix provides a method for correcting the axial component of actuator displacements measured during fault rupture tests. When a fault rupture test is performed, there is a small amount of axial expansion that occurs primarily by out of plane movement as the north part of the split basin is pushed by the actuators along the intended fault rupture plane. Although steel channel beams are used to guide and control relative movement of the north and south parts of the split basin, a small separation in the axial direction of the pipeline occurs.

This type of movement is substantiated by DCDT measurements. Two DCDTs were installed to measure separation across the fault rupture plane during each fault rupture test. Each DCDT was fixed to one basin such that its rod was able to slide across a beam attached to the other basin and aligned along the fault plane. Separations typically between 0.1 and 0.3 in. (2.5 and 7.6 mm) were measured during the tests. Although these measurements confirm load separation, it is not possible to use them to evaluate the extension along the longitudinal axis of the test pipeline.

The axial elongation of the pipeline in each fault rupture test was determined by adding all joint openings measured by the DCDTs or string pots until full slip was attained, and the locking mechanism was engaged at each joint. This estimate of axial elongation is plotted for the Kubota, McWane, and US Pipe fault rupture tests in Figures B.1, B.2, and B.3 respectively, relative to the fault axial movement, $d_f \cos \beta$, where d_f

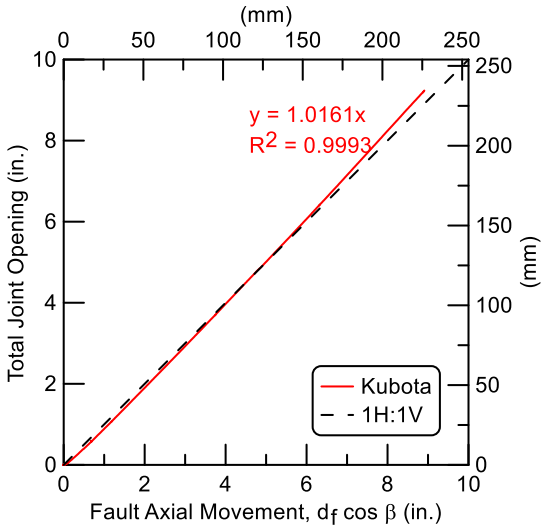

Figure B.1. Total Joint Opening vs. Fault Axial Movement for Kubota Fault Rupture Test

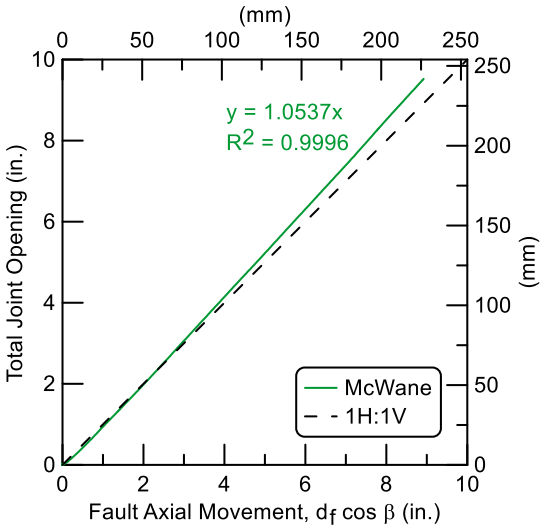

Figure B.2. Total Joint Opening vs. Fault Axial Movement for McWane Fault Rupture Test

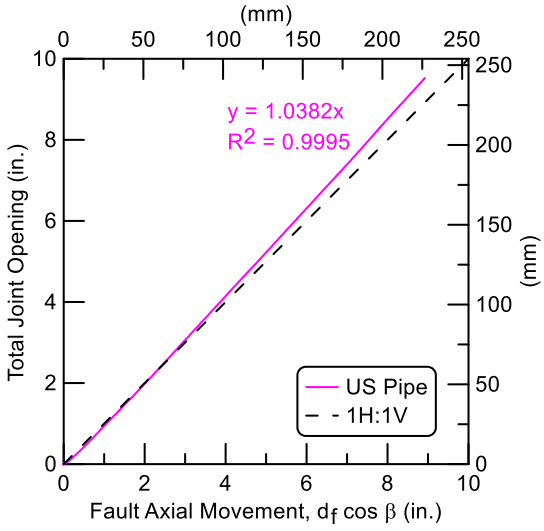

Figure B.3. Total Joint Opening vs. Fault Axial Movement for US Pipe Fault Rupture Test

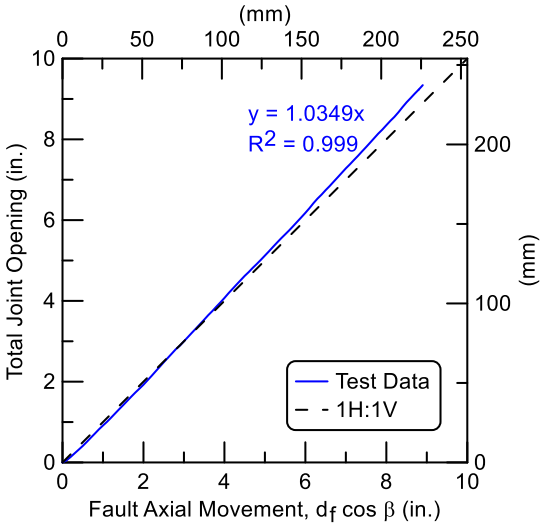

Figure B.4. Total Joint Opening vs. Fault Axial Movement for Combined Datasets

is a fault displacement and β is an intersection angle between the pipe and fault of 50°. The fault axial movement is associated with fault rupture movement imposed by the actuators.

In each figure a linear regression is plotted and compared with a 1H:1V line. The regression equation and r^2 is given for each test. Data from the AMERICAN fault rupture test were not used because there was some interference from the surrounding soil to the protective shields that affected the string pot measurements. (Pariya-Ekkasut, 2017).

Figure B.4 shows the linear regression for total joint opening vs. fault axial movement for the combined Kubota, McWane, and US Pipe datasets. The slope of the linear regression is a correction factor. When $d_f \cos \beta$ is multiplied by the slope, the axial extension along the pipeline is provided.

REFERENCES

Argyrou, C. (2018). "Pipeline Response to Earthquake-Induced Ground Deformation." PhD Dissertation: Cornell University, Ithaca, NY.

ASCE. (1984). "Guidelines for the Seismic Design of Oil and Gas Pipeline Systems." *Committee on Gas and Liquid Fuel Lifelines,* American Society of Civil Engineers, New York.

ASTM International (2013). "Standard Test Methods for Tension Testing of Metallic Materials." *Standard No. ASTM E8/E8M - 13a,* American Society for Testing and Materials International, West Conshohocken, PA.

AWWA. (2017). "Ductile Iron Pipe, Centrifugally Cast, for Water." *Standard No. ANSI/AWWA C151/A21.51-17,* American Water Works Association, Denver, CO.

Bouziou, D. O'Rourke, T. D., Cubrinovski, M., and Henderson, D. (2015). "Evaluation of Ground Deformations during the 2010-2011 Canterbury Earthquake Sequence", *6th International Conference on Earthquake Geotechnical Engineering*, Nov. 2015, Christchurch, NZ.

Ductile Iron Group. (1990). "Ductile Iron Data for Design Engineers." Chicago, IL. http://www.ductile.org/didata/ [accessed January 2018]

Honegger, D.G. and Nyman, D.J. (2004). "Guidelines for the Seismic Design and Assessment of Natural Gas and Liquid Hydrocarbon Pipelines", *Catalogue L51927, Pipeline Research Council International (PRCI)*, Arlington, Virginia.

JWWA. (2010). "Ductile Cast Iron Pipe for Water Supply." *Standard No. JWWA G113-10,* Japanese Water Works Association, Tokyo, JP. (in Japanese)

JWWA. (2010). "Water Ductile Cast Iron Profile Pipe." *Standard No. JWWA G114-10,* Japanese Water Works Association, Tokyo, JP. (in Japanese)

Jung, J. K., O'Rourke, T. D. and Argyrou C. 2016. "Multi-Directional Force Displacement Response of Underground Pipe in Sand." *Canadian Geotechnical Journal,* 53(11): 1763-1781.

Kishi, S., Kagawa, T., Kaneko, S., Kobuchi, K., and Miyajima, M. (2013). "A Study on Behavior of Earthquake Resistant Ductile Iron Pipeline at the 2011 Great East Japan Earthquake." *US-Taiwan-Japan Water System Seismic Practice*, Oakland, CA., Aug. 2013.

Maragakis, E. M., Siddharthan, R., and Meis, R. D. (1999). "Axial Behavior Characteristics of Pipe Joints under Static Loading." *Technical Report MCEER-03-0006,* Multidisciplinary Center for Earthquake Engineering Research, Buffalo, NY.

Mason, J A. (2006). "Earthquake Response and Seismic Strengthening of Welded Steel Pipelines." PhD Dissertation: Cornell University, Ithaca, NY.

Meis, R. D., Maragakis, E. M., and Siddharthan, R. (2001). "Static Axial Behavior of Some Typical Restrained Pipe Joints," *Journal of Testing and Evaluation*, 29(5): 485–491.

Meis, R. D., Maragakis, E. M., and Siddharthan, R. (2003). "Behavior of Underground Piping Joints Due to Static and Dynamic Loading," *Technical Report MCEER-03-0006,* Multidisciplinary Center for Earthquake Engineering Research, Buffalo, NY.

Meskele, T. and Stuedlein, A. W. (2015). "Static Soil Resistance to Pipe Ramming in Granular Soils" *Journal of Geotechnical and Geoenvironmental Engineering*, American Society of Civil Engineers, 141(3):04014108, 1–11.

Oda, K., Ishihara, T., and Miyajima, M. (2016). "Pipeline Design Method Against Large Displacement of Strike-Slip Fault." *ASME Pressure Vessels and Piping Conference, 8: Seismic Engineering:* V008T08A020. doi:10.1115/PVP2016-63699

O'Rourke, T. D. (1998). "An Overview of Geotechnical and Lifeline Earthquake Engineering", *Geotechnical Special Publication No. 75*, Geotechnical Earthquake Engineering and Soil Dynamics Conference, Seattle, WA, American Society of Civil Engineers, Aug. 1998, 2: 1392-1426.

O'Rourke, T. D. (2010). "Geohazards and Large, Geographically Distributed Systems." *Geotechnique,* 60(7): 505–543.

O'Rourke, T. D., Bonneau, A., Pease, J. W., Shi, P., and Wang, Y. (2006). "Liquefaction Ground Failures in San Francisco" *Earthquake Spectra*, EERI, Oakland, CA, 22(S2): 691-6112.

O'Rourke, T. D., and Druschel, S. J. (1989). "Improved Anchoring Practices for Plastic Gas Distribution Pipelines," *Report, Prepared for New York Gas Group,* Oct. 2015.

O'Rourke, T. D., Jeon, S-S., Toprak, S., Cubrinovski, M., Hughes, M., van Ballegooy, S., and Bouziou, D. (2014) "Earthquake Response of Underground Pipeline Networks in Christchurch, NZ", *Earthquake Spectra*, EERI, 30(1): 183-204.

O'Rourke, T. D., Jezerski, N. A. Olson, T., Bonneau, A. L., Palmer, M. C., Stewart, H. E., O'Rourke, M. J., and Abdoun, T. (2008). "Geotechnics of Pipeline System Response to Earthquakes", *Keynote Paper, Proceedings, Geotechnical Earthquake Engineering and Soil Dynamics IV (GEESD)*. Sacramento, CA, May.

O'Rourke, T. D., Jung, J. K., and Argyrou, C. (2016). "Underground Pipeline Response to Earthquake-Induced Ground Deformation", *Soil Dynamics and Earthquake Engineering*, 91:272-283.

O'Rourke, T. D. and Pease, J. W. (1997). "Mapping Liquefiable Layer Thickness for Seismic Hazard Assessment", *Journal of Geotechnical Engineering*, American Society of Civil Engineers, New York, NY, 123(1): 46-56.

Pariya-Ekkasut, C., Berger, B. A., Stewart, H. E., and O'Rourke, T. D. (2018). "Evaluation of McWane Seismic Flex Coupling for Resistance to Earthquake-Induced Ground Deformation", *Report, Prepared for McWane Corporate*, May, 2018, Cornell University, Ithaca, NY. https://sites.coecis.cornell.edu/lifelines/ [accessed April 2018]

Pariya-Ekkasut, C., Berger, B. A., Stewart, H. E., Wham, B. P., O'Rourke, T. D., and Bond, T. K. (2017). "Four-Point Bending Testing of 6-in. (150-mm), 12-in. (300-mm), and 16-in. (400-mm)-Diameter Kubota Earthquake Resistant Ductile Iron Pipes", *Report, Pre*pared for Kubota Corporation, Apr, 2017, Cornell University, Ithaca, NY. https://sites.coecis.cornell.edu/lifelines/ [accessed April 2018]

Pariya-Ekkasut, C., Stewart, H. E., Wham, B. P., O'Rourke, T. D., Argyrou, C., and Bond, T. K. (2015). "Four-Point Bending and Direct Tension Testing of Twelve Inch TR-XTREME™ Pipe Joint", *Report, Prepared for U.S. Pipe*, Sep, 2015, Cornell University, Ithaca, NY. https://sites.coecis.cornell.edu/lifelines/ [accessed April 2018]

Pariya-Ekkasut, C., Stewart, H. E., Wham, B. P., O'Rourke, T. D., Argyrou, C., and Bond, T. K. (2016). "Hazard Resilience Evaluation of US Pipe Ductile Iron TR-XTREME™ Joints: 4-16 in. (100-400 mm) Diameter Pipe", *Report, Prepared for U.S. Pipe*, Jan, 2016, Cornell University, Ithaca, NY. https://sites.coecis.cornell.edu/lifelines/ [accessed April 2018]

Pariya-Ekkasut, C., Stewart, H. E., Wham, B. P., O'Rourke, T. D., and Bond, T. K. (2016). "Direct Tension and Split Basin Testing of 6-in. (150-mm)-Diameter Kubota Earthquake Resistant Ductile Iron Pipe", *Report, Prepared for Kubota Corporation*, Feb, 2016, Cornell University, Ithaca, NY. https://sites.coecis.cornell.edu/lifelines/ [accessed April 2018]

Pariya-Ekkasut, C., Stewart, H. E., Wham, B. P., O'Rourke, T. D., Bond, T. K., and Argyrou, C. (2017). "American Earthquake Joint System for Resistance to Earthquake-Induced Ground Deformation", *Report, Prepared for American Cast Iron Pipe Company*, Jan, 2017, Cornell University, Ithaca, NY. https://sites.coecis.cornell.edu/lifelines/ [accessed April 2018]

Pease, J. W. and T. D. O'Rourke (1997), "Seismic Response of Liquefaction Sites", *Journal of Geotechnical Engineering*, American Society of Civil Engineers, New York, NY, 123(1): 37-45.

Singhal, A. C. (1984). "Behavior of Jointed Ductile Iron Pipelines." *Journal of Transportation Engineering*, American Society of Civil Engineers, 1120(2): 235-250.

Singhal, A. C. and Benavides, J. C. (1983). "Axial and Bending Behavior of Pipeline Joints" *Journal (American Water Works Association)*, American Water Works Association, 75(11): 572-578.

Stewart, H. E., Argyrou C., Bouziou, D., Bond, T. K., O'Rourke, T. D., & Wham, B. P. (2012). "Cornell - Axial Push Tests on Unlined Ductile Iron Pipe", Network for Earthquake Engineering Simulation (distributor), Dataset, DOI:10.4231/D3DV1CP5S.

Stewart, H. E., O'Rourke, T. D., Pariya-Ekkasut, C., Wham, B. P., Bond, T. K., Argyrou, C. (2015). "Hazard Resilience Testing of US Pipe Ductile Iron TR-XTREME™ Pipe Joints", *Report, Prepared for U.S. Pipe*, Feb, 2015, Cornell University, Ithaca, NY. https://sites.coecis.cornell.edu/lifelines/ [accessed April 2018]

Stuedlein, A. W., and Meskele, T. (2012). "Preliminary Design and Engineering of Pipe Ramming Installations." *Journal of Pipeline Systems Engineering and Practice*, American Society of Civil Engineers, 3(4): 125–134.

Tokimatsu, K. and Suzuki, H. (2004). "Pore Water Pressure Response around Pile and Its Effects on P-Y Behavior during Soil Liquefaction", *Soil and Foundations*, Japanese Geotechnical Society, 44(6): 101-110.

US. EPA. (2013). "Primer on Condition Curves for Water Mains." *Final Report, EPA/600/R-13/080*, United States Environmental Protection Agency, Cincinnati, OH. https://cfpub.epa.gov/si/si_public_record_report.cfm?dirEntryId=266113 [accessed April 2018]

Weber, W., and Hurtz, G. (1981). "Ermittlung der rohrreibung und entwicklung eines bohrgerätes." Tiefbau, Ingenieurbau, Stra*ß*enbau, 23(8), 550–555 (in German).

Weerasekara, L. (2011). “Pipe-Soil Interaction Aspects in Buried Extensible Pipes.” PhD Dissertation: University of British Colombia, Vancouver, BC, Canada.

Wijewickreme, D., Karimian, H., and Honegger, D. (2009). “Response of Buried Shell Pipelines Subjected to Relative Axial Soil Movement.” *Canadian Geotechnical Journal,* 46(7): 735–752.

Wham, B. P., Argyrou, C., Bouziou, D., O’Rourke, T. D., Stewart, H. E., and Bond, T. K. (2014). “Jointed Pipeline Response to Earthquake Induced Ground Deformation.” *Proc., 10th National Conf. on Earthquake Engineering*, Earthquake Engineering Research Institute, Anchorage, AK.

Wham, B. P., Berger, B. A., Pariya-Ekkasut, C., O’Rourke, T. D. (2018a) “Hazard-resilient Pipeline Joint Soil Structure Interaction under Large Axial Displacement.” Proc., *5th Conference on Geotechnical Earthquake Engineering and Soil Dynamics*, American Society of Civil Engineers, Austin, Texas, June 10-13, (accepted).

Wham, B. P., Berger, B. A., Pariya-Ekkasut, C., O’Rourke, T. D., Stewart, H. E., Bond, T. K., and Argyrou, C. (2018b). “Achieving Resilient Water Networks – Experimental Performance Evaluation.” *11th U.S. National Conf. on Earthquake Engineering*, EERI, Los Angeles, CA.

Wham, B. P. and O’Rourke, T. D. (2016). “Jointed Pipeline Response to Large Ground Deformation.” *Journal of Pipeline Systems Engineering and Practice*, American Society of Civil Engineers, 7(1): 04015009. doi:10.1061/(ASCE)PS.1949-1204.0000207.

Wham, B. P., Pariya-Ekkasut, C., Argyrou, C., Lederman, A., O’Rourke, T.D., and Stewart H. E. (2017). “Experimental Characterization of Hazard-Resilient Ductile Iron Pipe Soil/Structure Interaction under Axial Displacement.” *Congress on Technical Advancement*, American Society of Civil Engineers, Duluth, MN, 124–134. doi: 10.1061/9780784481028.013

Yang, H., Junfeng, D., Lingjing, J., and Yanyan, Q. (2011). “Bending Behavior of Jointed Ductile Iron Pipelines.” *Pipelines Conference*, American Society of Civil Engineers, Seattle, WA. https://doi.org/10.1061/41187(420)131